CENTRIFUGE MODELLING OF WET DEEP MIXING PROCESSES IN SOFT CLAYS

LEE CHEN HUI

NATIONAL UNIVERSITY OF SINGAPORE

2006

CENTRIFUGE MODELLING OF WET DEEP MIXING PROCESSES IN SOFT CLAYS

LEE CHEN HUI
(B. E. (Hons.), UTM)

A THESIS SUBMITTED
FOR THE DEGREE OF DOCTOR OF PHILOSOPHY
DEPARTMENT OF CIVIL ENGINEERING
NATIONAL UNIVERSITY OF SINGAPORE
2006

ACKNOWLEDGEMENTS

It is a pleasure to thank the many people who made this thesis possible.

My sincere thanks go to my PhD. Supervisors, Associate Professor Lee Fook Hou and Dr. Ganeswara Rao Dasari for providing me with an opportunity to work in the Center for Soft Ground Engineering, National University of Singapore; and for their invaluable time, assistance, advice on this thesis. Without them, I would not have completed this thesis.

Thanks are due also to several laboratory officers for their time, wisdom and assistance for the past few years, including Mr. Wong Chew Yuen, Mr. Tan Lye Heng, Miss Lee Leng Leng, Mr. Shen Ruifu, Mr. Choy Moon Nien, Mdm. Jamilah Bte Mohd, Mr. Foo Hee Ann, Miss. Ang Guek Hoon, Mr. Shaja Khan and Mr. Loo Leong Huat.

I would like to acknowledgement the research scholarship from the National University of Singapore, which allows me to undertake this study.

Finally, this research would not have been possible without the support and encouragement of my family and my friend, Miss Er Inn Inn.

TABLE OF CONTENTS

SUMMARY

Wet deep mixing (DM) is a commonly used in-situ soil improvement approach for improving soft clayey soils. The ability of DM improved soil to achieve designed strength is largely dependent on the mixing process. The strength of the improved soil in DM operations has been found to be often highly variable. This variability has been attributed to the non-uniformity of mixing in the improved soil mass. Partly because of the significant variation in strength of the improved soil and the need to ensure a very safe design, the design field strength of the stabilized soil is generally several times less than the strength obtained in laboratory by mixing the same relative amounts of soil and cement. However, various factors that affect the non-uniformity of wet DM i.e. mixing energy, density difference between soil and slurry, and configuration of mixing blade are not clearly understood. The aims of this study were to assess the feasibility of studying deep mixing processes by centrifuge modelling and to examine various factors that affect the uniformity of mixing. Scaling relationships relevant to modelling of DM were first derived. Results obtained in these analyses formed the basis for the subsequent development of centrifuge model equipment and the test procedures. After the centrifuge model equipment was developed, a series of parametric studies on various factors that affect the mixing quality were conducted under 1-g and 50-g centrifuge environment. From the analyses, it was found that the relationships between most of the significant forces in deep mixing processes could be satisfied using the centrifuge modelling with the exception of the Reynolds number. The Reynolds number cannot be preserved owing to the non-Newtonian viscous nature of cement slurry as well as the soil-cement mix. In particular, proper scaling of the viscosity of

the cement slurry typically used in the prototype DM would require a model viscosity less than that of water, which is difficult to achieve. Scaling of the viscosity of the soil-cement mix was easier to be preserved, by using zinc chloride solution in place of cement slurry. The mechanics of the mixing process is likely to be better modelled using zinc chloride than cement slurry in centrifuge model. The centrifuge results show that quality of mixing can be enhanced by lowering the viscosity of the binder, by increasing the work done in mixing, and by minimizing the density differences between soil and the binder. The consistency between the coefficient of variation of concentration obtained in centrifuge and that for strength obtained from field measurements indicate that the centrifuge modelling approach is promising and merits further study. On the other hand, comparison between 1-g and centrifuge results does not only show that there are significant differences between the two approaches, but it also highlights the important role of viscous forces in influencing mixing quality and the significance of viscosity scaling in achieving proper modelling.

NOMENCLATURE

$\bar{a}$	Sample mean
C	Concentration of tracer ions by total weight [%]
COV	Coefficient of variation
c	Mass of cement solids [kg]
c_o	Mass of the tracer ions per unit volume of slurry [g/cm^3]
cps	Centipoise [Metric (SI) unit= one millipascal-second]
c_{uo}	Undrained shear strength
D	Diameter of model mixing blade [D= 50mm]
d	Diameter of mixing blade [m]
DM	Deep mixing
E_s	Specific energy of mixing [N/m^2]
F_c	Centrifugal force [kg·m/s^2]
F_i	Inertial force [kg·m/s^2]
F_r	Froude number
G	Shear Modulus
g	Gravitational acceleration field [m/s^2, N/kg]
K	Consistency index of non-Newtonian fluid [Pa.s^n]
l	Characteristic dimension of soil debris or fluid body defining the centrifugal forces, F_c and inertial force, F_i [m]
M	Number of mixing blades
M_o	Mobility number
m_b	Masses of binder slurry in model ground [g]

m_s	Masses of soil in model ground [g]
N	Geometric scale factor
n	Flow behaviour index for non-Newtonian fluid
R	Rate of rotation of cutting tool per second [revs/s]
R_c	Radius of the model DM column [mm]
R_p	Rate of rotation of cutting tool per second during penetration [rpm]
R_w	Rate of rotation of cutting tool per second during withdrawal [rpm]
R_e	Reynolds number
R_i	Richardson number
r	Radial distance from the centre of rotation of mixing blade [m]
S	Separation distance between counter-rotating mixing blades [m]
s	Mass of dry soil [kg]
T	Total number of rotations of mixing blade per metre depth
t	Time of mixing [s]
V_s	Volume of the cut soil cavity [m^3]
V_w	Volume of the de-ionize water [l]
v	Characteristic velocity [m/s]
v_b	Volumes of binder slurry [cm^3]
v_p	Mixing tool penetration velocity [m/min]
v_s	Volumes of soil [cm^3]
v_w	Mixing tool penetration velocity [m/min]
W_d	Work done by the cutting and mixing tools [N·m]
W_s	Submerged weight of the soil debris [N]
w	Mass of water [kg]
w_{bp}	predicted mean binder mass [g/cm]

w_b measured mean binder mass [g/cm]

w_s Weight of soil sample [g]

z Depth defining the gravity stress, σ_g [m]

α Slurry insertion ratio

α_f Henkel's pore pressure parameter at failure state

α_i Area ratio account for the effect of axisymmetry of the DM column

$\Delta p_c'$ Excess expanding pressure on the cavity wall

ΔP_f Hydraulic pressure increment

$\Delta \sigma_{oct}$ Mean normal stress change

$\Delta \tau_{oct}$ Mean shear stress change

ρ General term for density [kg/m^3, g/cm^3]

ρ_s Densities of the soil debris defining the submerged weight, W_s [kg/m^3]

ρ_l Densities of the slurry defining the submerged weight, W_s [kg/m^3]

σ Characteristic drag force per unit area defining the work done by cutting and mixing tool, W_d [N/m^2]

σ^2 Sample variance

σ_d Dynamic pressure [N/m^2]

σ_g Gravity stress [N/m^2]

$\dot{\gamma}$ Shear strain rate [radian/s]

τ Viscous shear stress [N/m^2]

μ Dynamic viscosity [N·s/m^2]

ω Angular velocity for centrifugal forces, F_c and inertial force, F_i [radian/s]

LIST OF FIGURES

LIST OF TABLES

Chapter 1: Introduction and Literature Review

1.1 Overview

Deep mixing (DM) is a commonly used in-situ soil improvement approach for improving soft clayey soils (e.g. Porbaha 1998a, Fang et al 2001). In this approach, existing soil is mixed with strengthening agents, usually of cementitious nature, through hollow, rotating shafts with cutting tools, mixing paddles and/or augers mounted at various locations along the shafts (e.g. Bruce et al. 1998, Porbaha 1998a, Porbaha et al. 2001). Fig 1.1 shows an example of DM mixing blade, which is commonly used in Singapore. Fig. 1.2 shows the installation of DM column. In comparison with the untreated soil, the DM-treated soil mass has higher strength, lower compressibility, and lower permeability (e.g. Porbaha et al. 2000, Bruce 2001). The DM method can be classified into dry method and wet method based on the strengthening agent (binder) used (e.g. Porbaha et al. 2001). The former uses the dry powdered binder whereas the latter uses the water-binder slurry. This study focuses on the wet DM method.

According to Topolnicki (2004), the original concept of DM was developed in mid-1950s, when the Mixed in Place (MIP) piling technique was developed by Intrusion-Prepakt Inc. In this method a mechanical mixer was used to mix cementitious grout into the soil for the purpose of creating foundation elements and retaining walls. However, actual research works on DM were initiated in 1967, by the Port and Harbour Research Institute, Japan (PHRI), and the Swedish Geotechnical Institute,

Sweden (e.g. Porbaha 1998a, Bruce et al. 1998, Topolnicki 2004). Since then, extensive amount of research works have been conducted to gain insights into different aspects of DM. Extensive research in DM has also propelled the use of DM method in a wide variety of applications over the years, such as retaining earth pressure, foundations for structures, waterfront and marine applications, seepage control, environmental mitigation and liquefaction mitigation (e.g. Porbaha 1998b, Topolnicki 2004).

1.2 Uniformity of Strength in DM-Treated Ground

In spite of the wide acceptance of DM method, Silvester (1999) noted that deep soil mixing is not yet a technically mature process as much of the design is based on empirical experiences and case histories. Case histories and field data reported by several researchers have shown that the strength of the improved soil in DM operations is often highly variable (e.g. Babasaki et al. 1996, Mori et al. 1997, Porbaha et al. 2000, Porbaha 2002, CDIT Japan 2002). This variation in strength is often measured by coefficient of variation (COV), which represents the ratio of the standard deviation to the mean. Since the mean value is normalized out from the standard deviation, the COV is a useful statistical measure for comparing the degree of variation from one data series to another, even if the mean values are drastically different from one another (e.g. Montgomery and Runger 1999). This is especially useful in DM as the strength of the DM-improved ground varies across different construction sites and projects. Mori et al. (1997) reported that the COV for unconfined compressive (UC) strength of DM-improved soil in a thermal power station reconstruction project was 0.3. Babasaki et al. (1996) reported the COV for UC strength in a DM-improved soil

for open cut excavation was between 0.22 and 0.27. Hosomi et al. (1996) reported that the COV for UC strength of DM-improved soil for a port construction project in Tianjin was 0.33, based on 350 samples. Unami and Shima (1996) reported that the COV for UC strength of low strength type DM-improved soil in a shield tunnel was between 0.41 and 0.57. Thus, not only is the strength variable, but so is the COV, which underlines the large variation in performance characteristics between different DM operations.

Partly because of the significant variation in strength of the improved soil and the need to ensure a very safe design, the design field strength of the stabilized soil is generally several times less than the strength obtained in laboratory by mixing the same relative amounts of soil and cement (e.g. Nishida et al. 1996). This is often needed to ensure that a sufficient percentage of the cores have strength which exceeds the design value. For a given set of curing conditions, the ability of the treated ground to achieve the design strength depends mainly on the uniformity of the mixing. This high strength reduction factor could be attributed to the fact that mixing conditions in the field is often highly non-uniform, thereby leads to non-uniform strength distribution. This indicates that it may be possible to achieve potential savings by improving the uniformity of the field DM process.

1.3 Statistical Analysis on the Uniformity of Binder Distribution

The uniformity of deep soil mixing has still not been widely and systematically studied by researchers. Larsson (2001) noted that it is uncommon to use statistical methods to quantify the mixing quality. More often, subjective methods such as visual inspection

are used to describe the distribution of binder. Larsson (2001) studied the uniformity of binder contents of the field treated ground using dry DM method. Larsson's (2001) approach involved extraction of soil samples from field DM columns using split-tube-sampler. These soil samples were then collected for chemical analysis. The binder content in the soil samples was determined using ion chromatography with inductively coupled plasma. The uniformity of mixing could be determined based on the variation in the binder content. Larsson's (2001) research demonstrated the feasibility of studying the uniformity of binder contents in DM treated ground using statistical analysis. Fig. 1.3 shows the column cross-section with sample sizes and locations. Fig 1.4 shows the area ratio for the various sample locations. The sampling method as shown in Fig. 1.3 causes the central parts of the column's cross-section to be overrepresented, while the outer parts are underrepresented. Therefore, the mean and variance were adjusted using the corresponding area ratio, α to take into account the effect of axisymmetry of the DM column (Larsson 2001). The mean and variance is given by

$$\bar{a} = \frac{\sum_{j=1}^{3}\sum_{i=1}^{n_s}\left(a_{ij}\times\alpha_i\right)}{3\times\sum_{i=1}^{n_s}\alpha_i} \tag{1.1}$$

$$\sigma^2 = \frac{\sum_{j=1}^{3}\sum_{i=1}^{n_s}\left[\left(a_{ij}-\bar{a}\right)^2\times a_i\right]}{3\times\sum_{i=1}^{n_s}\alpha_i - 1} \tag{1.2}$$

Larsson (2001) stated that *"… The samples are numbered from the centre of the column, i = 1 to n_s where n_s = 6 for the small scale, n_s = 4 for the medium scale and n_s = 2 for the large scale. The samples are drawn in three directions from the centre of*

the column, numbered j = 1 to 3. The coefficient α represents the area ratio which the samples represent …".

More recently, Larsson et al. (2005a & 2005b) have measured the COV of the strength of lime-cement column for dry DM by using a hand-operated penetrometer. Although their studies were conducted using dry DM, Larsson et al. tried to extend their findings to wet DM method. However, owning to the different strengthening agents used in dry and wet DM, Larsson et al.'s field results are unlikely to be applicable to wet DM. As Larsson (2001) noted, field study on uniformity of binder distribution was a difficult, time-consuming and expensive process.

1.4 Influencing Factors on the Strength and Uniformity of DM Column

Some research has been conducted on factors influencing the strength and uniformity of DM column (e.g. Mizuno et al 1988, Matsuo et al. 1996, Dong et al. 1996, Yoshizawa et al. 1997, Al-Tabbaa et al. 1998, Al-Tabbaa and Evans 1999). Yoshizawa et al. (1997) reported the results of a survey on the factors influencing the strength and uniformity of DM columns in the field. The factors studied were types of cement, water-cement ratio for slurry, quantity of stabilizer, number of mixing shafts, configuration of mixer blades, rotational speed of the mixing blade, stabilizer injection method, penetration/withdrawal velocity and degree of mixing indicator. They reported that smaller variation in strength can be achieved

(1) by using blast furnace cement in place of ordinary Portland cement,

(2) by reducing the water-cement ratio,

(3) by increasing the quantity of stabilizer,

(4) by using a set of anti-rotation vanes to prevent rotation of the cut ground with the cutter blades and

(5) by increasing the total number of rotations of mixing blade per metre depth, *T*, *rev*/m. In penetration injection method, the number of rotations of mixing blade per metre depth, *T* is calculated from

$$T = \sum M \times \left[\left(\frac{R_p}{v_p}\right) + \left(\frac{R_w}{v_w}\right) \right] \quad (1.3)$$

where $\sum M$ is total number of mixing blades, R_p is the rotational speed of the mixing tool during penetration in rpm, v_p is the mixing tool penetration velocity in m/min, R_w is the rotational speed of mixing tool during retrieval in rpm and v_w is the mixing tool retrieval or withdrawal speed in m/min. On the other hand, in DM operations which involve binder feed only during withdrawal and where the binder outlet is located above the mixing blade, Topolnicki (2004) suggested that *T* can be defined as

$$T = \sum M \times \left(\frac{R_w}{V_w} \right) \quad (1.4)$$

Fig. 1.5 shows the variation of average strength and coefficient of variation of strength of the treated soil at different water cement ratio. Yoshizawa et al. (1997) also noted that the mixing quality deteriorates as the water-cement ratio increases in cases where the in-situ soil consists of highly viscous clay.

On the other hand, reasonably uniform treated soil with small coefficient of variation is achieved by increasing the number of rotations of mixing blade per metre depth above 360*rev*/m (Mizuno et al. 1988, Yoshizawa et al. 1997, CDIT 2002, Usui 2002). Fig. 1.6 shows the relationship between the blade rotation number and strength deviation of in-situ treated soil (Mizuno et al 1988). Based on Fig 1.6, CDIT (2002) noted that "…

The vertical axis of the figure shows the coefficient of variation for in-situ treated soils manufacture by the different blade rotation numbers. This particular field test was conducted to find out the possibility of uniform improvement of the loose sand layer. Among other factors, the influence of blade rotation number is exemplified here. At the blade rotation number of 360, the coefficient of variation ranges between 0.2 and 0.3, which is acceptable strength deviation for most of the practical applications. The figures also indicate the general trend that the deviation decreases with the increase of the "blade rotation number". The similar test data have been accumulated for the improvement of clay soils as well. …".

CDIT (2002) further recommended that a blade rotation number of 360*rev*/m or higher be used in Japan for wet deep mixing. This implied that the mixing effort plays a vital role in affecting the uniformity of the mixing. All these field data suggested that there are several key factors which would affect the uniformity of the mixing. However, the high cost of field test has, to date, precluded systematic and extensive parametric studies of the influence of these factors on the quality of mixing.

Due to the difficulties and high cost of conducting field test, several researchers have studied mixing operations under laboratory 1-g condition (Al-Tabbaa and Evans, 1998 & 1999, Dong et al. 1996, Matsuo et al. 1996). Al-Tabbaa and Evans (1999) conducted laboratory tests on wet soil-mixing using $1/10^{th}$-scale models at 1-g. The primary objective of their study was to establish a correlation between the laboratory models and the trial site. Fig. 1.7 shows the laboratory auger set-up. Fig. 1.8 shows the site trial prototype auger. Some visual assessment of the uniformity of mixing was reported by the authors, together with statistical variation in dry density and undrained

compressive strength. However, as the diameter of their UC samples was nearly as large as that of the model soil-mix columns, the reported statistical variation is unlikely to be a good reflection of the point-to-point variation in strength in a soil-mix column. Moreover, at Al-Tabbaa and Evans' (1998) trial site, the depth of mixing was only about 2.4m, and was meant to investigate the feasibility of using cement as a binder to treat contaminated soil rather than for strength enhancement. At such shallow depths, prototype overburden stress levels are relatively low, so that the effects of incorrect scaling of stress levels in 1-g model tests may not be significant. However, DM is often conducted down to much greater depths of about 20m or even more (e.g. Yoshida 1996, Isobe et al. 1996, Mizutani et al. 1996, Unami and Shima 1996, Matsuo et al. 1996, Kawasaki et al. 1984). At such great depths, discrepancy between 1-g model and prototype stress levels may significantly affect the results.

Various factors that affect the uniformity of 1-g laboratory mixing have been studied by several authors (e.g. Dong et al., 1996, Matsuo et al., 1996). Matsuo et al. (1996) studied the effect of the water-cement ratio and slurry insertion ratio, which is defined as the ratio of volume of slurry over volume of treated soil on uniformity of mixing. Matsuo et al.'s (1996) model mixing machine consists of a twin shaft mixer. Matsuo et al. (1996) noted that as the density of the ordinary Portland cement slurry becomes smaller (by increasing the water cement ratio of the slurry) the coefficient of variation in strength becomes larger. They attributed this to the difficulty in mixing soil and slurry when the density of the slurry is lighter than that of soil. This is consistent with the results of Yoshizawa et al.'s (1997) survey. Dong et al. (1996) studied the effect of tool geometry, mixing time and rotation speed in a series of laboratory tests. Fig. 1.9 shows the mixing blade used in their experiments to study the strength properties of

the cement treated soil. Dong et al. (1996) showed that the strength of the treated ground increases with the increase in the total number of blade revolution as shown in Fig. 1.10. Both studies were conducted in small scaled 1-g laboratory environment. Since DM is often conducted down to much greater depths, discrepancy between model and prototype stress levels may significantly affect the results. For this reason, even though small scale DM tests have been conducted (e.g. Dong et al. 1996, Matsuo et al. 1996), it is unclear that how such small scale test results can be scaled up to the prototype DM values.

In order to preserve prototype stress levels and therefore prototype soil behaviour in a reduced-scale model, centrifuge modelling is essential. Centrifuge modelling has been widely used to replicate the stress-strain behaviour of prototype scale on a reduced-scale model (e.g. Taylor 1995). In this approach, small-scale soil models are tested under conditions of elevated model gravity, simulated by the centrifugal acceleration field of a centrifuge. By doing so, prototype overburden stress levels can be reproduced in reduced-scale models, thereby enabling prototype soil behaviour to be manifested within the models. Thus, model results can be scaled up to large-scale prototype behaviour in a rigorous and self-consistent manner.

1.5 Centrifuge Modelling of Improved Ground

A number of centrifuge model studies have been conducted on the performance of ground improved by DM. (e.g. Miyake et al. 1991, Babasaki and Suzuki 1998, Hashizume et al. 1998, Kitazume et al. 1996, 2000 & 2001, Inagaki et al. 2002, Kimura and Matsuura 2002). Most of the tests were conducted to examine the

deformation and strength characteristic of the DM-treated ground. All those studies involved mixing of binder and soil in 1-g environment. Thus, the deep mixing process is not modelled in those studies. The following section presents few of the key studies published on the modelling of the DM improved ground by using high-g centrifuge.

Miyake et al. (1991) studied the deformation and strength characteristic of the group of cement treated soil column subjected to lateral force by using centrifuge model tests. According to Miyake et al. (1991), the remoulded alluvial marine clay was used in their studies. The model ground was subjected to self-weight consolidated under 80-g centrifugal acceleration until 85% degree of consolidation was achieved. The model was then placed on 1-g lab floor where a series of cylindrical holes were made by using thin wall samplers with a diameter of 20.2mm at the predetermined locations within the model ground. Next, vinyl chloride bars with a diameter of 20.2mm were inserted into the cylindrical holes. This “treated ground” was then subjected to high-g centrifuge consolidation until 85% degree of consolidation was achieved before embankment test and lateral loading test was conducted.

Kitazume et al. (1996, 2000 & 2001) studied the bearing capacity and failure envelope of DM improved ground subjected to caisson loading under centrifuge acceleration. In their centrifuge test, the soil-cement slurry was mixed and poured into acrylic pipes with 20mm diameter and subjected to vibration. The soil-cement mixture was then allowed to cure for 7days before the model DM columns were trimmed to the required length of 20cm. The trimmed DM columns were then kept for another 8days at room temperature under wet condition to ensure UC strength of about 500kN/m^2 was obtained. According to Kitazume et al. (1996), this UC strength almost corresponds to

the average strength in construction of embankment on DM improved ground. Upon completion of the curing stage, the soil-cement columns were placed in the middle of the container, surrounded by one dimensionally pre-consolidated model ground inside the container. Kaolin clay slurry was filled between the DM columns. The final model ground was subjected to high-g environment before subjected to various combinations of vertical and horizontal loads. Fig. 1.11 shows the typical modes of failure observed in centrifuge test. As can be seen, the mixing of binder and soil in 1-g environment allows a DM column with certain value of UC strength to be made. On the other hand, the field UC strength of DM improved ground is dependent on a number of factors as discussed earlier.

Hashizume et al. (1998) studied the behaviour of DM column under low improvement ratio (about 10%). The improvement ratio is defined as the ratio between the total cross sectional area of the columns and the improved area. Centrifuge tests were carried out to investigate the effect of the location and the length of the DM columns on the performance of the treated ground under embankment loading. In their test, the model columns were constructed from the slurry mixture of NSF clay, silica sand No.8, high early strength cement and water. The slurry mixture was then poured into a mold and cured for 28days. Toyoura sand was used to create the embankment loading. The model ground was prepared from clay slurry and pre-consolidated under 1-g load and followed by self-weight consolidation under 56-g for 16hours. Upon completion of self-weight consolidation, the DM columns were installed into model ground on 1-g lab floor. The final model ground was subjected to high-g centrifuge environment before testing was performed. Fig. 1.12 shows the deformation of the DM treated ground subjected to embankment loading.

Inagaki et al. (2002) studied the behaviour of the DM column under road embankment. The model columns were constructed from slurry-cement mixture containing cement of 6.0% in dry weight. The model columns were cured for 7days before insertion into the predrilled holes on the model ground. The model ground was prepared from kaolin slurry. The model ground was allowed to consolidate under 98kN/m^2 of surcharge loading before the model columns were inserted into the predrilled holes.

As can be seen, a number of centrifuge model studies have been conducted on the performance of ground improved by DM. However, no DM installation processes have been simulated in centrifuge models. The mixing quality of DM column is also not studied in reported tests.

1.6 Shortcomings in the Current Studies on Uniformity of Deep Mixing

As discussed earlier, the high cost of field test precluded systematic and extensive parametric studies of the influence of these factors on the uniformity of mixing. While some research has been devoted to study various factors that affect the uniformity of mixing in 1-g laboratory tests, the overburden stress level is not reproduced. It is well established that soil behaviour depends on the effective stress level. Because of this, it is uncertain how those 1-g laboratory results can be applied to prototype scale. To date, the uniformity of mixing is not studied using centrifuge model. Although numerous centrifuge model studies have been conducted on the performance of ground improved by DM, all studies involved mixing of the binder and soil in 1-g environment (e.g. Miyake et al. 1991, Hashizume et al. 1998, Kitazume et al. 1996, 2000 & 2001, Inagaki et al. 2002). This does not allow the mixing process to be accurately modelled.

Moreover, the quality of mixing was not investigated in these studies. To date, DM processes have not been simulated in centrifuge models, therefore it is not known whether centrifuge modelling is a viable approach, since DM is likely to involve, not just solid phase deformation and failure, but also fluid-solid mixing as well as fluid-fluid mixing. This provides the motivation for the current study on centrifuge modelling of DM installation process.

1.7 Objectives of the Study

The purposes of this study were

1. To assess the feasibility of studying DM processes by means of centrifuge modelling through

(a) derivation of scaling relationship which characterizes the installation and mixing behaviours of DM,

(b) examination on the possibility of satisfying all the pivotal dimensionless groups, and

(c) the design, fabrication and use of the DM installer.

2. To examine various factors that affect the uniformity of DM including the configuration of the mixing blade, mixing energy, viscosity of the binder and density difference between the soil and binder. This will be achieved by using statistical analysis based on the coefficient of variation and mean.

Unless otherwise stated, the term “DM” used hereinafter refers to wet DM. This research was only limited to 1-g and high-g laboratory investigation that utilize a

simple twisted mixing blade with constant blade angle to simulate the wet-mixing processes These model tests do not account for the effect arising out of the setting and curing process. These processes in any case, do not correctly scale in centrifuge environment.

1.8 Value of this Study

Up to now, the only means of studying quality of mixing in DM is in the field, which is often difficult and costly. If proven to be viable, centrifuge modelling can potentially offer a much less expensive solution than the field test. The main limitation of the previous 1-g laboratories DM studies is that the results cannot be applied to the field in a consistent manner due to the inaccurate scaling of 1-g tests. In contrast, centrifuge modelling of DM installation offers the advantage of correct scaling of the overburden stress level which is important.

Fig. 1.1 Example of mixing blade which is commonly used in Singapore.

Fig. 1.2 Installation of DM column.

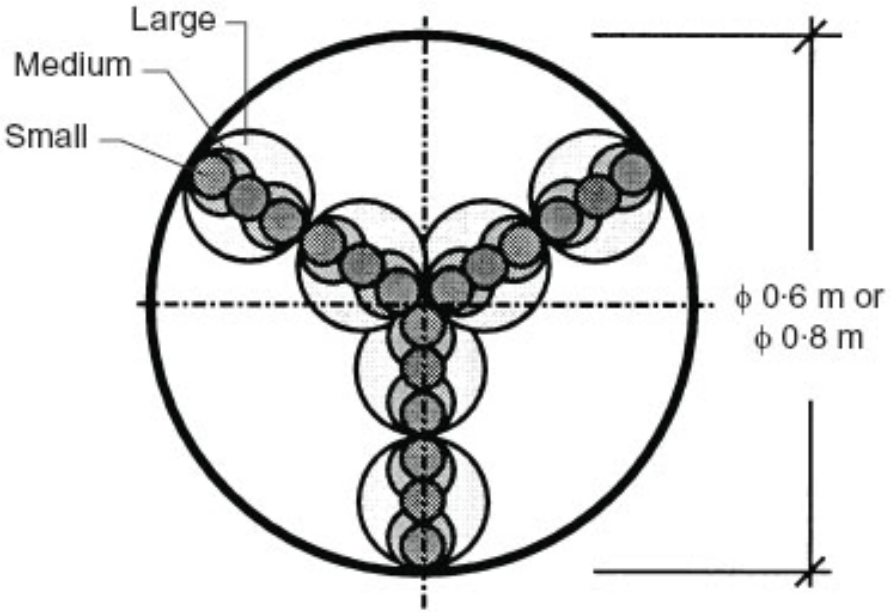

Fig. 1.3 Column cross-section with sample sizes and locations (Larsson 2001).

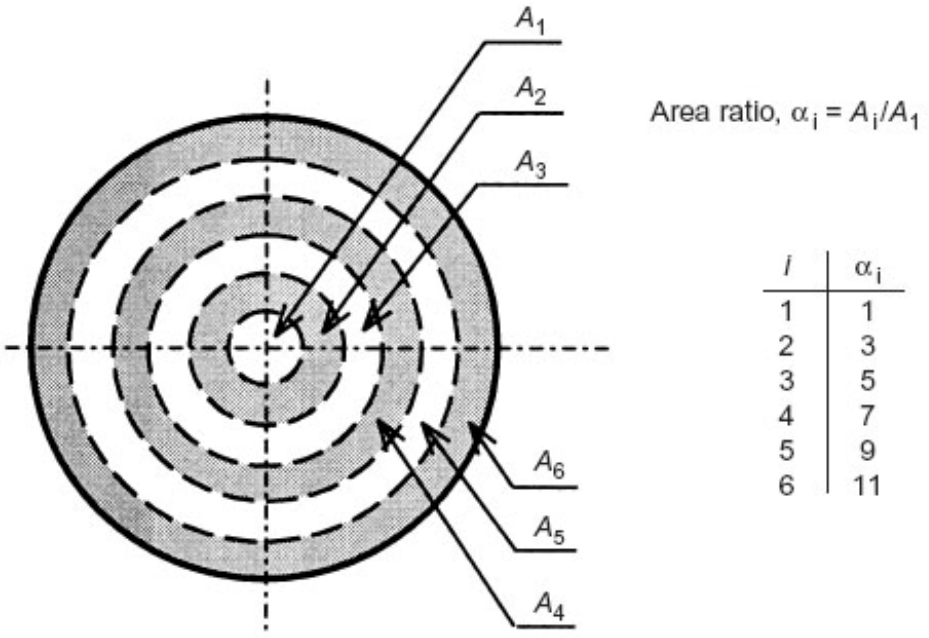

i	α_i
1	1
2	3
3	5
4	7
5	9
6	11

Fig. 1.4 Area ratio for the various sample locations (Larsson 2001).

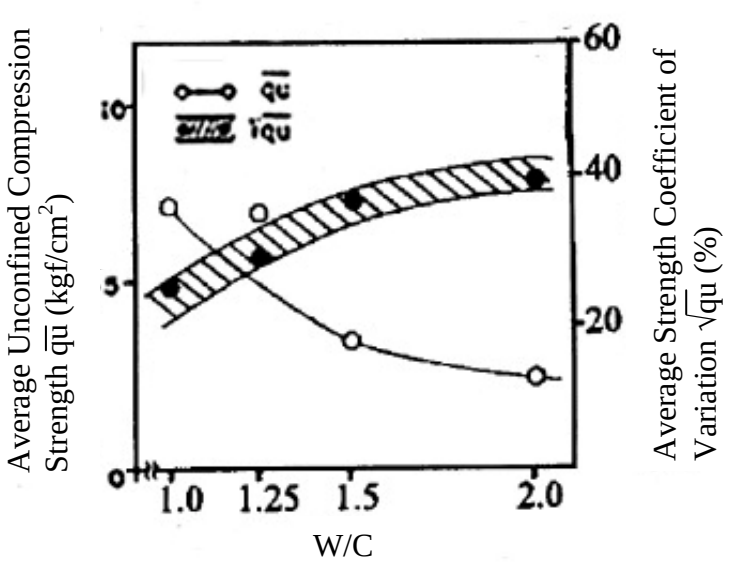

Fig. 1.5 Variation of average unconfined compression strength and coefficient of variation in strength of the treated ground at various water cement ratio (Yoshizawa et al. 1997).

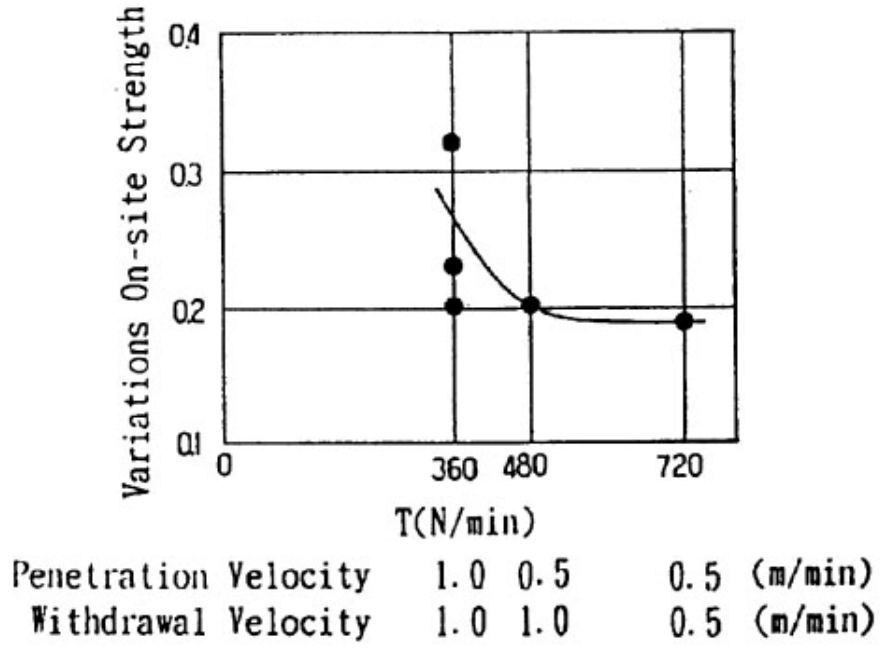

Fig. 1.6 Variation in on-site strength with blade rotation number (CDIT 2002).

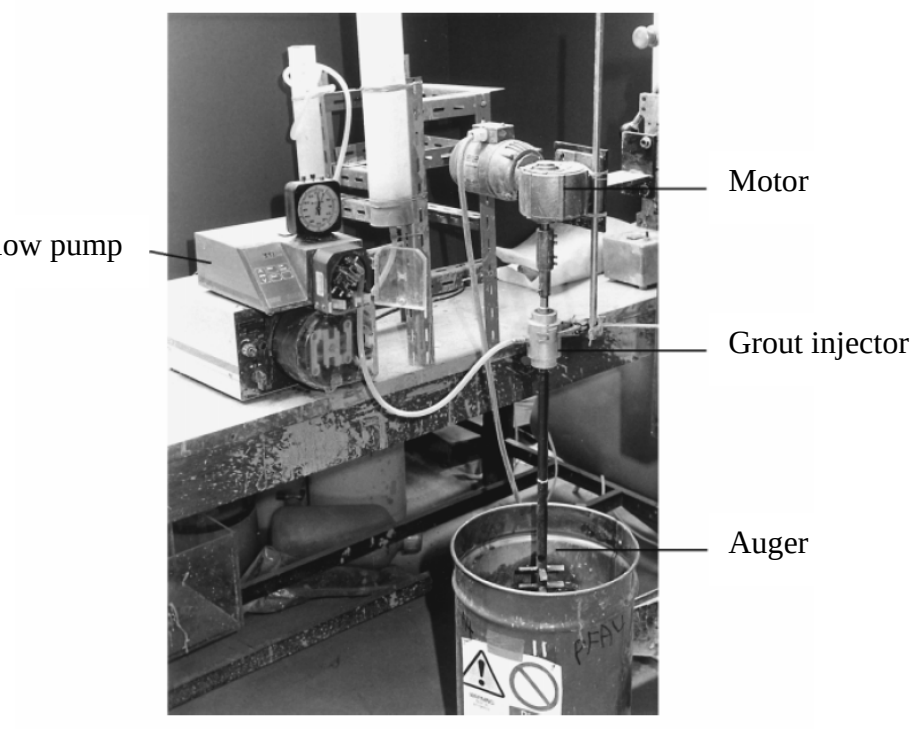

Fig. 1.7 Laboratory auger set-up (Al-Tabbaa and Evans 1999).

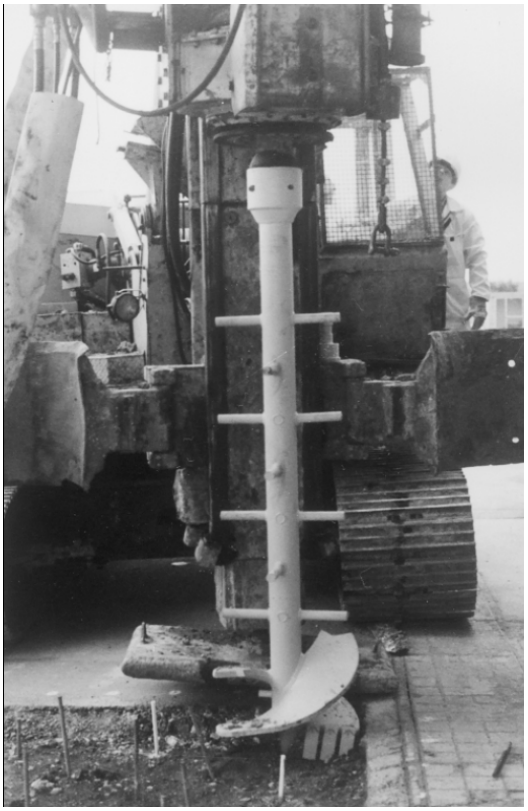

Fig. 1.8 The site trial prototype auger (Al-Tabbaa and Evans 1999).

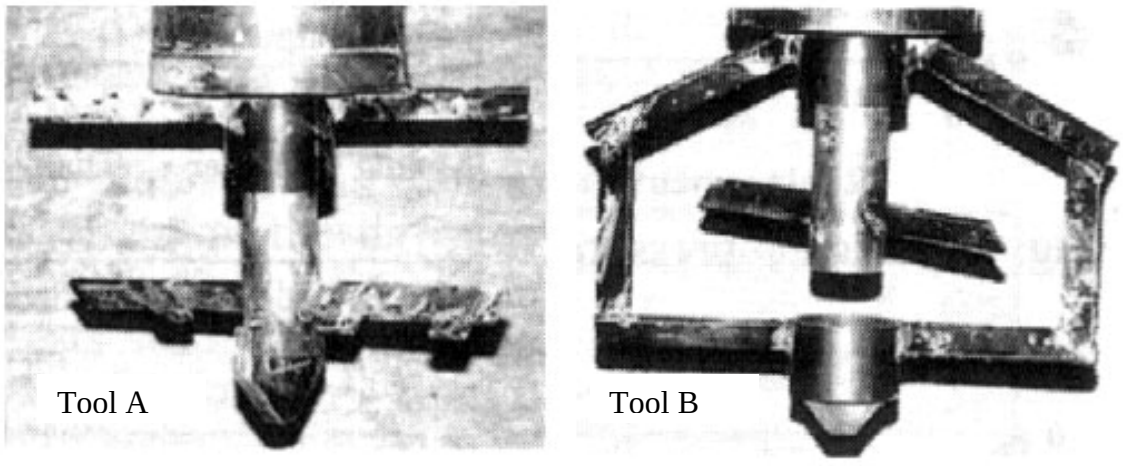

Fig. 1.9 Mixing blade used to study the strength properties of the cement treated soil (Dong et al. 1996).

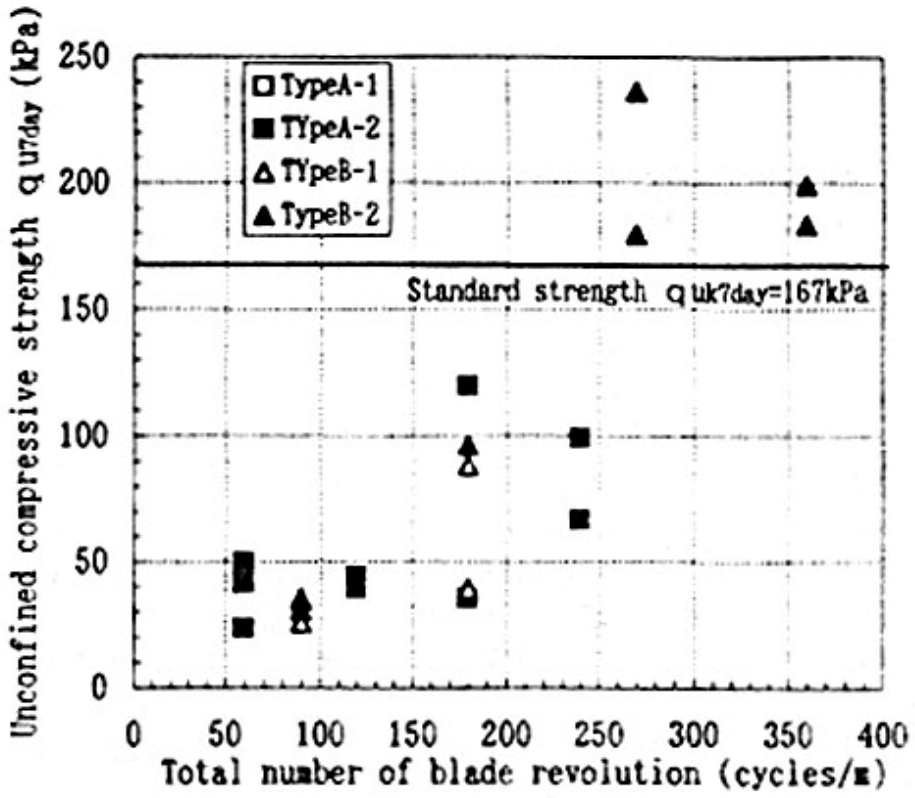

Fig. 1.10 Relationship between total number of blade revolution (Dong et al. 1996).

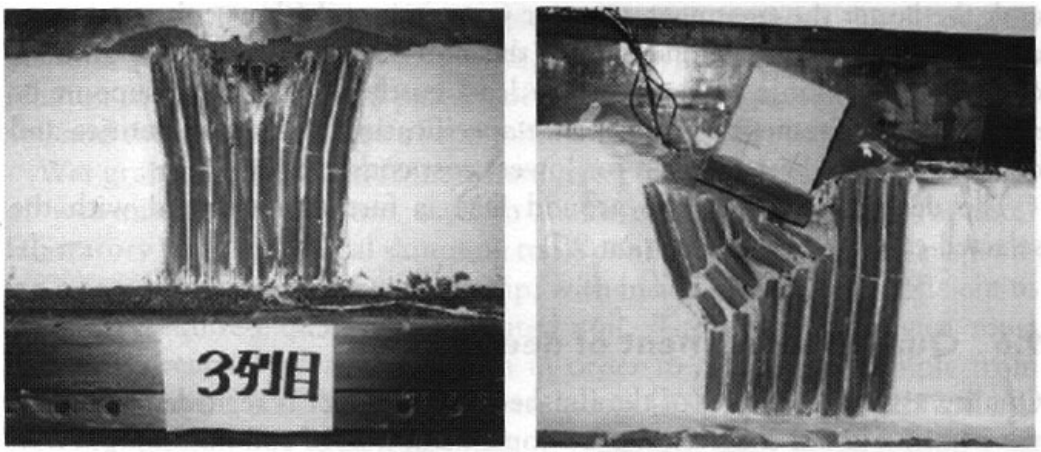

Fig. 1.11 Typical modes of failure observed in centrifuge test (Kitazume et al. 2000).

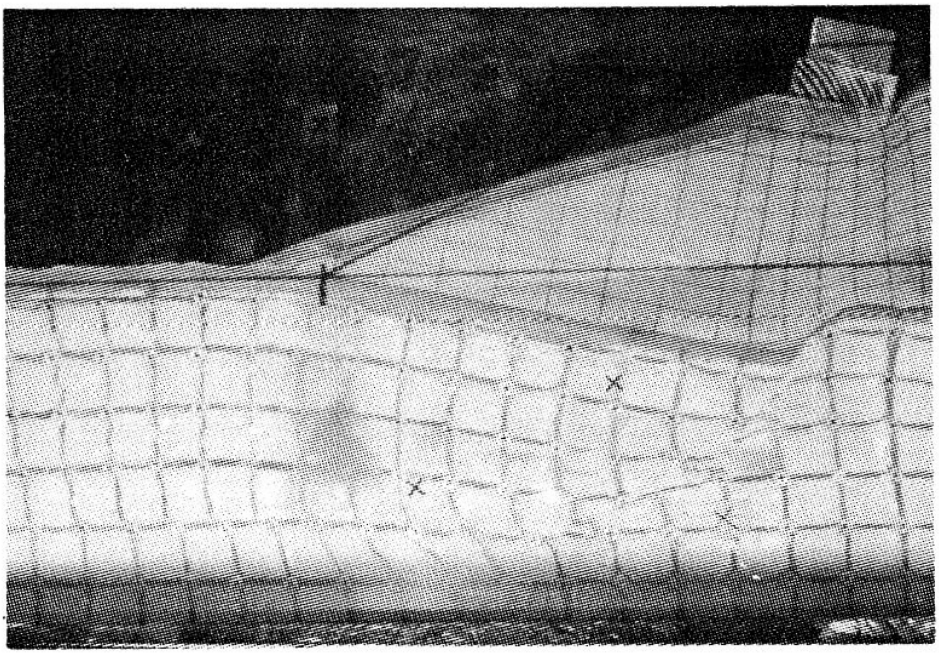

Fig. 1.12 Deformation of the DM treated ground subjected to embankment loading (Hashizume et al. 1998).

Chapter 2: Modelling Considerations and Scaling Laws

In this chapter, scaling relationships relevant to the modelling of wet DM will be presented and the likelihood of satisfying them in centrifuge is examined. The following section will derive the important dimensionless groups that are related to DM. Subsequently, the implication on the modelling of DM will be discussed. Details of these works have been reported in Lee et al. (2004) and Lee et al. (2006).

2.1 Dimensionless Groups

Although little is known about the detailed mechanics of DM, one may surmise that DM operations must invariably involve cutting and remoulding of the in-situ soil mass as well as entrainment and mixing of the cut soil debris with the binder (Lee et al. 2006). The “cutting process” referred here merits some elaboration since it is applied to many different processes. In metal cutting and machining, the material of the work piece is usually assumed to fail in shear (e.g. Zorev 1966). In DM, the cutting process is actually the intrusion of a blunt cutting blade into the soil matrix to break up and remould the latter. This process is similar to that of a drag anchor cutting through a soil mass (e.g. O’Neill and Randolph 2001, O’Neill et al. 2003). The cutting process of a drag anchor fluke is often analysed as a plasticity problem and characterized by the undrained shear strength.

The remoulding of the cut soil is also a problem of shear deformation and failure. Thus, both the cutting and remoulding processes can be addressed by conventional centrifuge scaling laws. The entrainment and mixing of the cut soil debris with the binder involve liquid-solid entrainment and liquid-liquid mixing. Liquid-liquid mixing processes have been extensively studied in chemical and process engineering (e.g. Sterbacek and Tausk 1965, Ulbrecht et al. 1985, Harnby et al. 1992), where it is well-established that the Reynolds number plays a pivotal role (e.g. Sterbacek and Tausk 1965). However, DM is usually implemented in deep cylindrical columns, where gravity forces as well as buoyancy and entrainment effects may assume added significance. The effects of these factors are still not well-understood. The objective of this discussion is to examine the feasibility of scaling these processes in reduced-scale centrifuge models.

2.1.1 Froude and Reynolds Numbers

For a single fluid, the similarity condition can be satisfied by the preservation of the Froude and the Reynolds numbers (e.g. Sterbacek and Tausk 1965, McDonough 1992), which together define the ratios between inertial, gravity and viscous forces. The Froude number is given by

$$F_r = \frac{v^2}{g \cdot d} \tag{2.1}$$

in which, d is a characteristic length, v is a characteristic velocity and g is the gravity acceleration. The gravity stress σ_g at any depth can be as expressed as

$$\sigma_g = \rho \cdot g \cdot z \tag{2.2}$$

in which ρ is the density of the fluid and *z* the depth. Since the depth is proportional to the characteristic length for geometrically similar prototype and model,

$$\sigma_g = C_1 \cdot \rho \cdot g \cdot d \tag{2.3}$$

in which C_1 is a constant of proportionality. Similarly, the inertial stress in a moving fluid can be expressed as the dynamic pressure σ_d such that

$$\sigma_d = \frac{1}{2} \cdot \rho \cdot v^2 \tag{2.4}$$

Thus, the ratio $\frac{\sigma_d}{\sigma_g}$ is given by

$$\frac{\sigma_d}{\sigma_g} = \frac{v^2}{2 \cdot C_1 \cdot g \cdot d} \propto \mathrm{F_r} \tag{2.5}$$

In other words, the Froude number expresses the ratio of inertial force to gravity force in a fluid. In geometrically similar reduced-scale DM models, all dimensions are reduced by *N* times from the corresponding prototype dimension. In addition, if the soil is sufficiently fine-grained so that the particle sizes are much smaller than the dimensions of the model, then particle size effects become insignificant. In such a case, any one of the geometric dimensions, such as the diameter of the cutting tool *d,* may be used. The characteristic velocity may be taken to be the velocity at the outer edge of the cutting tool.

$$v = \pi \cdot d \cdot R \tag{2.6}$$

in which *R* is the rate of rotation of the cutting tool in revolutions per second, and *v* can be taken to be the characteristic velocity. Hence, the ratio of model to prototype Froude number can then be expressed as

$$\frac{F_{rm}}{F_{rp}} = \frac{R_m^2}{R_p^2} \cdot \frac{d_m}{d_p} \cdot \frac{g_p}{g_m} \tag{2.7}$$

in which R is the rate of rotation of the cutting tool in revolutions per second and the subscripts m and p denote model and prototype quantities, respectively.

For a Newtonian fluid, the Reynolds number is given by

$$R_e = \frac{\rho \cdot v \cdot d}{\mu} \tag{2.8}$$

in which ρ and μ are the density and dynamic viscosity respectively. The viscous shear stress at any point in the moving fluid τ can be expressed in the form

$$\tau = \mu \cdot \frac{dv}{dx} = C_2 \cdot \mu \cdot \frac{v}{d} \tag{2.9}$$

In the term $\frac{dv}{dx}$ denotes the velocity gradient at the point in question. Thus, the Reynolds number is a measure of the ratio of the inertial stress (or dynamic pressure) to the viscous shear stress in the moving fluid. The fluids involved in DM methods are non-Newtonian. Hence, the definition of the Reynolds number for Newtonian fluid cannot be used directly. For non-Newtonian fluids, the Reynolds number has been variously expressed in other forms. For instance, for a fluid with viscosity obeying a power-law (Khatib and Richardson 1984), that is

$$\tau = K \cdot \left(\frac{dv}{dx} \right)^n \tag{2.10}$$

In which τ is the viscous shear stress, $\frac{dv}{dx}$ denotes the velocity gradient at the point in question, K and n are constants defined as the consistency index and flow behaviour index (e.g. Sterbacek and Tausk 1965). A log-log plot of shear stress to shear rate need to be constructed to obtain constants K and n. K is the intercept of the flow curve on the stress axis at unit rate of shear, and is a measure of consistency. The higher is the K, the more viscous is the fluids. n, the slope of the line, is a measure of non-

Newtonian behaviour. For $n < 1$, the fluid is yield-pseudoplastic and for $n > 1$, the fluid is yield-dilatant. For n=1, K is the Newtonian viscosity, μ (Bourne 1964).

Govier and Aziz (1972) suggested that the Reynolds number can be expressed in the form

$$R_e = \frac{\rho \cdot d^n \cdot v^{2-n}}{K} \cdot 8 \cdot \left(\frac{n}{2+6n} \right)^n \tag{2.11}$$

Rearranging Eq. 2.11 leads to

$$R_e = \frac{\rho \cdot v^2}{\left(\frac{1}{8 \cdot \left(\frac{n}{2+6n} \right)^n} \right) \cdot K \cdot \left(\frac{v}{d} \right)^n} \tag{2.12}$$

in which d is characteristic length, v is velocity, ρ is the density, K and n is power-law parameters as show in Eq. 2.10. Eq. 2.12 indicates that for non-Newtonian fluids, Reynolds number is also an expression of the ratio of the inertial stress (or dynamic pressure) to the viscous shear stress.

2.1.2 Buoyancy Effects

The Froude and Reynolds numbers alone do not completely express the interaction between forces in DM processes. During the mixing, cut soil debris may be moved around by the cement slurry. The degree to which cut soil debris is mobile may have a significant influence on the uniformity of mixing. The forces affecting the mobility of the cut soil debris are the submerged weight of the soil debris and the inertial force (i.e. the dynamic pressure) of the fluid. The submerged weight W_s of the soil debris can be expressed as

$$W_s = \left(\rho_s - \rho_f\right) \cdot g \cdot l^3 \tag{2.13}$$

in which ρ_s and ρ_f are the densities of the soil debris and the slurry, respectively, and l is a characteristic dimension of the soil debris. The dynamic pressure F_i can be expressed in the form

$$F_i = ½ \cdot \rho_f \cdot v^2 \cdot l^2 \tag{2.14}$$

(e.g. Olson 1966). Dividing Eq. 2.14 by Eq. 2.13, substituting Eq. 2.6 and ignoring the constant π leads to a dimensionless force ratio M_o, such that

$$M_o = \frac{\left(R \cdot d\right)^2}{\left(Cs - 1\right) \cdot g \cdot l} \tag{2.15}$$

in which $Cs = \frac{\rho_s}{\rho_f}$ (2.16)

This dimensionless group is similar in form to the Shields parameter as well as the mobility number used in the sedimentation studies (e.g. Hanes 2001). The M_o will be termed herein as the mobility number, since it defines the mobility of the soil debris in the mixing process. Since the dimensions of DM column and cutting tool are scaled down by the same factor from prototype to model, it can be surmised that the characteristic dimension of soil debris will be reduced by approximately the same factor as that of the model. Based on this assumption, the ratio of the model mobility number to the prototype mobility number can then be expressed as

$$\frac{M_{om}}{M_{op}} = \frac{R_m^2}{R_p^2} \cdot \frac{d_m}{d_p} \cdot \frac{\left(Cs - 1\right)_p}{\left(Cs - 1\right)_m} \cdot \frac{g_p}{g_m} \tag{2.17}$$

The counterpart of the mobility number, which controls the mixing of two fluids with different densities (Rielly & Pandit 1988) is the Richardson number which is defined as

$$R_i = \frac{\Delta\rho \cdot g \cdot d}{\rho_L \cdot v^2} \qquad (2.18)$$

in which $\Delta\rho$ is the density difference between the two fluids and ρ_L is the density for lighter fluid. Eqs. 2.15 and 2.18 are similar in form.

2.1.3 Centrifugal Effects

Centrifugal forces also arise from the motion of the soil debris and fluid in the DM column. For a piece of soil debris or fluid body of characteristic dimension *l*, the centrifugal force F_c may be expressed in the form

$$F_c = \rho_s \cdot l^3 \cdot \varpi^2 \cdot d \qquad (2.19)$$

in which ρ_s is the density of the soil debris under consideration and ω is the angular velocity of the flow. The inertial force F_i is given by

$$F_i = ½ \cdot \rho_s \cdot \varpi^2 \cdot r \cdot l^3 \qquad (2.20)$$

in which *r* is the radial distance from the centre of rotation. Dividing Eq. 2.19 by Eq. 2.20 and ignoring the constant ½ leads to

$$\frac{F_c}{F_i} = \frac{d}{r} \qquad (2.21)$$

which will be preserved in a geometrically similar model. The centrifugal force can also be normalized by the viscous force; this is equivalent to multiplying Eq. 2.8 by Eq. 2.21 and will result in a number which is akin to the Dean number used for flow in curved channels (e.g. Gelfgat et al. 2001).

2.1.4 Effects of Work Done in Mixing

Apart from forces, the work done in mixing has also been shown to influence the degree of mixing. Niranjan et al. (1994) reported that the work done in mixing per unit volume of the DM column significantly influences quality of mixing. Dong et al. (1996) used the number of turns of the mixing tool per metre depth as a measure, while Yoshizawa et al. (1997) and Usui (2002) used the sum total of the number of turns of the mixing blades per metre of the DM column, which took into account the number of mixing blades on the shaft. The work done by the cutting and mixing tools W_d may be expressed in the form

$$W_d = C_3 \cdot \sigma \cdot d^3 \cdot R \cdot t \tag{2.22}$$

in which σ is a characteristic drag force per unit area on the mixing tool and t the time of mixing and C_3 a constant. The volume of the cut soil cavity V_s is given by

$$V_s = C_4 \cdot d^3 \tag{2.23}$$

in which C_4 is a constant for a cut soil cavity of given aspect ratio. Dividing Eq. 2.22 by Eq. 2.23 yields the specific energy of mixing E_s

$$E_s = \left(\frac{C_3}{C_4} \right) \cdot \sigma \cdot R \cdot t \tag{2.24}$$

The drag force on the mixing tools is the sum of the form and viscous drag components, both of which can be related to the inertial force, so that

$$\frac{\sigma}{\rho \cdot (R \cdot d)^2} = C_5 \tag{2.25}$$

in which C_5 is a constant. Substituting Eq. 2.25 into Eq. 2.24 leads to

$$E_s = \left(\frac{C_3 \cdot C_5}{C_4} \right) \cdot \rho \cdot R^3 \cdot d^2 \cdot t \tag{2.26}$$

2.2 Implications for Centrifuge Modelling

For a geometrically scaled model to yield results which are scalable to prototype values in a self-consistent manner, the above dimensionless groups need to be preserved in the model. The following section discussed centrifuge scaling of DM.

2.2.1 Froude Number

Eq. 2.7 shows that the Froude number can be preserved if

$$\frac{g_p}{g_m} = \frac{1}{N} \tag{2.27}$$

$$\frac{R_m}{R_p} = N \tag{2.28}$$

in which N is the geometric scale factor. Thus, the scale factor for the rate of rotation of the mixing tool is the same as that for the scale factor of inertial force of dynamic events in the centrifuge. This is not surprising since the Froude number expresses a similar requirement as that for the scaling of inertial force.

2.2.2 Reynolds Number

In the wet mixing method, cement slurry is often used as the stabilising agent, so that the fluid inside the DM cavity consists essentially of cement slurry with varying amounts of soil mixed into it. As shown in Table 2.1, the typical water-cement ratio used in the cement grout ranges from 0.8 to 1.2. Fig. 2.1 shows the viscometer used for viscosity measurement. Fig. 2.2 shows the shear stress of cement slurry at various water-cement ratios, measured over a wide range of shear strain rate, the latter being

defined as the velocity gradient between two layers of fluid (e.g. Dinsdale and Moore 1962, Harris 1977, Ferguson and Kemblowski 1991). The estimation on the range of shear strain rate will be discussed later. As can be seen, the shear stress does not increase linearly with shear strain rate, which indicates that cement slurry is a non-Newtonian fluid, the Reynolds number cannot be explicitly evaluated.

There is, however, another way to assess Reynolds scaling. Eq. 2.8 can also be expressed in the form

$$R_e = \frac{\rho \cdot v^2}{\left(\mu \cdot v / d\right)} \tag{2.29}$$

in which μ is the dynamic viscosity. The numerator in Eq. 2.29 represents the dynamic pressure, which arises from inertial forces. The denominator represents the stresses arising from viscous shear in the fluid. In such situations, recourse can be made to the concept of the Reynolds number being the ratio of inertial to viscous forces in the fluid, which has been discussed earlier. This leads to

$$R_e = \frac{\rho \cdot v^2}{\tau} \tag{2.30}$$

in which $\tau = \frac{\mu \cdot v}{d}$ represents the viscous shear stress in the fluid. Similarly, as mentioned earlier, the Froude number in Eq. 2.1 can be written as

$$F_r = \frac{\rho \cdot v^2}{\rho \cdot g \cdot d} \tag{2.31}$$

In centrifuge modelling, prototype gravity stresses are preserved in the model, that is, $\rho \cdot g \cdot d$ is the same for the model and prototype. If the Froude number is also preserved, then the term $\rho \cdot v^2$ must be the same in model and prototype. Thus preservation of the Reynolds number dictates that the viscous shear stress τ should be

the same in the model and the prototype. The following paragraphs describe how this could be achieved.

Examination of the some of the mixing blades configuration (e.g. Kawasaki et al. 1984, Nishibayashi et al. 1988, Yoshizawa et al. 1997) show that the separation distance S between mixing blades typically ranges from 0.5r to 2r where r is the radius of the mixing blade. The rate of rotation of cutting tool R ranges from about 0.33revs/s to 1revs/s. If we consider a commonly used configuration in which successive layers of mixing blades rotate in opposite directions, then the average shear strain rate $\dot{\gamma}$ between successive mixing blades can be defined by

$$\dot{\gamma} = \frac{8 \cdot \pi \cdot R \cdot r}{3 \cdot S} \tag{2.32}$$

As above examples show, the average shear strain rate in prototype DM operations may range from about 1radian/s to about 30radian/s.

Fig. 2.3 shows the variation of shear stress as the shear strain rate increases from 0 to 50 radian/s, which is the low strain rate end of curves shown in Fig. 2.2. As can be seen, as the strain rate increase from 0 to about 2radian/s, the shear stress increases rapidly. Thereafter, it moderates significantly. If only strain rates of between 2radian/s and 30radian/s are considered, the shear-stress-strain-rate curve can be reasonably fitted by the Bingham relationship, as Gallagher (2000) has noted.

In a centrifuge model, the velocity is preserved while the dimensions are reduced by N times. Thus,

$$\dot{\gamma}_m = N \cdot \dot{\gamma}_p \tag{2.33}$$

With a scale factor N of 50, the average shear strain rate in the model is about 1500radian/s, with typical field rotation of 30radian/s.

Fig. 2.4 shows the ratios of viscous shear stress in the model to that in the prototype at various water-cement ratios, inferred from the viscous measurements, for N of 50. Those shear stress ratios were calculated from the viscous shear stress of cement slurry at different water-cement ratio and the corresponding model and prototype strain rate. The lower solid curve represents the ratio at a prototype strain rate of 2radian/s and a corresponding model strain rate of 100radian/s. The higher solid curve represents the ratio at a prototype strain rate of 18radian/s and a corresponding model strain rate of 900radian/s. The shear stress ratio for prototype strain rate of 30radian/s could not be determined since the corresponding model strain rate of 1500radian/s is beyond the range of the viscometer used for this study. Since correct scaling requires the shear stress ratio to be 1, the shear stress ratio represents the deviation from correct scaling of viscous shear stresses; with a higher ratio implying a larger deviation. As can be seen, the use of cement slurry will result in significant overscaling, which is particularly severe at high water-cement ratio and high strain rates. At low water-cement ratio and low strain rates, the overscaling is mitigated by the presence of the Bingham yield stress, which contributes substantially to the shear stress. As such, Reynolds number is difficult to preserve since both the cement and soil slurries are non-Newtonian fluids. In particular, proper scaling of the viscosity of the cement slurry typically used in prototype DM require that the viscosity of the model binder to be less than that of water, while maintaining the same density, which is difficult to achieve.

One way of mitigating this problem is to use a liquid tracer with the same density but a lower viscosity, so that overscaling of the viscous shear stresses can be mitigated. An example of such a liquid tracer is zinc chloride solution, the density of which can be adjusted to be approximately equal to that of cement slurry. As shown in Fig. 2.5, the viscosity of zinc chloride increases with its density. Fig. 2.4 also shows the effect of using zinc chloride of the same density as that of cement slurry with the specified water-cement ratio. As can be seen, the overscaling in model viscous shear stress can be reduced using lower viscosity zinc chloride as model binder, albeit not completely eliminated.

It is clear that zinc chloride is chemically very different from cement slurry. For instance, the former has a pH of between 3 and 4 whereas the latter has a pH of about 12. It is therefore worthwhile to consider the possible effects that these chemical differences may have on the validity of the modelling. Mixing can occur via several mechanisms such as convective processes, molecular diffusion and shearing mixing (e.g. Rielly et al. 1994). However, it is widely recognised that the most efficient mixing mechanism is convective mixing, which is the physical process that the mixers and mixing blades such as those used in DM, seeks to promote (e.g. Sterbacek and Tausk 1965, Ulbrecht et al. 1985, Harnby et al. 1992). Molecular processes are almost invariably far slower than convective processes (e.g. Rielly et al. 1994). For this reason, in mechanically assisted mixing processes, molecular diffusion is almost invariably not a considered mechanism. It is for this reason that mixing efficiency can often be characterised by the Froude and Reynolds numbers (e.g. Sterbacek and Tausk 1965, Ulbrecht et al. 1985, Harnby et al. 1992). Given this background, it seems unlikely that any differences in molecular diffusion properties between zinc chloride

and cement slurry will significantly influence the results of the mixing process. There is, however, another possible effect; the chemical interaction between the cement slurry and soil may result in a mixture which has a different flow constitutive behaviour from that resulting from zinc chloride and soil. In the mixing of incompressible fluids, the important constitutive parameter is the relation between shear stress and velocity gradient; in a Newtonian fluid, it is expressed by the viscosity. This is evident from the foregoing discussion above, wherein the only material parameters which appear in the entire dimensionless group are the density and viscosity of the fluids. Thus, it is important to determine how the shear-stress-velocity-gradient characteristics of the mixture of cement-slurry-soil (hereafter termed "soil-cement mix") and zinc-chloride-soil mixtures will impact the modelling. This measured constitutive behaviour of the mixtures would take into account any chemical interaction that might present slurry-mixture. Fig. 2.6 shows the variation of shear stress with shear strain rate for kaolin-cement slurry at cement and water contents which are representative of those used in DM. The water content is defined herein as the ratio of the mass of water, w to the mass of dry soil and cement solids while the cement content is defined as the ratio of the mass of cement to the mass of dry soil, s and cement solids, c. As can be seen, the shear stress does not increase linearly with shear strain rate and there is also a discernible Bingham stress especially at low water contents. The magnitudes of the Bingham stress for the corresponding water content and cement content are shown in Table 2.2.

Fig. 2.7 shows the variation in shear stress with shear strain rate for kaolin-zinc chloride mixture for different slurry density and volumetric slurry-soil ratios. These parameters are selected so as to simulate a combination of water and cement contents

which are representative of DM parameters, based on an in-situ water content of 61%. This water content represented the average water content of the model clay bed for the model tests. The magnitudes of the Bingham stress for the kaolin-zinc chloride mixture (Table 2.3) are significantly lower than kaolin-cement slurry (Table 2.2) for the corresponding water content and cement content. Fig. 2.8 shows model-prototype viscous shear stress ratios at two prototype strain rates of 2radian/s and 18radian/s, for kaolin-cement slurry mixture and kaolin-zinc chloride mixture at different cement and water contents, at N=50. These ratios were inferred from the viscous shear stress in Fig. 2.6 and Fig. 2.7. Once again, prototype viscous shear stress level is much better preserved with zinc chloride as a model binder instead of cement slurry. Hence, the mechanics of the mixing process is likely to be better modelled using zinc chloride than cement slurry. It should, however, be noted that these considerations do not apply to the setting and curing processes, which, in any case, involve chemical reactions that are not well-scaled in centrifuge models.

2.2.3 Mobility and Richardson Numbers

Eqs. 2.17 and 2.18 show that if the rate of rotation of the mixing tool is increased by N times in the model and if the densities of the various solid and liquid phases are preserved, then the mobility and Richardson numbers are automatically preserved in the model.

2.2.4 Work Done in Mixing

Consideration of Eq. 2.26 shows that, in order to preserve the specific work done in mixing,

$$\rho_m \cdot (R_m)^3 \cdot {d_m}^2 \cdot t_m = \rho_p \cdot (R_p)^3 \cdot {d_p}^2 \cdot t_p \qquad (2.34)$$

There are actually several different possible fluid phases, but if the components' densities are preserved, then $\rho_p = \rho_m$ for all phases. This leads to

$$\frac{t_m}{t_p} = \frac{1}{N} \qquad (2.35)$$

Eq. 2.35 is same as the result which can be obtained by preserving the dimensionless mixing time or simultaneity number (Sterbacek and Tausk 1965).

Table 2.1 Operating parameters in some reported deep cement mixing projects.

Author Year	Site	Diameter of Mixing Blade [m]	Reported Depth of Improvement [m]	Blade Revolution [rpm]	Penetration Rate [m/min]	Withdrawal Rate [m/min]	W/C Ratio	Type of Cement	Coefficient of Variation
Yoshida 1996	NA	1.0	-22	22 or 45	0.5	1.0	1	Retardation type cement	NA
Isobe et al. 1996	Osaka-Kunishima, Japan	1.5	-6 ~ -18	20 or 40	0.5	1.0	0.8	Cement	NA
Mizutani et al. 1996	Sakai-machi, Ibaraki, Japan	1.0	Approximately -6 (Field trial)	30	0.5	1.0	1.0 and 1.2	Cement	0.363-0.383
Unami and Shima 1996	Ukishima, Japan	1.0	Approximately -30	40 (Penetration) 50 (Withdrawal)	0.3-1.0	1.0	1.0	Cement slurry & additive agent	0.41-0.57
Matsuo et al. 1996	NA	NA	-16.5	25 (Penetration) 50 (Withdrawal)	0.5	1.0	1.0	Cement	NA
Kawasaki et al. 1984	Tokyo (Test construction)	NA	T.P. -9.0 ~ -39.0	35 (Penetration) 50-55 (Withdrawal)	2.0	1.5	-	Ordinary Portland cement	0.331
	Saga A	NA	G.L. -1.0 ~ -8.0	25 (Penetration) 50-60 (Withdrawal)	1.0	1.0	-	Portland blast-furnace slag cement	0.485
	Hiroshima	NA	D.L. -9.0 ~ -22.0	20-30 (Penetration) 40-60 (Withdrawal)	1.0	1.0	-	Ordinary Portland cement	0.353
	Osaka	NA	D.L. -12.0 ~ -17.0	20-30 (Penetration) 20-60 (Withdrawal)	1.0	0.5	-	Portland blast-furnace slag cement	0.277
		NA	D.L. -17.0 ~ -29.0	20-30 (Penetration) 20-40 (Withdrawal)	1.0	0.5	-	Portland blast-furnace slag cement	0.381
	Saga B (Test construction)	NA	D.L. -4.0 ~ -19.0	20-30 (Penetration) 40-60 (Withdrawal)	1.0	1.0	-	Portland blast-furnace slag cement	0.296
	Saga B	NA	D.L. -4.0 ~ ~21.0	20-30 (Penetration) 40-60 (Withdrawal)	1.0	1.0	-	Portland blast-furnace slag cement	0.299
	Chiba (Test construction)	NA	A.P. -11.0 ~ -31.0	20-30 (Penetration) 40-50 (Withdrawal)	2.0	1.0	-	Ordinary Portland cement	0.292
	Chiba	NA	A.P. -9.0 ~ -22.0	20-30 (Penetration) 40-50 (Withdrawal)	2.0	1.0	-	Ordinary Portland cement	0.207

NA - Not available

Table 2.2 Bingham yield stress for kaolin-cement slurry at various water and cement contents.

Water contents, w/(s+c)	**Cement contents, s/(s+c)**	**Bingham yield stress [Pa]**
0.9	0.2	58
0.8	0.1	875
0.8	0.2	184
0.8	0.3	80
0.7	0.2	220

Table 2.3 Bingham yield stress for kaolin-zinc chloride slurry at various modelled water and cement contents.

Water contents, w/(s+c)	**Cement contents, s/(s+c)**	**Bingham yield stress [Pa]**	**Zinc chloride density [g/cm^3]**	**Volumetric slurry-soil ratios**
0.9	0.2	18	1.29	0.60
0.8	0.1	60	1.24	0.32
0.8	0.2	20	1.36	0.48
0.8	0.3	10	1.43	0.68
0.7	0.2	30	1.49	0.35

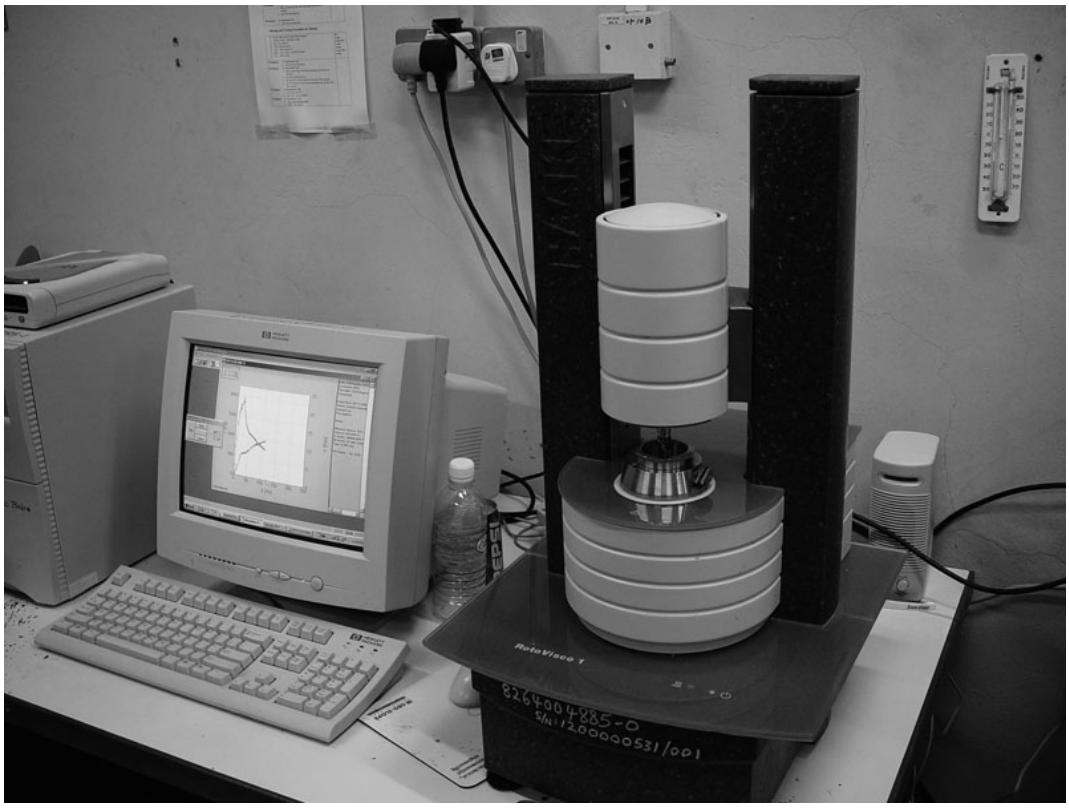

Fig. 2.1 Viscometer used for viscosity measurement.

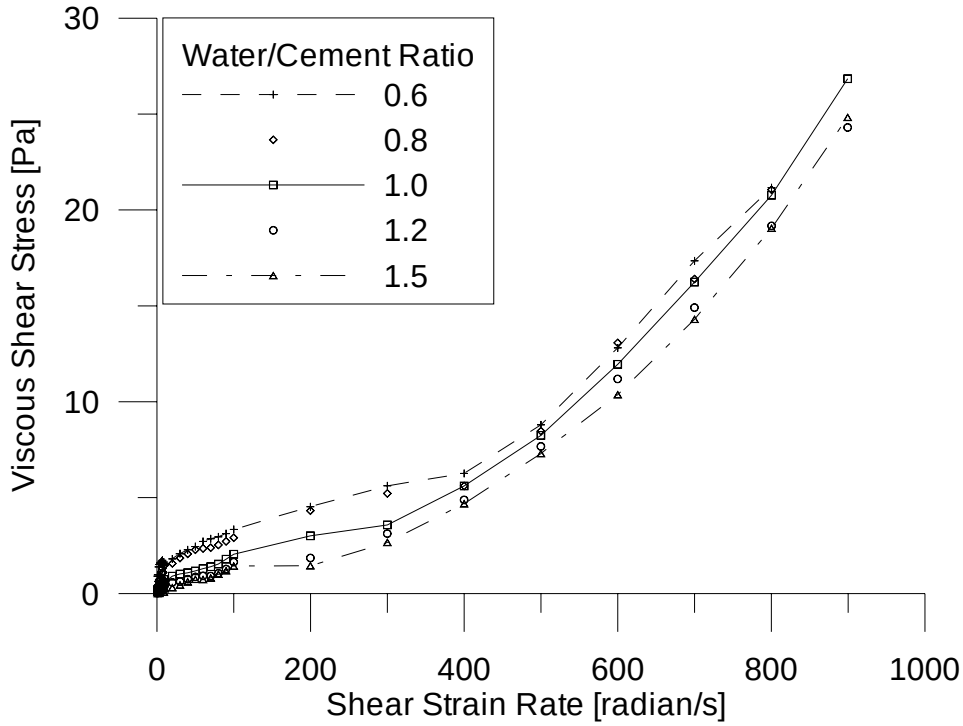

Fig. 2.2 Viscous shear stress against shear strain rate of cement slurry at various water-cement ratios.

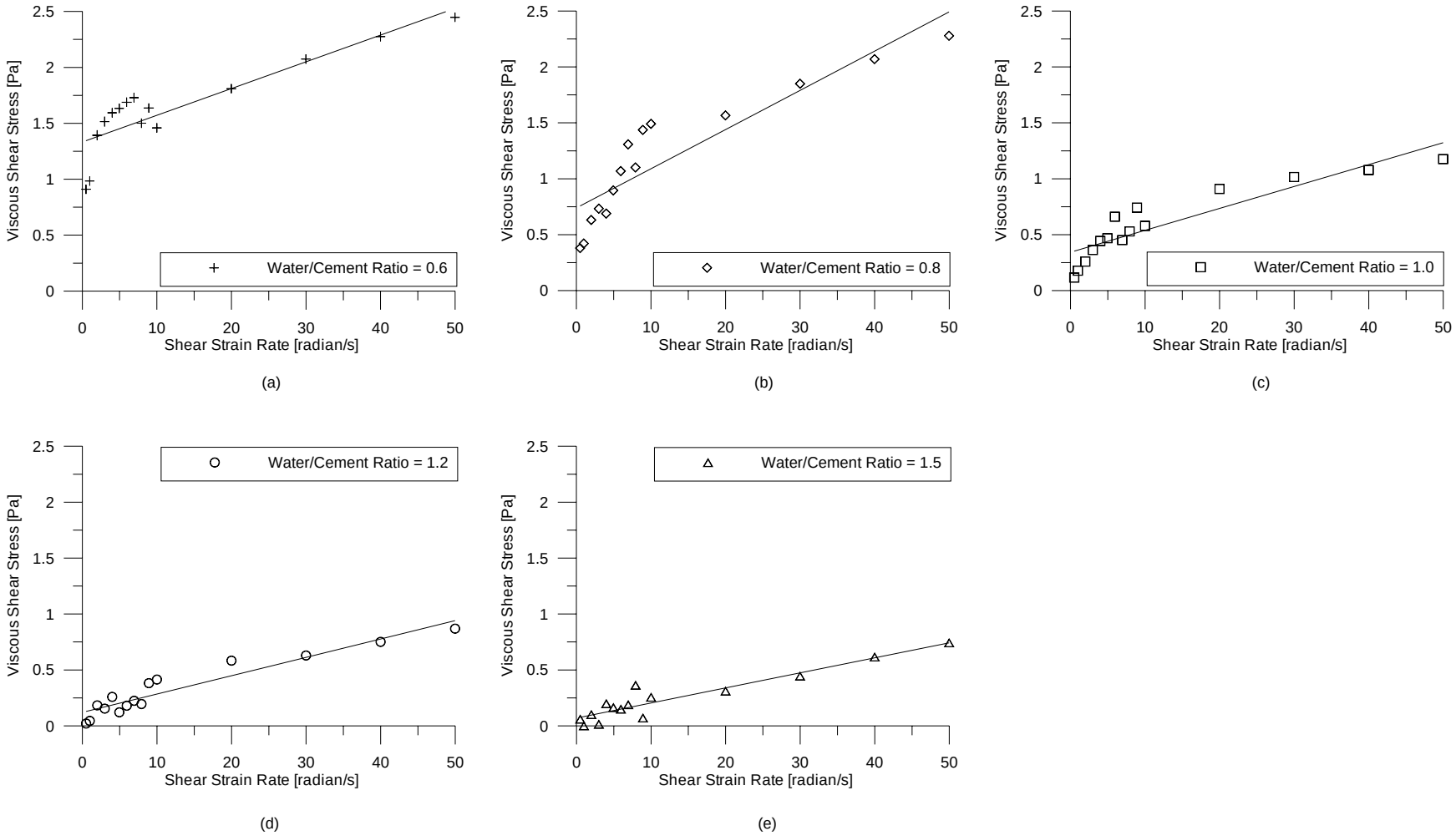

Fig. 2.3 Variation of viscous shear stress at low shear strain rate of cement slurry at various water-cement ratios.

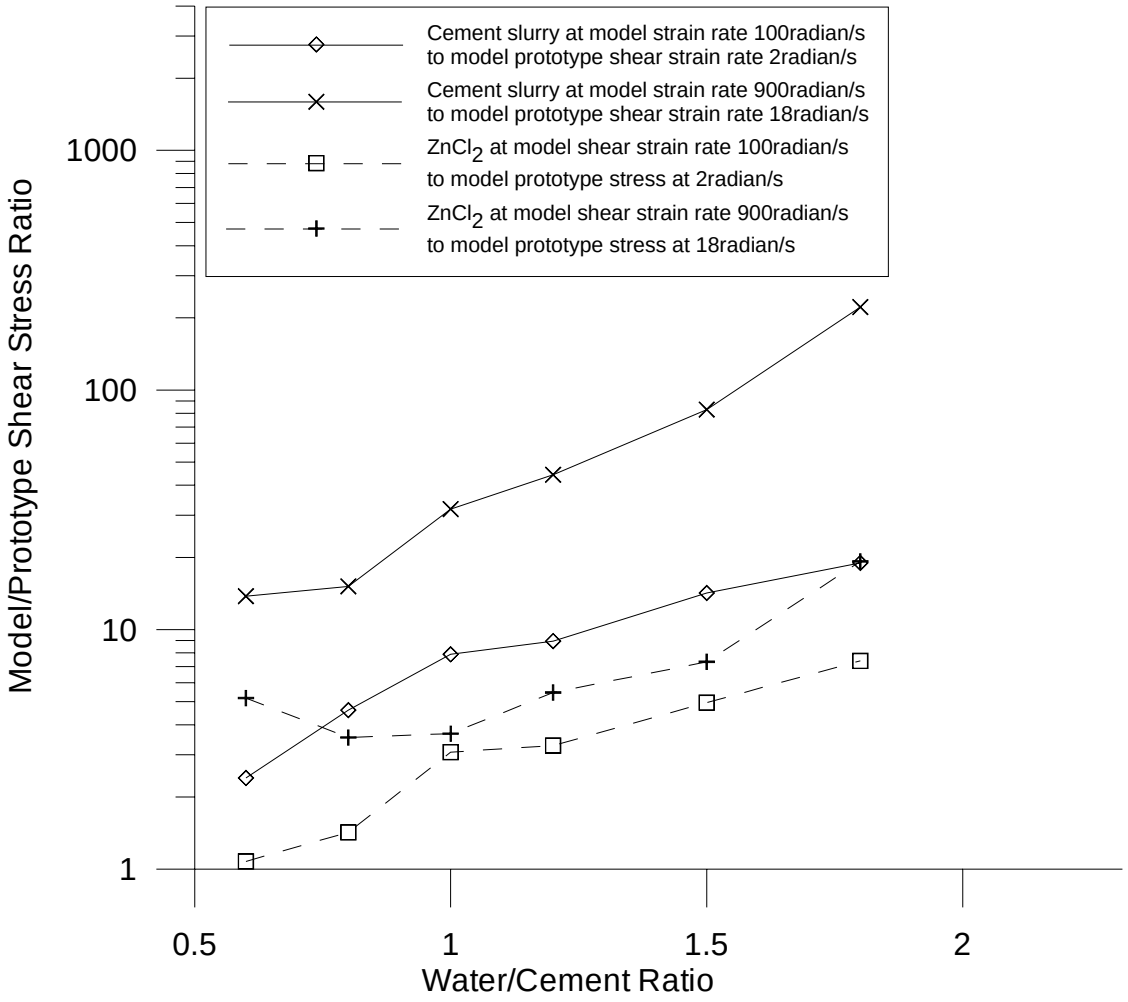

Fig. 2.4 Model-to-prototype viscous shear stress ratios for cement slurry at various water-cement ratios and zinc chloride solution at same density.

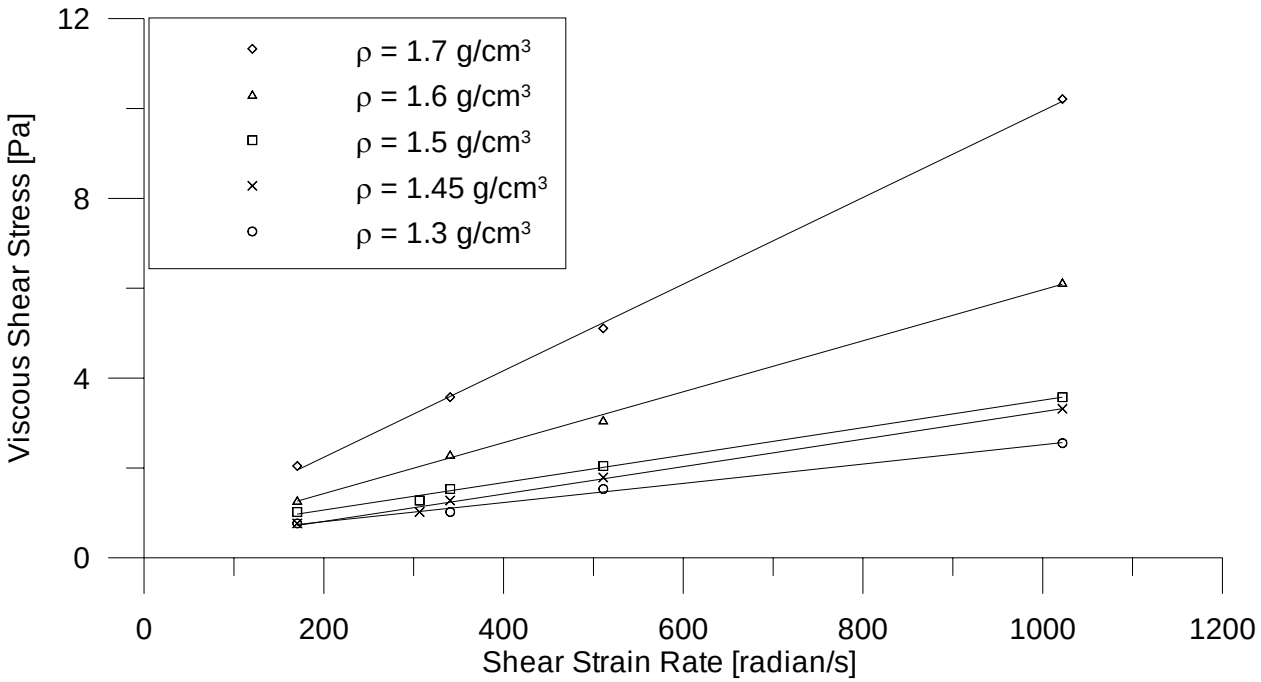

Fig. 2.5 Viscous shear stress against shear strain rate for zinc chloride at various densities.

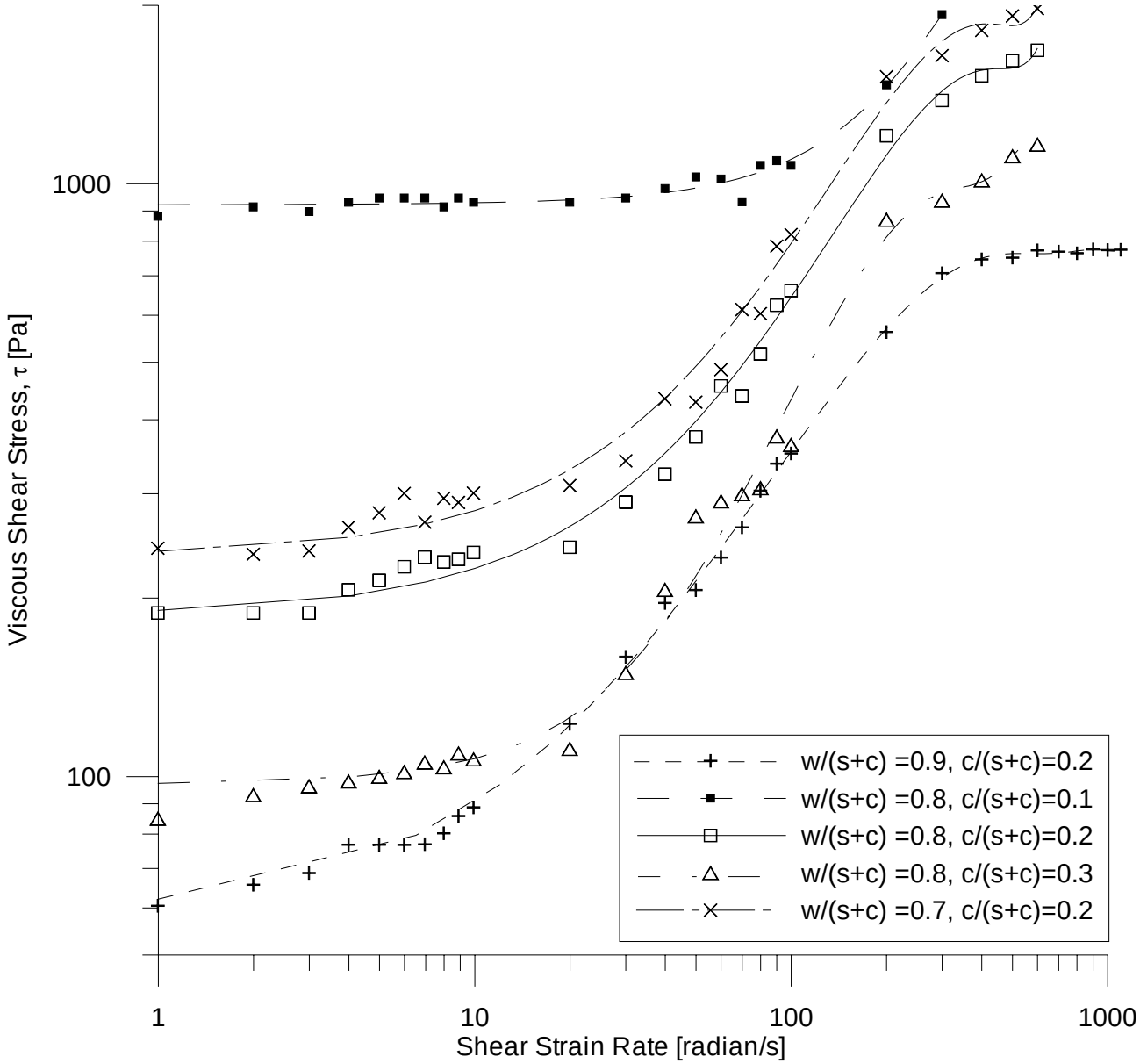

Fig. 2.6 Viscous shear stress against shear strain rate for kaolin-cement slurry at various water and cement contents.

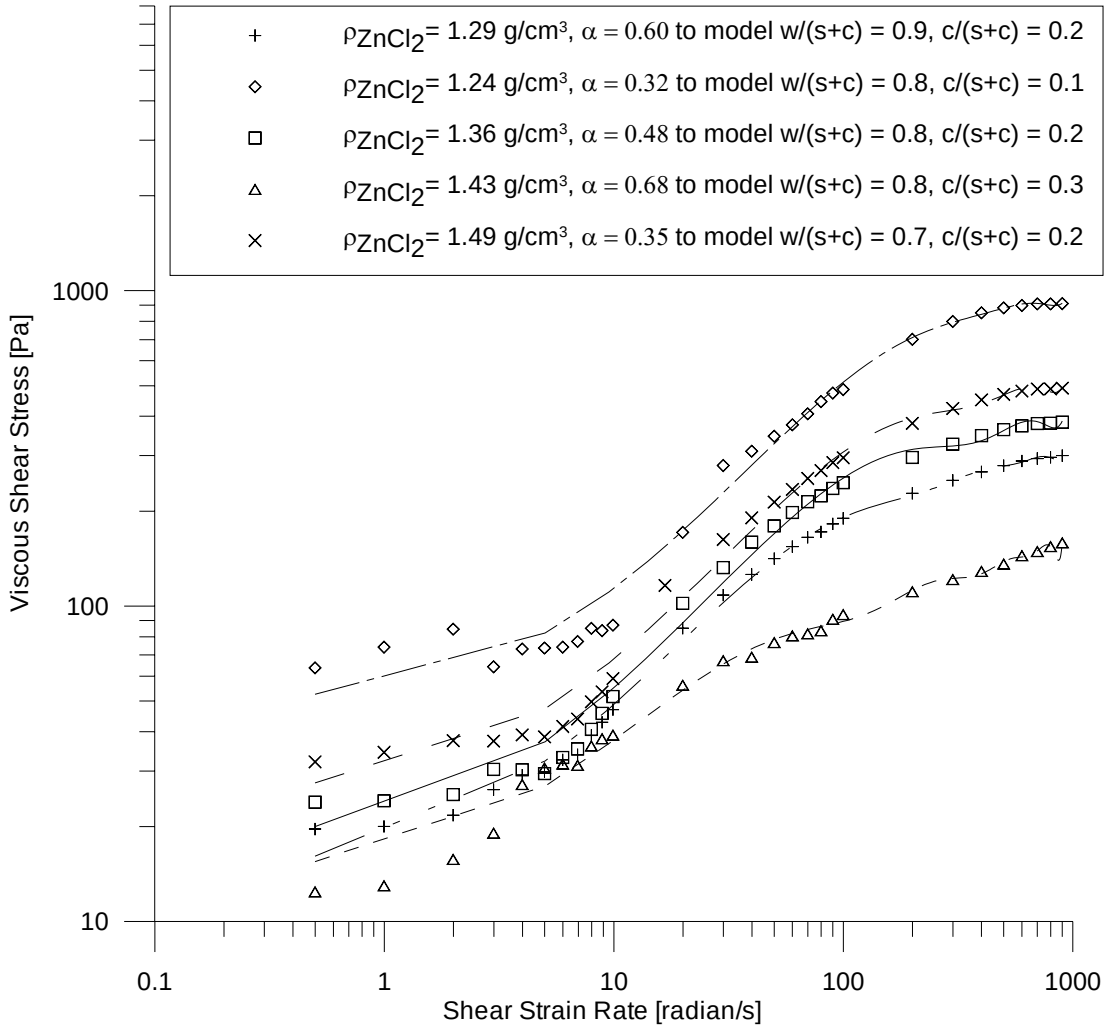

Fig. 2.7 Viscous shear stress against shear strain rate for kaolin-zinc chloride slurry at various mix ratios, based on an in-situ water content of 61%.

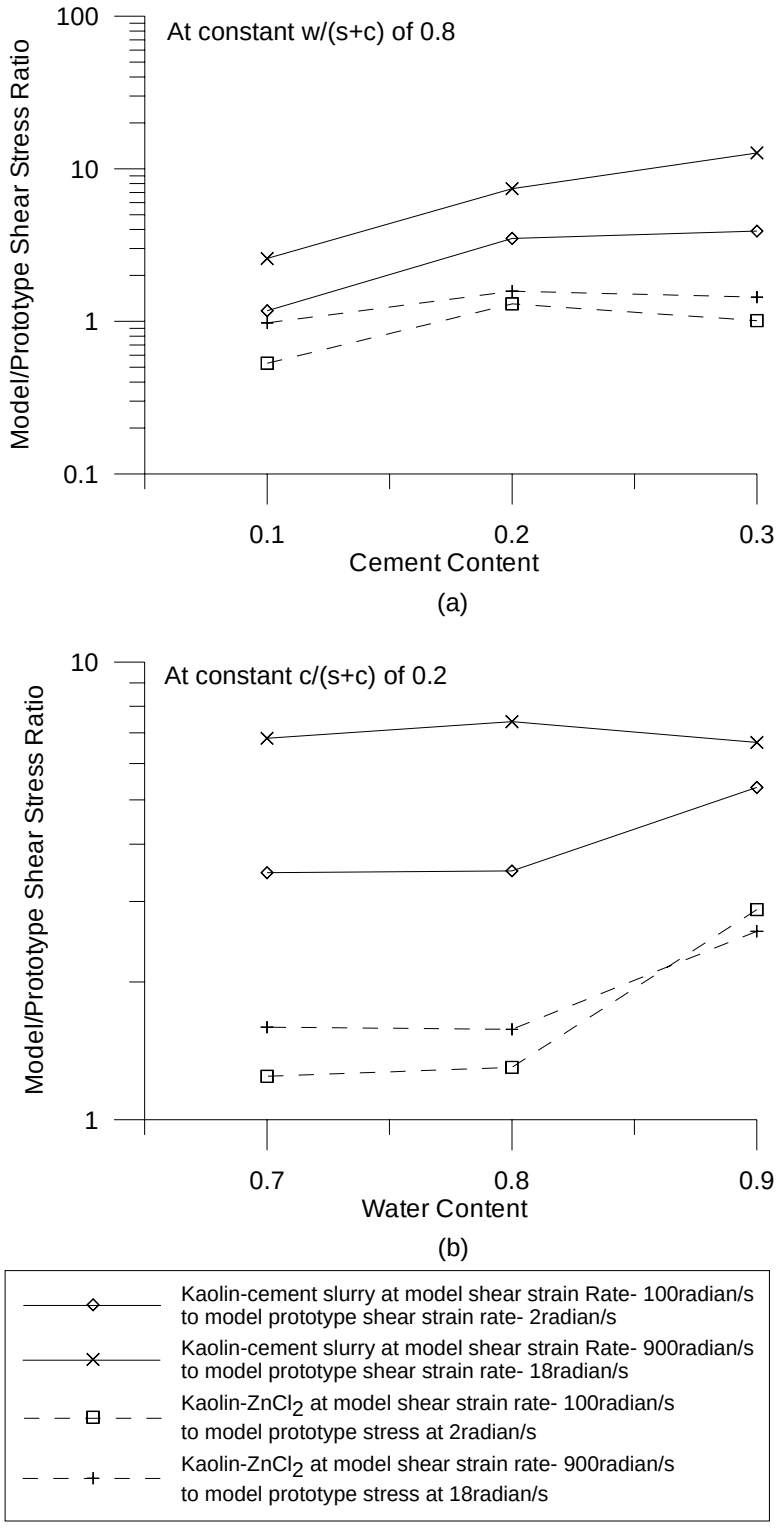

Fig. 2.8 Model-to-prototype viscous shear stress ratios for kaolin-cement slurry at various water and cement contents, as well as for equivalent kaolin-zinc chloride slurries for in situ kaolin water content of 61%.

Chapter 3: Model Development and Experimental Methods

In this chapter, the development of centrifuge model and the experimental method will be presented. The following section will present an overview of the deep mixing (DM) equipment in field. Subsequently, the development work of three different model DM installers will be described. These DM installers will be used for parametric study of uniformity of DM. Finally, the model preparation and test procedure for centrifuge test and 1-g test will be presented.

3.1 Overview of Deep Mixing in Field

A variety of soils mixing tools have been manufactured for various DM purposes. Porbaha et al. (2001) categorized these mixing tools into two types, namely blade-based mixing tools and auger-based mixing tools. According to Porbaha et al. (2001), the installation of a single DM column consists of several steps. After setting the position of the DM machine and confirming the designated location, the shaft is advanced into the ground to reach the required depth. The slurry is fed through the orifice (or nozzle) at the tip and/or through the blades and/or through the main shaft. The bottom of the column is formed at the prescribed depth by steady injection of the stabilizer and mixing for a certain period of time. The mixing is continued while the shafts are being withdrawn. This process is continued until the column reaches the required height above its toe. As can be seen, DM comprises of shearing, intrusion and

remoulding of the in-situ soil mass, entrainment of the cut-up soil mass by the slurry and mixing of the softened, pulverized soil by the slurry.

3.2 Model Deep Mixing Equipment

As part of this study, both centrifuge and 1-g model tests of DM process were carried out. The centrifuge model experiments were conducted under 50-g in the National University of Singapore (NUS) geotechnical centrifuge facility. As shown in Fig. 3.1, the National University of Singapore (NUS) centrifuge is a balanced-beam centrifuge comprising of a central spindle [1] supporting a centrifuge arm [2], both ends of which carry swing platforms [3] on which the test package [4] and counterweight [5] are placed. The 2m radius centrifuge has a payload capacity of 40g-tonnes. Each of the two swing platforms has a working area of about 750mm x 700mm and maximum model headroom of approximately 1200mm. The main camera [6], mounted on centrifuge arm, provides continuous in-flight monitoring of the test package. Electrical and hydraulic slip rings [7] mounted on the central spindle allows the model test to be controlled and monitored from an adjacent control room. When in-flight, the base of the swing platform is normal to the resultant of the centrifugal acceleration field and the earth's gravitational field. Details of the NUS centrifuge and its operation are available in Lee et al. (1991) and Lee (1992).

In this study, centrifuge model tests were conducted using three different DM installer configurations. Hereafter, these DM installers will be termed as DM installer A, DM installer B and DM installer C. In the first series of centrifuge model tests, all tests were conducted with DM installer A, which has a single twisted-blade. All the tests in

the second series were conducted with DM installer B which has two twisted-blades arranged in a double-layered, cruciform fashion. In the third series, all model tests were conducted with DM installer C equipped with three pairs of double-layered twisted-blades, arranged in stacked cruciform fashion. The detailed description of each DM installer will be presented in the following section.

3.2.1 Model Setup for DM Installer A

The first series of in-flight DM apparatus i.e. DM installer A, was developed by modifying the in-flight sand compaction pile installer (Ng et al. 1998, Lee et al 2001, 2002). As shown in Figs. 3.2, 3.3 and 3.4, the DM installer A comprises of a primary storage tank [8] welded to an underslung hollow casing with internal diameter of about 12mm and external diameter of about 14mm [9], which encases a rotating shaft [10]. A variety of mixing blades [11] could be attached to the bottom end of the rotating shaft. The latter was connected to a miniature hydraulic motor [12] mounted on top of the primary storage tank as shown in Fig. 3.2 and a Pepperl & Fuchs OBS2000-F28-E4 retro-reflective photoelectric sensor [13] was used to monitor the rotational speed of the shaft. Fig. 3.5 shows the close-up view of the retro-reflective photoelectric sensor. This retro-reflective photoelectric are equipped with an emitter and detector in the same housing and rely on a reflector attached in the mixing shaft to bounce the beam back across the path of the target. During DM installation, an infrared beam was sent by a transmitter to the rotating mixing shaft. The infrared beam was then reflected back to a receiver by a reflective strip attached to the rotating mixing shaft. The signal from the retro-reflective photoelectric was then interpreted by a KFU8-FSSP-1.D frequency-voltage converter manufactured by Pepperl & Fuchs (Fig. 3.6) and the rotational speed

of the mixing blade was then reported. The miniature hydraulic motor [12] was connected to the shaft of the hydraulic cylinder [14] which controlled the penetration and withdrawal of the DM installer as shown in Figs. 3.7 and 3.8. The miniature hydraulic motor [12] was powered by an on-board hydraulic power pack [15] which located on the top of the centrifuge arm as shown Fig. 3.8. As shown in Fig. 3.9, a potentiometer [16] was mounted on the miniature hydraulic motor [12] to monitor the depth of installation during penetration and withdrawal phase.

The zinc chloride flowed into the DM installer A through a feeder [17] (Fig. 3.3) which was connected by a feeding tube [18] (Fig. 3.8) to the zinc chloride storage tank [19] located on the centrifuge arm as shown in Fig. 3.8. The feed rate of the zinc chloride was controlled by the Swagelok SS-4MG-MH metering valve [20] as shown in Figs. 3.9 and 3.10, which was calibrated and preset before the experiment. The DM installer was mounted on an XY-table, which allows accurate in-flight XY positioning, if needed. The details of this XY-table have been reported by Ng et al. (1998) and will not be repeated herein. The original hydraulic cylinder mounted on the XY-table has a limited stroke length. In order to facilitate greater penetration depth, a new hydraulic cylinder [14] with maximum stroke length of 210mm was designed and fabricated, as shown in Figs. 3.7, 3.8 and 3.9.

Fig. 3.11 shows a typical relationship between the flow rate of the zinc chloride, which was used as the model binder in the model experiments. Fig. 3.10 shows the vernier scale [21] of the metering valve provides accurate flow control. The actual flow rate is likely to be affected by the viscosity of the liquid tracer; thus the metering valve was recalibrated and reset before each test.

In order to study the effect of blade angle on the uniformity of mixing, two simple twisted-blades with blade angle of 45° and 90° were fabricated. The blade angle is defined herein as the angle made by the plane of the blade with the direction of rotation. This definition is similar to that for the angle of attack used in aeronautics (e.g. Springer, 2003). Both simple-twisted blades have a blade height of 5mm and blade diameter of 50mm as shown in Figs. 3.12, 3.13 and 3.14. The prototype diameter represented by that of the model DM column is larger than diameters used in the field, which are often 2m or less. This is needed to facilitate measurement of chloride concentration in the model DM columns at multiple locations, which would have been more difficult with narrower columns. The mixing blade was fastened to the rotating shaft [10] of DM installer A as shown in Fig. 3.3. The zinc chloride was introduced into the soil through an opening located at the top of the mixing blade as shown Fig. 3.14.

The DM installer A used in the first series study are simpler than many prototype DM equipment, which often have more than one layer of cutting and mixing blades. However, this does not detract from the objective of these model tests which is to study the feasibility of reproducing DM mechanics in centrifuge models rather than to replicate the performance of specific prototype DM equipment. For such fundamental studies, simple blade configurations may allow salient features of the mixing process to be more clearly manifested. As will be seen later, installers B and C employed more complex blade configurations. The use of simple model blades is not unprecedented; Al-Tabbaa and Evans (1999) also used a simple model blade in their 1-g model study and found it to give much better cement-mixed columns that a geometrically similar model blade.

3.2.2 Model Setup for DM Installer B

The model setup for DM installer B was similar to the model setup presented in section 3.2.1, with the exception that the entire DM installer A was replaced by the DM installer B. As shown in Fig. 3.15, the key difference between DM installer A and DM installer B is that the latter has two twisted-blades arranged in a stacked cruciform fashion, instead of simple twisted-blade found on DM installer A. As discussed earlier, DM installer A was developed by modifying the in-flight sand compaction pile installer. In designing DM installer B, it was decided to develop a generic configuration that is scaleable into a multi-mixing blade configuration. For this reason, DM installer B has a different architecture from DM installer A. DM installer B was essentially comprises of a crown [22] mounted to the miniature hydraulic motor [12] as shown in Figs. 3.15 and 3.16. Fig. 3.17 shows the schematic drawing of the crown. Fig. 3.18 shows the close-up view of the crown. The crown comprises of a miniature primary storage tank that receives the zinc chloride from the stationary feeder pipe [23] and channelling it into the hollow casing. A hollow casing [24] connected between the crown and the mixing blade [25]. A stationary feeder pipe was used to introduce the zinc chloride into the DM installer through the crown of the DM installer. The schematic diagram of the stationary feeder is shown Fig. 3.19. Fig. 3.20 shows the close-up view of the feeder. A retro-reflective photoelectric sensor was mounted on the stationary feeder as shown in Fig. 3.21. The retro-reflective photoelectric sensor was used to monitor the in-flight rotational rate of the mixing blade.

The mixing blade used in this series of study comprised of two twisted-blades arranged in a double-layered cruciform fashion as detailed in Figs. 3.22 and 3.23. These twisted-

blades have the same blade dimension as the DM installer A, i.e. blade height of 5mm and blade diameter of 50mm. Four injection nozzles were located next to each blade to facilitate zinc chloride injection during DM installation.

3.2.3 Model Setup for DM Installer C

The model setup for DM installer C was essentially similar to the model setup presented in section 3.2.2, with the exception that the DM installer C equipped with three stacked pairs of double-layered twisted-blades [26] as shown as shown in Figs. 3.24, 3.25 and 3.26. As discussed in section 3.2.2, the DM installer B can be easily extended to multiple blades by attaching additional mixing blades to the hollow casing. In this study, three pairs of double-layered twisted-blades were used, as illustrated by the schematic diagram in Fig. 3.25. Fig. 3.26 shows the DM installer C with three stacked pairs of double-layered twisted-blades.

3.3 Sample Preparation Procedure

The model soft clay beds used in the both centrifuge model tests and 1-g model test were prepared using de-aired kaolin clay slurry and consolidated to the required stress level. Some of the physical properties of the clay are presented Table 3.1 (after Ong 2004). All 22 centrifuge model tests were consolidated by self-weight under centrifuge gravity. All 6 1-g model test were consolidated by surcharge loading.

3.3.1 Centrifuge Model Preparation

The soil used in the study is speswhite kaolin. The inside walls of the container were coated with silicone grease. A thin layer of fine sand was placed over the container base to facilitate drainage during consolidation. A layer of polypropylene geotextile filter was then placed over the sand layer. The container was partially filled with de-aired water. The clay slurry was de-aired in a de-airing chamber as shown in Fig. 3.27. De-aired clay slurry with water content of 1.5 times the liquid limit was then placed into the container under water, thereby minimising the possibility of trapping air voids in the kaolin. The slurry was then allowed to consolidate first under its own self-weight. Subsequently, a surcharge was applied on the clay surface; the surcharge pressure being gradually increased in stages to 10kPa, with each stage being maintained till the clay was considered to have achieved sufficient strength to bear the next stage. The model clay bed inside the container was then subjected to self-weight consolidation at 50-g model gravity until an average degree of consolidation of 95% was achieved before in-flight installation of the DM column was carried out.

In model test DM05, DM06, DM07, DM08 and DM09, the side wall of the container was removed and holes were drilled into the sides of the clay bed at prescribed locations using drill bits upon the completion of 1-g consolidation by surcharge. Druck PDCR81 PPTs were inserted to the prescribed location to measure the changes in pore pressure during DM installation. The prescribed locations are shown in Fig. 3.28. The performance of these PPTs in model clay beds has been reported by Konig et al. (1994) and will not be repeated herein. The container side was then re-fitted and the whole assembly was then subjected to self-weight centrifuge consolidation at 50-g

until an average degree of consolidation of at least 95% was achieved before in-slight installation of the DM column was carried out.

3.3.2 1-g Model Preparation

The model clay bed for the 1-g model tests follow the same preparation as centrifuge model preparation, with the exception that the surcharge pressure being gradually increase to 31kPa, with each stage being maintained till the clay was considered to have achieved sufficient strength. Finally, the model was subjected to 31kPa until an average consolidation of 95% was achieved. The average water content was about 63%. The 1-g model has a similar effective stress level as the centrifuge model at model depth 2D, in which *D* is the diameter of the mixing blade. Fig. 3.29 shows the 1-g model under surcharge loading. Upon completion of the consolidation, the loading platen on the top of the clay surface was removed and 1-g installation of DM is carried out. Soil samples were collected at model depth 1D, 2D and 3D.

The 1-g model has a uniform effective stress level of about 31kPa. The effective stress level of the entire 1-g model is similar to the centrifuge model at about model depth 2D. At model depth 1D, the effective stress in 1-g tests was higher than that of 50-g test; at model depth 3D, the effective stress in 1-g tests was lower than the 50-g tests. However, the differences in effective stress between 1-g model and 50-g model does not detract from the objective of these model tests which is to provide an overview on mixing quality for DM conducted at 1-g environment and high-g environment. This will be discussed further on chapter 4.

3.4 Test Procedure

During the model tests, the installer was jacked into the model clay bed at a constant speed, with the mixing shaft rotating to break up and remould the clay mass. In order to monitor the in-flight rotational speed of the mixer, an OBS2000-F28-E4 miniature retro-reflective photoelectric sensor (e.g. Figs. 3.5 and 3.21) manufactured by Pepperl & Fuchs was attached to the side of the DM installer. A small amount of water-based ink was added into the zinc chloride to enable visualization of the spread of the zinc chloride. The zinc chloride was then placed into the zinc chloride storage tank prior to the test. Upon reaching the required depth, the direction of rotation was reversed and the zinc chloride solution in the secondary storage tank was introduced into the clay through the bottom of the casing at the prescribed rate, thereby mixing the zinc chloride and soil while the installer was withdrawing. This procedure is similar to the withdrawal injection method (Porbaha et al. 2001). In actual DM operation, the binder can be introduced during the penetration or withdrawal phase, or both (e.g. Porbaha et al. 2001, European Standard: Execution of Special Geotechnical Works- Deep Mixing 2003). However, Porbaha et al. (2001) noted that the withdrawal injection method, in which binder is introduced during the withdrawal phase, is likely to create fewer problems as soil has already been broken up during the penetration phase. The rotational speed of the model mixer for both the penetration and withdrawal phases was approximately 770revs/min (rpm); this being the maximum achievable by the hydraulic system driving the DM installer. This is equivalent to approximately 15rpm in prototype scale, which is similar to that used by Dong et al. (1996) in their study, but is slightly lower than the typical range of 20 to 60rpm used in field DM operations, as shown in Table 2.1. The penetration and withdrawal rate were ranging from

0.03m/min to 0.432m/min. In model test DM20, DM26 and DM27, re-penetration and remixing were conducted immediately after the first withdrawal. During the re-penetration and remixing of the DM installer, no zinc chloride was introduced. In these centrifuge tests, the blade rotation number was ranging from 35.6rev/m to 513rev/m.

Approximately 124ml of the zinc chloride was introduced into the kaolin clay bed in each DM installation. This is equivalent to approximately 35% of the total volume of a single DM column. As shown in Fig. 3.30, this produces a DM column with a diameter of 50mm and height of about 180mm, which is equivalent to a prototype column with 2.5m diameter and 9m height. As discussed earlier, the prototype diameter represented by that of the model DM column is larger than diameters used in the field. However, this is needed to facilitate measurement of chloride concentration in the model DM columns at multiple locations.

Sampling of soil samples were carried out immediately after in-flight installation. The side of the container were removed as shown in Fig. 3.31. The model clay bed was trimmed at prescribed levels using a wire cutter. At each level, soil samples were collected at various locations within the DM column, by using a miniature scoops shown in Fig. 3.32 and stored separately in a sealed sample bottle. The soil samples were then weighed and the tracer ion concentration is analyzed using ion chromatography.

The test procedure for the 1-g model tests was similar to the in-flight DM, the only difference is that the rotational speed of the model mixer for both the penetration and withdrawal phases was approximately 15revs/min, which was far lower than that used

at high-g. Initial attempts to use the rotational speed used in high-g models for the 1-g tests resulted in severe splashing of the zinc chloride. This can be attributed directly to the fact that, at higher rotation rates, the Froude number is no longer preserved and the centrifuge force in the mixing cavity became much higher than the gravity force. The penetration and withdrawal rate for these 1-g tests were 0.03m/min. Model test were conducted using zinc chloride as well as cement slurry in model tests 1gG, 1gH and 1gI.

3.5 Chemical Analysis of Tracer Ion Concentration

The concentration of the tracer ion was analyzed using DIONEX ion chromatograph as shown in Fig 3.33. The chloride ion was selected as the tracer ion for model tests conducted using zinc chloride. For cement slurry, calcium ion was selected as the tracer ion for measuring concentration. In order to analyze the chloride concentration, the soil samples were first diluted into de-ionized water. Each sample was stored in separate testing tubes as shown in Fig. 3.34. These diluted samples will be subjected to ion chromatography analysis. Calcium concentration was analyzed by adding a small amount of strong hydrochloric acid to the soil sample to dissolve a portion of the non-water soluble ion. These dissolved soil samples were then diluted into the de-ionize water and subjected to ion chromatography analysis. The concentration of chloride in zinc chloride solution was about 0.27g/cm^3, 0.40g/cm^3 0.53g/cm^3 for zinc chloride density of 1.3g/cm3, 1.5g/cm3 and 1.7g/cm3 respectively. The concentration of calcium in cement slurry was about 0.18g/cm^3, 0.24g/cm^3 and 0.37g/cm^3 for cement slurry density of 1.3g/cm^3, 1.5g/cm^3 and 1.7g/cm^3 respectively. In addition, the raw kaolin clay also tested for the baseline calcium content and chloride content. The

concentration of the baseline ion was then subtracted from the corresponding spot concentration of the soil-binder mix. The mean concentration of baseline calcium in kaolin clay was about 0.44% by total weight of kaolin clay and the concentration of baseline chloride in kaolin clay was insignificant.

The results of the analysis were reported in part per million (ppm), and this value was then converted to the ratio of the weight of tracer ion to the weight of soil sample using the relationship

$$C = \frac{c_o \cdot V_w}{w_s} \cdot 100 \qquad (3.1)$$

where C is the concentration of tracer ion in % by weight, c_o concentration of tracer ions in de-ionize water in g/l, V_w the volume of the de-ionize water used in dilution in litre, w_s the weight of soil samples in gram.

Table 3.1 Physical properties of kaolin clay (Ong, 2004).

Properties	**Value**
Specific Gravity (G_s)	2.65
Liquid Limit (W_L)	80%
Plastic Limit (W_P)	40%
Compression Index (C_c)	0.64
Swelling Index (C_S)	0.13
Coefficient of Permeability at 100kPa on Normally Consolidated Condition (k)	1.36×10^{-8} m/s
Effective Internal Friction Angle (ϕ')	25°
Lamda (λ)	0.27
kappa (κ)	0.06
Ratio of Undrained Shear Strength, c_u to the Effective Overburden Pressure, q' for Normally Consolidated Condition	0.20 - 0.30

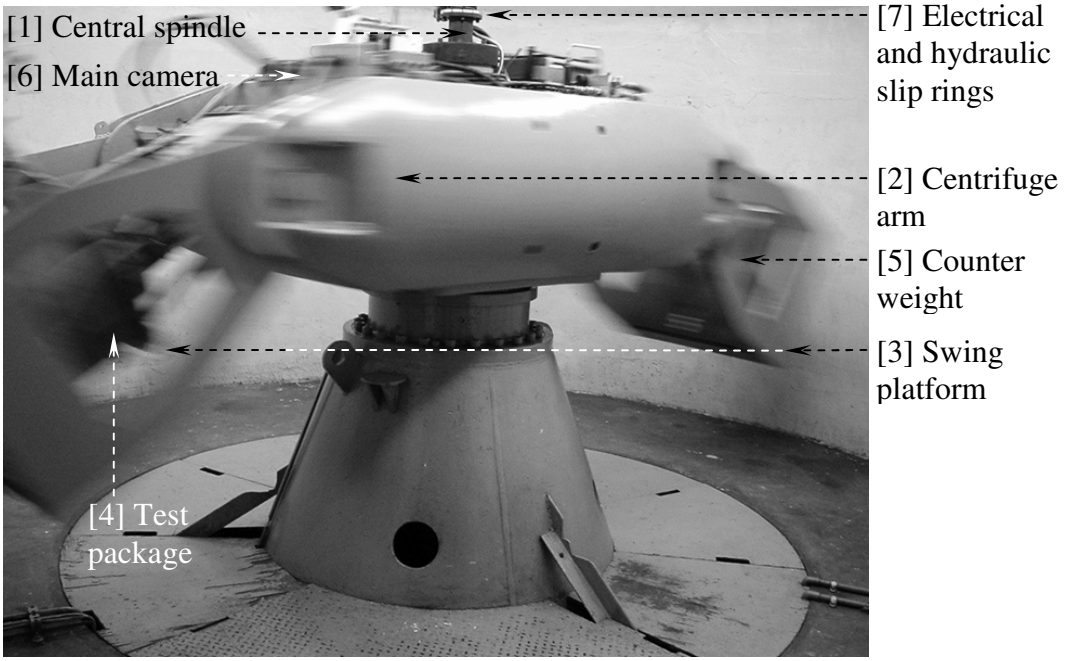

Fig. 3.1 National University of Singapore (NUS) Geotechnical Centrifuge facility in action.

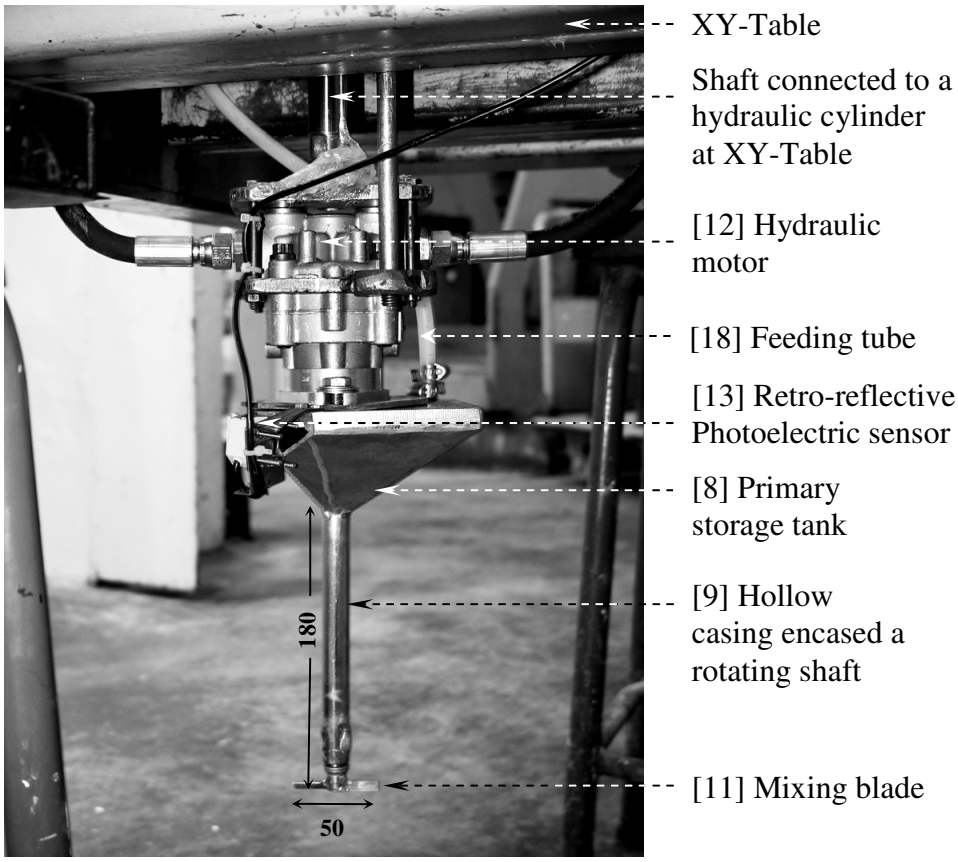

Fig. 3.2 DM installer A mounted on the XY-table (all dimension in mm).

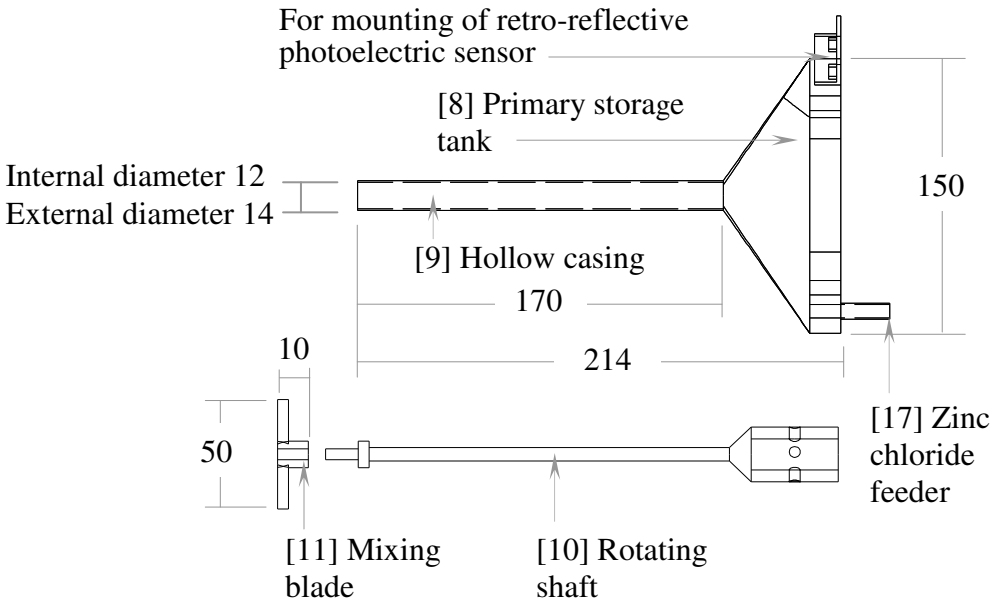

Fig. 3.3 Schematic of in-flight DM cutting and mixing equipment (all dimensions in mm).

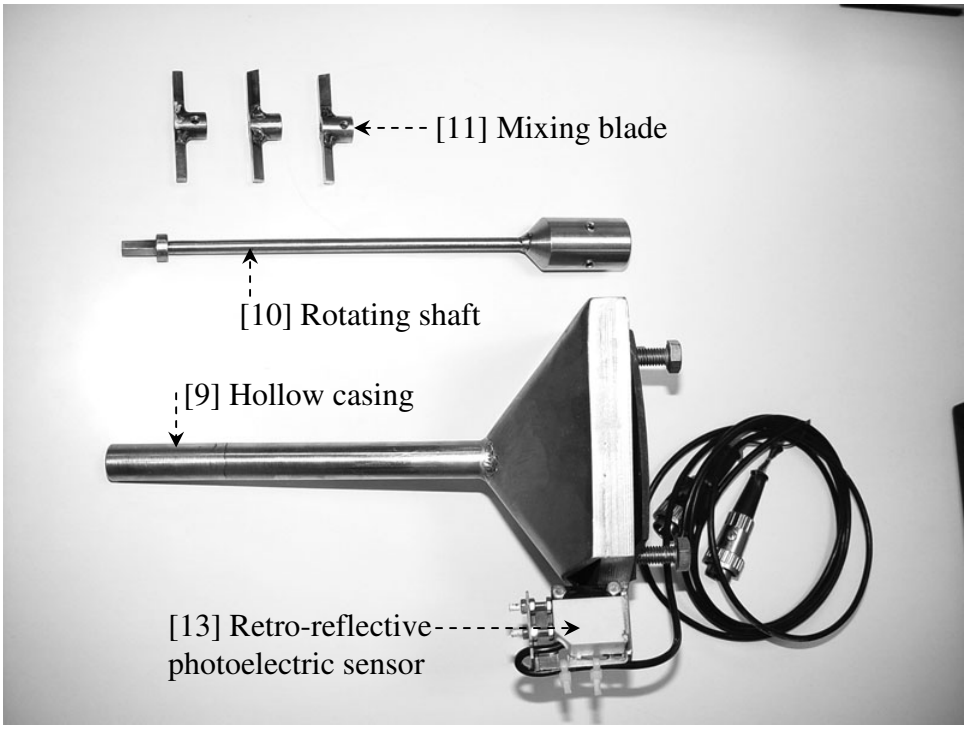

Fig. 3.4 DM installer A with a variety of mixing blades could be attached to the bottom end of the rotating shaft.

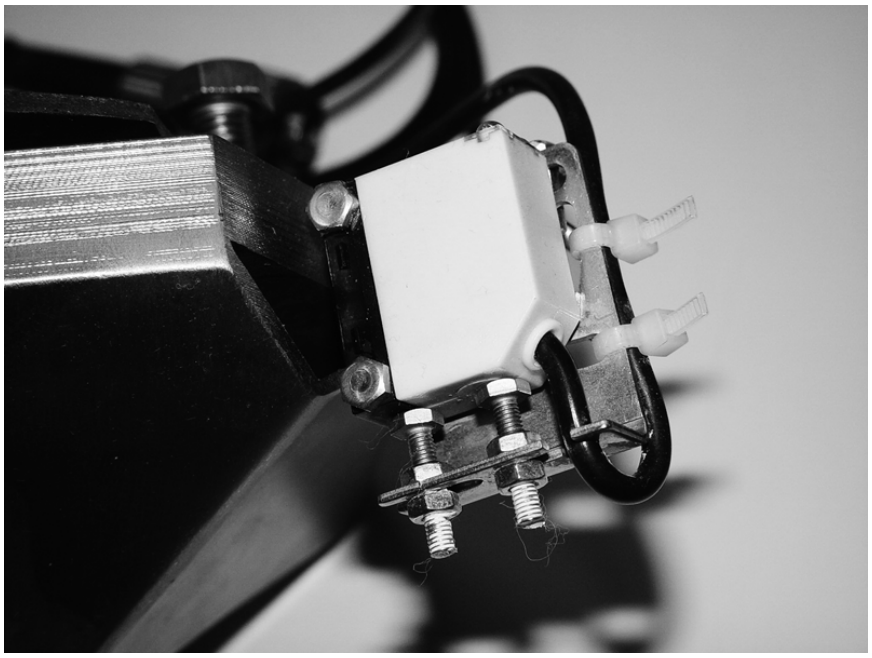

Fig. 3.5 Pepperl & Fuchs OBS2000-F28-E4 retro-reflective photoelectric sensor.

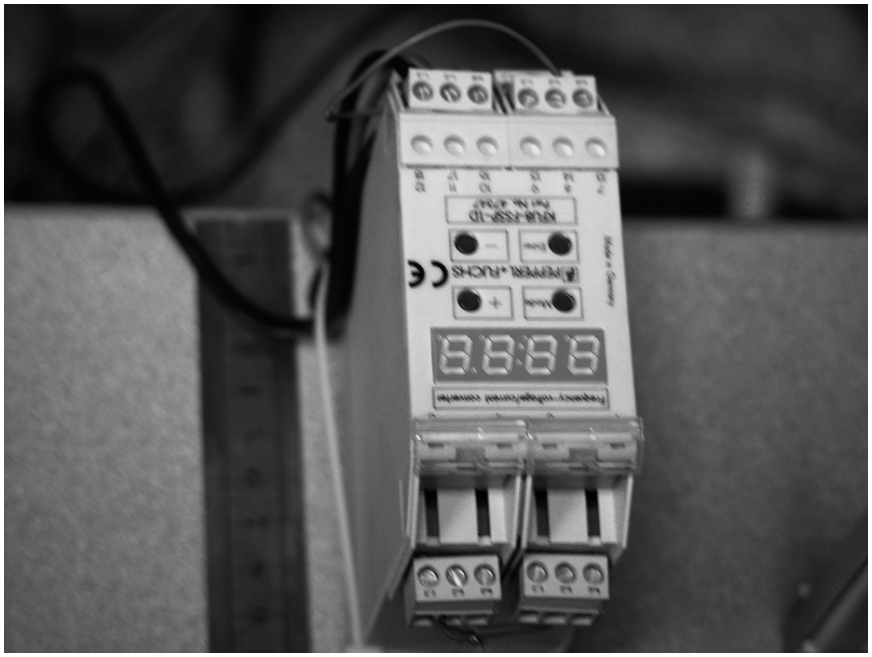

Fig. 3.6 KFU8-FSSP-1.D frequency-voltage converter translates the signal for from retro-reflective photoelectric sensor into rotational rate of the mixing blade.

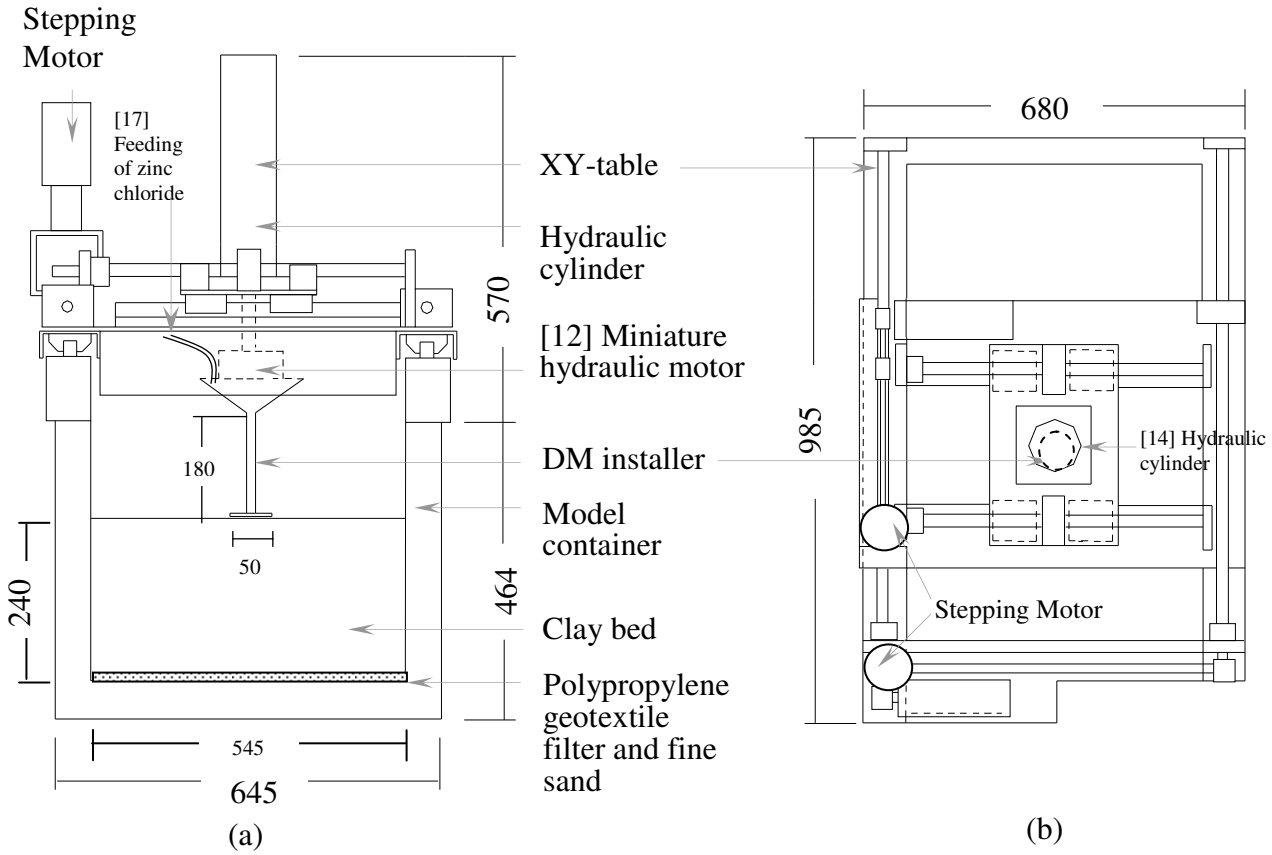

Fig. 3.7 (a) Side view of DM installer mounted on the model container (b) Plan view of DM installer (all dimensions in mm).

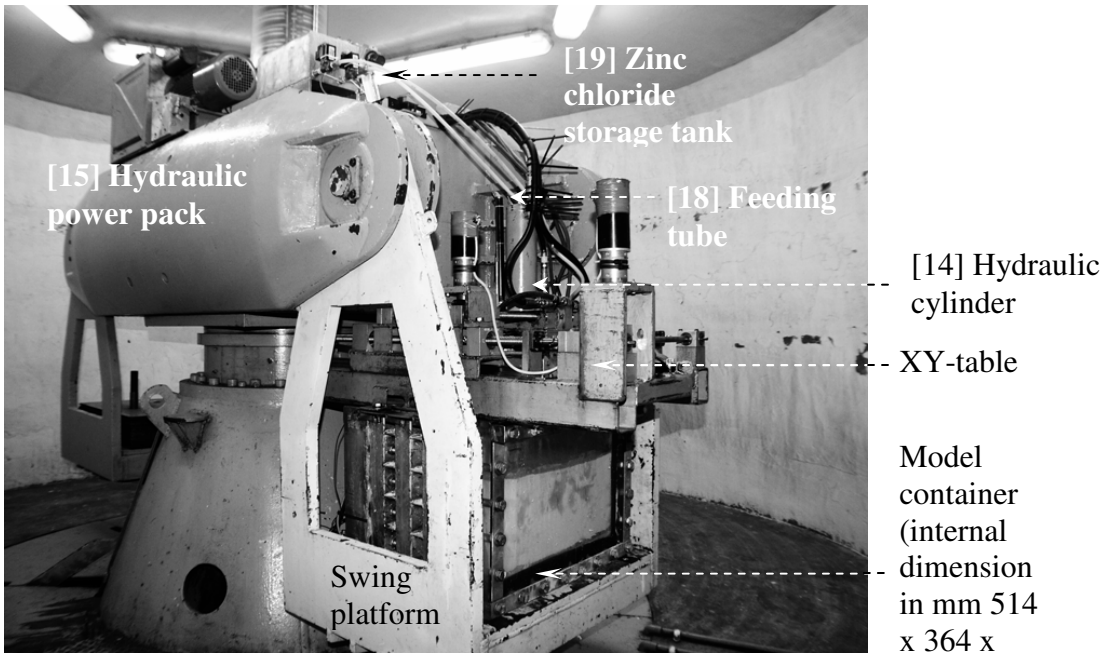

Fig. 3.8 Setup of the model test on a 2m radius centrifuge with a maximum payload capacity of 40g-tonnes (all dimension in mm).

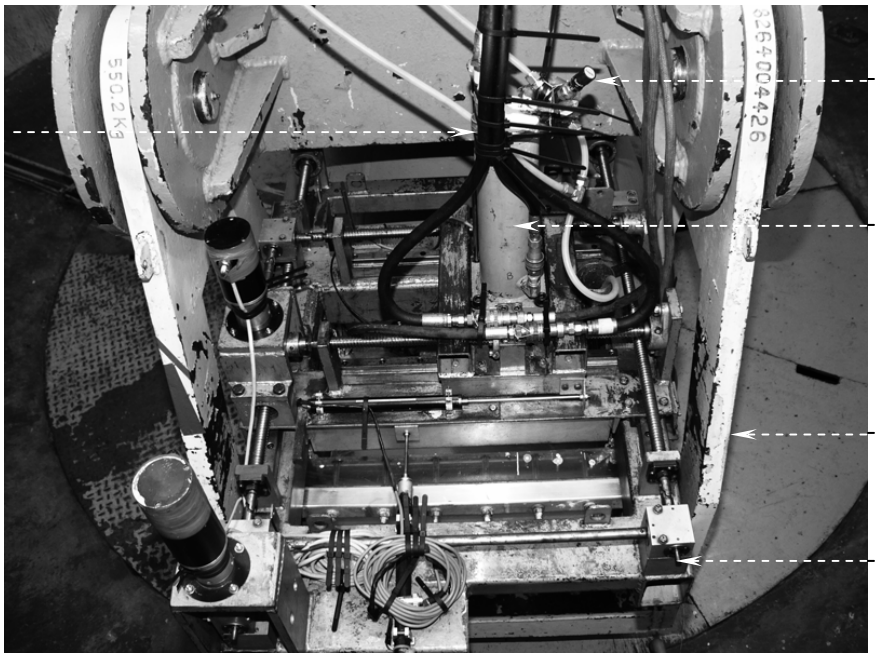

Fig. 3.9 Top view of XY-table (all dimension in mm).

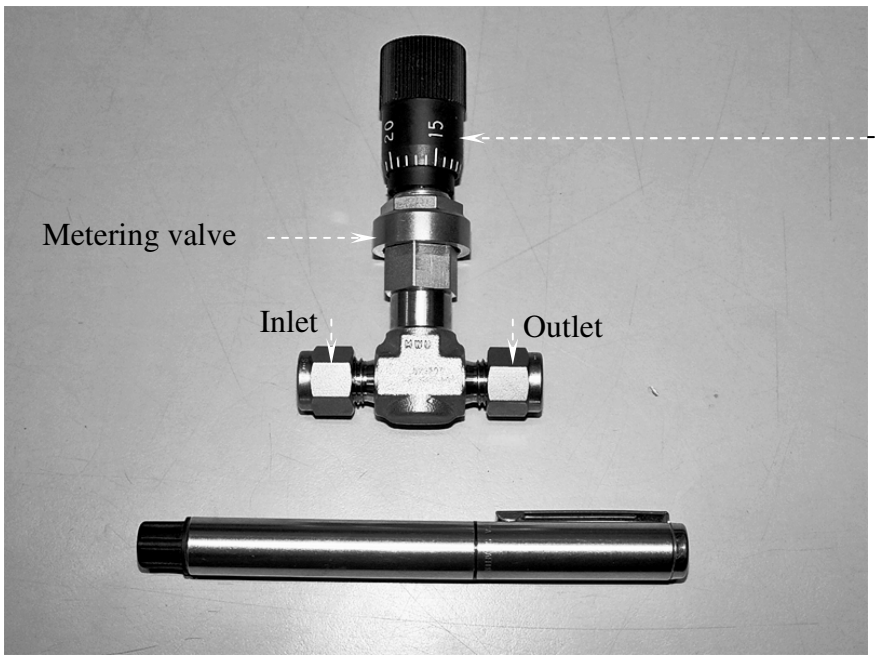

Fig. 3.10 Swagelok SS-4MG-MH metering valve.

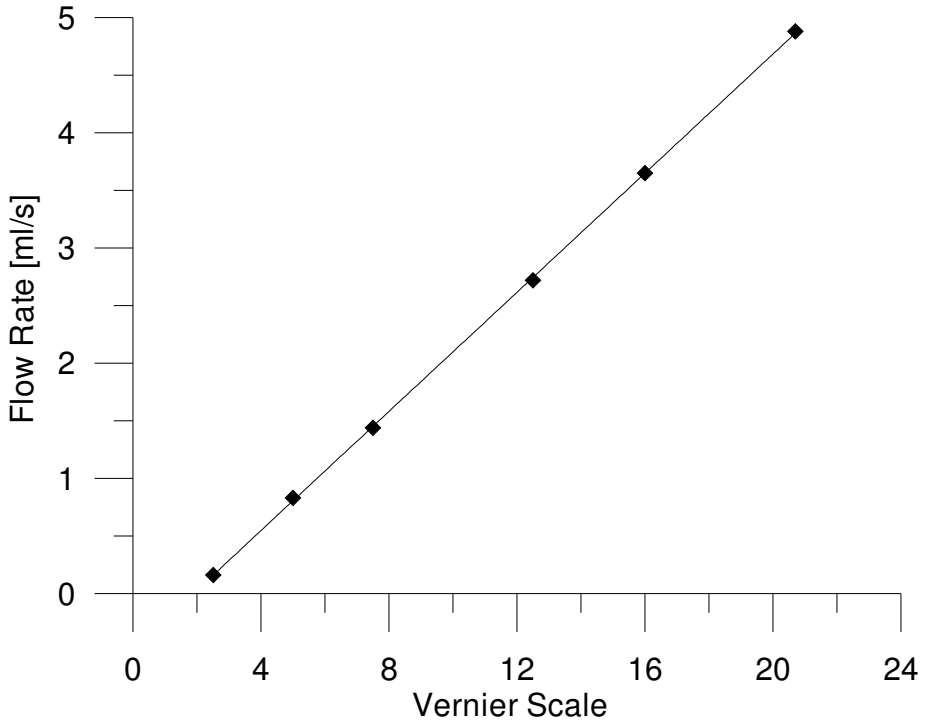

Fig. 3.11 Typical relationship between the flow rate of the zinc chloride and setting of the metering valve.

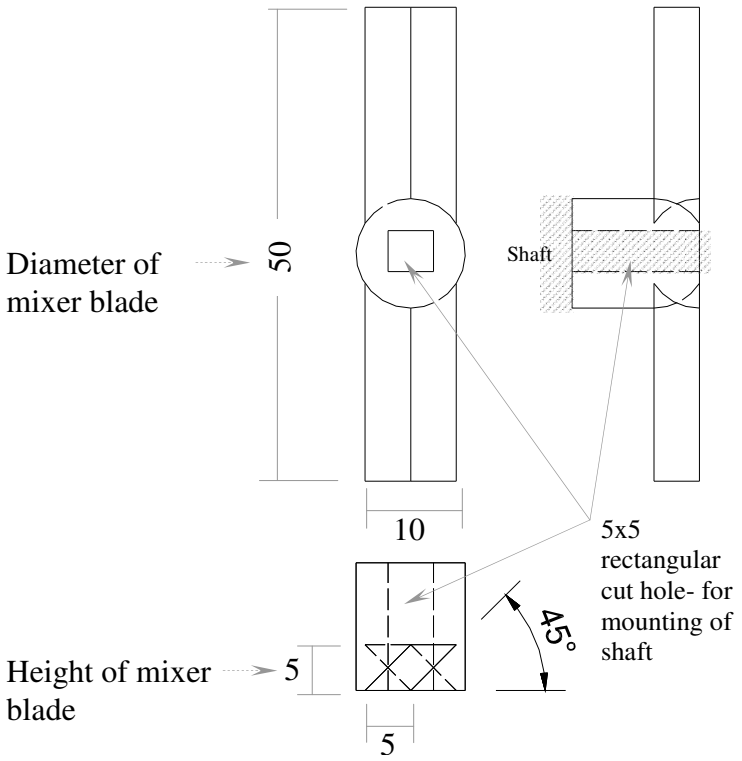

Fig. 3.12 Schematic of 45° blade for DM installer A (all dimensions in mm).

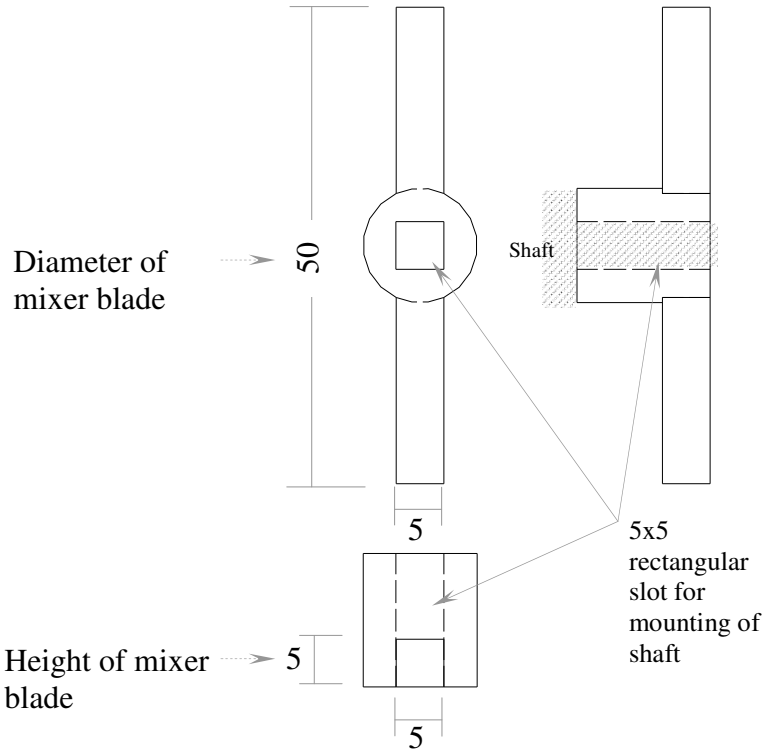

Fig. 3.13 Schematic of 90° blade for DM installer A (all dimensions in mm).

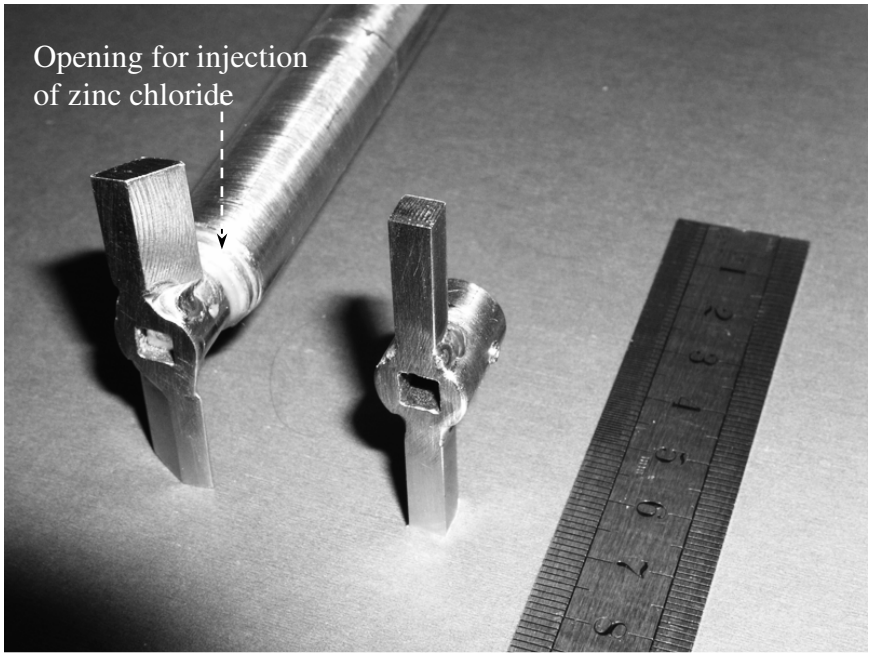

Fig. 3.14 Left- 45° blade for DM installer A, right- 90° blade for DM installer A.

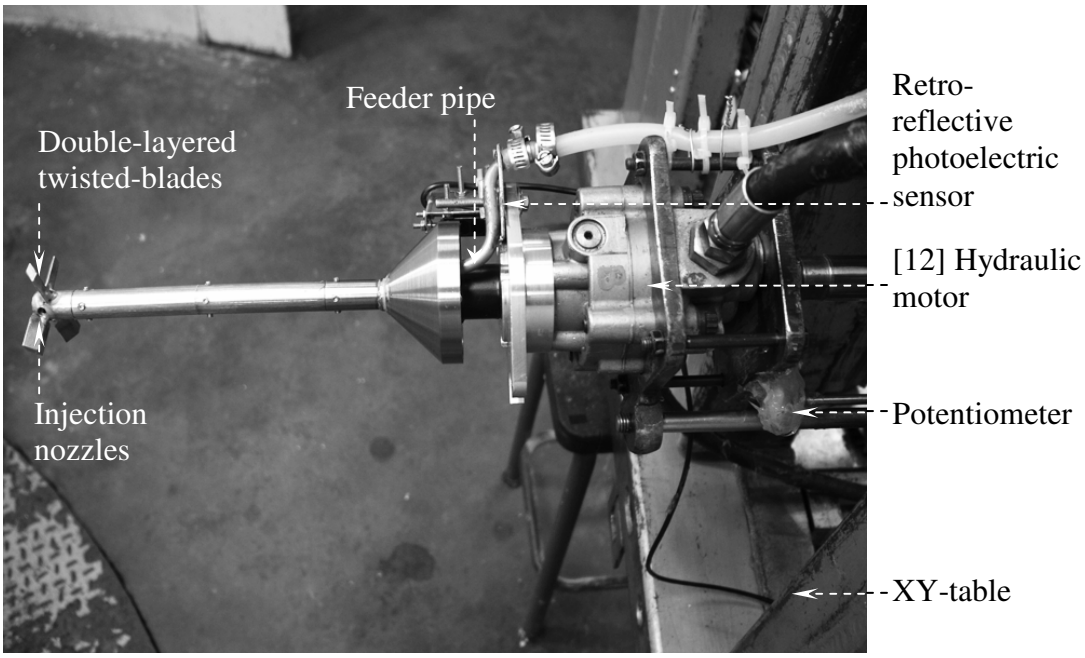

Fig. 3.15 DM installer B mounted on the XY-table.

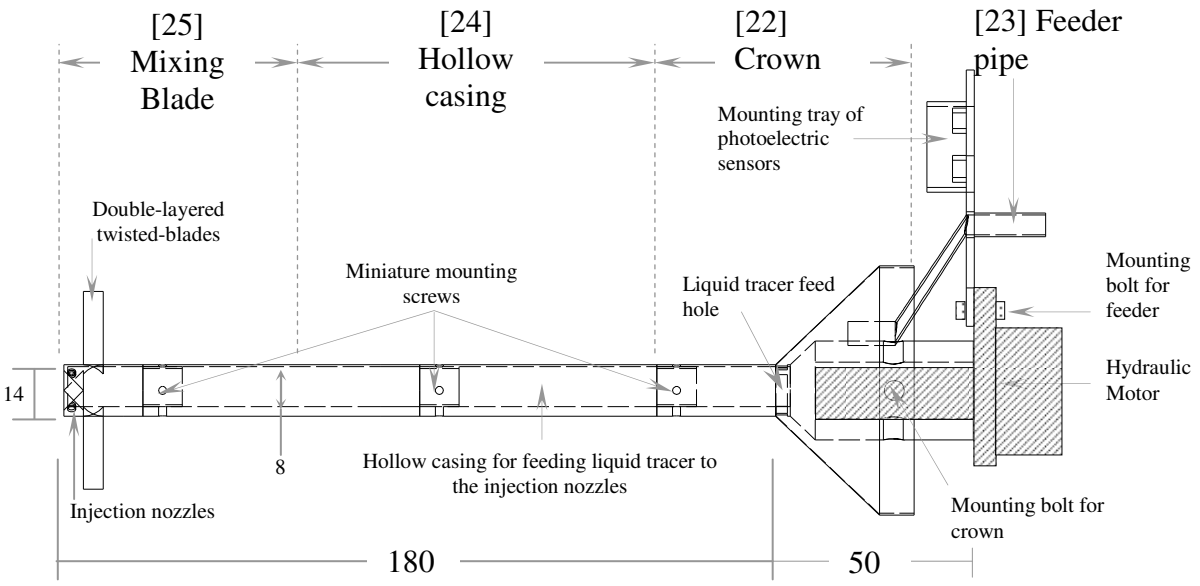

Fig. 3.16 Schematic of in-flight DM installer B (all dimensions in mm).

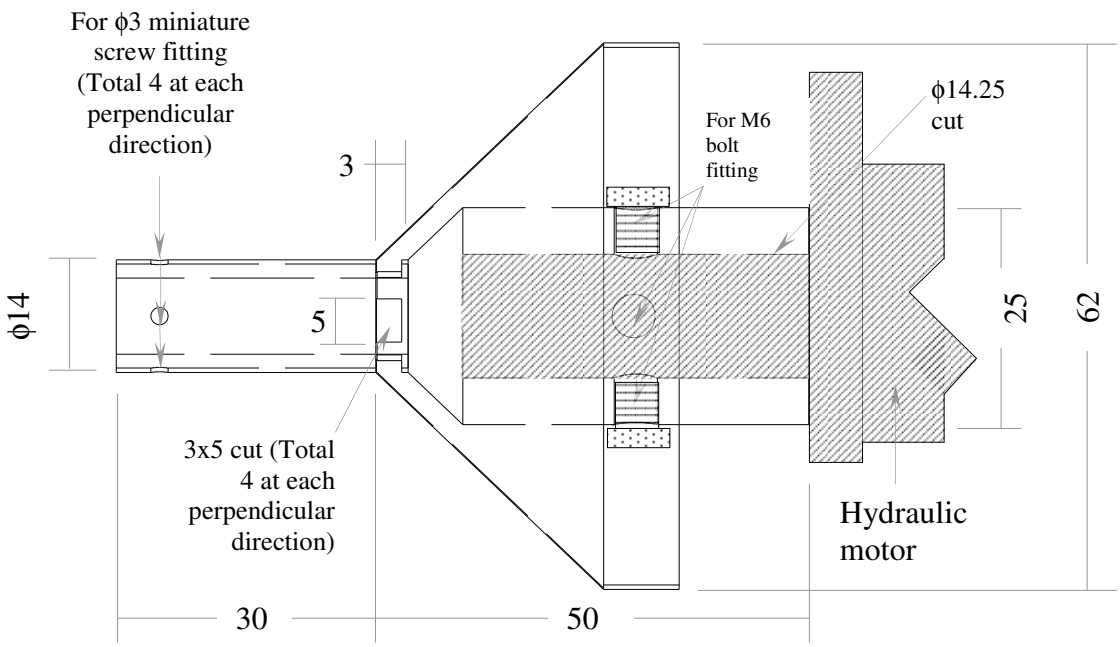

Fig. 3.17 Schematic of crown of DM installer B. The crown rotated together with the mixing blade during installation (all dimensions in mm).

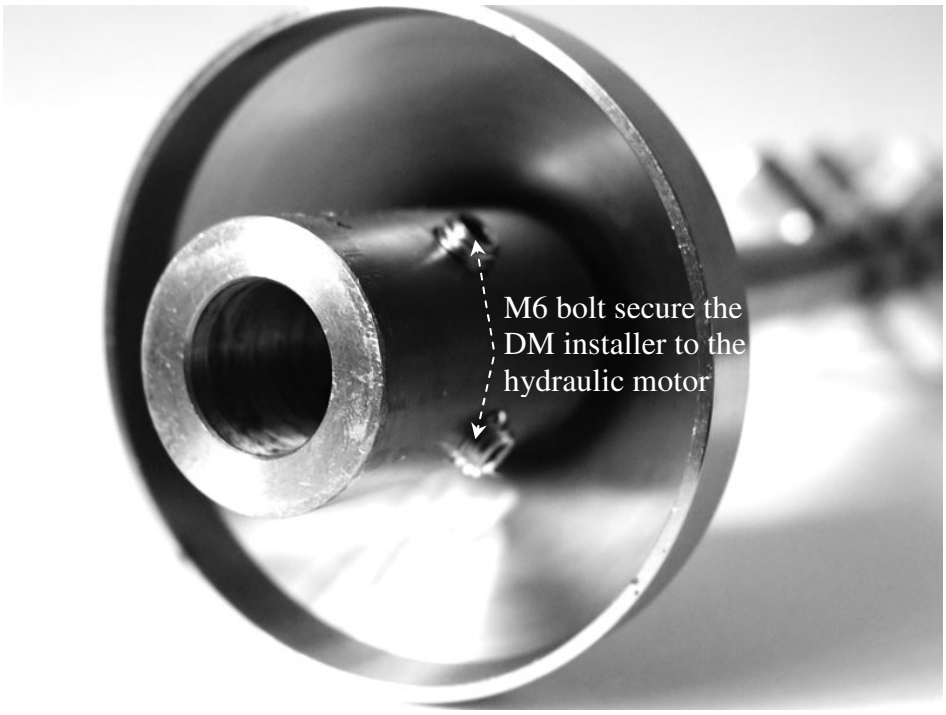

Fig. 3.18 Close-up view of the crown.

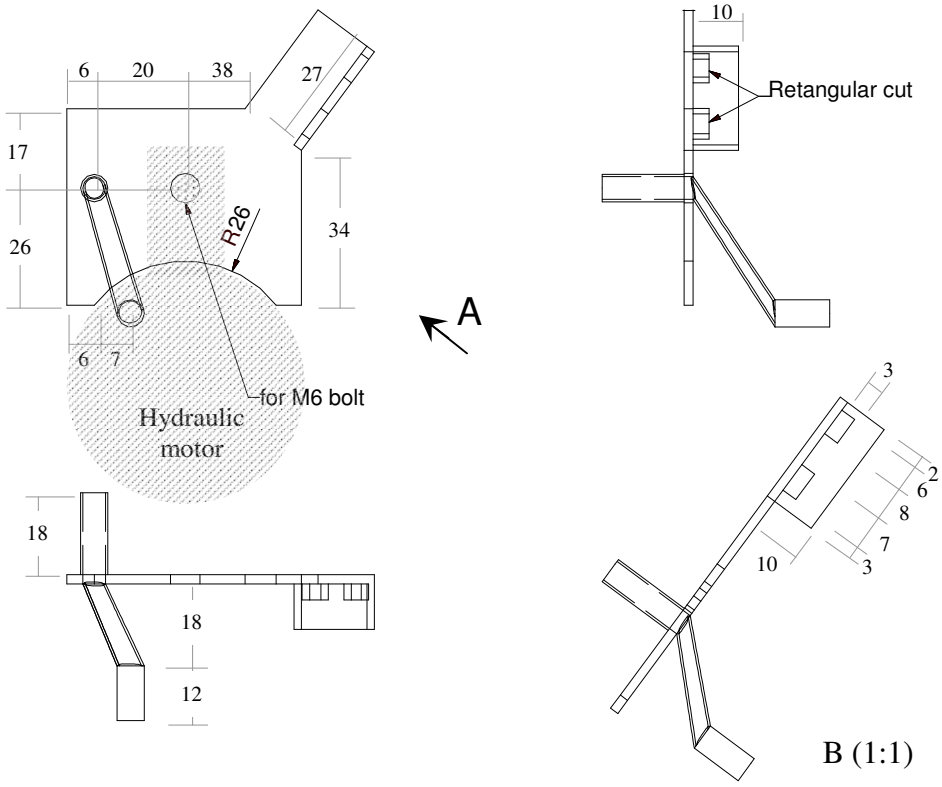

Fig. 3.19 Schematic of feeder used in DM installer B and C (all dimensions in mm).

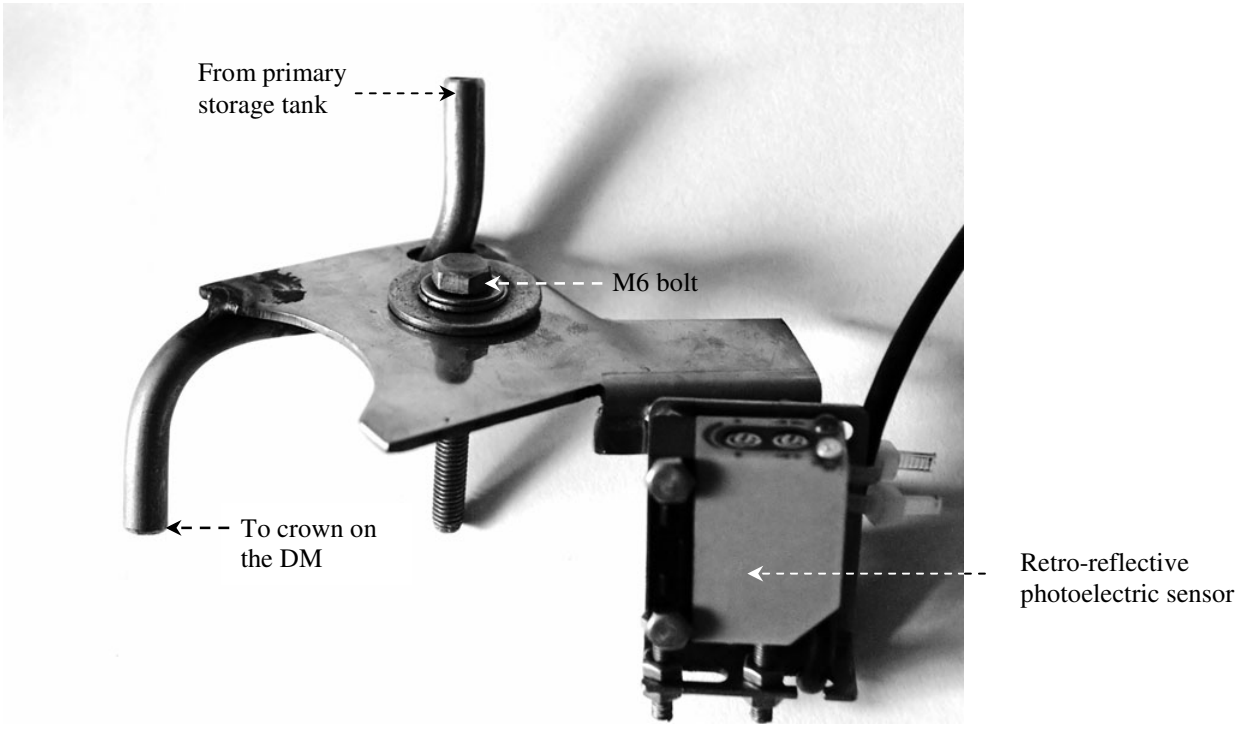

Fig. 3.20 Close-up view of the feeder.

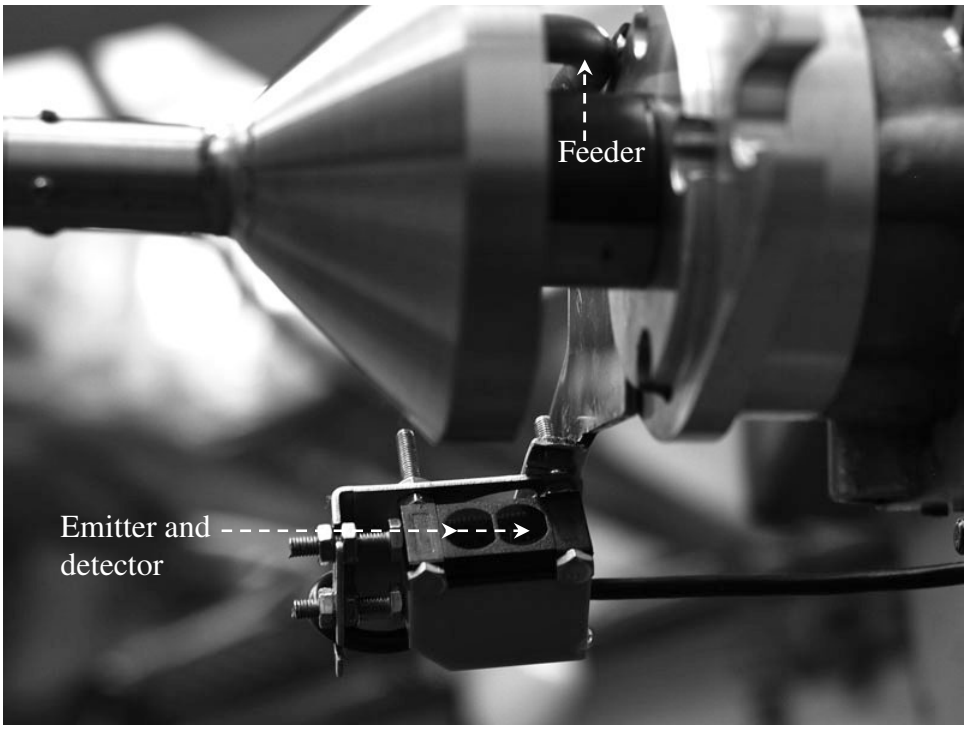

Fig. 3.21 Mounting of the retro-reflective photoelectric sensor on DM installer B.

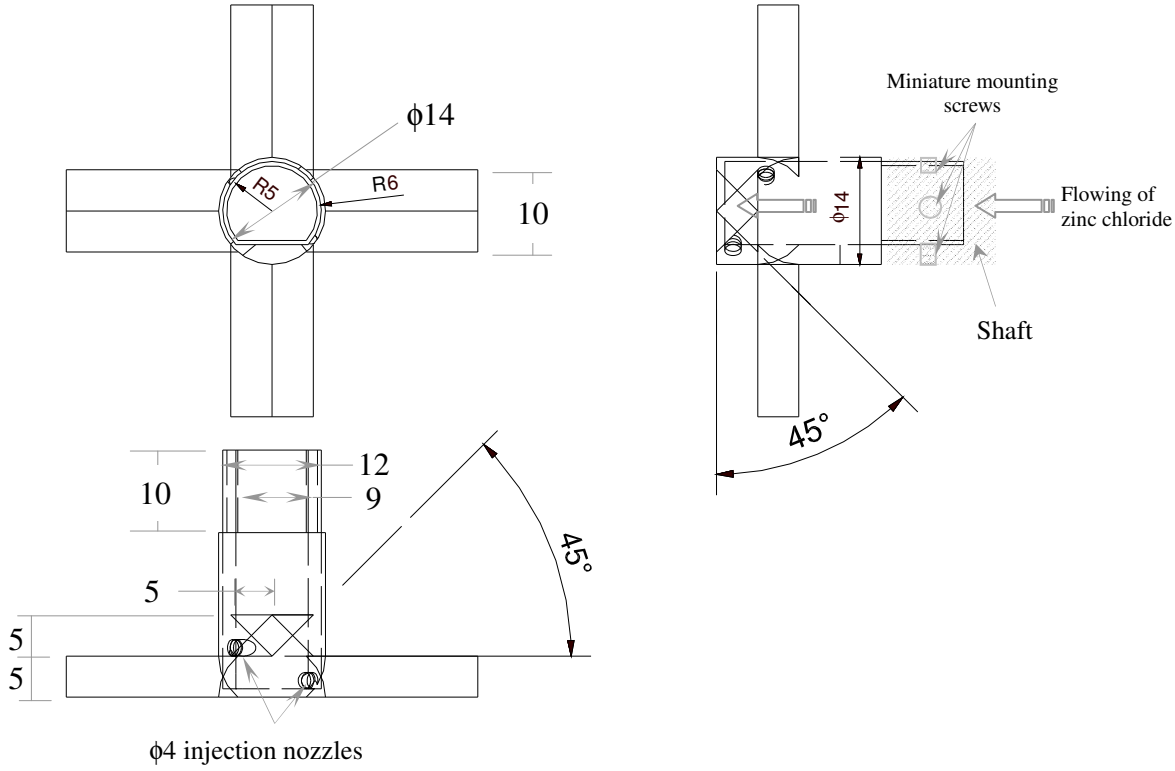

Fig. 3.22 Schematic of mixing blade for DM installer B and C (all dimensions in mm).

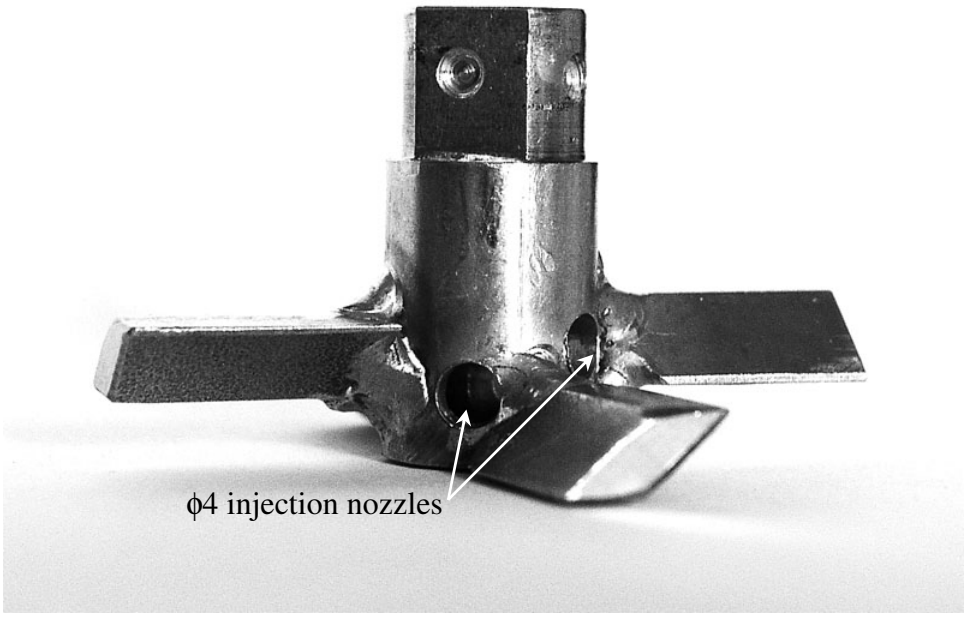

Fig. 3.23 Mixing blade for DM installer B which has two twisted-blades arranged in a double-layered, cruciform fashion.

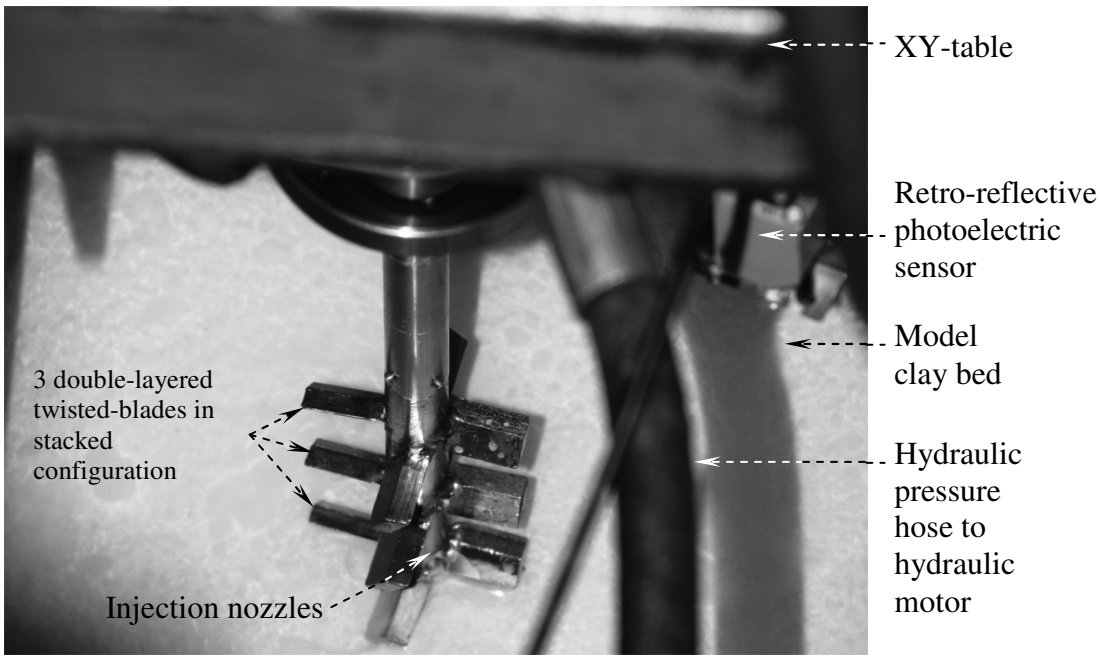

Fig. 3.24 DM installer C mounted on XY-table. The DM installer was positioned at the designated location.

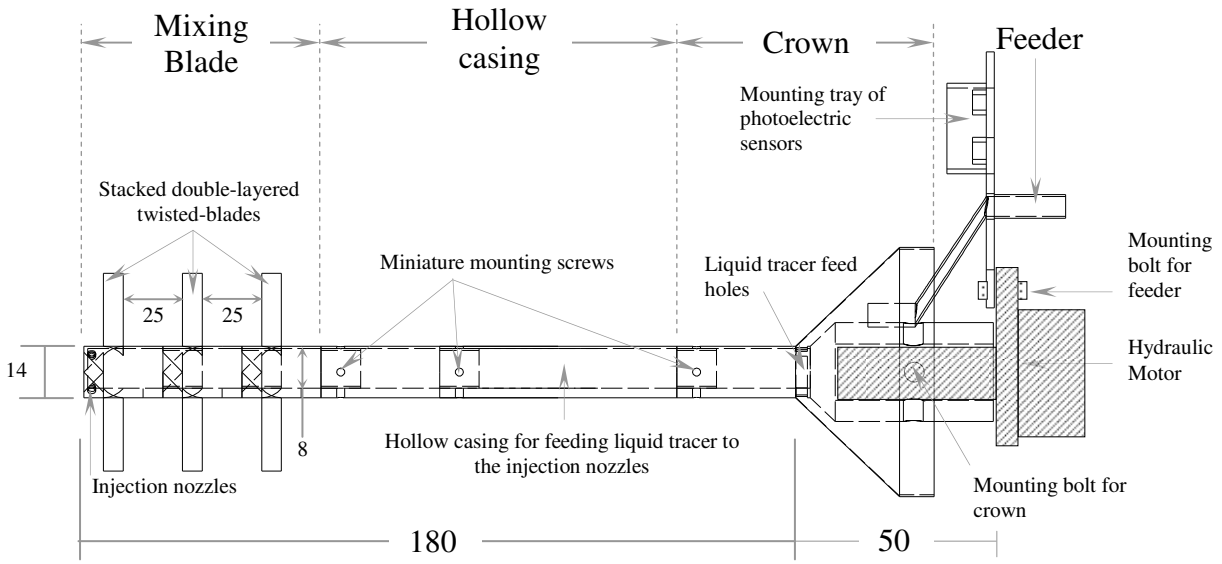

Fig. 3.25 Schematic of in-flight DM installer C (all dimensions in mm).

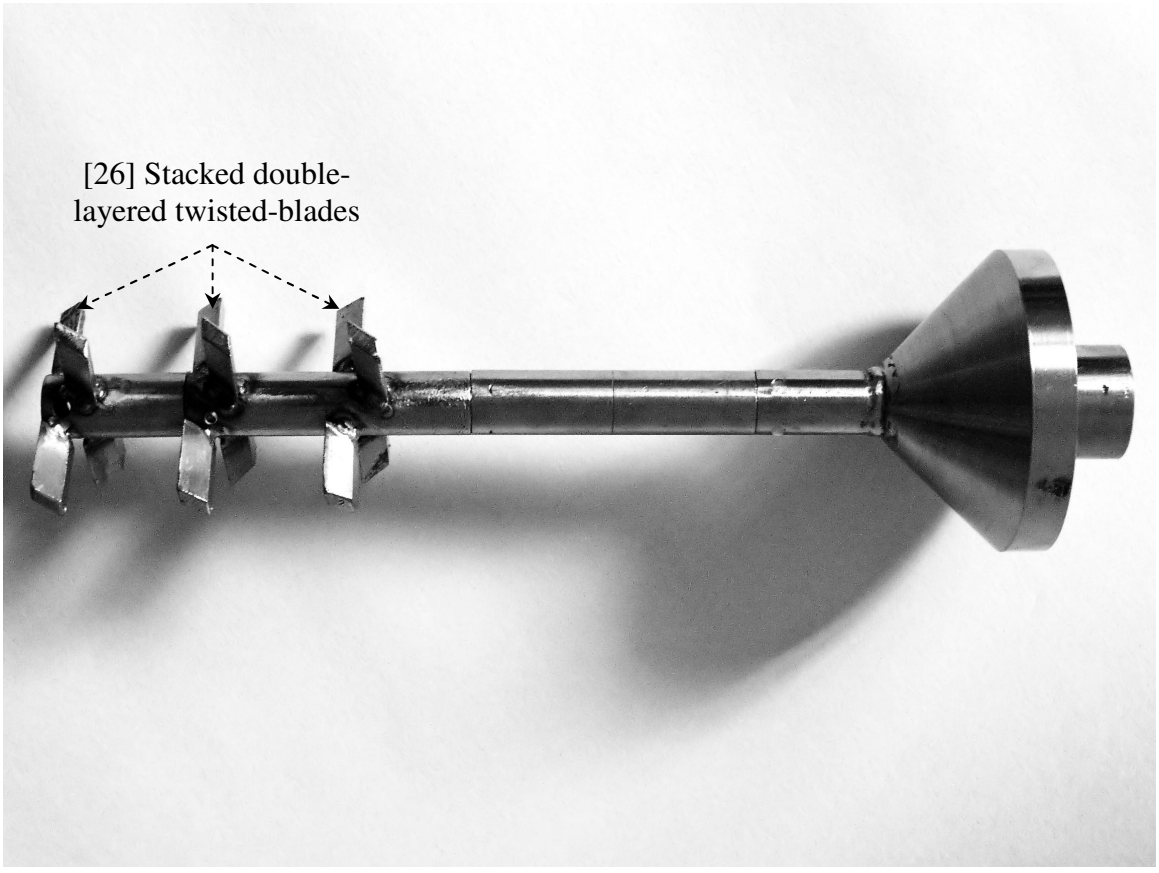

Fig. 3.26 DM installer C with three stacked pairs of double-layered twisted-blades.

Fig. 3.27 De-aring chamber use in remoulding of the kaolin powder.

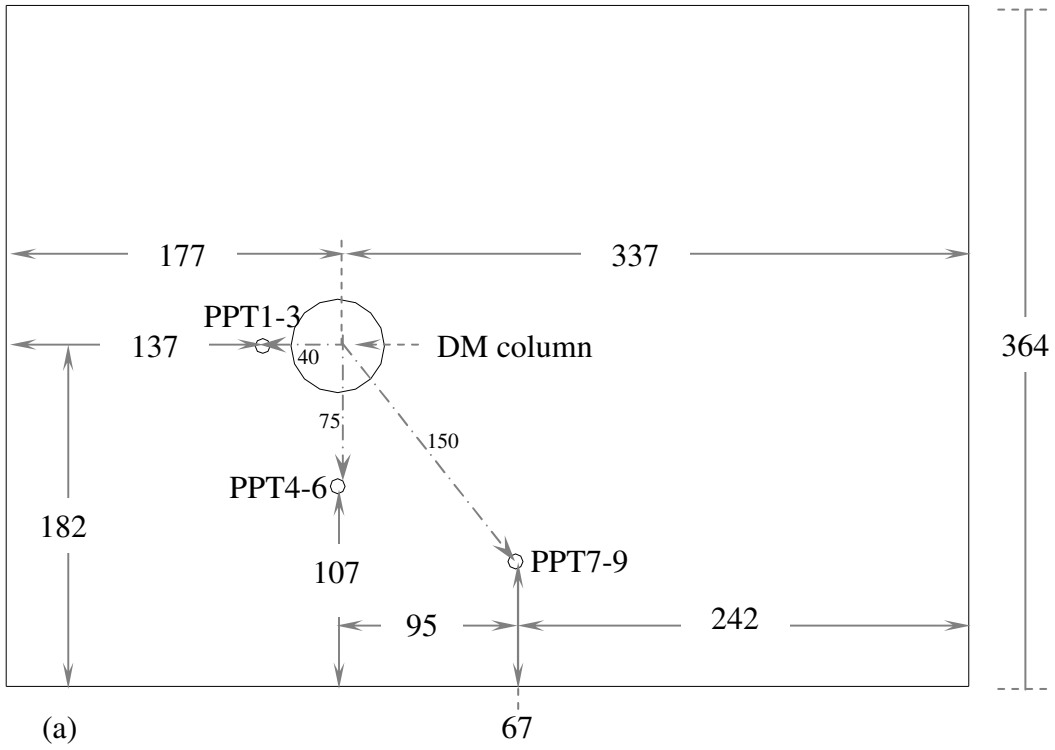

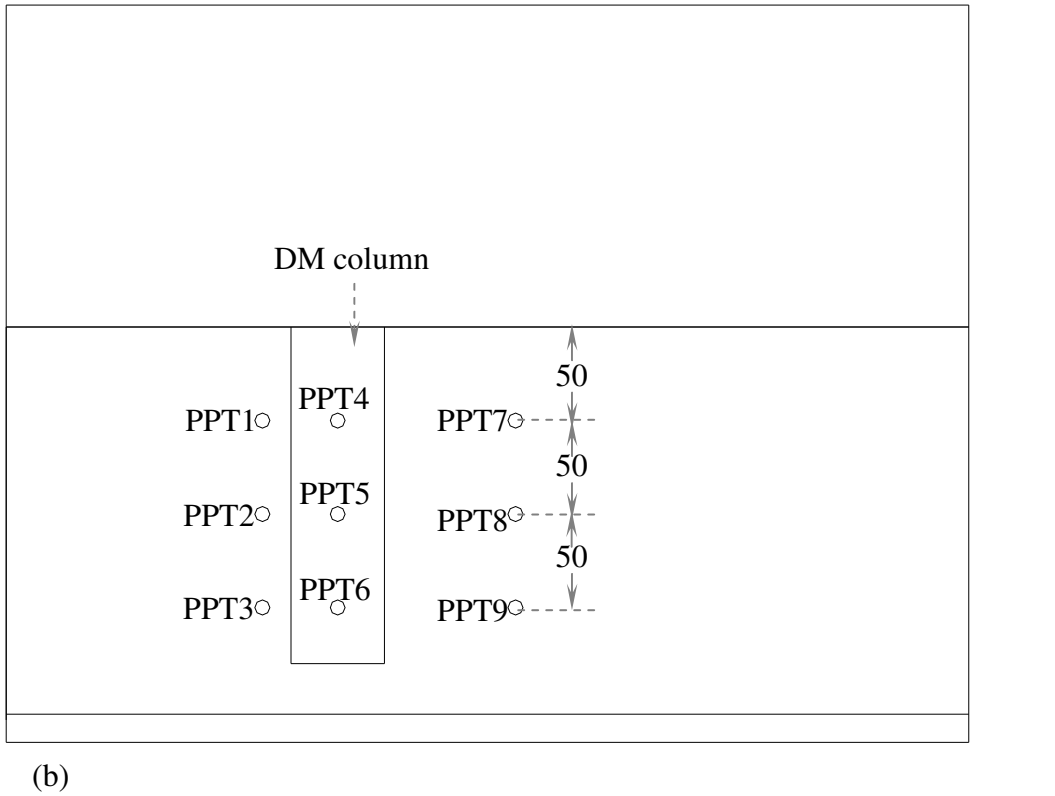

Fig. 3.28 Location of PPTs installed in centrifuge model (a) Plan view (b) Sectional view.

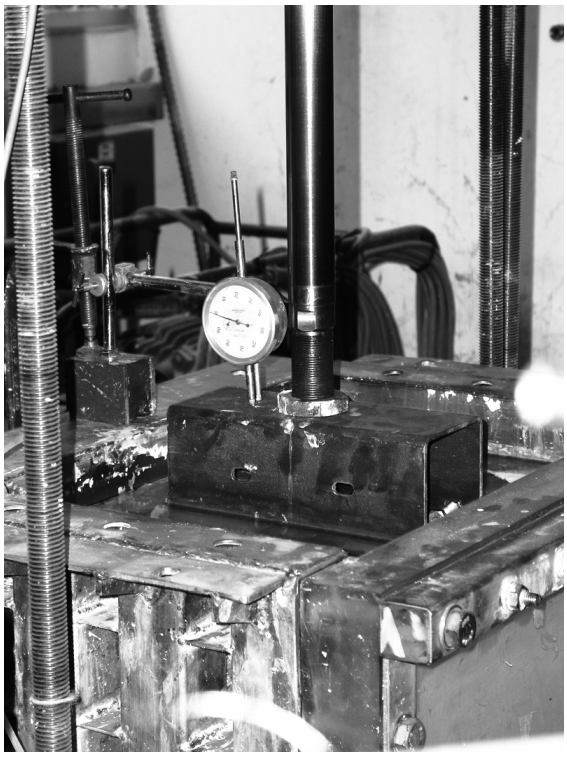

Fig. 3.29 1-g model under surcharge loading.

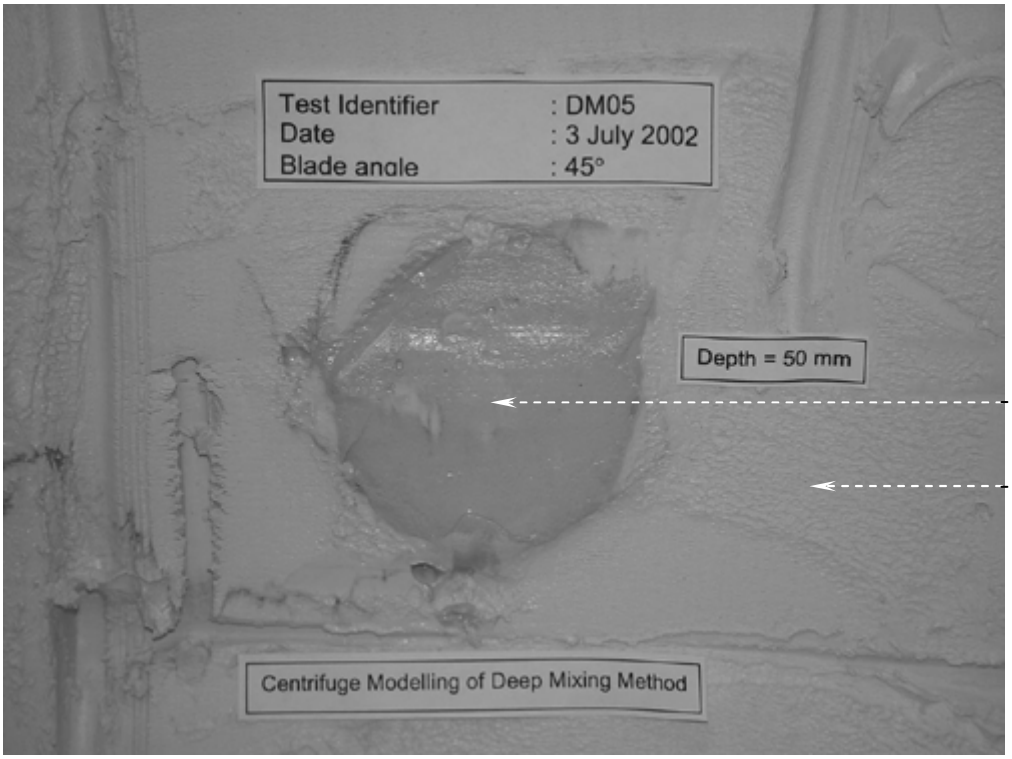

Fig. 3.30 Plane-sectional view of a DM column with a diameter of 50mm at model depth 50mm.

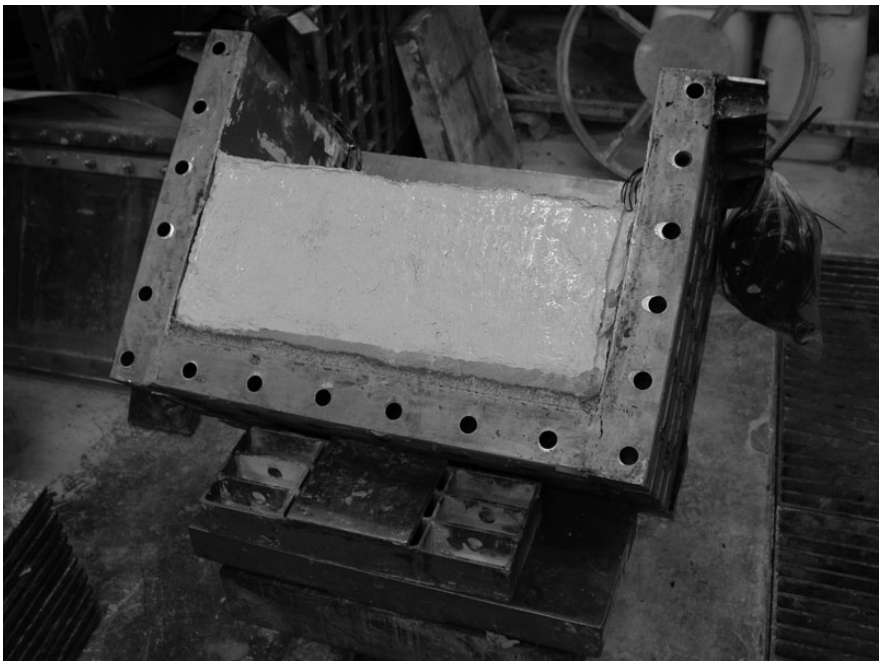

Fig. 3.31 Side wall of the model container were removed so that the model clay bed can be trimmed at prescribed levels using a wire cutter.

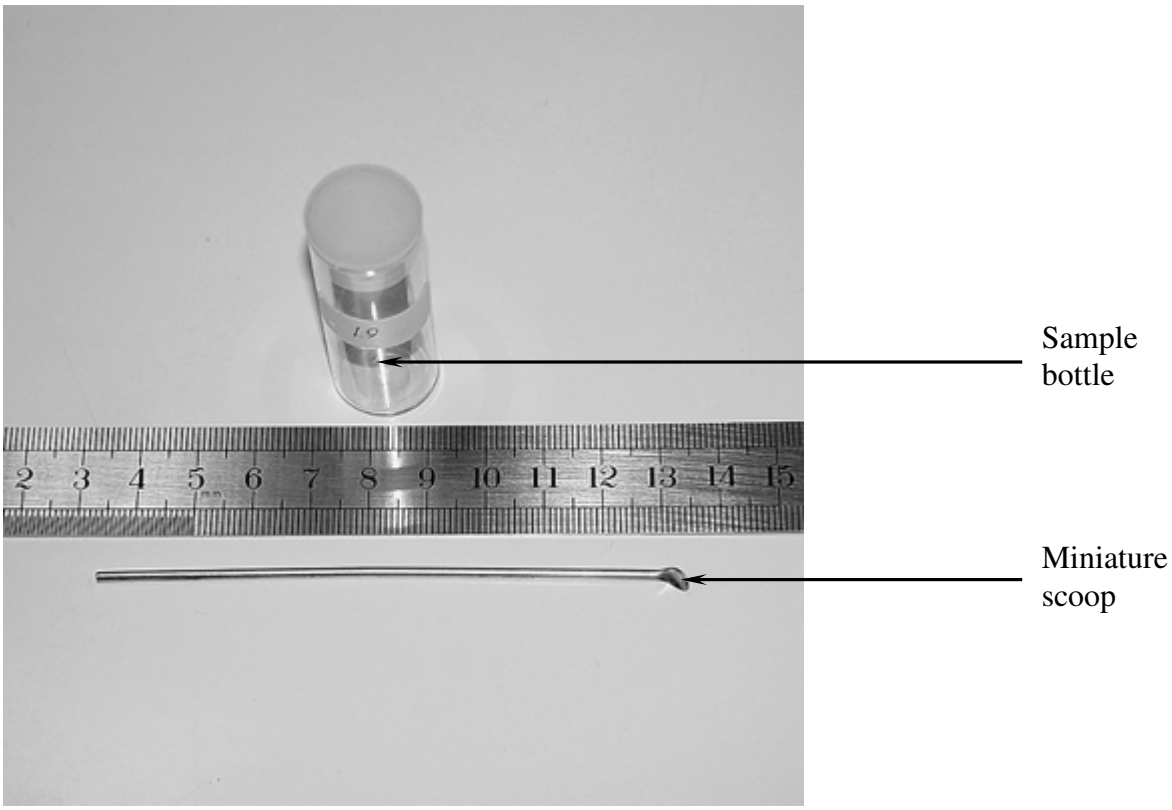

Fig. 3.32 Sample bottle and miniature scoop used to collect soil samples at various locations within the DM column.

Fig. 3.33 DIONEX ion chromatograph.

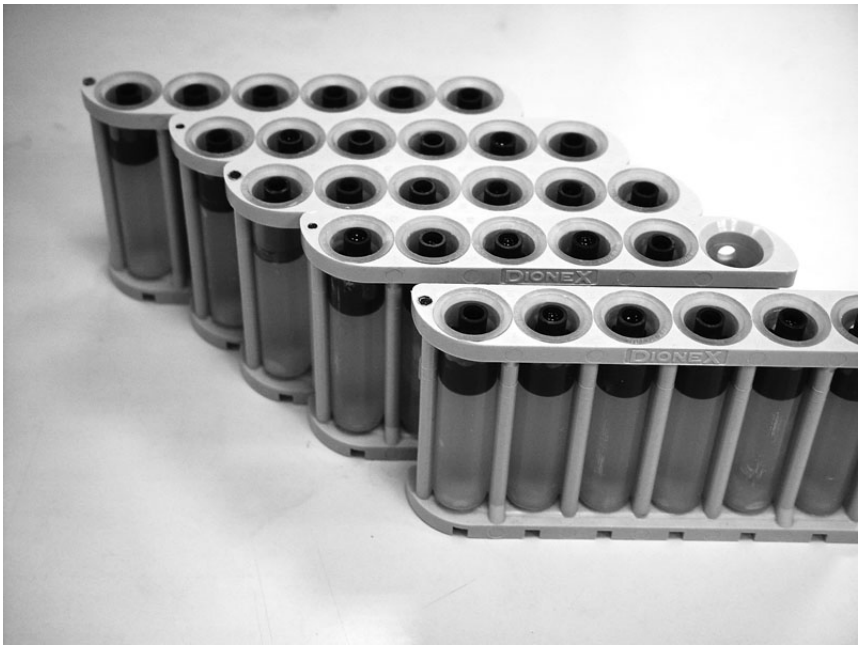

Fig. 3.34 Soil samples were first diluted into de-ionized water and stored in testing tubes.

Chapter 4: Comparison of 1-g Laboratory Model Mixing and Centrifuge Model Mixing

In order to experimentally evaluate the effect of 1-g scaling on the DM method, this chapter will examine and compare experimental results obtained from both 1-g mixing and centrifuge mixing of model binder and soil. As shown in Table 4.1, a series of 14 model tests were conducted in this part of the study. DM installer A was used for all 14 model tests. Model tests 1gD, 1gE and 1gF were performed using zinc chloride as the model binder, with different slurry densities of 1.7g/cm^3, 1.5g/cm^3 and 1.3g/cm^3 respectively. Model tests 1gG, 1gH and 1gI were performed using cement slurry as model binder, with different slurry densities of 1.3g/cm^3, 1.5g/cm^3 and 1.7g/cm^3 respectively. Model tests 1gJ and 1gK were performed using zinc chloride with a high pH (i.e. pH ±13) as model binder, with different slurry densities of 1.3g/cm^3 and 1.5g/cm^3. The high pH was obtained by replacing a portion of the zinc chloride solution with sodium hydroxide. Model tests 1gL, 1gM and 1gN were performed using zinc chloride with high-viscosity as model binder, with different slurry densities of 1.3g/cm^3, 1.5g/cm^3 and 1.7g/cm^3. The higher viscosity was obtained by replacing a portion of the zinc chloride solution with glycerine. Finally, model tests DM05, DM07 and DM08 were performed at 50-g under centrifuge environment using zinc chloride as model binder, with different slurry densities of 1.7g/cm^3, 1.5g/cm^3 and 1.3g/cm^3 respectively.

4.1 Typical Distribution of Concentration of Tracer Ion

Fig. 4.1 shows spot concentration of tracer ion calculated using Eq. 3.1 at various radial distances in some of the model tests. As can be seen, all of the tests show significant variation in spot concentration of tracer ion over the deep-mixed column, which is defined by the diameter of the mixing blade. Comparison also shows that the 1-g tests appear to have a higher level of variation in tracer ion than the 50-g tests. This qualitative impression will be confirmed by quantitative evaluations to be discussed later. The results also show the presence of tracer ion in the region just beyond the reach of the mixing blade. The radius of the model mixing blade was 25mm. As Fig. 4.1 shows, tracer ion is indicated at radii up to about 50mm or twice the mixing blade radius. The reasons for this will be discussed later together with the pore pressure measurements. However, it may be noted that this may not be unrealistic. Shen (1998) reported evidence of hydrofracturing in his field tests on Ariake Clay, in the form of vertical cracks in the core samples and extremely rapid dissipation of excess pore pressure around the DM column He also reported that "…*after the column hardens, there exists a hardened zone in the vicinity of the column (within several percentage of column radius* R_c*) in which the strength is almost same as that of the column. Moreover, in the region to 2.0*R_c*, the shear strength is inclined to be greater than that of the original ground*…". Thus, infiltration of binder outside of the DM column also occurs in field tests.

4.2 Verification of Measured Mean Tracer Ion Mass to the Predicted Value

In this section, the mean tracer ion mass deduced from the mass of model binder used in the test is compared with that deduced from spot concentrations measurements using the mass balance approach. The mean tracer ion mass per unit depth of soil was deduced from the relation

$$w_{bp} = C_o \times \alpha \times \pi \times r_i^2 \qquad (4.1)$$

in which C_o is the mass of the tracer ions per unit volume of slurry, α is the actual volumetric slurry-soil ratio as summarized in Table 4.1, and r_i is the radius of the DM column. The mean tracer ion mass so determined will hereafter be designated as "predicted mean tracer ion mass".

The mean tracer ion mass per unit depth of soil can also be deduced from the measured spot concentration values, using the relation

$$w_b = \left(\frac{a_i}{100} \times (\rho_i \times \pi \times r_i^2)\right) + \left(\frac{a_o}{100} \times \left(\rho_o \times \pi \times (r_o - r_i)^2\right)\right) \qquad (4.2)$$

in which a is the concentration of tracer ions in percentage by total weight. This concentration was calculated using Larsson's (2001) expression, which takes into account the effect of asymmetry of the DM column. ρ is the final density of the soil-binder mixture, r_o is the radius of influence zone when the concentration of tracer ions approaching zero, as illustrated in Fig. 4.2 and the subscripts i and o denote inner column and outer column quantities respectively. As shown in Fig. 4.2, the outer column zone is defined to account for the infiltration of the tracer ion beyond the deep mixing (DM) zone. In Eq.4.2, the first term represents the measured mean tracer ion mass inside the DM zone whereas the second term represents the measured mean

tracer ion mass which has infiltrated to the outside of the DM zone. The mean tracer ion mass deduced using Eq. 4.2 will hereafter be designated as the "measured mean tracer ion mass". In Eq. 4.2, r_i is taken to be the radius of the mixing blade whereas r_o is taken to be the radius at which the concentration falls to a negligible value, typically $2r_i$.

Fig. 4.3 shows the predicted mean tracer ion mass, w_{bp} against the measured mean tracer ion mass, w_b. The predicted mean tracer ion mass and measured mean tracer ion mass are expressed in mass per unit depth [g/cm]. The binder-soil mix density ρ_i and ρ_o can be estimated by assuming that there is no chemical reaction between binder and soil during mixing. Let

$$c_i = \frac{m_b}{m_b + m_s} \tag{4.3}$$

in which m_b and m_s are the masses of binder and soil in the mix. Re-arranging the terms leads to the relation

$$\frac{m_b}{m_s} = \frac{c_i}{1 - c_i} \tag{4.4}$$

The combined density ρ of the binder-soil mix is given by the total mass of binder and soil divided by sum of the volumes of binder and soil v_b and v_s, respectively, i.e.

$$\rho = \frac{m_b + m_s}{v_b + v_s} = \frac{m_b + m_s}{\frac{m_b}{\rho_b} + \frac{m_s}{\rho_s}} \tag{4.5}$$

Substituting Eq. 4.4 into 4.5 leads to

$$\rho = \frac{\rho_b \cdot \rho_s}{\rho_b \cdot (1 - c_i) + \rho_s \cdot c_i} \quad (4.6)$$

The test results indicate that the measured mean tracer ion mass agree well with the predicted value. The mass balance calculation showed that most of the data points fall within ±15% of the actual predicted value. This indicates that the measured tracer ion concentration values sum up to a total mass that is in reasonably good agreement with the total mass of tracer ion used in the mixing.

4.3 Effect of Binder Viscosity

Fig. 4.4 shows the mean concentration and coefficient of variation (COV) in chloride concentration for all depths within the DM column for both 50-g centrifuge tests and 1-g model tests at different slurry density of 1.3g/cm^3, 1.5g/cm^3 and 1.7g/cm^3. The COV in chloride concentration in the DM column was also calculated using Larsson's (2001) expression, which normalizes the variation with respect to the mean concentration. In other words, the mean concentration has already been taken into account in the COV. Table 4.1 summarizes the mean tracer ion concentration and COV in mean tracer ion concentration for all depth within the DM column as plotted in Fig. 4.4. As Fig. 4.4 shows, the lowest COV is obtained in the 50-g centrifuge tests using zinc chloride (model binder) as the replacement prototype binder (cement slurry). The 1-g tests show significantly higher COV than the 50-g tests. This will be discussed further below.

Amongst the 1-g tests, the COV of kaolin-zinc chloride mixture was slightly but consistently lower than that of kaolin-cement slurry mixture at all slurry densities. This

trend is also reflected by the comparison of the relevant tests in Table 4.1 (e.g. 1gF vs. 1gG, 1gE vs. 1gH and 1gD vs. 1gI). This could be explained by the effect of model binder's viscosity on the mixing quality. As discussed in chapter 2, the viscosity of zinc chloride solution is always lower than the viscosity of cement slurry at the same slurry density. Thus under same volumetric slurry-soil ratio, α and slurry density, the kaolin-cement slurry mixture will definitely have a higher viscosity than those of kaolin-zinc chloride mixture. Furthermore, the difference of mixing quality between kaolin-zinc chloride mixture and kaolin-cement mixture also appears to increase when the binder density increases. The details of this effect will be presented in the later section. As discussed, both the cement slurry's and zinc chloride's viscosity will increase with their density. However, this increment of viscosity is more significant in cement slurry than the increment in zinc chloride. Thus, higher viscosity in cement slurry leads to an increase in the COV, which is suggestive of deterioration in mixing quality.

In order to further confirm the above observation, i.e. the effect of model binder's viscosity on the COV, model tests 1gL, 1gM and 1gN have been conducted. Model tests 1gL, 1gM and 1gN were performed using high-viscosity zinc chloride with a low pH as model binder, with different slurry densities of 1.3g/cm^3, 1.5g/cm^3 and 1.7g/cm^3 respectively. The viscosity of zinc chloride for each test was increased so that it is closer to the viscosity of cement slurry at low shear strain rate at its respective densities. The higher viscosity model binder in model tests 1gL, 1gM and 1gN was obtained by replacing approximately 18%, 24% and 26% of the zinc chloride solution by glycerine, which has a density of about 1260kg/m^3 but a viscosity about 600 times that of water. As a result, the viscosity of zinc chloride solution in model tests 1gL,

1gM and 1gN was approximately 14 centipoise (cps) (slurry density 1.3g/cm^3), 20cps (slurry density 1.5g/cm^3) and 24cps (slurry density 1.7 g/cm^3) respectively. The viscosity of zinc chloride-glycerine mixtures is in the same range as that of cement slurry (i.e. about 13.6 to 23.9cps). It is also significantly higher than that of zinc chloride solution used in tests 1gF, 1gE and 1gD, which has a viscosity of 2.7cps (slurry density 1.3g/cm^3), 3.7cps (slurry density 1.5g/cm^3) and 10cps (slurry density 1.7g/cm^3) respectively. Figs. 4.5 to 4.7 show the spot tracer ion concentration at various model depths (denoted by 1D, 2D and 3D; in which D is the diameter of the mixing blade) and radial distances for 1-g test at slurry density of 1.3g/cm^3, 1.5g/cm^3, 1.7g/cm^3. Fig. 4.8 shows the mean tracer ion concentration and COV for different model depth within the DM column for 1-g model tests at different slurry density of 1.7g/cm^3, 1.5g/cm^3 and 1.3g/cm^3. Fig. 4.9 shows mean tracer ion concentration and COV for all depth within the DM column. As can be seen, the mean chloride concentration in the DM column is consistently lower in tests conducted with zinc chloride-glycerine mixture than tests conducted with zinc chloride solution. This is due to the lower concentration of zinc chloride in the binder. Amongst the 1-g zinc chloride tests, the COV of kaolin-zinc chloride-glycerine mixture at higher binder viscosity was consistently higher than that of kaolin-zinc chloride mixture at lower binder viscosity for the corresponding model binder density (e.g. kaolin-zinc chloride-glycerine mixture vs. kaolin-zinc chloride mixture at 1.7g/cm^3). Similar observation was found for the entire range of model binder density (i.e. 1.3g/cm^3, 1.5g/cm^3 & 1.7g/cm^3).These results clearly showed that raising the viscosity of the binder leads to an increase in the COV, which is suggestive of deterioration in mixing quality. Furthermore, the difference in COV for all depth between kaolin-zinc chloride-glycerine mixture and kaolin-cement mixture is smaller than the difference in COV for all depth between

kaolin-zinc chloride mixture and kaolin-cement mixture. This is explained by the fact that the viscosity of zinc chloride-glycerine mixture was adjusted to be closer to the viscosity of cement slurry at low shear strain rate at its respective densities.

4.4 Effect of pH of Model Binder

As pointed out in chapter 2, zinc chloride is chemically very different from cement slurry. For instance, the former has a pH of between 3 and 4 whereas the latter has a pH of about 12. In this section, the possible effects that these chemical differences may have on the validity of the modelling are examined. Two model tests, i.e. 1gJ and 1gK have been conducted to examine the possible effects of these chemical differences. Model tests 1gJ and 1gK were performed using zinc chloride solution with a high pH ±13 as model binder, with different slurry densities of 1.3g/cm^3 and 1.5g/cm^3. The model binder used in model tests 1gJ and 1gK was obtained by replacing approximately 57% and 66% of the zinc chloride solution by sodium hydroxide. The model binder was then filtered to remove all suspensions. The results obtained from this series of tests were then compared with model test 1gF and 1gE. Test 1gF and 1gE were performed using zinc chloride with a low pH ±4 as model binder, with different slurry densities of 1.3g/cm^3 and 1.5g/cm^3. Figs. 4.10 to 4.11 show the spot concentration of tracer ion at various model depths and radial distances for 1-g test at slurry density of 1.3g/cm^3, 1.5g/cm^3. Fig. 4.12 shows the mean tracer ion concentration and COV for difference model depth within the DM column for 1-g model tests at difference slurry density of 1.5g/cm^3 and 1.3g/cm^3. Fig. 4.13 shows mean tracer ion concentration and COV for all depth within the DM column. As can be seen, the differences between COV for all depth obtained from both set of tests i.e. pH ±4 vs.

pH ±13 are rather marginal. At depths of 1D, test 1gJ yields a marginal lower COV than test 1gF; at depth of 3D, test 1gE yields marginally lower COV than test 1gK. The overall COV for both set of tests are nearly equal. This indicates that the pH of binder has trivial effect on the quality of mixing. This is not surprising since in design of mixers, the chemical properties of the substances are usually not considered. The mixing efficiency can often be characterised by the Froude and Reynolds numbers in mechanical mixing process (e.g. Sterbacek and Tausk 1965).

4.5 Effect of Density Difference between Soil and Slurry

Fig. 4.14 shows the variation in mean tracer ion concentration and COV against model binder density in 50-g zinc chloride tests, 1-g zinc chloride tests and 1-g cement slurry tests. In all cases, there is a decrease in the COV as the model binder density increase. This is in spite of the fact that the viscosity will increase with the model binder density, which would have, in the light of previous discussion, result in an increase in COV. It indicates that, apart from the viscosity, the binder density also has a significant effect on the mixing quality. In the case of cement slurry and zinc chloride binders with the same density, then the differences in model binder viscosities can be seen to play a role in affecting the mixing quality; this was discussed in the previous section. In this case, the comparison is between same types of model binder with different densities. The results show that, in this case, the difference in density has a more predominant effect on the mixing quality than differences in viscosity. Thus density difference between binder and soil plays more dominant role than the viscosity in determining the mixing quality, at least in cases where same type of binder is used. This is consistent with previous studies which showed that it is more difficult to

achieve uniform mixing when the density of slurry is different from that of the soil (Yoshizawa et al. 1997). A similar observation has also been reported by Rielly & Pandit (1988) and they showed that Richardson number is the dimensionless group which controls the mixing of two fluids with different density.

4.6 Effect of Centrifuge Scaling on Deep Mixing

Figs. 4.15 to 4.17 show spot tracer ion concentration at various model depths and radial distances for 50-g centrifuge model tests and 1-g model tests at different slurry density of 1.7g/cm^3, 1.5g/cm^3 and 1.3g/cm^3. Fig. 4.18 shows the mean tracer ion concentration and COV for different model depth within the DM column for 50-g centrifuge model tests and 1-g model tests at different slurry density of 1.7g/cm^3, 1.5g/cm^3 and 1.3g/cm^3. Both model tests were intended to model the prototype DM at blade revolution of 15rpm and withdrawal rate of 0.03m/min. As Fig. 4.18 shows, for a given model binder density, the COV is lowest for 50-g mixing with viscosity scaling of the model binder (i.e. zinc chloride), followed by 1-g mixing with a low-viscosity model binder (i.e. zinc chloride) and is the highest for 1-g mixing with a high-viscosity model binder. As can be seen, at all three depths and for all three model binder densities, the lowest COV was obtained in centrifuge tests using zinc chloride, while the highest COV was obtained in 1-g tests using cement slurry. In other words, centrifuge model tests using zinc chloride achieve the most uniform mixing whereas 1-g tests using cement slurry achieve the least uniform mixing. This is readily correlated to the relative magnitude of the viscous forces to other forces (e.g. dynamic pressure and gravity stress), which is lowest in centrifuge tests using zinc chloride and highest in 1-g tests using cement slurry. It is also consistent with the fact that a higher

viscosity and lower rotational rate suppresses turbulence which promotes efficient mixing (e.g. Harnby et al. 1992).

Yoshizawa et al. (1997) measured COV of unconfined compressive strength of field coring in deep-mixed piles formed using slurries of different water-cement ratios. Fig. 4.19 shows their results, obtained by converting water-cement ratio to slurry density, based on a specific gravity of cement of 3.15. Plotted in this figure are also the depth-averaged COV from Fig. 4.18. Strictly speaking, the model tests' results and Yoshizawa et al.'s (1997) results cannot be compared quantitatively since the former relates to chloride and calcium ions concentration whereas the latter relates to unconfined compressive strength. Nonetheless, the general agreement between centrifuge model test and field results, as well as the similarity in the two trends is striking. The 1-g test results, on the other hand, show COV which are far higher than those reported by Yoshizawa et al. (1997).

The observed differences between 1-g and centrifuge models can be explained through the scaling relations. In the 1-g models where the model binder and rate of rotation is the same as the prototype, the model Froude number and model Mobility number are reduced by N times. The model Reynolds number is not so readily defined since cement slurry and the slurry-soil mix are both non-Newtonian. For a Newtonian liquid, the Reynolds number would also have been reduced by N^2 times compared to prototype values. In view of this, even though the liquid is non-Newtonian, one would expect a similar order of magnitude of reduction. This implies that, in the 1-g models, viscous stress is magnified N^2 times relative to the dynamic pressure and N times relative to the gravity stress.

The situation is illustrated in Table 4.2 which summarises the way the various kinds of stresses are altered under different conditions. Each type of stress is normalized with respect to its own prototype level. In this table, the models are assumed to be 100^{th}-scale and are geometrically similar to the prototype. Furthermore, all materials used in the model are assumed to have the same density as their prototype counterparts. As can be seen, centrifuge modelling with full viscosity scaling of the model binder will result in all the stresses being maintained at their prototype values, which will lead to correct scaling. As shown in chapter 2, the use of zinc chloride does not confer full viscosity scaling since the model-to-prototype shear stress ratio ranges between 1 and about 8 depending on the shear strain rate. In this table, a value of 5 has been adopted for illustration. As can be seen, in a 1-g model using cement slurry with rotation rate equal to the prototype rate, the viscous stress is much higher than all the other stresses. In addition, the ratio of the dynamic pressure to the gravity stress is also incorrectly modelled.

The predominance of viscous stress has been known to be detrimental to mixing quality (e.g. Sterbacek and Tausk 1965, Harnby et al. 1992). The viscous effects can be mitigated in 1-g models by increasing the rate of rotation. It can be shown that if $R_m = \sqrt{N} \cdot R_p$, the ratio between inertial, gravity, buoyancy and centrifugal stress can be preserved at prototype values, but viscous stress are still over-scaled by roughly $N^{3/2}$ (1000 times in Table 4.2) times. Thus, the degree of viscosity scaling needed in 1-g model will still be higher than that for centrifuge models, in fact, of the order of $N^{3/2}$ times, see Table 4.2. Increasing R_m beyond $\sqrt{N} \cdot R_p$ will lead to overscaling of inertial

and centrifugal stress in relation to gravity stress; preliminary tests showed that this was manifested by increased splashing of the tracer-soil mix.

One possible case wherein over-scaling of viscous stress might have degraded the mixing quality in the model is in the 1g-model tests reported by Al-Tabbaa and Evans (1999). In their experiments, cement slurry was used as a model binder. Two different model augers were used in their experiments as shown in Fig. 4.20. Auger 1 is geometrically similar to the prototype auger whereas Auger 2 is not. Al-Tabbaa and Evans (1999) reported that "… *Auger 2 produced higher strengths, which were almost twice those produced by auger 1. In addition, auger 1 produced far more variability between the top and base halves of the columns: in the made ground, the UCS of the top sample was half that of the base sample, while in the sand and gravel the top sample was 50% stronger than the base sample. Weaker column bases have been reported in the literature (Day and Ryan, 1995) and have been related to the presence of insufficient grout and inadequate mixing. The observation of a weaker top part is possibly related to the same effects. Hence these results show that the design of auger 2 is far more effective in producing homogeneous mixing than that of auger 1*…". It is uncertain what rotation rate was used by Al-Tabbaa and Evans (1999). Nonetheless, the symptoms reported by them seem strongly suggestive of poor mixing arising from over-scaling of viscous stresses.

Table 4.1 Mean concentration and coefficient of variation (COV) for all depth within the DM column for 50-g and 1-g model tests at different slurry density of 1.3g/cm^3, 1.5g/cm^3 and 1.7g/cm^3.

Model test identifier	**Model Env. [g]**	**Type of Model Binder**	**Density of Model Binder [g/cm^3]**	**Model Blade Revolution [rpm]**	**Model Penetration Rate [m/min]**	**Model Withdrawal Rate [m/min]**	**Mean Tracer Ion Concentration [% by Total Weight]**	**Mean Tracer Ion Concentration COV**	**Slurry Insertion ratio, α**
DM08	50	Zinc chloride	1.3	770	0.03	0.03	7.36	0.44	0.37
1gF	1	Zinc chloride	1.3	15	0.03	0.03	7.2	0.60	0.37
1gG	1	Cement slurry	1.3	15	0.03	0.03	3.37	0.62	0.33
1gJ	1	Zinc chloride + Sodium hydroxide	1.3	15	0.03	0.03	2.87	0.59	0.37
1gL	1	Zinc chloride + glycerine	1.3	15	0.03	0.03	5.68	0.65	0.36
DM07	50	Zinc chloride	1.5	770	0.03	0.03	8.01	0.32	0.36
1gE	1	Zinc chloride	1.5	15	0.03	0.03	7.80	0.50	0.33
1gH	1	Cement slurry	1.5	15	0.03	0.03	5.26	0.57	0.35
1gK	1	Zinc chloride + Sodium hydroxide	1.5	15	0.03	0.03	2.89	0.52	0.36
1gM	1	Zinc chloride + glycerine	1.5	15	0.03	0.03	6.53	0.59	0.35
DM05	50	Zinc chloride	1.7	770	0.03	0.03	9.75	0.13	0.36
1gD	1	Zinc chloride	1.7	15	0.03	0.03	9.45	0.46	0.32
1gI	1	Cement slurry	1.7	15	0.03	0.03	7.25	0.54	0.34
1gN	1	Zinc chloride + glycerine	1.7	15	0.03	0.03	6.97	0.54	0.34

Table 4.2 Relation between various stresses (normalized with respect to its own prototype level) under different conditions.

Condition	Viscous Stress	Inertial Stress (dynamic pressure)	Gravity Stress	Centrifugal Stress	Buoyancy Stress
Prototype	1	1	1	1	1
100-g centrifuge model with cement slurry	100	1	1	1	1
100-g centrifuge model with zinc chloride (at model/prototype stress ratio of 5)	5	1	1	1	1
100-g centrifuge model with full viscosity scaling (i.e. using model binder with 100 times reduced in viscosity)	1	1	1	1	1
1-g model with cement slurry, model rotation rate = prototype rotation rate	1	0.0001	0.01	0.0001	0.01
1-g model with zinc chloride, model rotation rate = prototype rotation rate	0.05	0.0001	0.01	0.0001	0.01
1-g model with cement slurry, model rotation rate = 10×prototype rotation rate	10	0.01	0.01	0.01	0.01
1-g model with zinc chloride, model rotation rate = 10×prototype rotation rate	0.5	0.01	0.01	0.01	0.01
1-g model with model binder with 100 times reduced in viscosity, model rotation rate = 10×prototype rotation rate	0.1	0.01	0.01	0.01	0.01

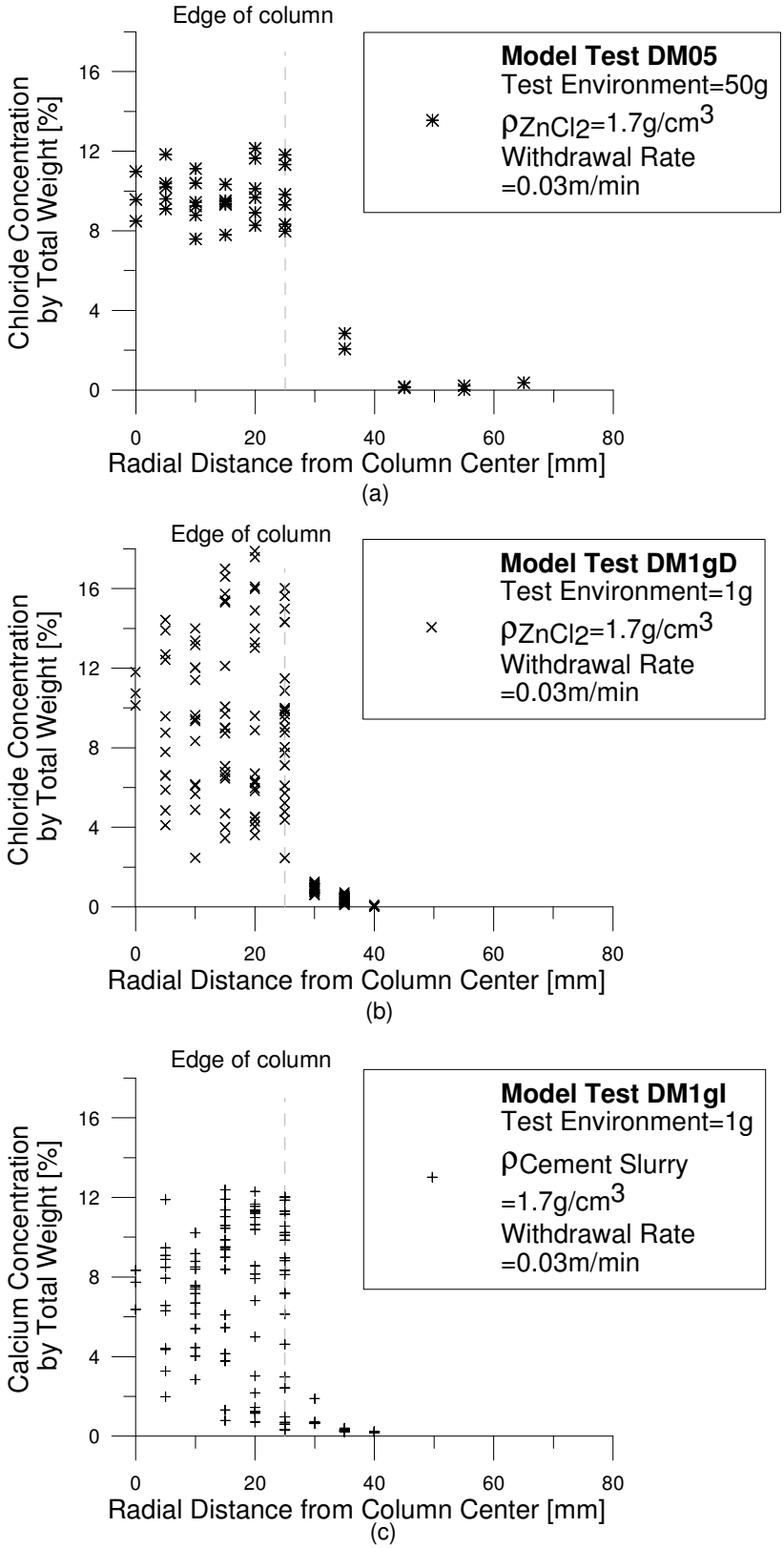

Fig. 4.1 Variation of spot concentration at various radial distances in some of the model tests.

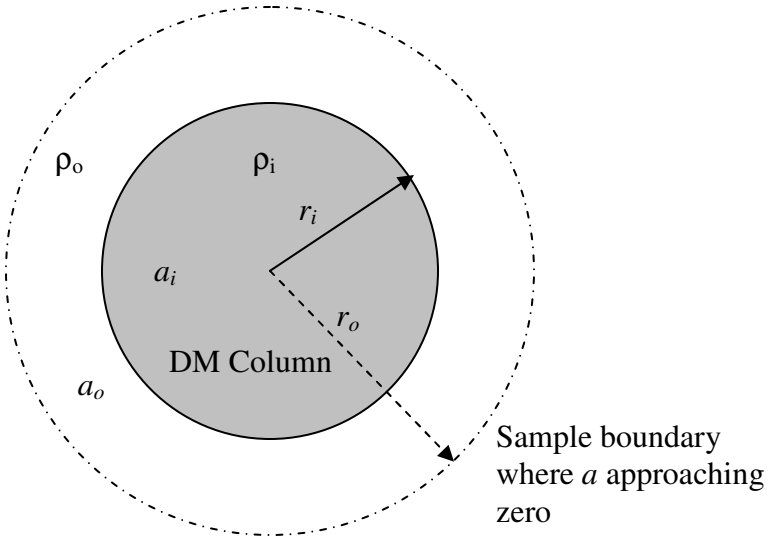

Fig. 4.2 Calculation of mean tracer ion mass in unit depth of soil from soil samples.

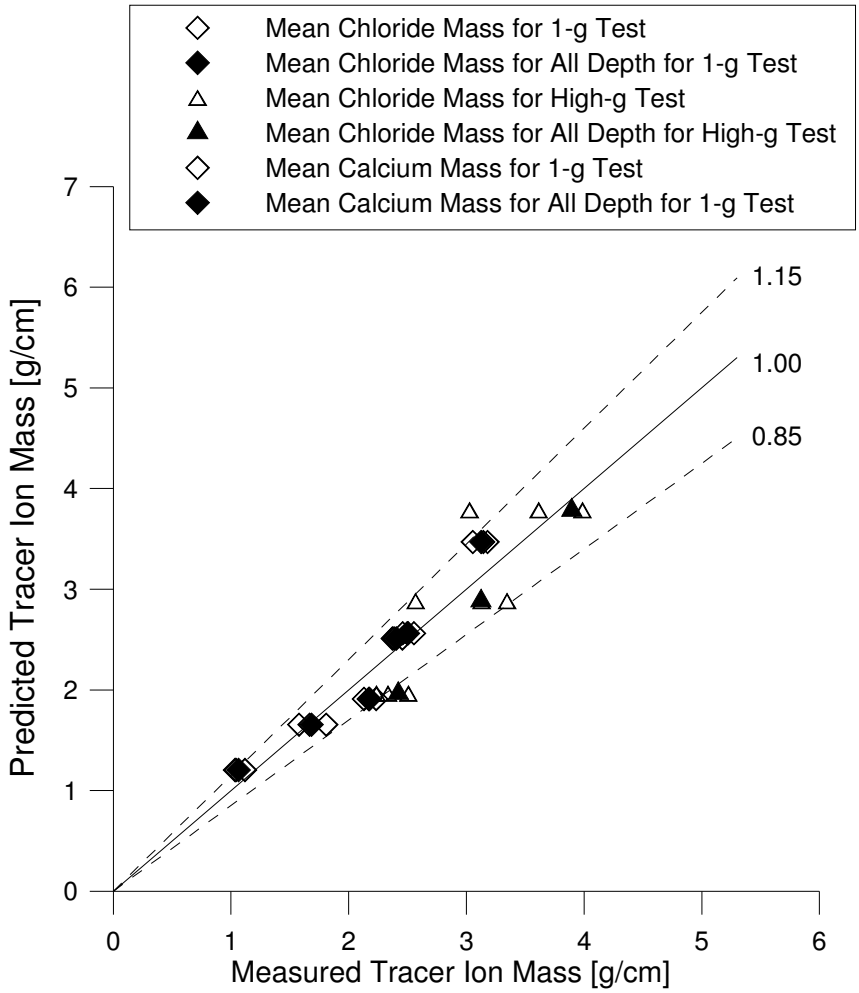

Fig. 4.3 Predicted mean tracer ion mass to the measured mean tracer ion mass of the model tests.

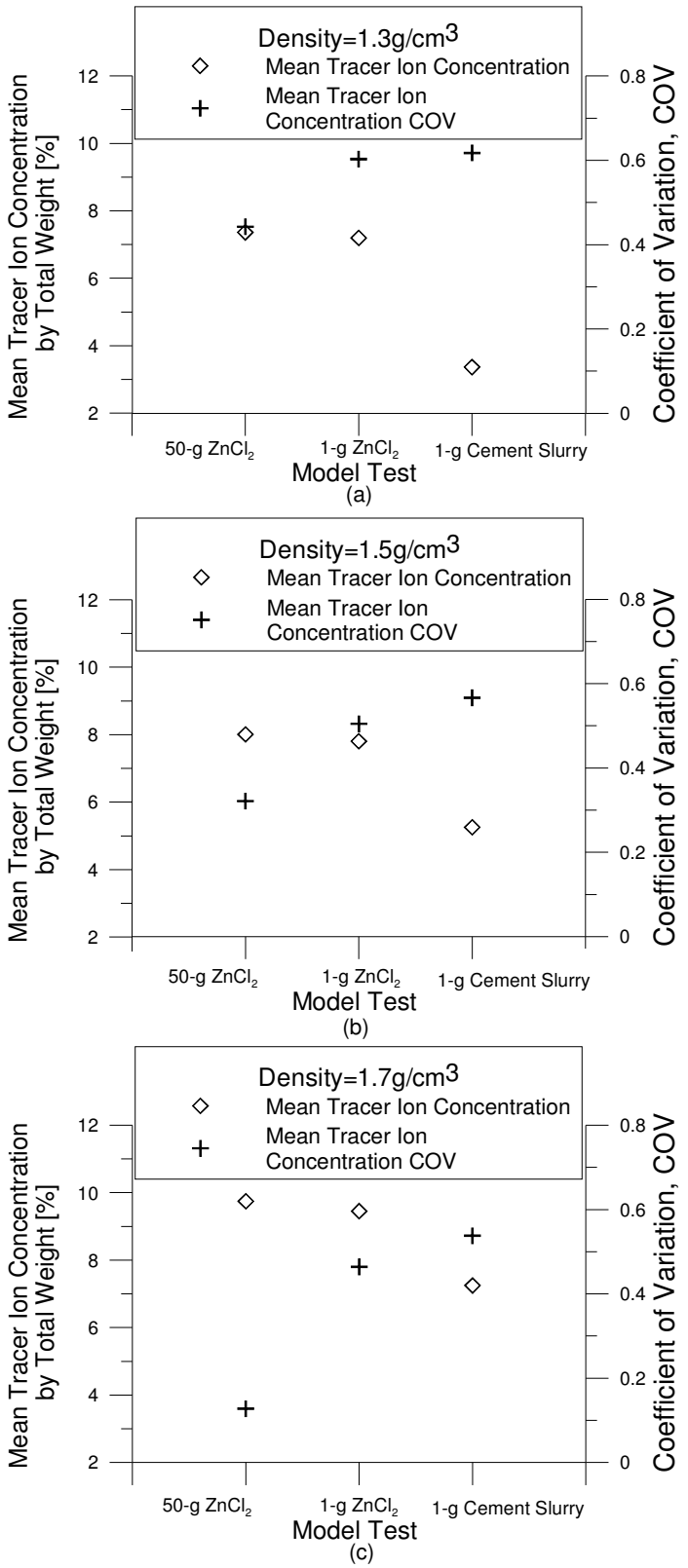

Fig. 4.4 Mean concentration and coefficient of variation for all depth within the DM column for high-g and 1-g model tests at different slurry density of 1.3g/cm^3, 1.5g/cm^3 and 1.7g/cm^3.

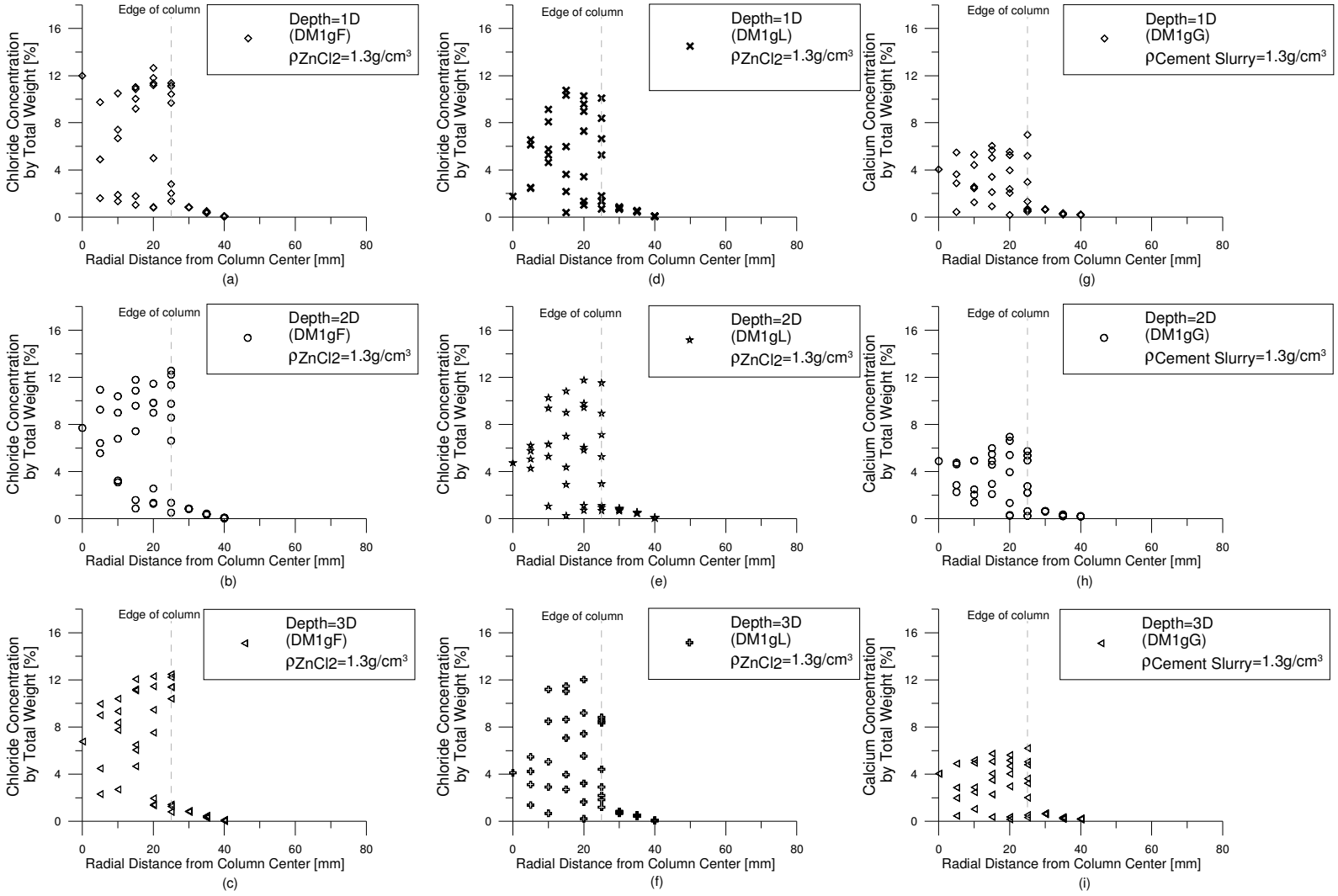

Fig. 4.5 Spot concentration at various model depths and radial distances for 1-g test DM1gF ($ZnCl_2$), 1-g test DM1gL ($ZnCl_2$-glycerine) and DM1gG (cement slurry) at slurry density of 1.3g/cm^3.

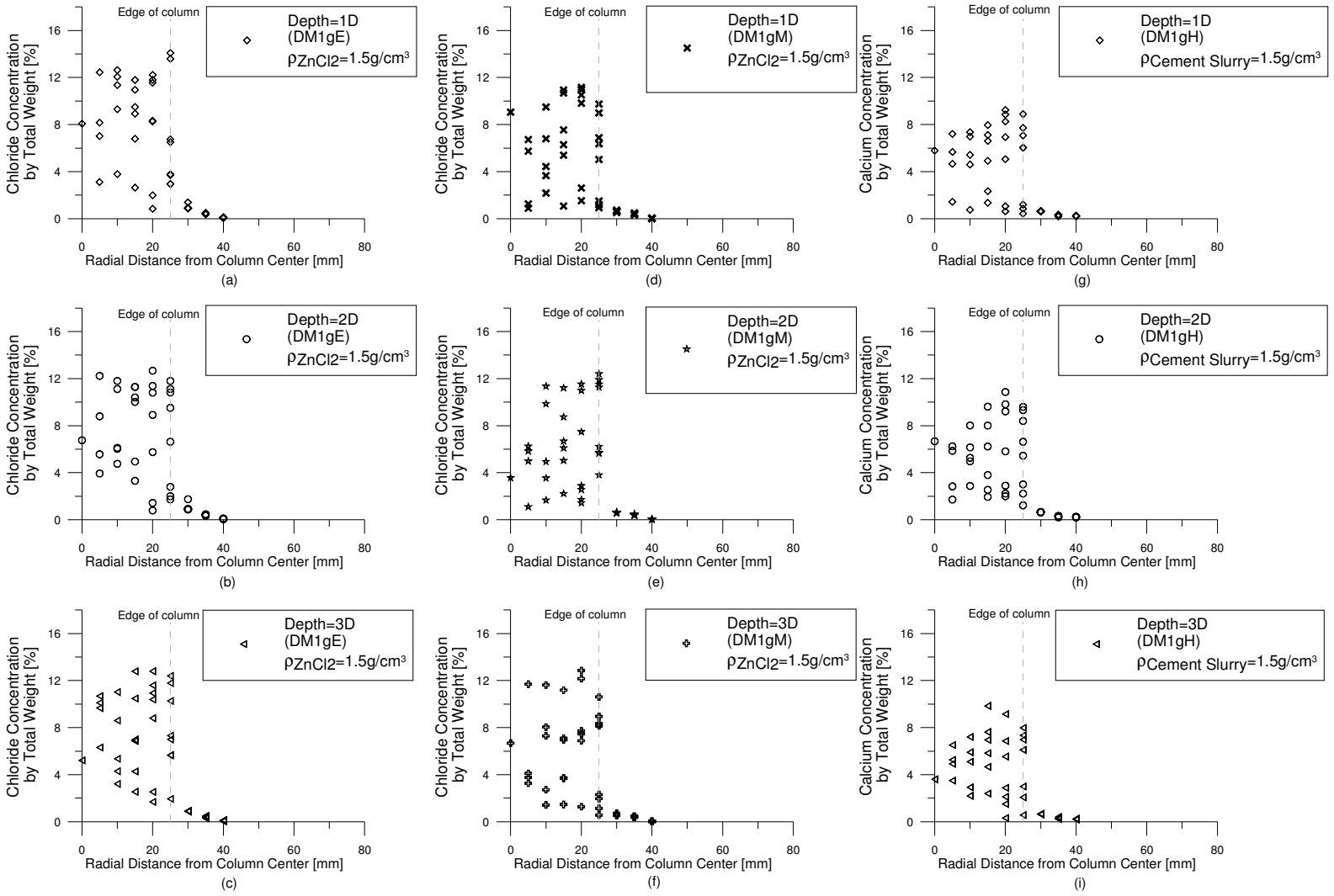

Fig. 4.6 Spot concentration at various model depths and radial distances for 1-g test DM1gE ($ZnCl_2$), 1-g test DM1gM ($ZnCl_2$-glycerine) and DM1gH (cement slurry) at slurry density of 1.5g/cm^3.

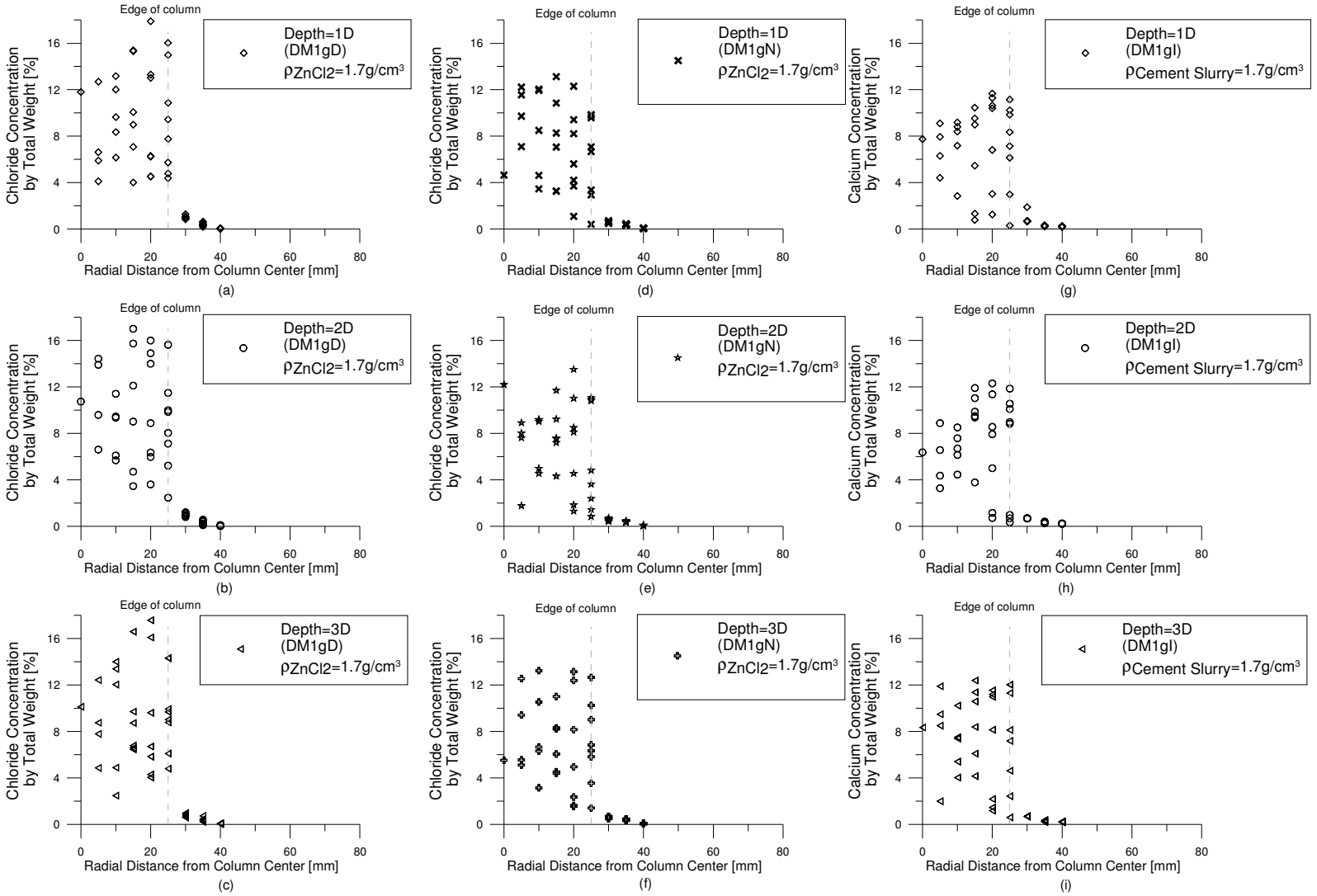

Fig. 4.7 Spot concentration at various model depths and radial distances for 1-g test DM1gD ($ZnCl_2$), 1-g test DM1gN ($ZnCl_2$-glycerine) and DM1gI (cement slurry) at slurry density of 1.7g/cm^3.

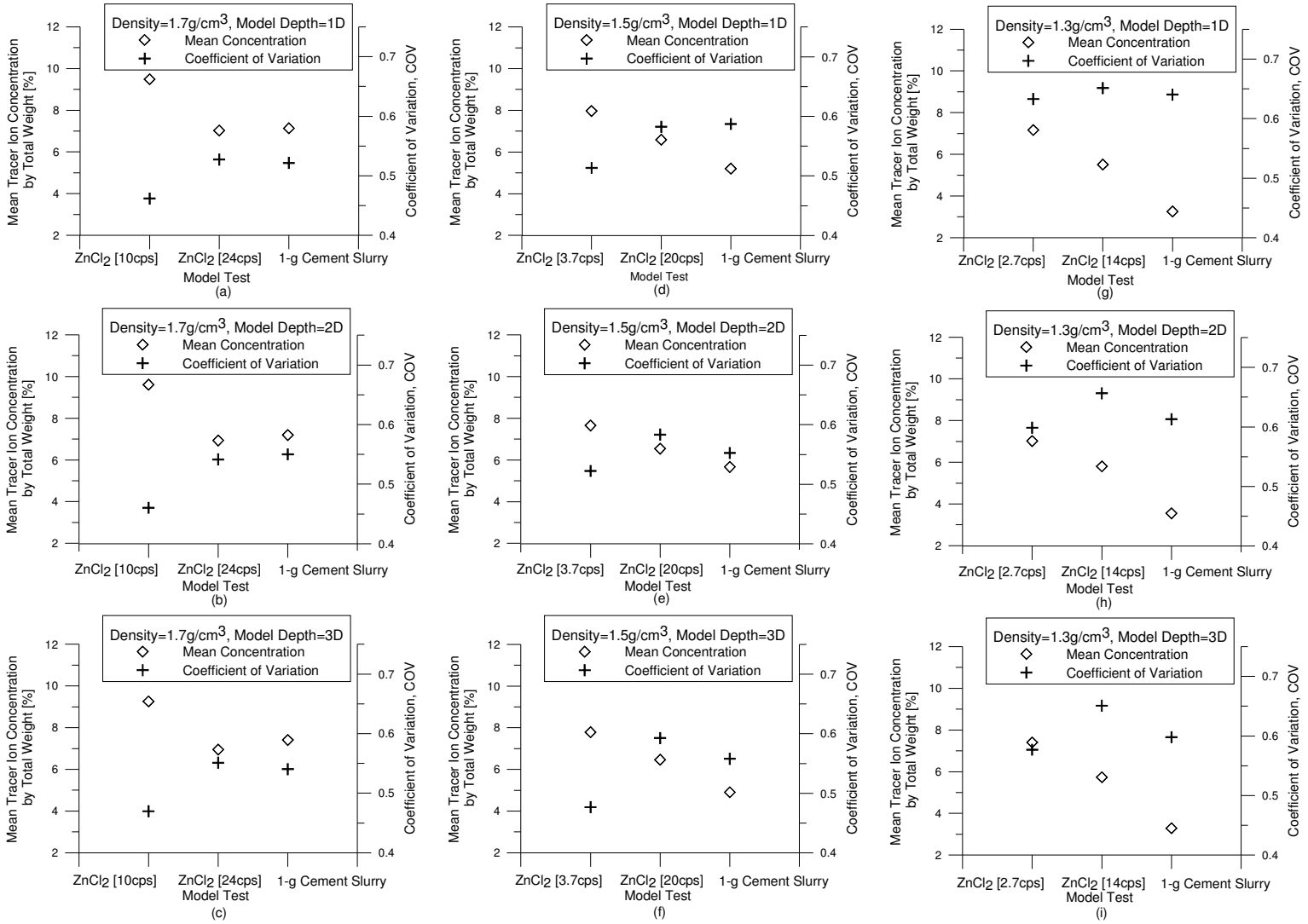

Fig. 4.8 Mean concentration and coefficient of variation for difference model depth within the DM column for 1-g model tests at difference slurry density of 1.7g/cm^3, 1.5g/cm^3 and 1.3g/cm^3.

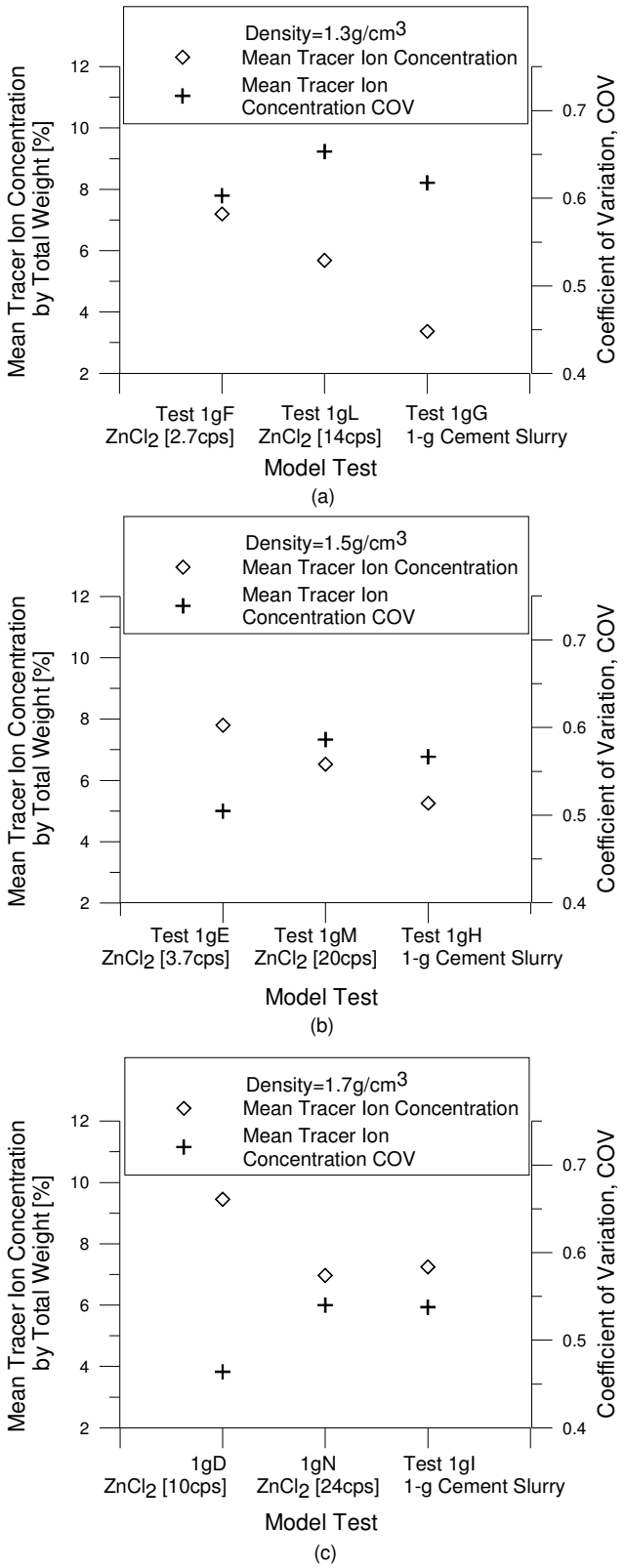

Fig. 4.9 Mean concentration and coefficient of variation for all depth within the DM column for 1-g model tests at different slurry density of 1.3g/cm^3, 1.5g/cm^3 and 1.7g/cm^3.

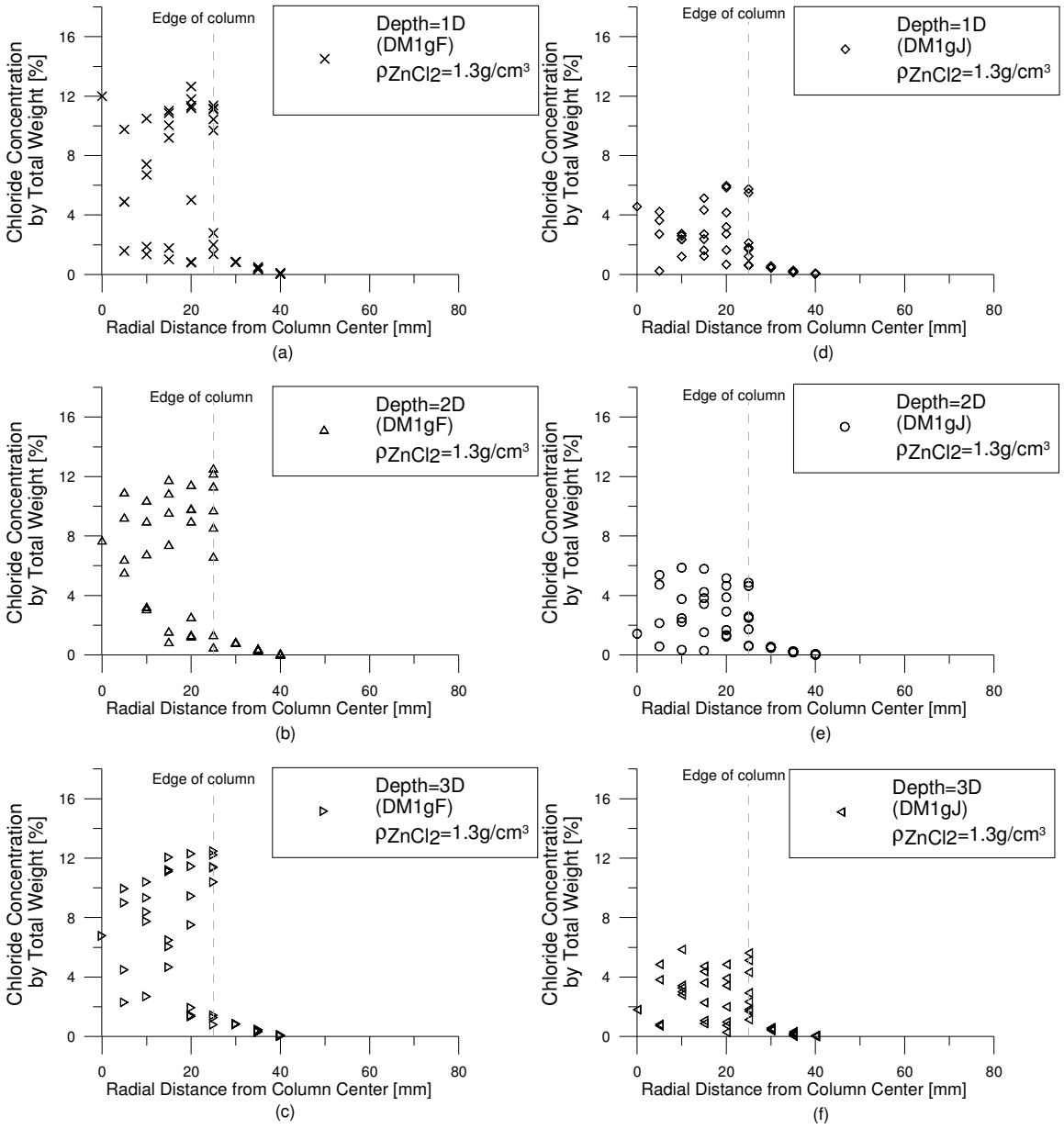

Fig. 4.10 Spot concentration at various model depths and radial distances for 1-g test DM1gF (binder pH ±4) and DM1gJ (binder pH ±13) at slurry density of 1.3g/cm^3.

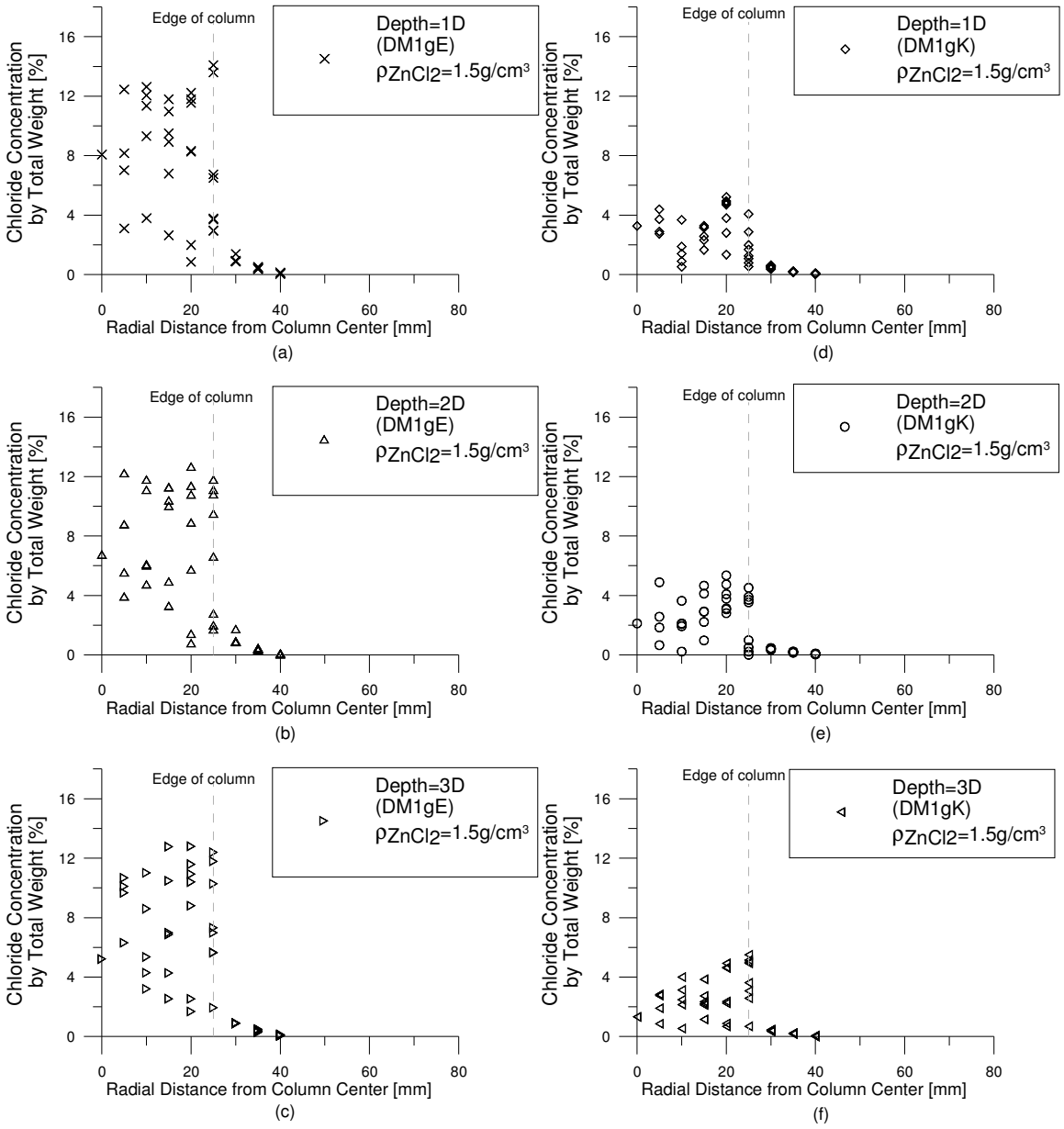

Fig. 4.11 Spot concentration at various model depths and radial distances for 1-g test DM1gE (binder pH ±4) and DM1gK (binder pH ±13) at slurry density of 1.5g/cm^3.

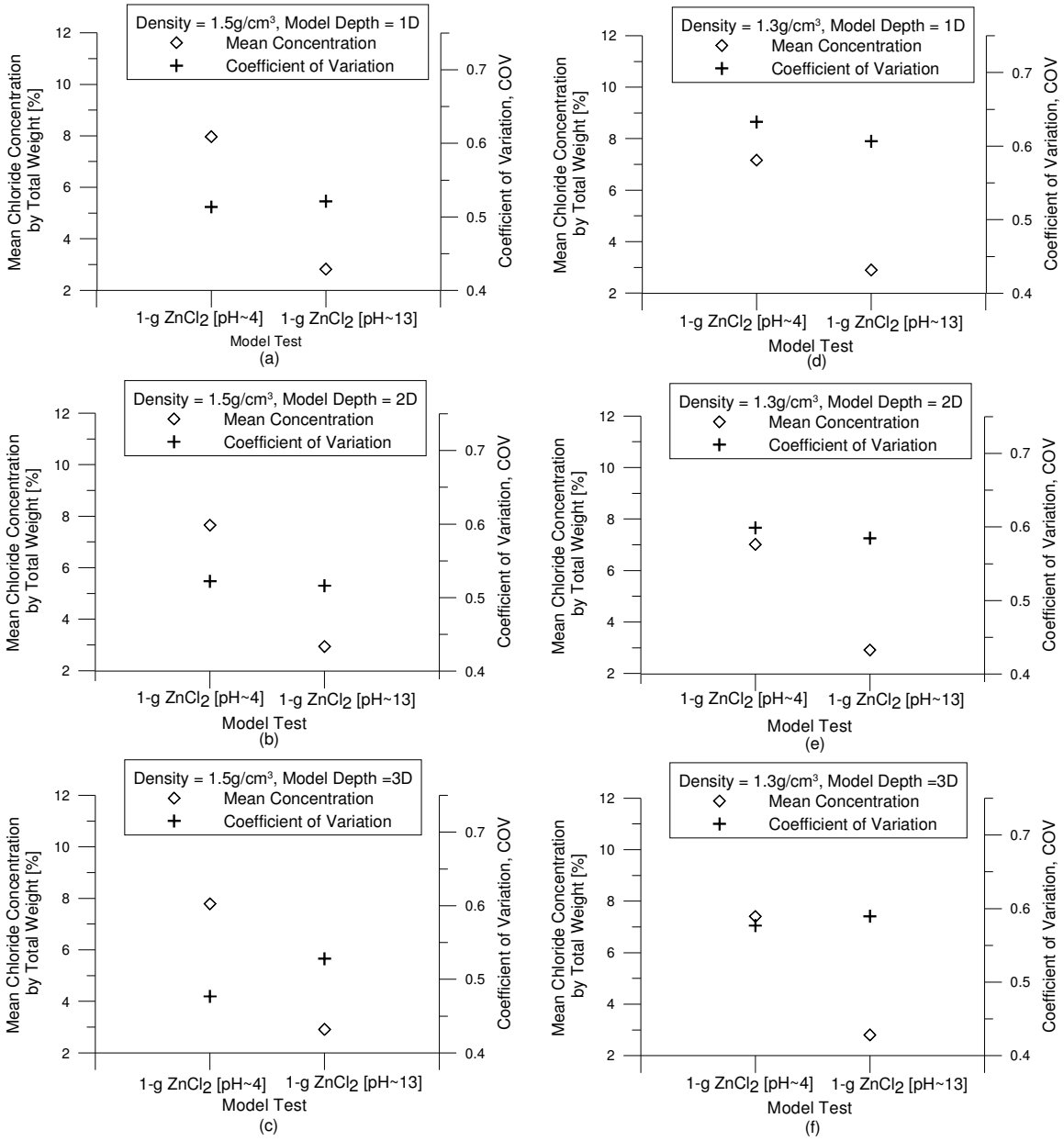

Fig. 4.12 Mean concentration and coefficient of variation for difference model depth within the DM column for 1-g model tests at difference slurry density of 1.5g/cm^3, 1.3g/cm^3.

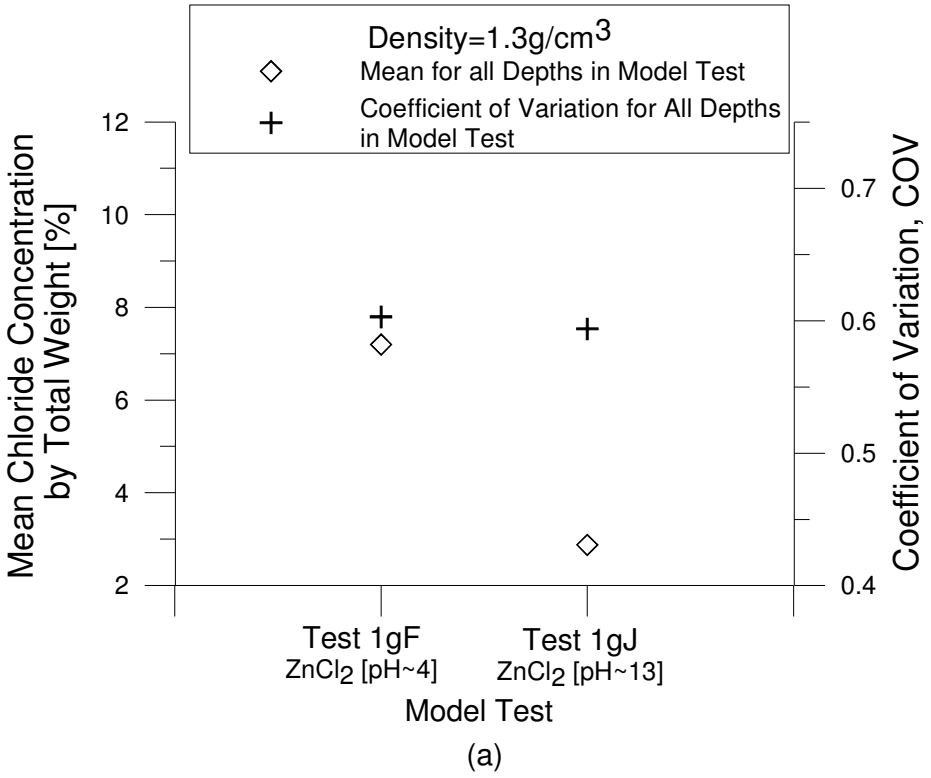

(a)

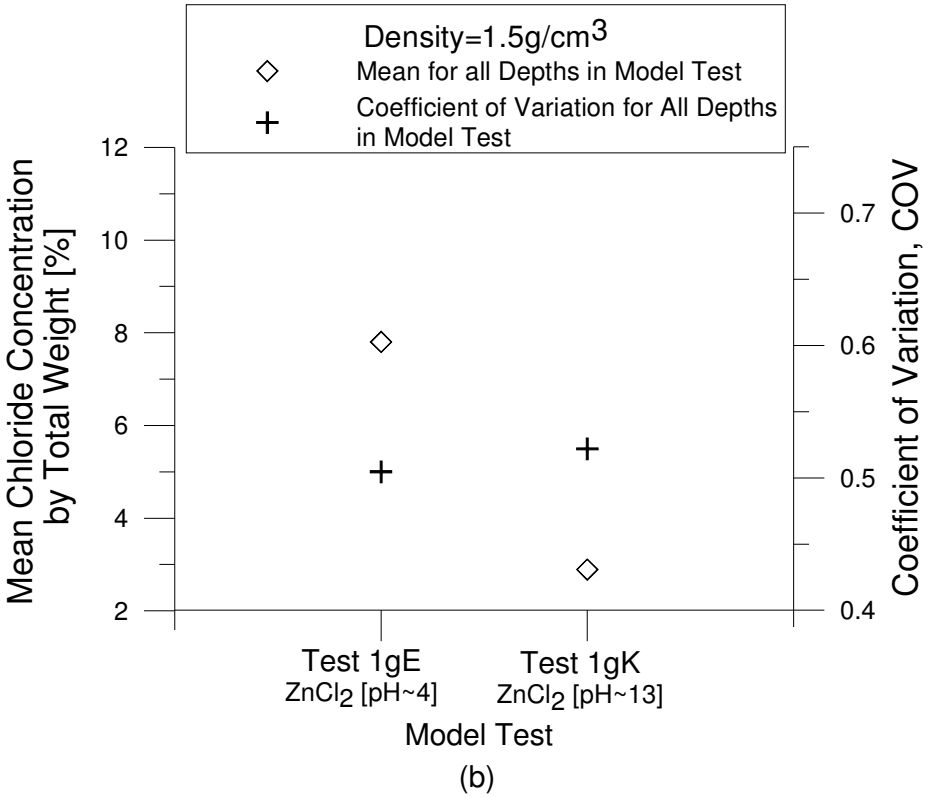

(b)

Fig. 4.13 Mean concentration and coefficient of variation for all depth within the DM column for 1-g model tests at different slurry density of 1.3g/cm^3, 1.5g/cm^3.

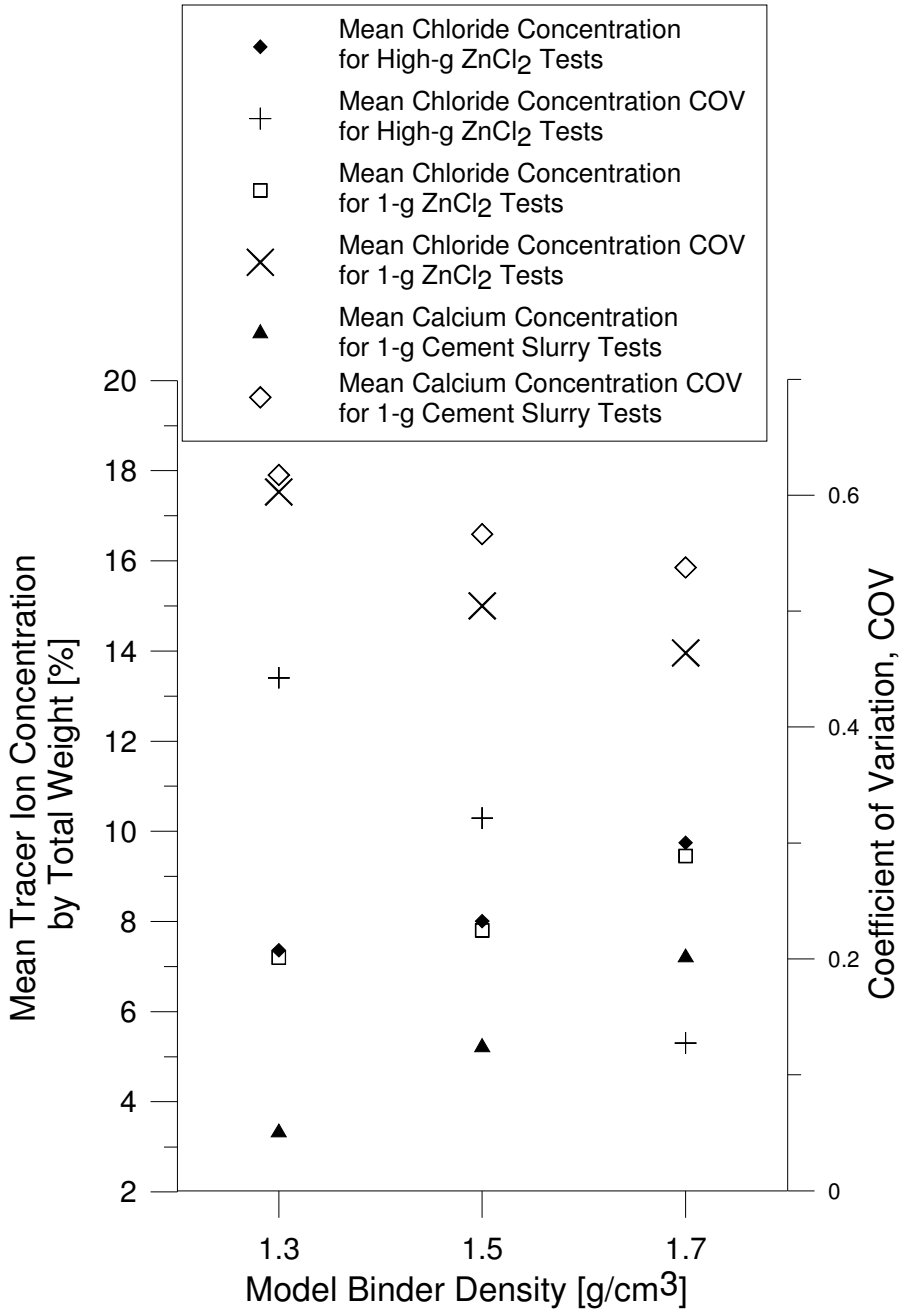

Fig. 4.14 Mean concentration and coefficient of variation for all depth within the DM column for high-g and 1-g model tests at different slurry density of 1.3g/cm^3, 1.5g/cm^3 and 1.7g/cm^3.

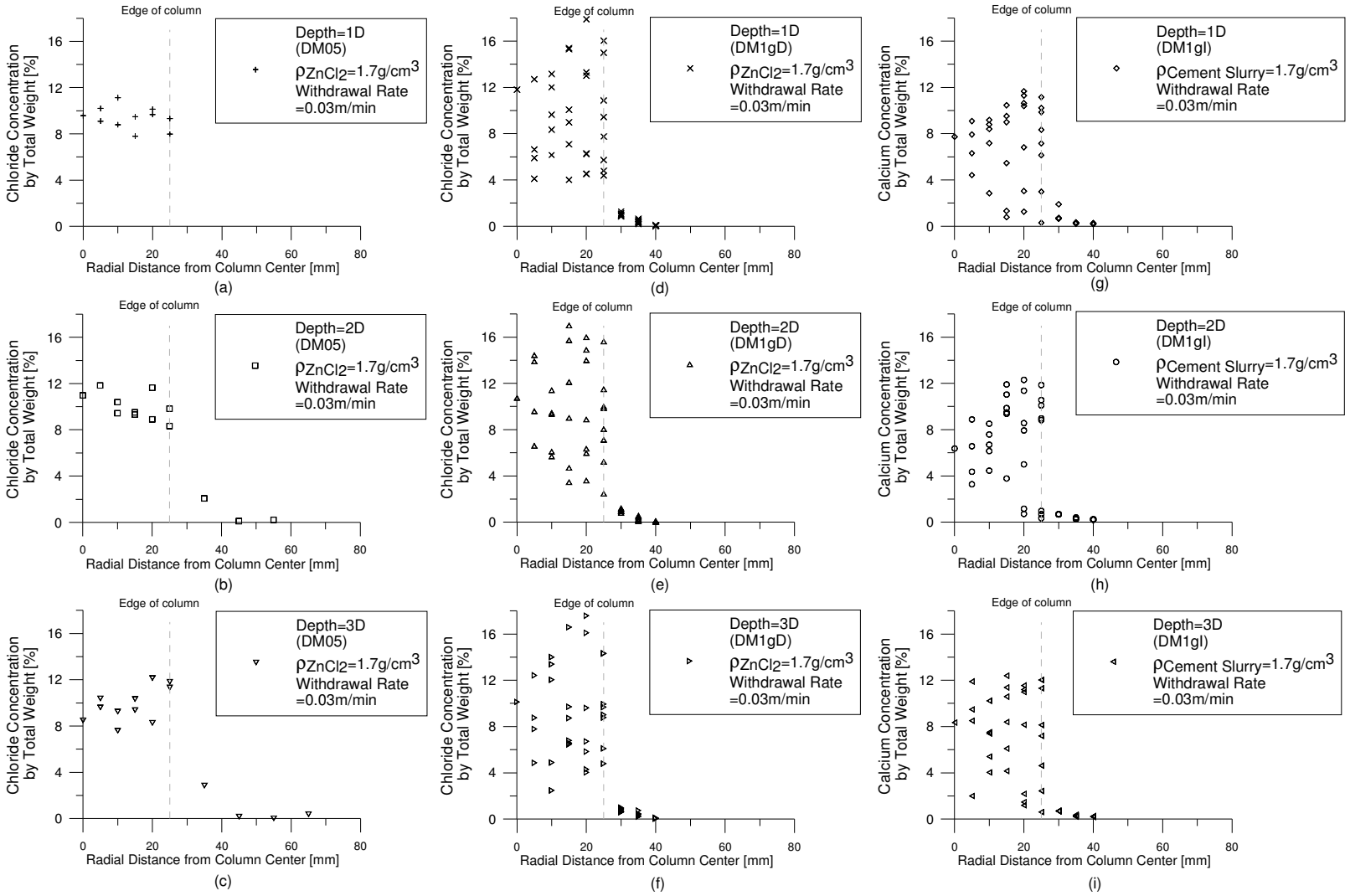

Fig. 4.15 Spot concentration at various model depths and radial distances for high-g test DM05 ($ZnCl_2$), 1-g test DM1gD ($ZnCl_2$) and DM1gI (cement slurry) at slurry density of 1.7g/cm^3.

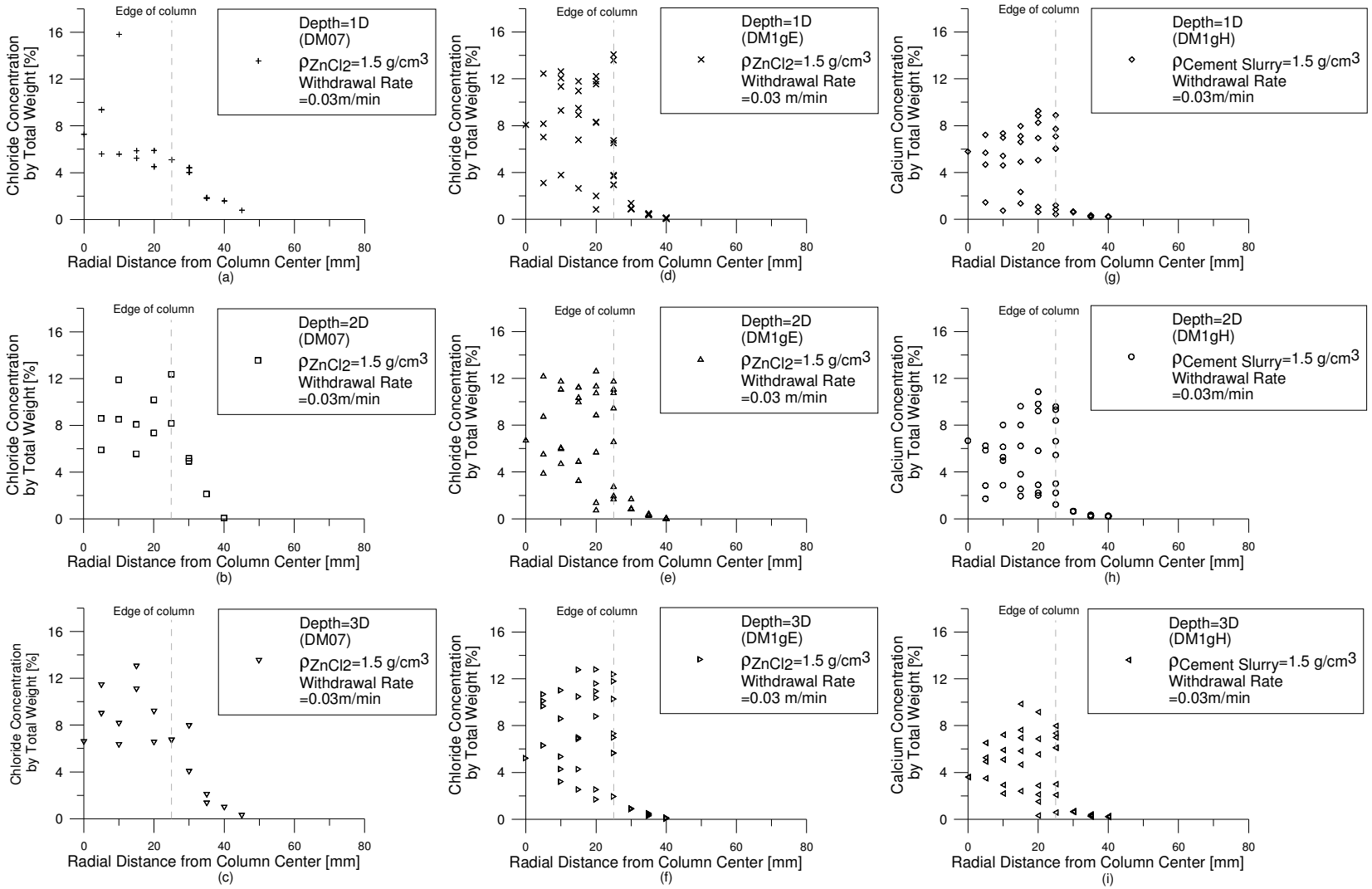

Fig. 4.16 Spot concentration at various model depths and radial distances for high-g test DM07 ($ZnCl_2$), 1-g test DM1gE ($ZnCl_2$) and DM1gH (cement slurry) at slurry density of 1.5g/cm^3.

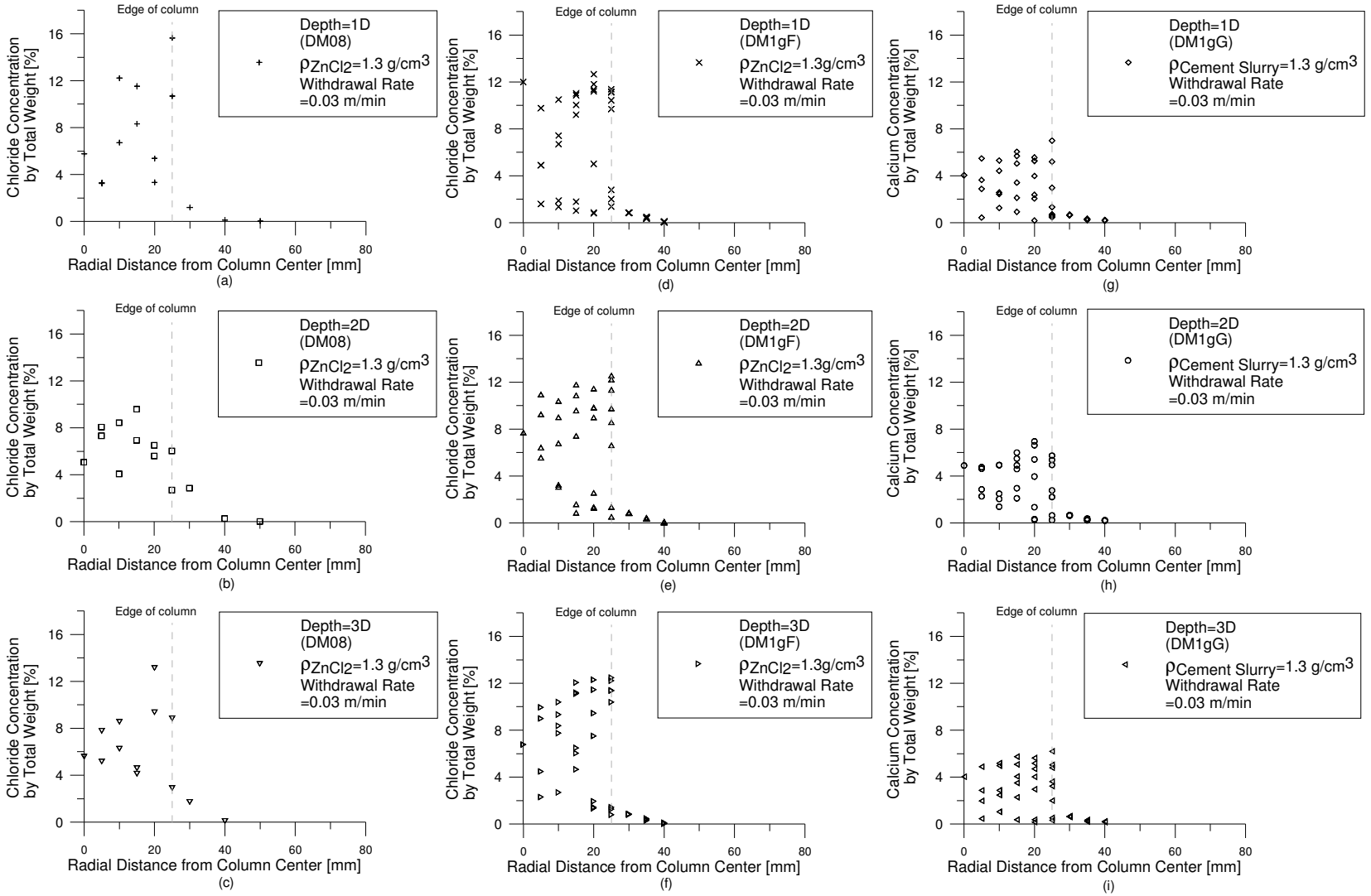

Fig. 4.17 Spot concentration at various model depths and radial distances for high-g test DM08 ($ZnCl_2$), 1-g test DM1gF ($ZnCl_2$) and DM1gG (cement slurry) at slurry density of 1.3g/cm^3.

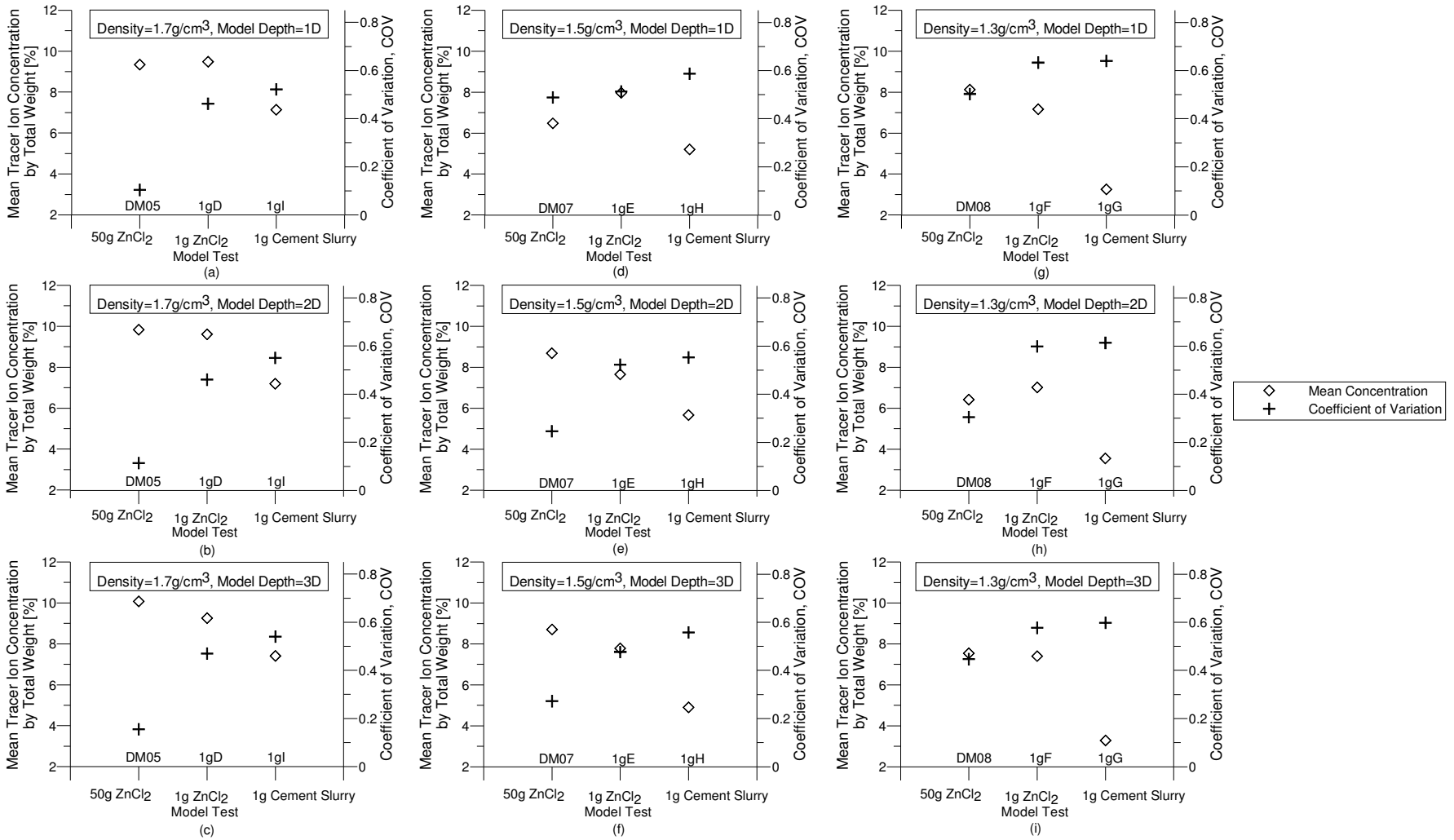

Fig. 4.18 Mean concentration and coefficient of variation for difference model depth within the DM column for high-g and 1-g model tests at difference slurry density of 1.7g/cm^3, 1.5g/cm^3 and 1.3g/cm^3.

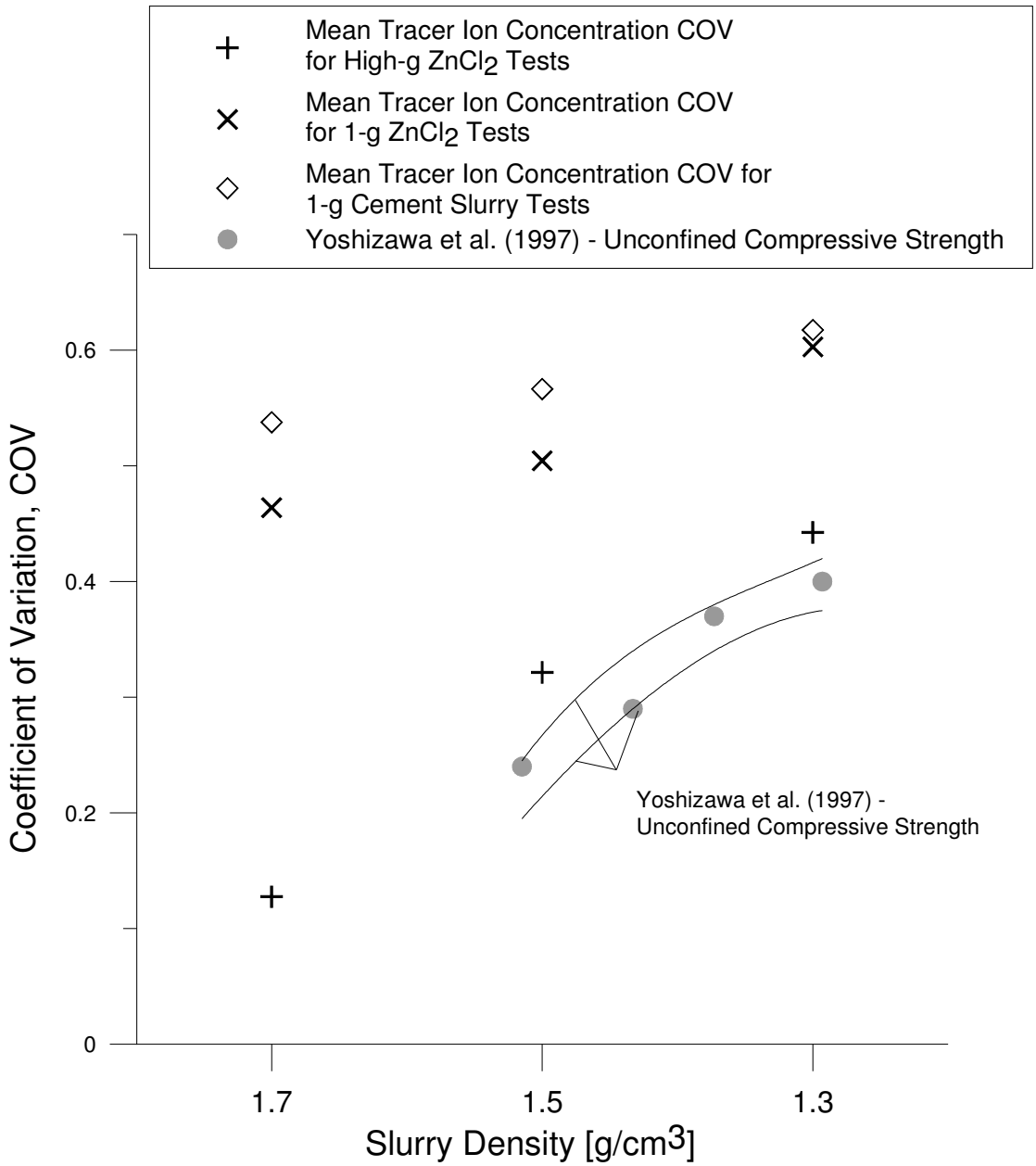

Fig. 4.19 Comparison between high-g tests, 1-g tests and Yoshizawa et al. (1997)'s COV at difference slurry density of 1.7g/cm^3, 1.5g/cm^3 and 1.3g/cm^3.

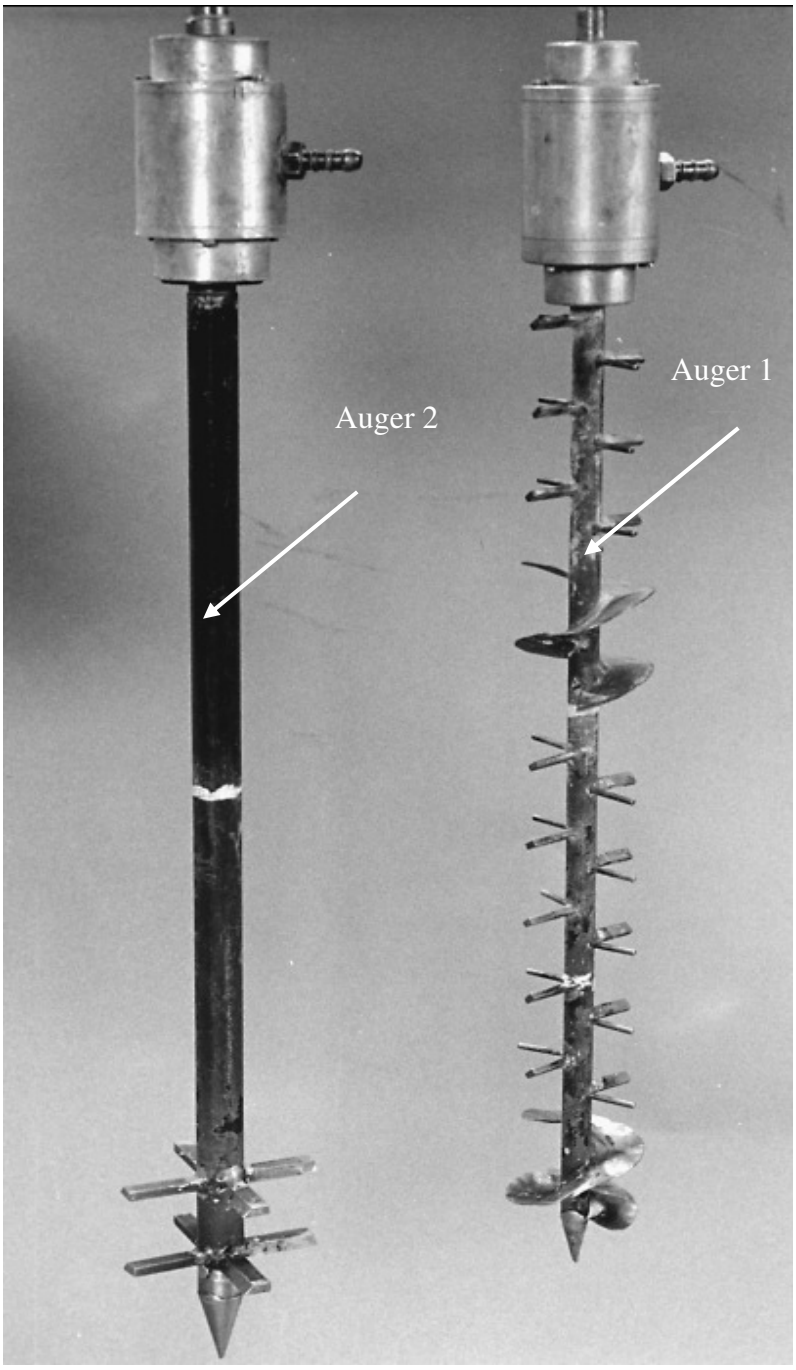

Fig. 4.20 Two different model augers were used in Al-Tabbaa and Evans's (1999) 1-g experiments.

Chapter 5: Parametric Studies

In this chapter, the effects of various parameters on the mixing quality are examined using centrifuge test data. As a precursor to the parametric studies, the reliability of the centrifuge test data was first examined by the mass balance approach used in the previous chapter and the repeatability of four of the centrifuge model tests. The parameters studied are the mixing blade angle, viscosity, withdrawal rate, buoyancy effects, blade rotation number and re-penetration of the DM installer. As shown in Table 5.1, 22 centrifuge model tests were conducted as part of this study. All centrifuge model tests were performed at model blade rotational rate of 770rpm, which is corresponding to the prototype blade rotational rate of about 15rpm. Three different types of DM installer were used for the in-flight installation of DM, as shown in Figs. 3.4, 3.15 and 3.26. These DM installers are labelled as types A, B and C installer. DM installer A has a single twisted-blade. DM installer B with two twisted-blades arranged in a double-layered, cruciform fashion. DM installer C has three pairs of double-layered twisted-blades as shown in Fig.3.26.

In the next section, the measured mean chloride mass will be verified against the predicted value in order to examine the total amount of zinc chloride introduced into the soil.

5.1 Verification of Measured Mean Chloride Mass to the Predicted Value

Fig. 5.1 shows the predicted mean chloride mass, w_{bp} in term of mass per unit depth of soil [g/cm] plotted against the measured mean chloride mass, w_b in unit depth of soil. The method of calculation for both the predicted mean chloride mass and the measured mean chloride mass has been reported in chapter 4 and will not be repeated herein. As Fig. 5.1 shows, most of the data points fall within two straight lines with slopes of 1.15 and 0.85 respectively. This indicates that the measured mean chloride mass fall within ±15% of the predicted value. Thus the mass of the chloride used is adequately accounted for by summing up the statistical distribution of chloride concentration throughout the soil.

5.2 Repeatability of the Experiments

In order to examine the repeatability of the experiments, model tests DM12A, 14A, 16A and 19A (hereafter denoted as repeated model tests) were conducted using the same test parameters as tests DM12, DM14, DM16, DM19 (hereafter denoted as initial model tests) respectively. Tests DM12 (and DM12A) and DM14 (and DM14A) were conducted using DM installer A, but with a zinc chloride density of 1.3g/cm^3 and 1.7 g/cm^3 respectively. Model tests DM16 (and DM16A) and DM19 (and DM19A) were conducted using DM installer B, also with zinc chloride density of 1.7g/cm^3 and 1.3g/cm^3 respectively. Figs. 5.2 to 5.5 show the spot concentration at various model depths and radial distances for model tests, DM12 (and DM12A), DM14 (and DM14A), DM16 (and DM16A), DM19 (and DM19A) respectively. The distribution of spot concentration for each test appears similar to its repeated counterpart. However, it

is difficult to quantify the similarity or differences based on spot concentration. Fig. 5.6 shows the mean chloride concentration and coefficient of variation (COV) at 3 model depths. The mean and COV was computed from the spot concentration. As can be seen, the mean chloride concentration and the COV for each model test agree well with the corresponding value of its repeated counterpart. In most cases, the discrepancy between the pairs of values does not exceed 10% of the mean. The similarity between the model tests and their repeated counterparts suggests that the results obtained from centrifuge experiments are consistent and repeatable.

5.3 Parametric Studies

In the next section, the effects of various parameters on the mixing quality are examined using centrifuge test data. The parameters studied are the mixing blade angle, viscosity, withdrawal rate, buoyancy effects, blade rotation number and re-penetration.

5.3.1 Influence of Mixing Blade Angle

In order to examine the influence of the mixing blade angle on the quality of mixing, DM05 and DM06 were performed using the same zinc chloride density and penetration rates, but with different blade angle of 45° and 90° respectively. The blade angle is defined herein as the angle subtended by the central plane of the blade and the plane of rotation. This definition is similar to that for the angle of attack used in aeronautics (e.g. Springer, 2003). Fig. 5.7 shows mean chloride concentration and COV within the DM column for model tests DM05 and DM06. As can be seen, the

COV is much lower when the blade angle of 45° was used. This suggests that the mixer blade angle may influence the dispersion of zinc chloride. Fig. 5.8 shows the measured spot concentration at the three depths for DM05 and DM06. As can be seen, a larger amount of chloride was dispersed toward the outer part of the column in DM06. The same trend persists at all three depths. On the contrary, DM05 has much more uniform radial distribution throughout the column in test.

During mixing, the blades of the DM installer were rotated counter clockwise to mix the model binder and soil. The flow pattern within the deep mixing column is extremely complex since the mixing blade is likely to be moving at a higher velocity that the surrounding slurry. Some of the slurry particles may be moving at a velocity that is quite near to that of the blade whilst others may be moving much slower. The situation inside the deep mixing cavity is not the same as that within an impeller pump wherein the liquid motion is almost uniform. For this reason, it is difficult to represent the physics of the flow in a mathematical way.

However, one possible explanation relates to the centrifugal effects of the slurry within the deep mixing cavity. In both tests, the density of the zinc chloride used is 1.7g/cm^3, which is heavier than the surrounding fluid. A 90º-blade may be able to impart a larger rotational velocity to the slurry than a 45º-blade owing to its larger projected area. It is therefore a larger tendency for the heavy zinc chloride being centrifuged to locations outside of the cavity before it is effectively mixed. If this is true, then the mixing velocity within the cavity is likely to have a significant effect on the radial distribution of the mixing components, if they are of different densities.

5.3.2 Influence of Binder Viscosity

Test DM05 and DM09 were performed at the different zinc chloride's viscosities of 10cps and 17.7cps respectively to examine the effect of binder's viscosities on mixing. These tests employed zinc chloride with the same density, but the viscosity of the zinc chloride model binder in test DM09 was about 77% higher than that in DM05. The higher viscosity was obtained by replacing approximately 22% of the zinc chloride solution by glycerine, which has a density of about 1260kg/m^3 but with a viscosity about 600 times that of water. Fig. 5.9 shows the spot chloride concentration for model tests DM05 and DM09. As can be seen, the spot chloride concentration in the DM column is generally lower in test DM09 than DM05. This is due to the lower concentration of zinc chloride in the model binder in DM09. Fig. 5.10 shows mean and COV of chloride concentration in the DM column. The mean chloride concentration in Fig. 5.10 reflects the generally lower spot concentration in Fig. 5.9. In addition, raising the viscosity of the binder leads to an increase in the COV, which is an indication of deterioration in mixing quality. This is consistent with the fact that a higher viscosity suppresses turbulence which promotes efficient mixing (e.g. Harnby et al. 1992). Thus, these results suggest that one way of enhancing the quality of mixing in DM columns is by reducing the viscosity of the cement slurry. In field mixing, the quality can be improved also if the viscosity of cement slurry can be lowered, say by means of chemical additives, without adversely affecting the cured strength of the soil-cement mix.

5.3.3 Influence of Penetration and Withdrawal Rates

In order to examine the effect of withdrawal rate, a series of 11 model tests has been conducted at the withdrawal rate of 0.03m/min, 0.072m/min, 0.216m/min and 0.432m/min. The first 7 tests were conducted using the DM installer A. DM08, DM11 and DM12 were performed at the same zinc chloride density of 1.3g/cm^3, but with different penetration and withdrawal rates. The penetration and withdrawal rate of test DM08 was 0.03m/min. This is much lower than the value used in DM11 and DM12, which have the same penetration rate of 0.432m/min, but different withdrawal rates of 0.216m/min and 0.432m/min respectively. Fig. 5.11 shows the spot chloride concentration for these three tests. The mean and COV of chloride concentration at different model depth were also computed and presented in Fig. 5.12. As this figure shows, the COV for all depths in test DM08 is slightly lower than the COV of tests DM11 and DM12. The overall COV also shows that the lowest COV is obtained for DM08, followed by DM11 and then DM12. The fact that DM11 has a lower COV than DM12 suggests that using a lower withdrawal speed will improve the quality of mixing, presumably by increasing the work done in mixing. One way to represent the work done in mixing is by using blade rotation number which will be discussed in the later section. The difference between DM08 and the other two tests is somewhat more difficult to interpret since DM08 also has a much slower penetration rate than DM11 and DM12, and this may also contribute to the quality of mixing. Notwithstanding this, one may surmise that the withdrawal speed is more likely to have a more significant influence since the zinc chloride was only introduced during the withdrawal phase.

The effect of withdrawal rate is also examined by using zinc chloride of different densities. Tests DM07 and DM15 were conducted with a zinc chloride density of 1.5g/cm^3, using withdrawal rates of 0.03m/min and 0.432m/min respectively. Tests DM05 and DM14 were conducted with a zinc chloride density of 1.7g/cm^3, using withdrawal rates of 0.03m/min and 0.432m/min respectively. Fig. 5.13 shows the spot chloride concentration for DM07 and DM15, while Fig. 5.14 shows the corresponding concentration for DM05 and DM14. These two figures show that the scatter in spot concentration seems to be higher for the tests with a higher withdrawal rate, compared to the corresponding test with a lower withdrawal rate. Figs. 5.15 and 5.16 show the mean chloride concentration and COV for the two pairs of model tests (i.e. with zinc chloride density of 1.5g/cm^3 and 1.7g/cm^3). Once again, there is a general decrease in COV as the withdrawal rate is reduced. In particular, the COV of DM05 is much lower than that in DM14. In other words, between DM05 and DM14, a lower withdrawal rate appears to have the most significant effect in improving the uniformity of the mixing. These two tests used zinc chloride with a density of 1.7g/cm^3. The result indicates that the significance of the withdrawal rate may be enhanced or reduced depending upon the density. This is suggestive of an interaction between withdrawal rate and buoyancy effects. The latter will be further elaborated in Section 5.3.4.

Another 4 model tests were conducted using DM installers B and C. DM16 and DM17 were conducted using DM installer B using a zinc chloride density of 1.7g/cm^3 and penetration rate of 0.432m/min, but with different withdrawal rates of 0.432m/min and 0.216m/min respectively. Tests DM21 and DM28 were conducted using DM installer C using a zinc chloride density of 1.7g/cm^3 and penetration rate of 0.432m/min, but with different withdrawal rates of 0.432m/min and 0.076m/min respectively. Figs. 5.17

and 5.18 show the spot chloride concentration for the four model tests. Figs. 5.19 and 5.20 show the mean chloride concentration and COV for DM installers B and C, respectively. In both pairs of tests, the test with the slower withdrawal rate yielded a lower COV than its counterpart with a faster withdrawal rate. Thus, regardless of the DM installation used, the results show that the withdrawal rate of the DM installer has a measurable influence on the quality of the mixing and this is also consistent with the field observation that the final quality of the DM treated ground is improved by using a slower withdrawal rate.

5.3.4 Influence of Buoyancy Effects

A series of 12 model tests were conducted to study the effect of mixing of binder and soil in situations where the density of the binder is different from that of the soil. All model tests were conducted at a penetration rate of 0.432m/min. For DM installer A, tests DM05, DM07 and DM08 were conducted at zinc chloride density of 1.7g/cm^3, 1.5 g/cm^3 and 1.3 g/cm^3 respectively at a withdrawal rate of 0.03m/min. Another three tests, viz. DM14, DM15, and DM12, were conducted by using DM installer A at a higher withdrawal rate of 0.432m/min. For DM installer B, tests DM16, DM18 and DM19 were conducted at zinc chloride density of 1.7g/cm^3, 1.5g/cm^3 and 1.3g/cm^3 respectively at a withdrawal rate of 0.432m/min. For DM installer C, tests DM20, DM26 and DM27 were conducted with different zinc chloride density of 1.7g/cm^3, 1.5g/cm^3 and 1.3g/cm^3 respectively at a withdrawal rate of 0.432m/min. For this series of model test, re-penetration and remixing were conducted at 0.432m/min after the DM installer has been withdrawn.

Fig. 5.21 shows the overall COV for all depths for the model tests. Fig. 5.22 shows the COV for different model depths within the DM column at different zinc chloride density of 1.3g/cm^3, 1.5g/cm^3 and 1.7g/cm^3. As shown in Fig. 2.5, as the density of the zinc chloride solution increases, so does its viscosity, which should lead to deterioration in the quality of mixing. If the viscosity is the sole factor in determining the quality of mixing, DM05 which used zinc chloride with density of 1.7g/cm^3 should be more viscous and this should result in the poorest mixing quality. However, model test results differ from the previous deduction. As shown in Fig. 5.21, DM05 has the highest quality of mixing, followed by DM07 and then DM08. A similar observation was also found in model tests DM14, DM16 and DM20 which used zinc chloride with density of 1.7g/cm^3. These three tests yielded the higher mixing quality than the corresponding model tests using zinc chloride density of 1.5g/cm^3 and 1.3g/cm^3. A similar trend exists at all three depths as presented in Fig. 5.22. Therefore, our results suggest that, apart from viscosity, density differences between model binder and soil may impact the mixing quality. From our results, it is obvious that, over the ranges of parameters investigated, the influence of density differences between model binder and soil is more dominant than the influence of viscosity.

Fig. 5.21 also presents Yoshizawa et al.'s (1997) results, which were obtained by converting water-cement ratio to density of cement slurry, based on the assumption that the specific gravity of cement is 3.15. The model tests' results and Yoshizawa et al.'s (1997) results cannot be compared quantitatively since the former relates to chloride concentration whereas the latter relates to unconfined compressive strength. Nonetheless, the similarity in the two trends is clear and suggests that Yoshizawa et al.'s (1997) results on the COV in strength for different water-cement ratios may be

attributed, at least in part, to the degradation in mixing quality as the binder density decreases, i.e. buoyancy effect.

Matsuo et al. (1996) also noted a similar variation in the COV of the unconfined compressive strength with water-cement ratio and suggested that the degradation in mixing quality can be attributed to buoyancy effects arising out of density differences between slurry and soil. The significance of density differences between two fluids in the mixing was also noted by Rielly & Pandit (1988) who characterised the mixing behaviour using the Richardson number. Thus, over the range of properties studied in this series of model tests, buoyancy force appears to have a very significant influence on the quality of mixing.

5.3.5 Influence of Blade Rotation Number

DM installer A has fewer blades than many prototype DM equipments, which often have more than one layer of cutting and mixing blades. CDIT (2002) noted that it is not the number of turns or withdrawal rate which determines the mixing quality, but rather the blade rotation number, this being defined as number of rotations of mixing blade per metre depth of improved soil. Indeed, in Japan, the degree of mixing is often expressed in terms of blade rotation number (Mizuno et al. 1988). Thus, increasing the number of cutting and mixing blades would increase the blade rotation number which should improve the mixing quality, if CDIT (2002) is correct. In order to further investigate the impact of blade rotation number on the mixing quality, a series of 6 model tests has been conducted. Two different DM installers were designed and used in our study i.e. DM installers A and B. DM installer A is equipped with single

twisted-blade inclined at blade angle of 45° while DM installer B is equipped with two twisted-blades inclined at blade angle of 45° arranged in a double-layered orientation. Model tests DM12, DM15 and DM14 were conducted using DM installer A with zinc chloride density of 1.3g/cm^3, 1.5/cm^3 and 1.7g/cm^3 respectively. Model tests DM19, DM18 and DM16 were conducted using DM installer B with the same corresponding zinc chloride density of 1.3g/cm^3, 1.5/cm^3 and 1.7g/cm^3 respectively. All models tests were performed at the same penetration and withdrawal rate of 0.432m/min. Figs. 5.23 to 5.25 present the spot chloride concentration for model test using zinc chloride density of 1.3g/cm^3 (i.e. DM12 and DM19), 1.5/cm^3 (i.e. DM15 and DM18) and 1.7g/cm^3 (i.e. DM14 and DM16) respectively. Fig. 5.26 shows mean chloride concentration and COV for the similar model tests. Our previous results on the effect of withdrawal rates on the mixing quality suggested that the mixing quality increases with a decrease in withdrawal rate. If withdrawal rate is the sole factor affecting the quality of mixing, then the mean and COV of the chloride concentration should remain unchanged within each pair of tests using the same withdrawal rate and zinc chloride of the same density. As Fig. 5.26 shows, the COV for DM installer B is consistently lower than the COV of DM installer A for all depths examined. The difference is particularly evident in the cases where the zinc chloride density is much lower than that of the soil. It should be noted that the additional layer of mixing blades on DM installer B doubles the prototype blade rotation number from 35.6rev/m (in the case of DM Installer A) to 71.3rev/m. This is consistent with the observation of Mizuno et al. (1988).

On the other hand, it appears to contradict the 1-g laboratory test observation of Al-Tabbaa and Evans (1999). As shown in Fig. 4.20, Al-Tabbaa and Evans (1999) used

two different auger designs in their mixing experiments. Auger 1 is geometrically similar to that used in the field, whereas Auger 2 is a much simpler auger consisting of only 2 layers of blades. Al-Tabbaa and Evans (1999) noted that "…*Auger 2 produced higher strengths, which were almost twice those produced by auger 1. In addition, auger 1 produced far more variability between the top and base halves of the columns: in the made ground, the UCS of the top sample was half that of the base sample*….". It is not entirely clear what is the cause of the heterogeneity observed by Al-Tabbaa and Evans (1999), especially since the field trials appeared to produce satisfactory results with Auger 1 design. One possible explanation is the scale distortion which arises from performing the experiments in 1-g environment. Al-Tabbaa and Evans (1999) did not report the auger's RPM used in their laboratory experiments. Assuming that their 1-g laboratory tests used the same RPM as the field prototype, then it can be shown that the shear strain rate, and therefore viscous stress are both preserved at prototype level. On the other hand, gravity and inertial stresses would be reduced by $1/N$ and $1/N^2$ times, respectively. The predomination by the viscous stresses would probably inhibit effective mixing. In particular, the reduction in gravity stresses might have interacted with the multiple layers of blades in Auger 1 to prevent effective top-bottom mixing, resulting in variability between top and bottom of the columns. If this is true, then it lends further support to the case of using centrifuge modelling, instead of 1-g modelling, to study DM processes.

In addition to the blade rotation number, the blade configuration itself may also affect the quality of mixing. To investigate this, a series of model tests were performed using DM installers A and B with the same blade rotation number i.e. 71.3rev/m, this being achieved by varying their withdrawal rate. Model tests DM11 and DM19 were

performed using zinc chloride density of 1.3g/cm^3 with DM installer A and B, respectively. As shown in Fig. 5.27, at depths of 1D and 2D, Installer B appears to give slightly lower COV than Installer A. At depth of 3D, there is no significant difference between the two sets of installers. Overall, DM installer B seems to give a slightly lower COV compared to DM installer A, this being explainable by the differences at depths of 1D and 2D. Thus, the difference between the two DM installers does appear to have a discernible effect; in this case, the double-layered configuration seems to produce a better quality of mixing than the single layer blade configuration. However, this effect seems to be smaller than that due to differences in blade rotation number.

Fig. 5.28 summarizes the effects of zinc chloride density, blade rotation number and blade configuration on the COV. As can be seen, within the ranges of parameters investigated herein, the most significant effect seems to arise from model binder density (probably relative to soil slurry density). This is followed by the blade rotation number and finally the blade configuration. Mizuno et al.'s (1998) results are also superimposed into Fig. 5.28. Strictly speaking, the results from the current model tests and those of Mizuno et al. (1998) cannot be compared quantitatively, since Mizuno et al.'s COV refer to the of strength rather than tracer ion concentration. Nonetheless, the fact that both set of results lie on a similar band and show a similar trend with blade rotation number lends further confidence to the centrifuge model test results.

5.3.6 Influence of Re-penetration of DM Installer

As discussed in chapter 3, the additional mixing blades on DM installer C along the shaft may not contribute much to improving the quality of mixing due to the withdrawal injection method used in our study. In the withdrawal injection method, zinc chloride was only introduced into the cut soil during the withdrawal phase via the injection nozzles, which are located at the bottom end of the shaft. This causes most of the zinc chloride to be injected around the first pair of blades which are located nearer to the injection nozzles. Thus, it is likely that mixing is achieved primarily by the first, and to a lesser extent second, pair of blades. The third pairs of blades along the shaft (for Installer C) are located further away from the injection nozzles. Therefore these two pairs of blades may not be fully utilized in the withdrawal injection process. To achieve optimal mixing efficiency, we may install additional injection nozzles next to the second and the third pair of blades. However, this design is not feasible in the current model mixing equipment since the amount of injection at each nozzle, in a multi-nozzle situation, cannot be controlled accurately. This control is likely to be crucial in our parametric study in order to ensure that the amount of zinc chloride injected at each depth is controlled. Hence, this approach was excluded from this study.

Another method to achieve optimal mixing and better utilize the additional mixing blades along the shaft is to conduct re-penetration of the installer into the DM column. The re-penetration of mixing installer will increase the blade rotation number and re-utilize the upper layers of blade, both of which should lead to an improvement in mixing quality. To study the impact of re-penetration i.e. the remixing effect of the

installer, model tests DM20, DM21 and DM28 were performed at the same zinc chloride density of 1.7g/cm^3 and penetration rate of 0.432m/min using DM installer C. DM20 and DM21 was performed at withdrawal rate of 0.432m/min. Re-penetration was conducted at 0.432m/min immediately after the first withdrawal for DM20, but not for DM21. DM28 was conducted at a withdrawal rate of 0.076m/min. Therefore, the blade rotation number for both DM20 and DM28 was 404rev/m, whereas that for DM21 was 71.3rev/m. Fig. 5.29 shows the spot chloride concentration for tests DM21, DM28 and DM20 whilst Fig. 5.30 shows the mean chloride concentration and COV for the same tests. As Fig. 5.30 shows, the differences between the COV of DM 20 and DM28 are rather marginal. At depths of 1D and 3D, DM28 yields marginally lower COV; at depth of 2D, DM20 yields a lower COV. The overall COV for the tests are nearly equal. This suggests that a similar mixing quality can be obtained by using a similar blade rotation number, which can, in turn, be achieved either by using a slower withdrawal rate or by re-penetration. As expected, DM21 yielded a higher COV than DM20 and DM28. This is readily attributable to the lower blade rotation number of DM21 than the other two tests.

Combining the observations from Section 5.3.3 and 5.3.5, blade rotation number can significantly affect the mixing quality in our model tests. Since the blade rotation number is determined by the withdrawal rate and the number of mixing blade, the same blade rotation number can be obtained by different installers by adjusting withdrawal rate. A comparable mixing quality was achieved by using all three DM installers under the same blade rotation number. The main advantage of a many-bladed installer is that, by using a larger number of mixing blades, the withdrawal rate can be increased leading to a reduction in the total DM installation time. To fully utilize the

upper layers of blades, re-penetration can also be utilized. In the model tests, DM installers A and B took about 5.67 and 2.83 times the duration of DM installer C takes to achieve a comparable mixing quality.

Table 5.1 Parameters used in the high-g model tests.

Model Test Identifier	**Type of DM Installer**	**Blade Angle [°]**	**Density of Zinc Chloride [g/cm^3]**	**Density Difference Between Soil and Slurry, ρ_b-ρ_s [g/cm^3]**	**Model Blade Revolution [rpm]**	**Slurry Insertion Ratio, α**	**Average Blade Rotation Number [rev/m]**	**Model Penetration Rate [m/min]**	**Model Withdrawal Rate [m/min]**	**Dynamic Viscosity of Zinc Chloride [cps]**
DM05	A	45	1.7	0.07	770	0.36	513.3	0.03	0.03	10
DM06	A	90	1.7	0.07	770	0.37	513.3	0.03	0.03	10
DM07	A	45	1.5	-0.13	770	0.36	513.3	0.03	0.03	3.7
DM08	A	45	1.3	-0.33	770	0.37	513.3	0.03	0.03	2.7
DM09	A	45	1.7	0.07	770	0.34	513.3	0.03	0.03	17.7
DM11	A	45	1.3	-0.33	770	0.39	71.3	0.432	0.216	2.7
DM12	A	45	1.3	-0.33	770	0.38	35.6	0.432	0.432	2.7
DM12A	A	45	1.3	-0.33	770	0.36	35.6	0.432	0.432	2.7
DM14	A	45	1.7	0.07	770	0.34	35.6	0.432	0.432	10
DM14A	A	45	1.7	0.07	770	0.33	35.6	0.432	0.432	10
DM15	A	45	1.5	-0.13	770	0.33	35.6	0.432	0.432	3.7
DM16	B	45	1.7	0.07	770	0.35	71.3	0.432	0.432	10
DM16A	B	45	1.7	0.07	770	0.34	71.3	0.432	0.432	10
DM17	B	45	1.7	0.07	770	0.33	142.6	0.432	0.216	10
DM18	B	45	1.5	-0.13	770	0.32	71.3	0.432	0.432	3.7
DM19	B	45	1.3	-0.33	770	0.36	71.3	0.432	0.432	2.7
DM19A	B	45	1.3	-0.33	770	0.37	71.3	0.432	0.432	2.7
DM20	C	45	1.7	0.07	770	0.35	404.0	0.432 x2	0.432 x2	10
DM21	C	45	1.7	0.07	770	0.34	71.3	0.432	0.432	10
DM26	C	45	1.5	-0.13	770	0.32	404.0	0.432 x2	0.432 x2	3.7
DM27	C	45	1.3	-0.33	770	0.36	404.0	0.432 x2	0.432 x2	2.7
DM28	C	45	1.7	0.07	770	0.32	404.0	0.432	0.076	10

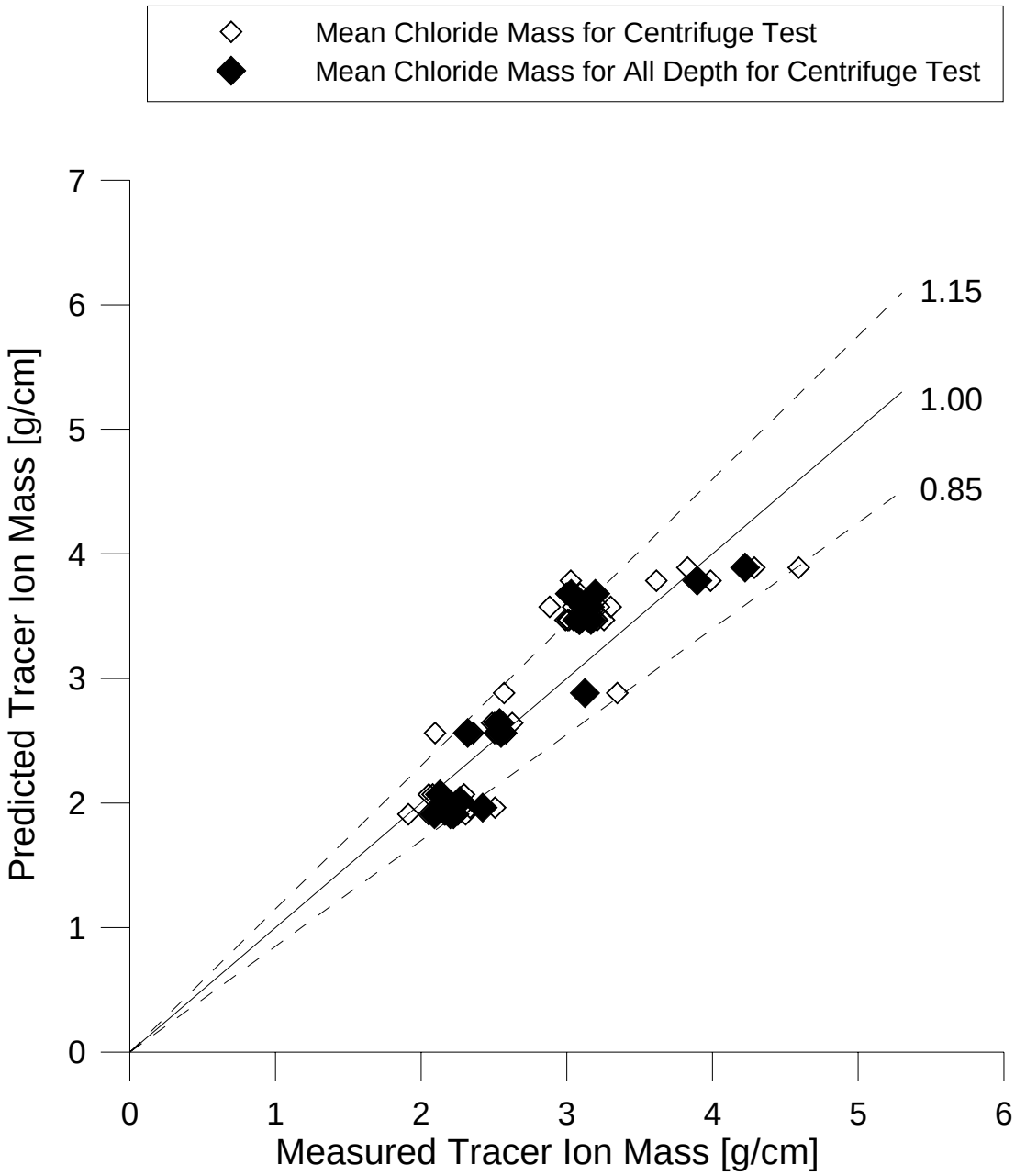

Fig. 5.1 Predicted mean tracer ion mass to the measured mean tracer ion mass of the model tests.

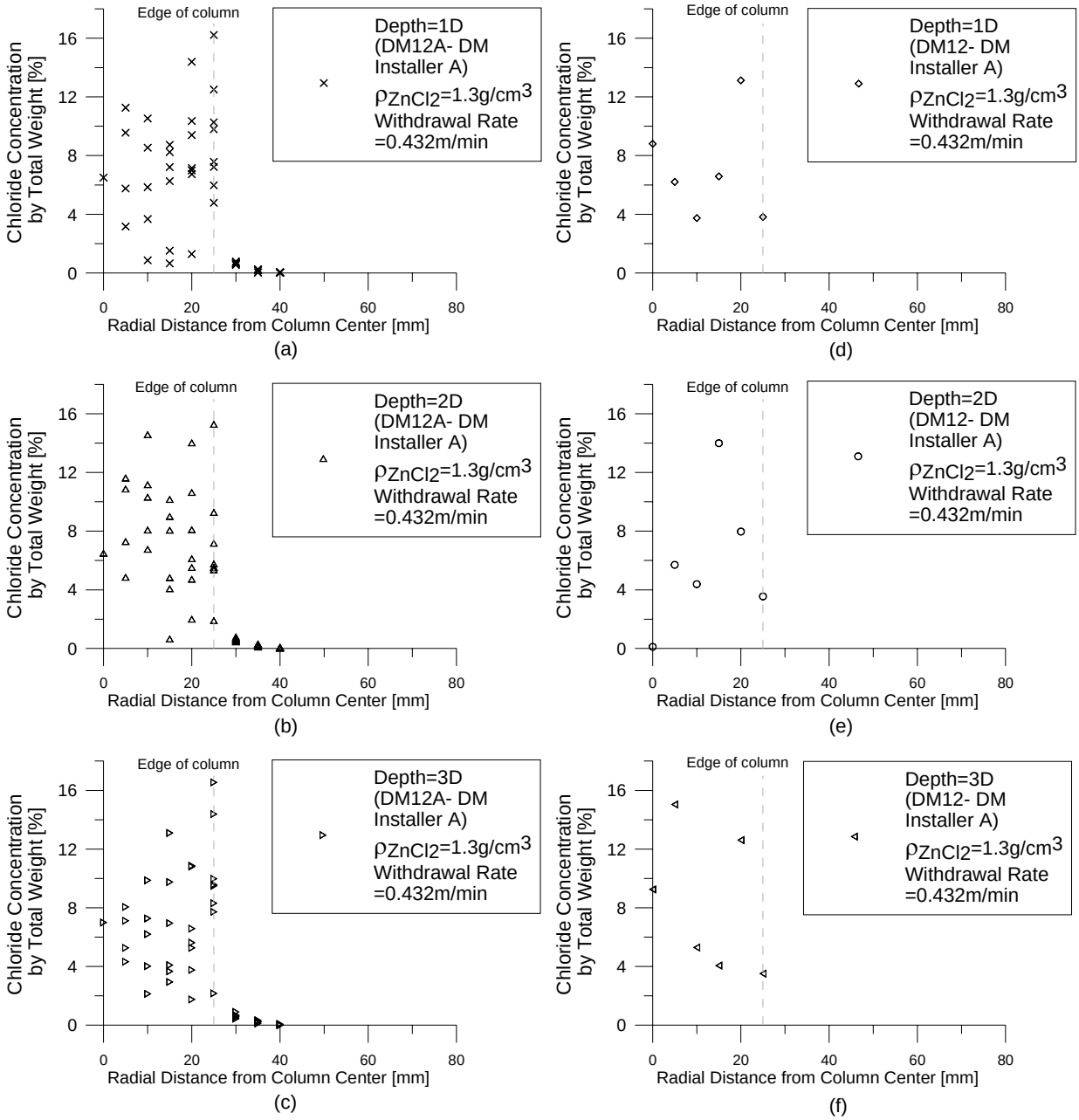

Fig. 5.2 Spot chloride concentration at various model depths and radial distances in model tests DM12A and DM12.

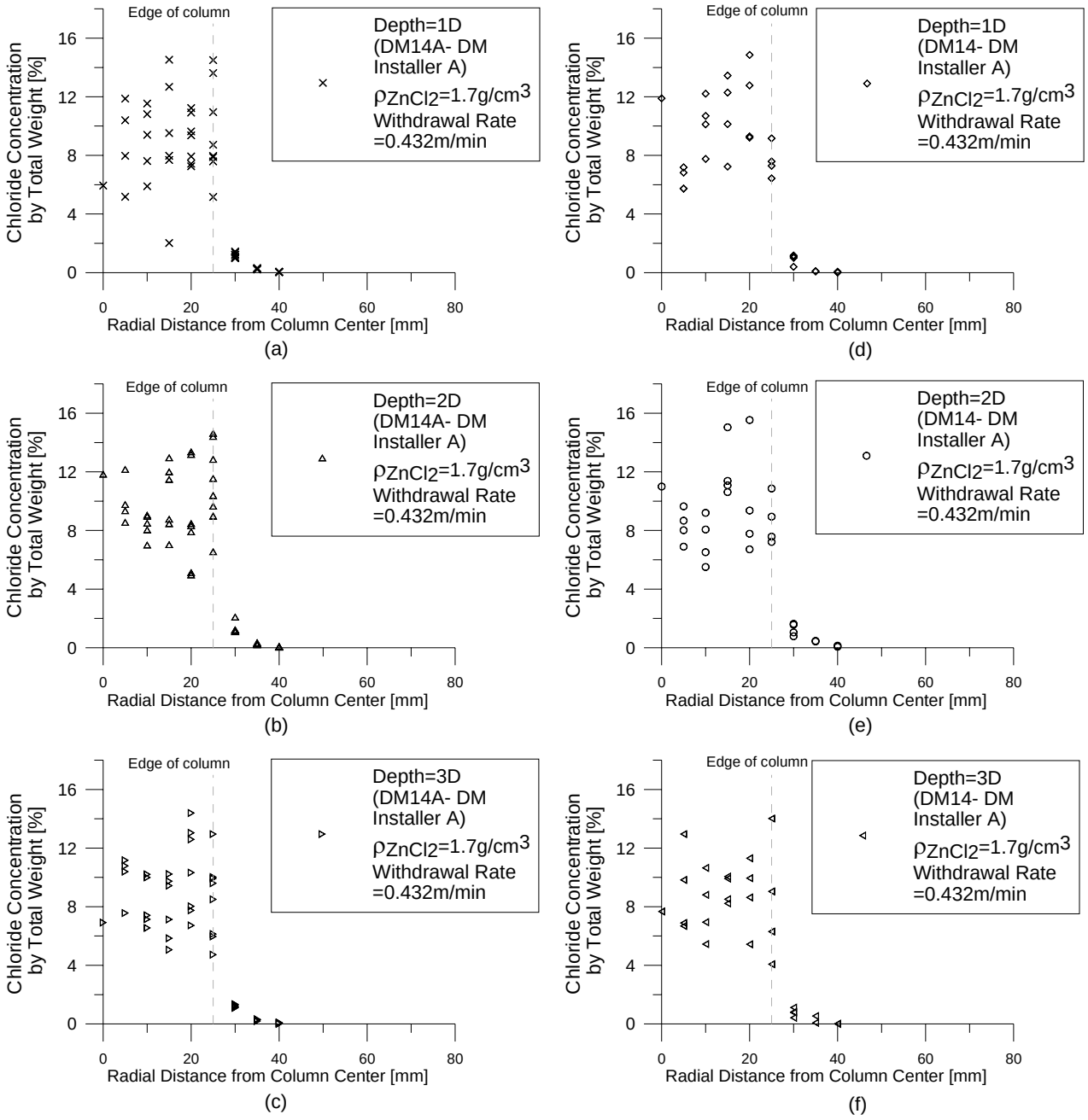

Fig. 5.3 Spot chloride concentration at various model depths and radial distances for model tests DM14A and DM14.

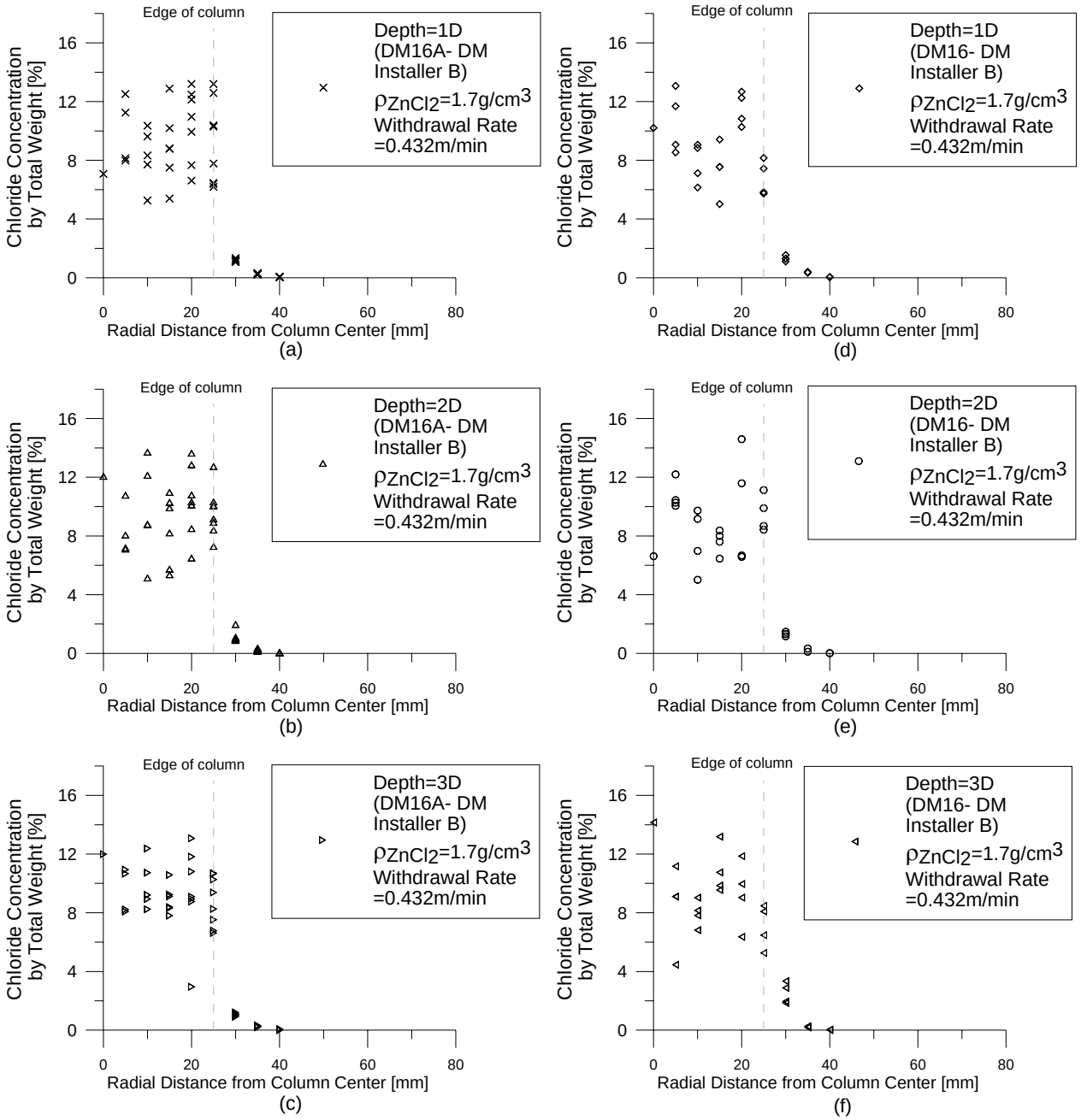

Fig. 5.4 Spot chloride concentration at various model depths and radial distances for model tests DM16A and DM16.

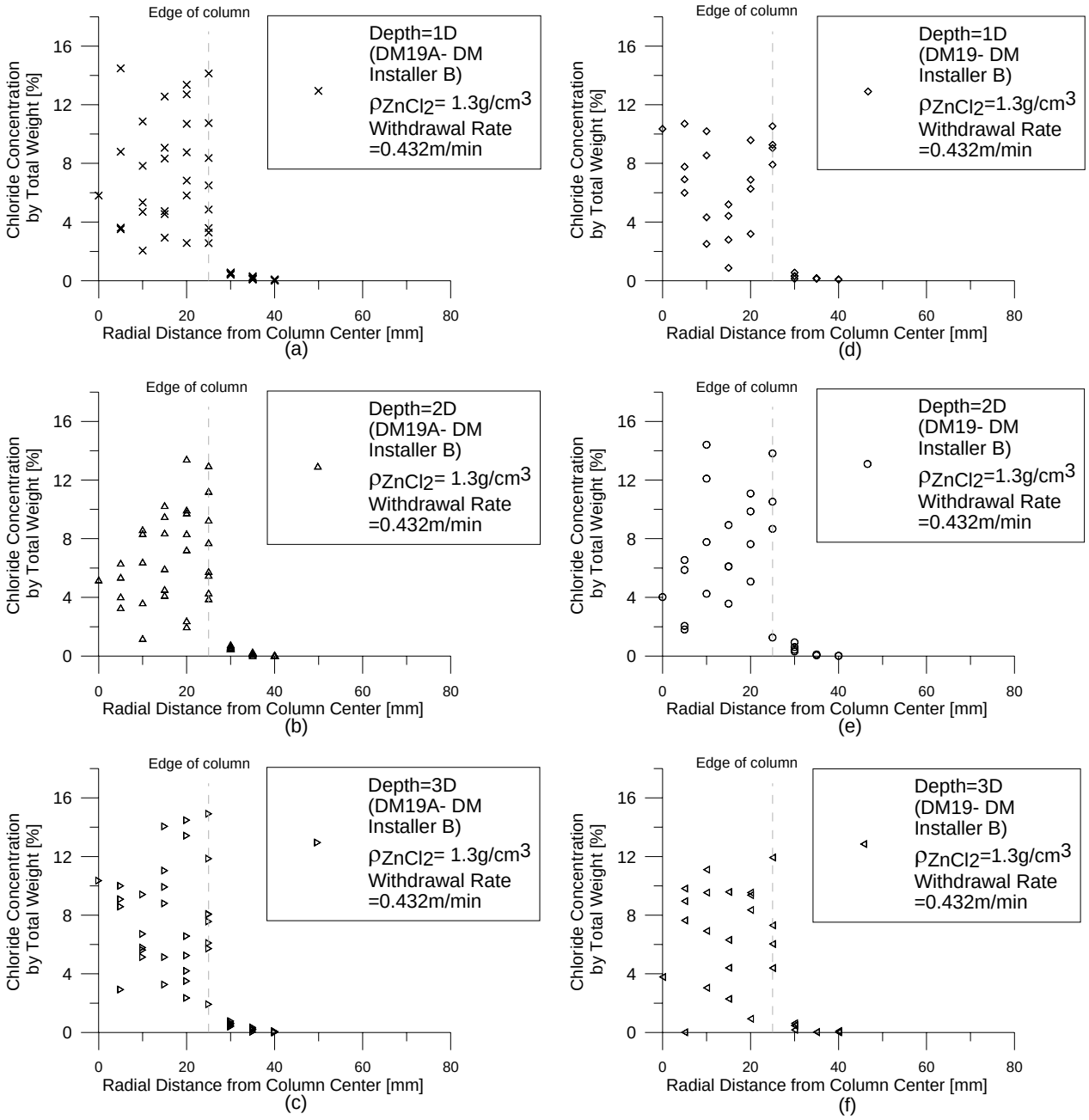

Fig. 5.5 Spot chloride concentration at various model depths and radial distances for model tests DM19A and DM19.

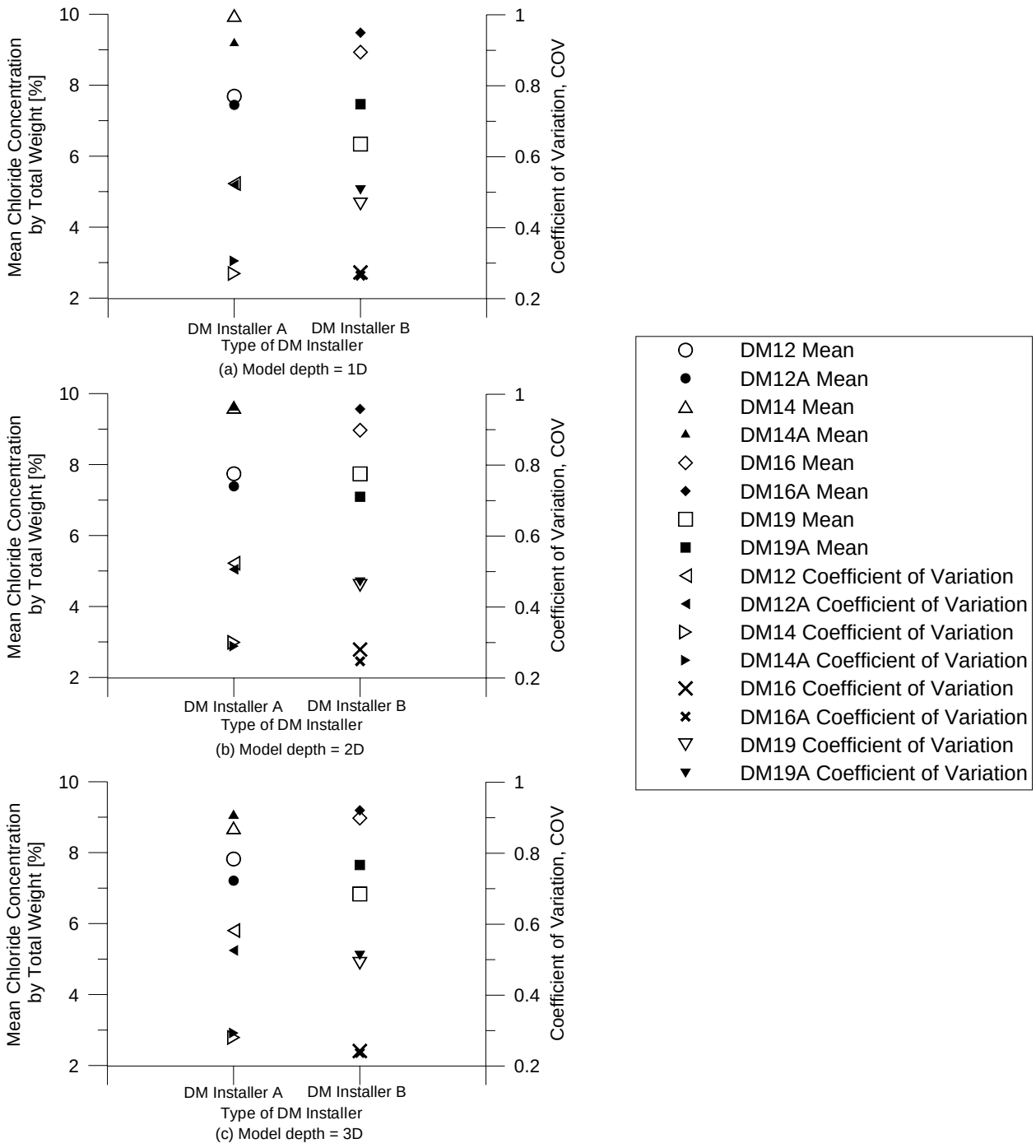

Fig. 5.6 Mean chloride concentration and COV for a series of 8 model tests in the analysis of repeatability.

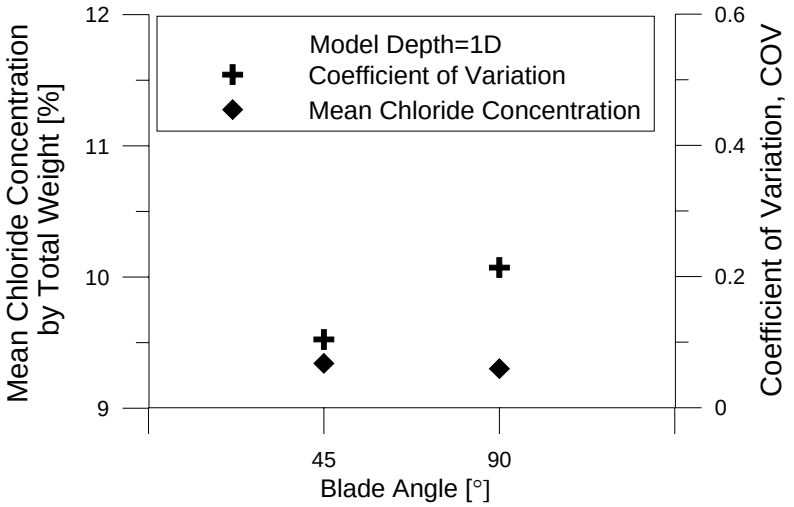

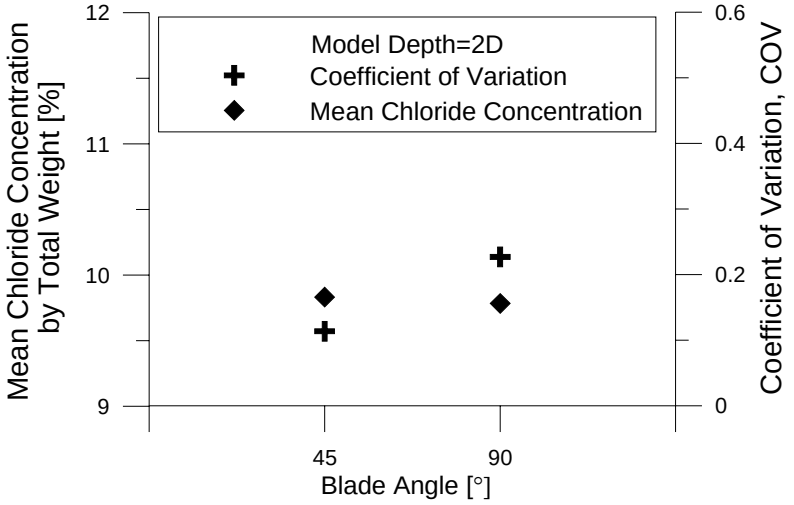

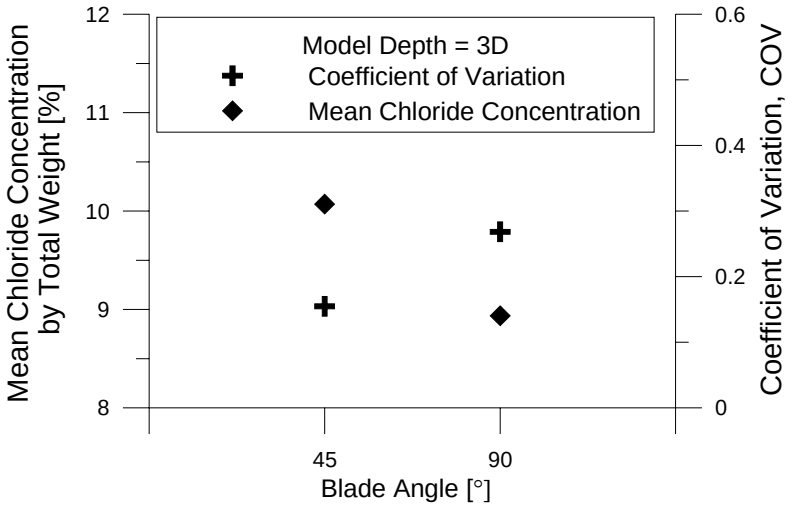

Fig. 5.7 Mean chloride concentration and COV within the DM column for model tests DM05 and DM06.

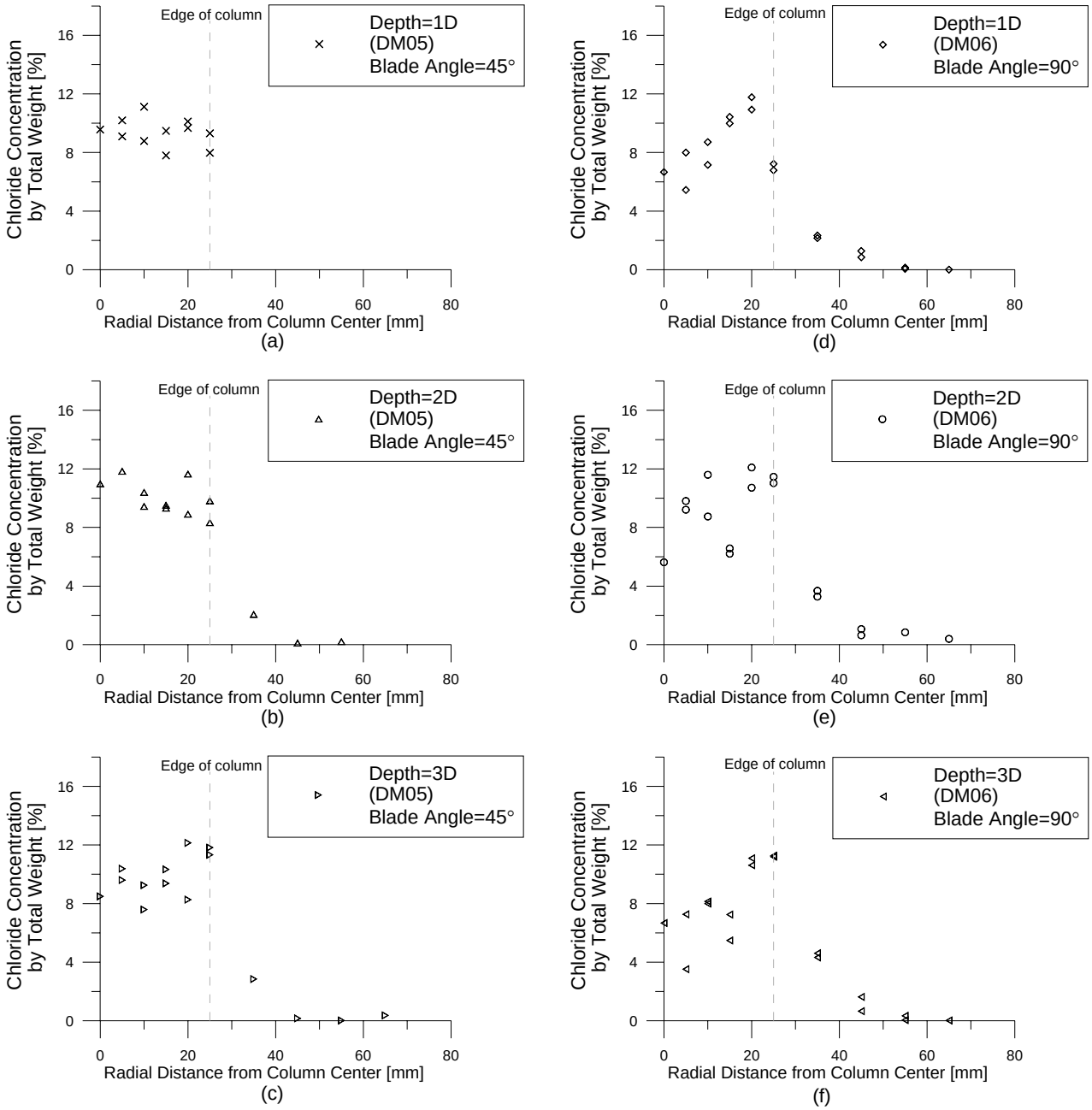

Fig. 5.8 Measured spot chloride concentration at the three depths for model tests DM05 and DM06.

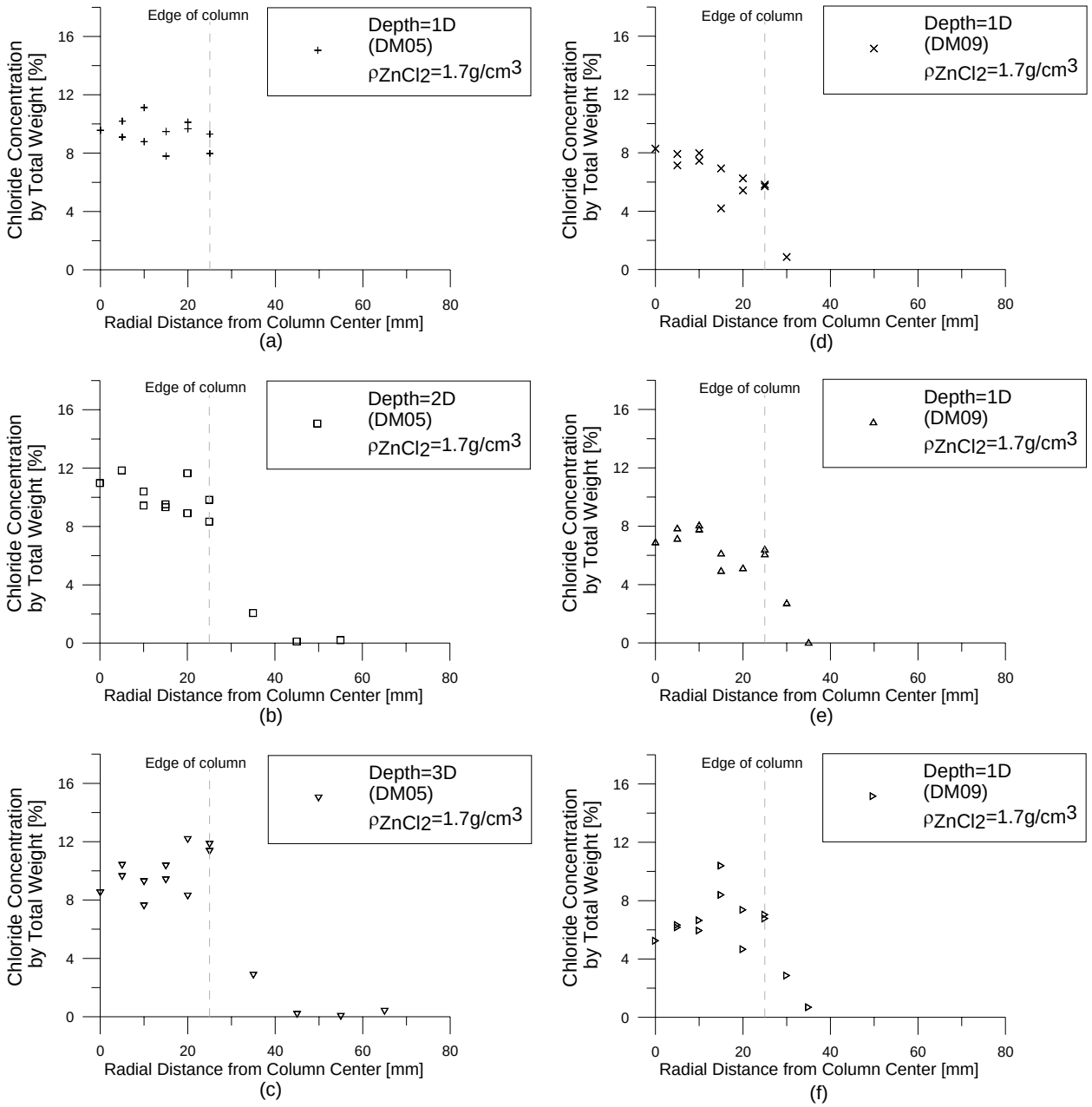

Fig. 5.9 Spot chloride concentration for model tests DM05 (10cps) and DM09 (17.7cps).

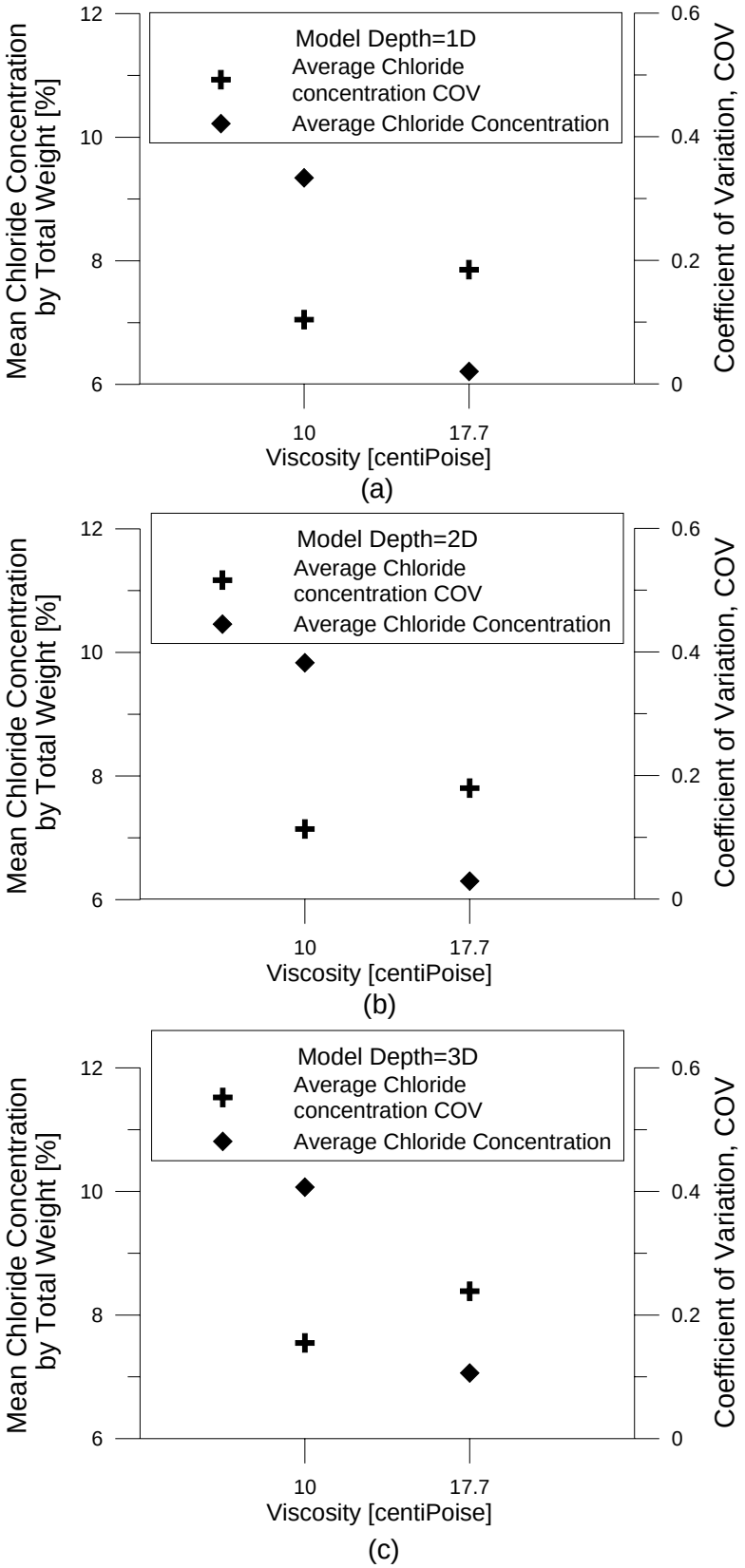

Fig. 5.10 Mean chloride concentration and coefficient of variation within the DM column for model tests DM05 (10cps) and DM09 (17.7cps).

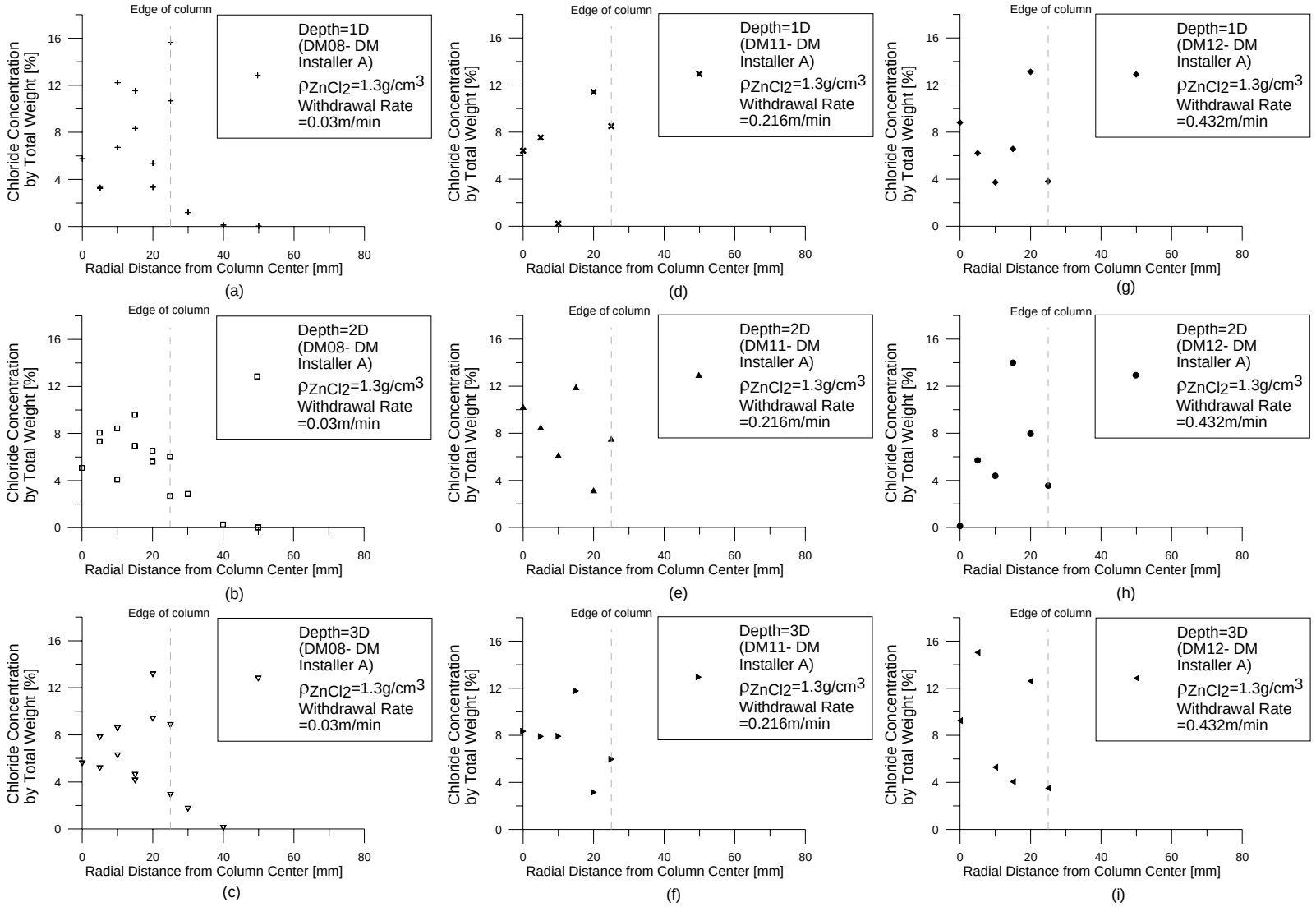

Fig. 5.11 Spot chloride concentration for model tests DM08, DM11 and DM12.

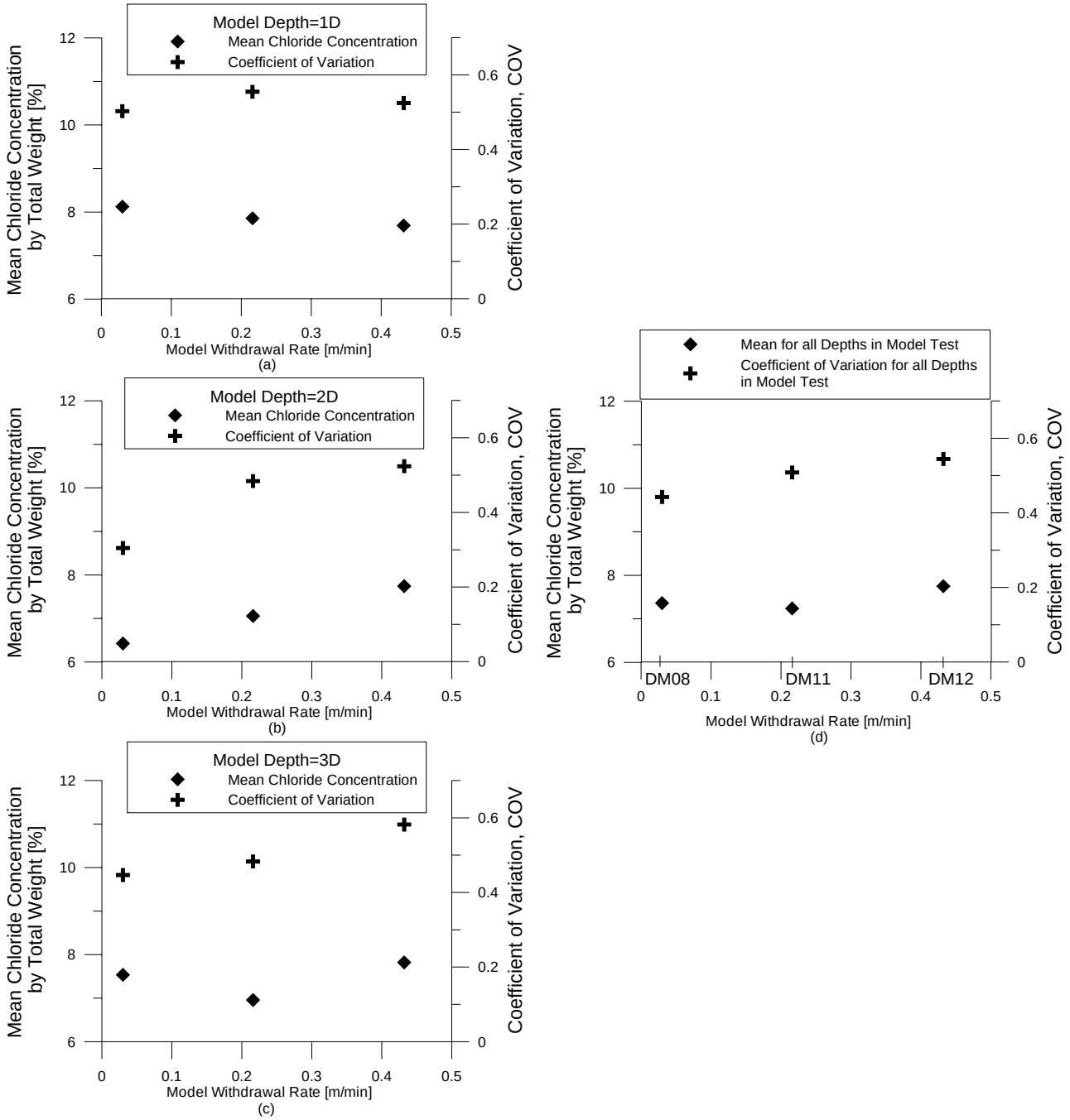

Fig. 5.12 Mean chloride concentration and coefficient of variation within the DM column for model tests DM08, DM11 and DM12.

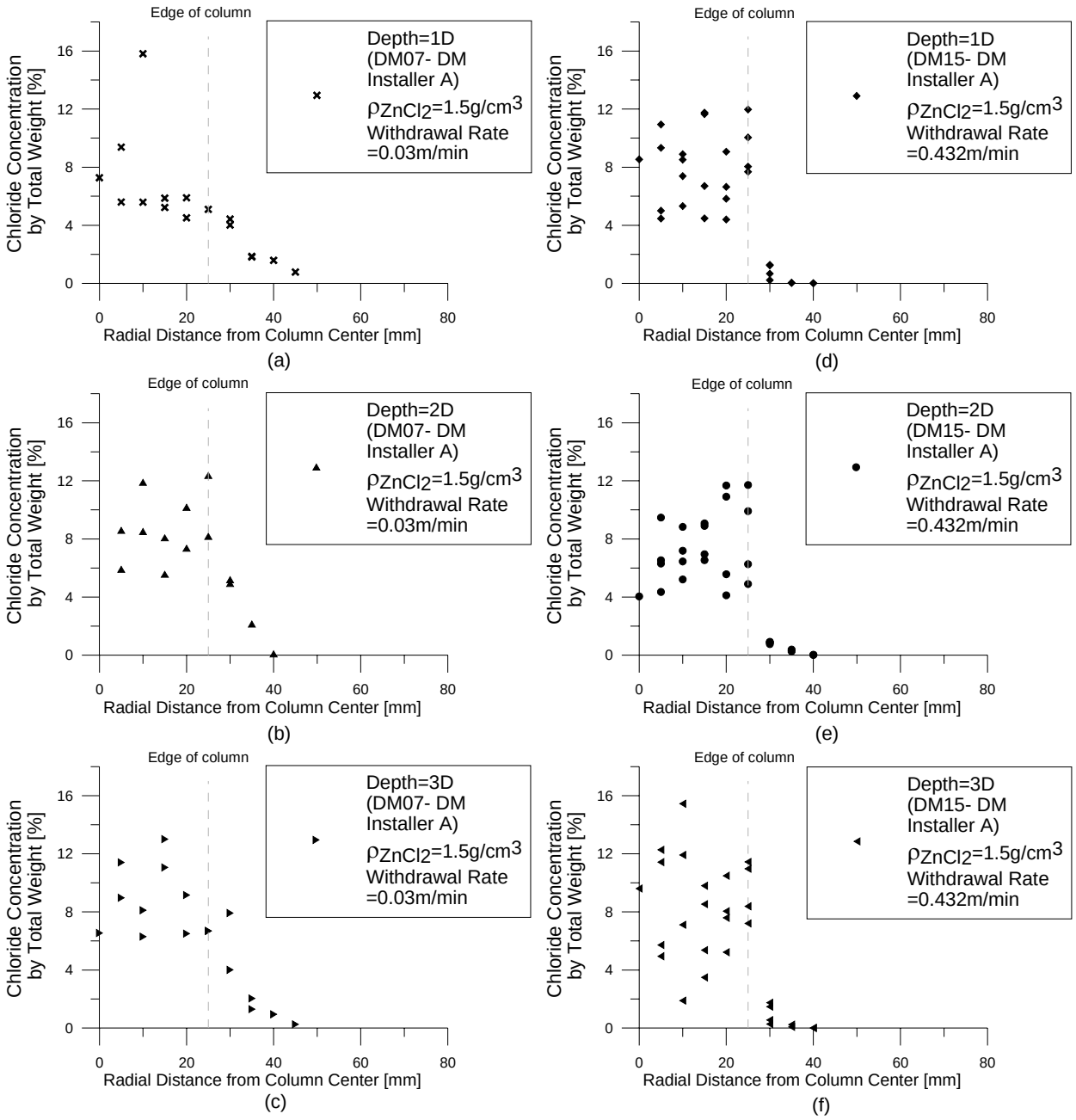

Fig. 5.13 Spot chloride concentration for model tests DM07 and DM15 at binder's density of 1.5g/cm^3.

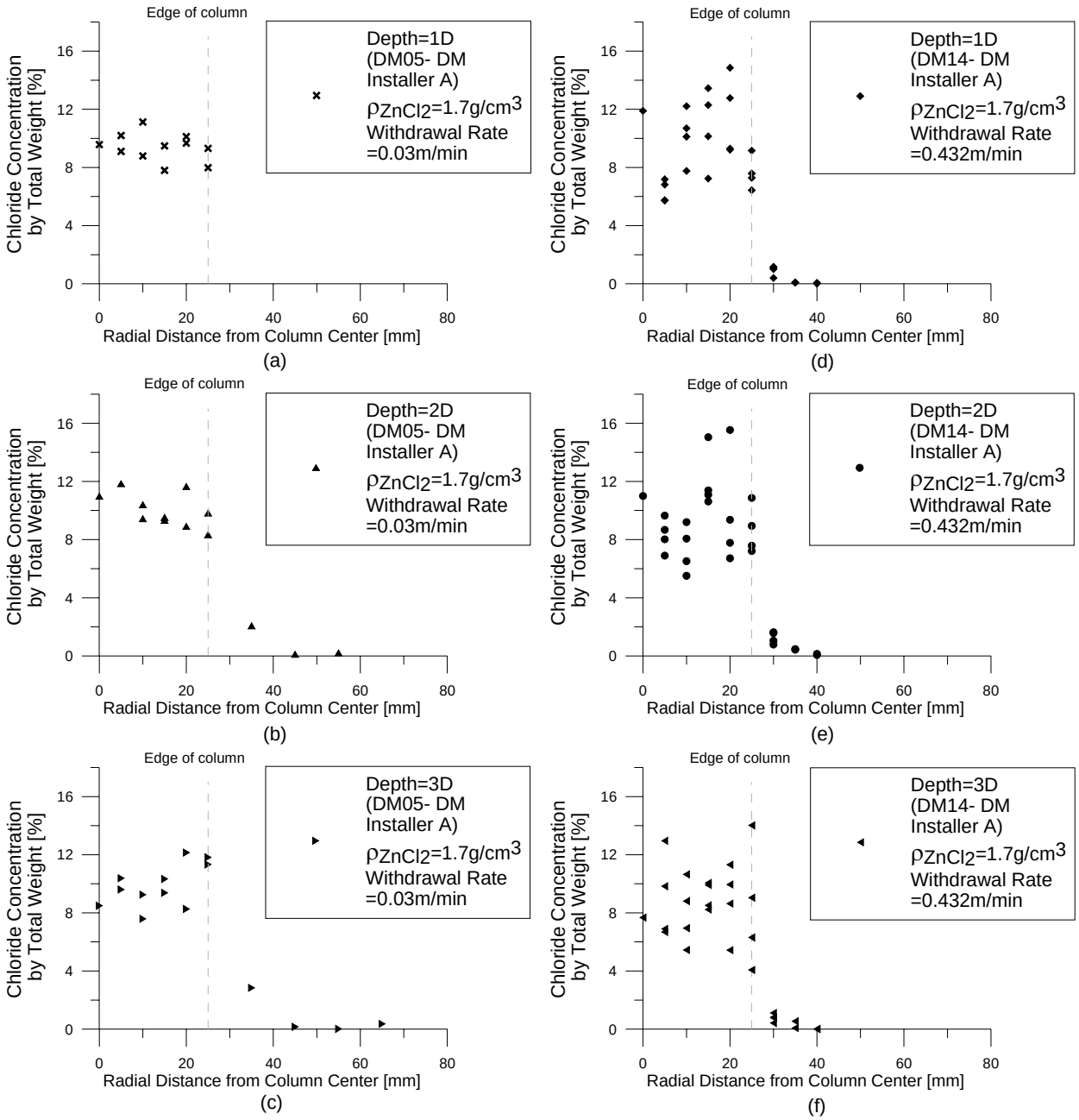

Fig. 5.14 Spot chloride concentration for model tests DM05 and DM14 at binder's density of 1.7g/cm^3.

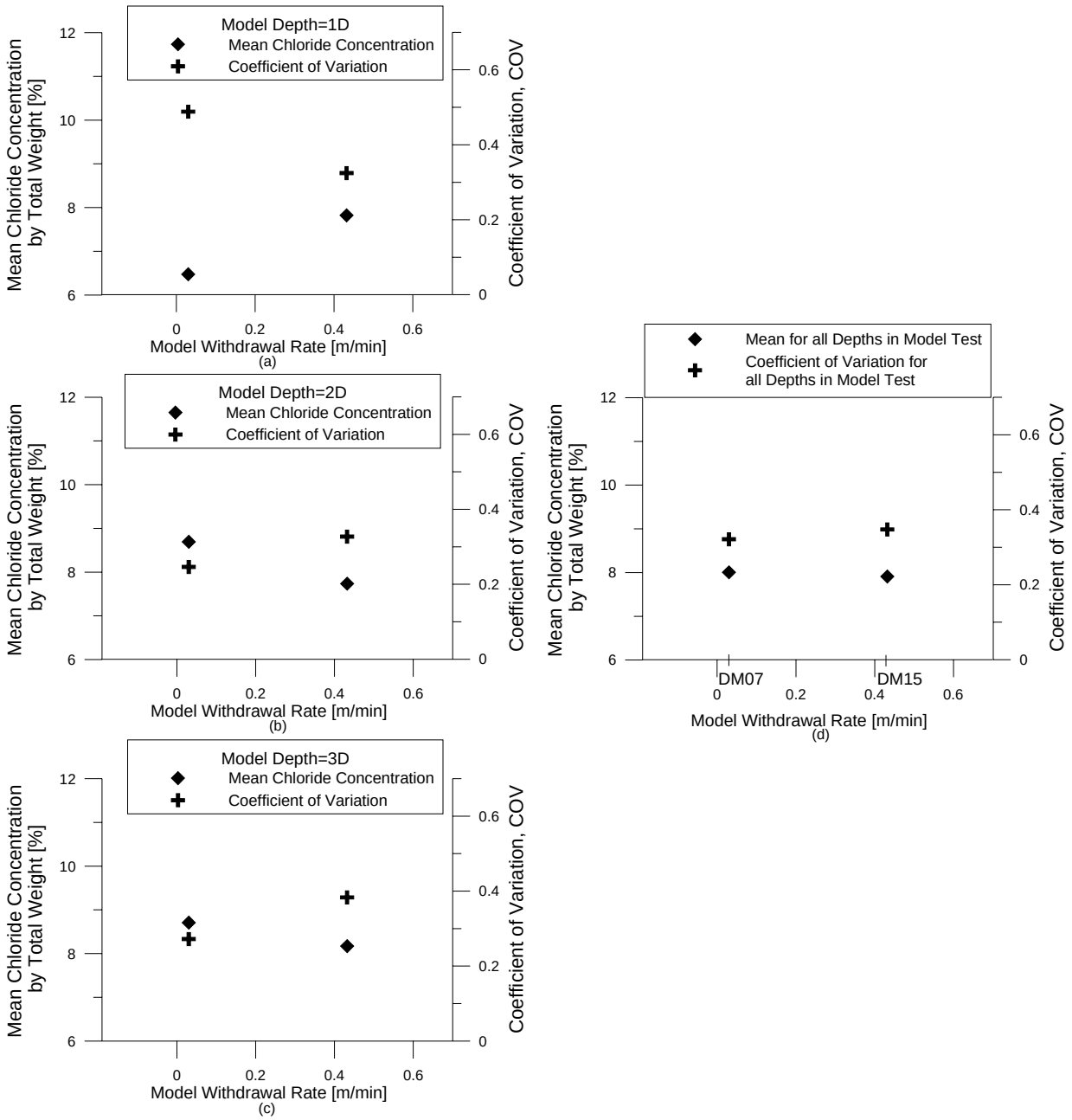

Fig. 5.15 Mean chloride concentration and coefficient of variation within the DM column for model tests DM07 and DM15 at binder density of 1.5g/cm^3.

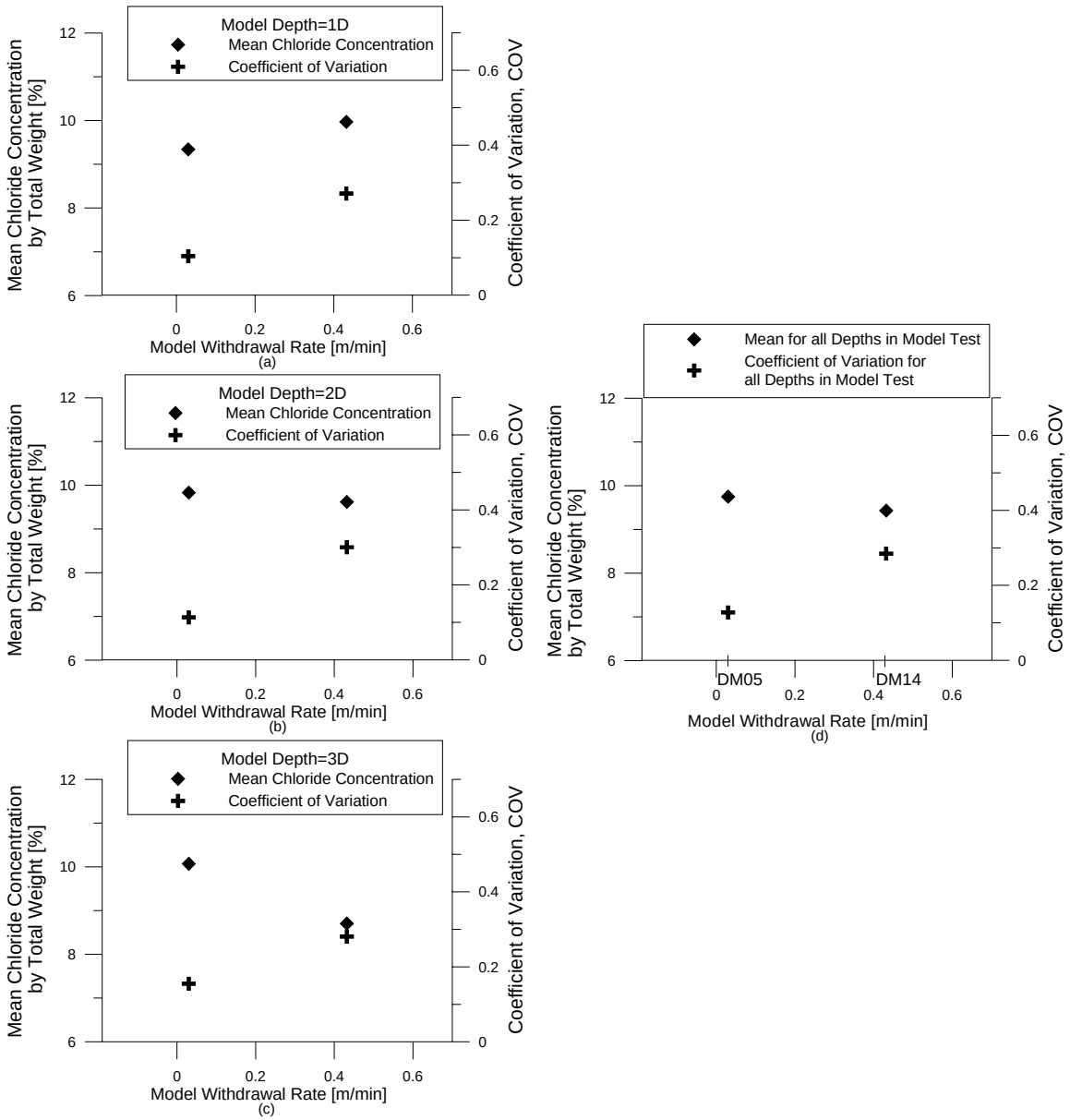

Fig. 5.16 Mean chloride concentration and coefficient of variation within the DM column for model tests DM05 and DM14 at binder density of 1.7g/cm^3.

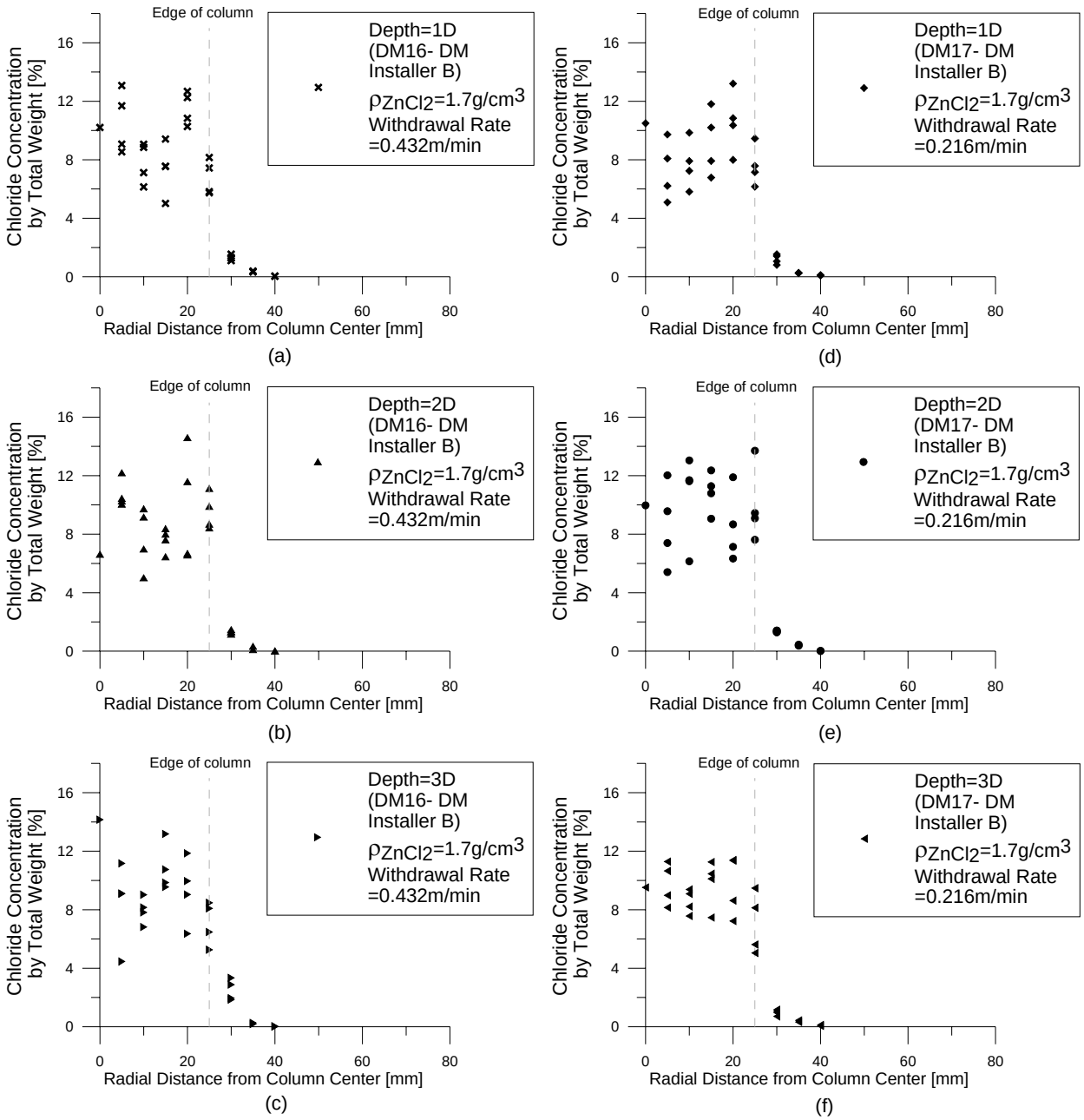

Fig. 5.17 Spot chloride concentration for model tests DM16 and DM17.

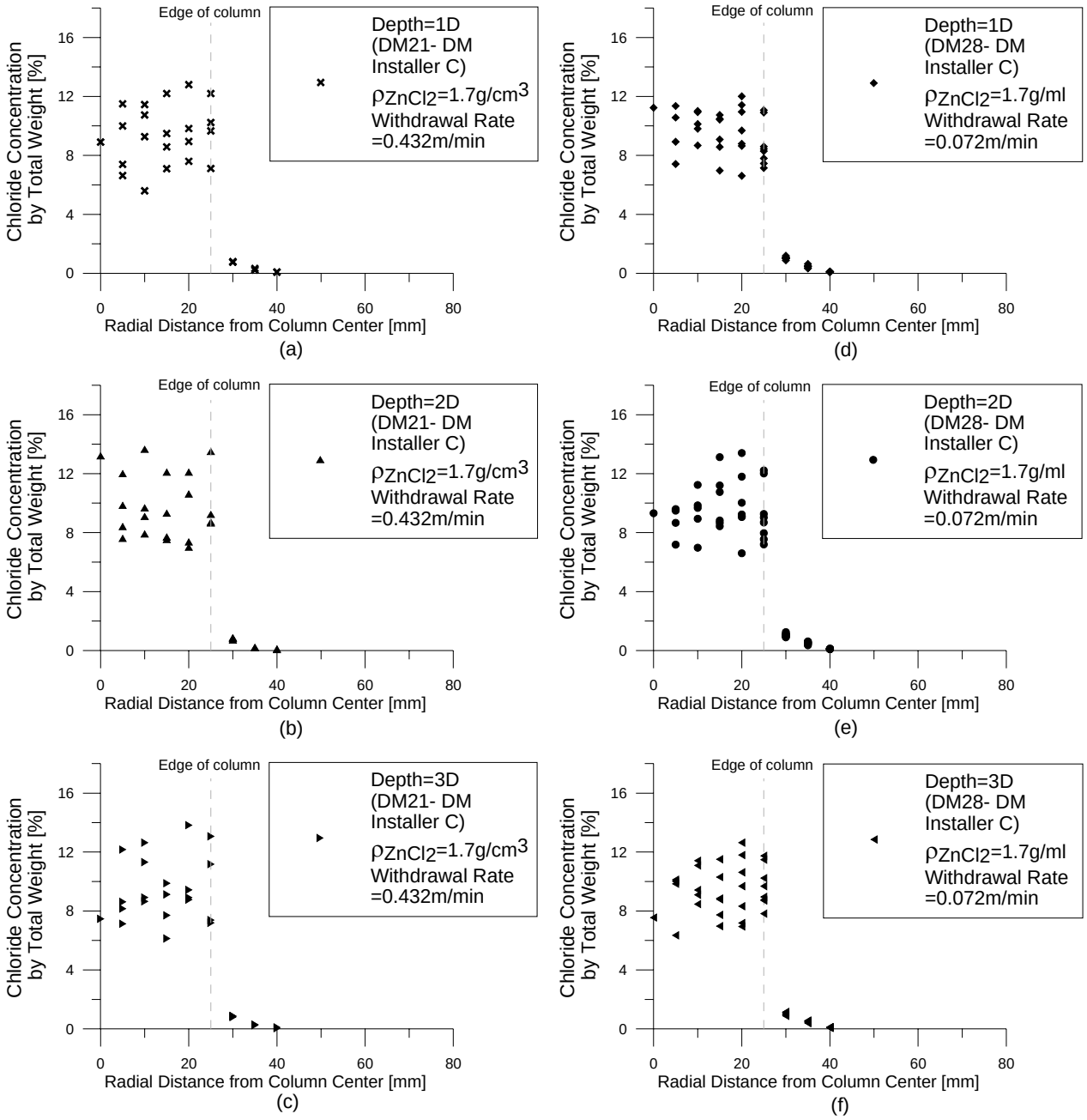

Fig. 5.18 Spot chloride concentration for model tests DM21 and DM28.

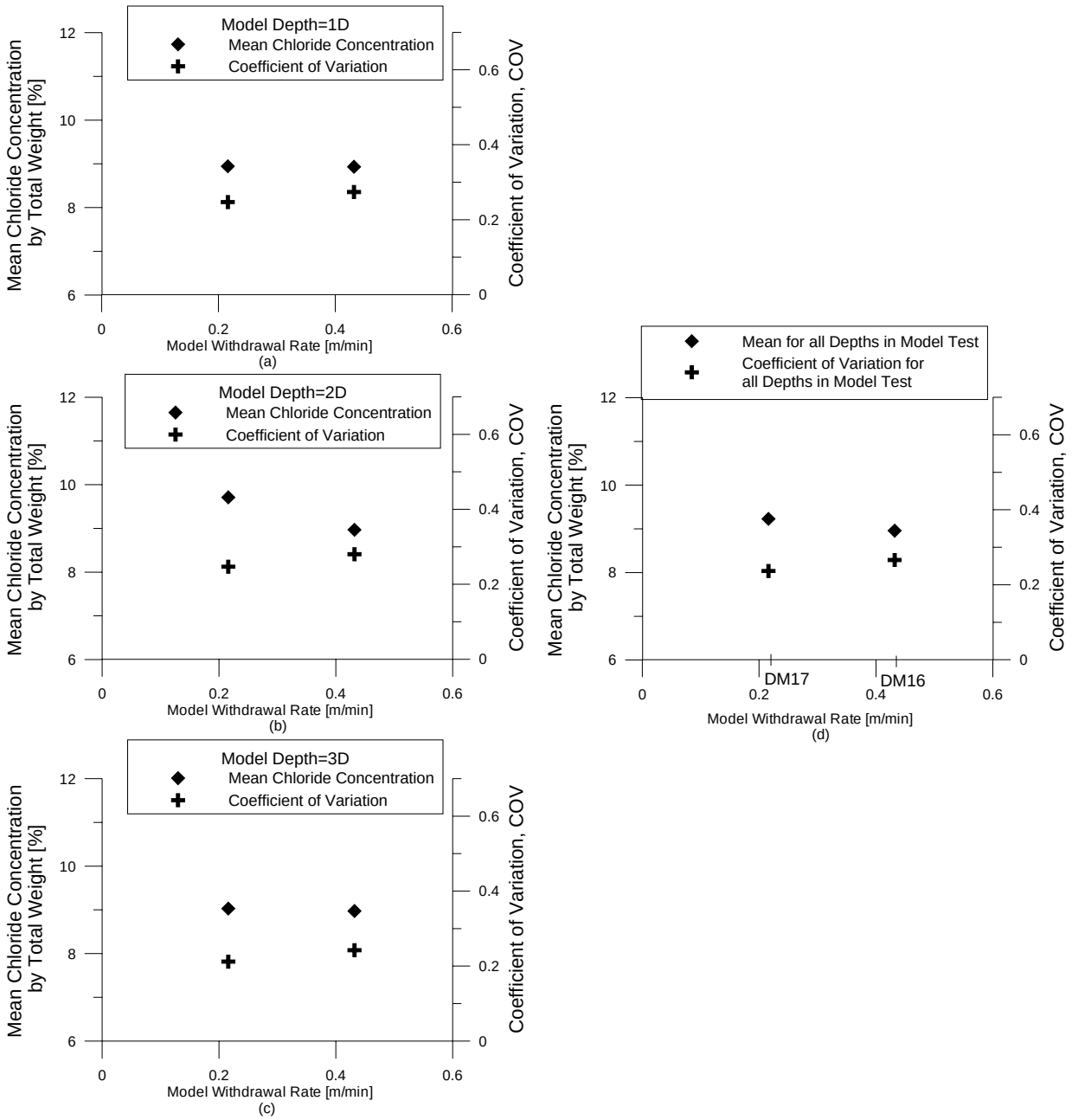

Fig. 5.19 Mean chloride concentration and coefficient of variation within the DM column for model tests DM16 and DM17.

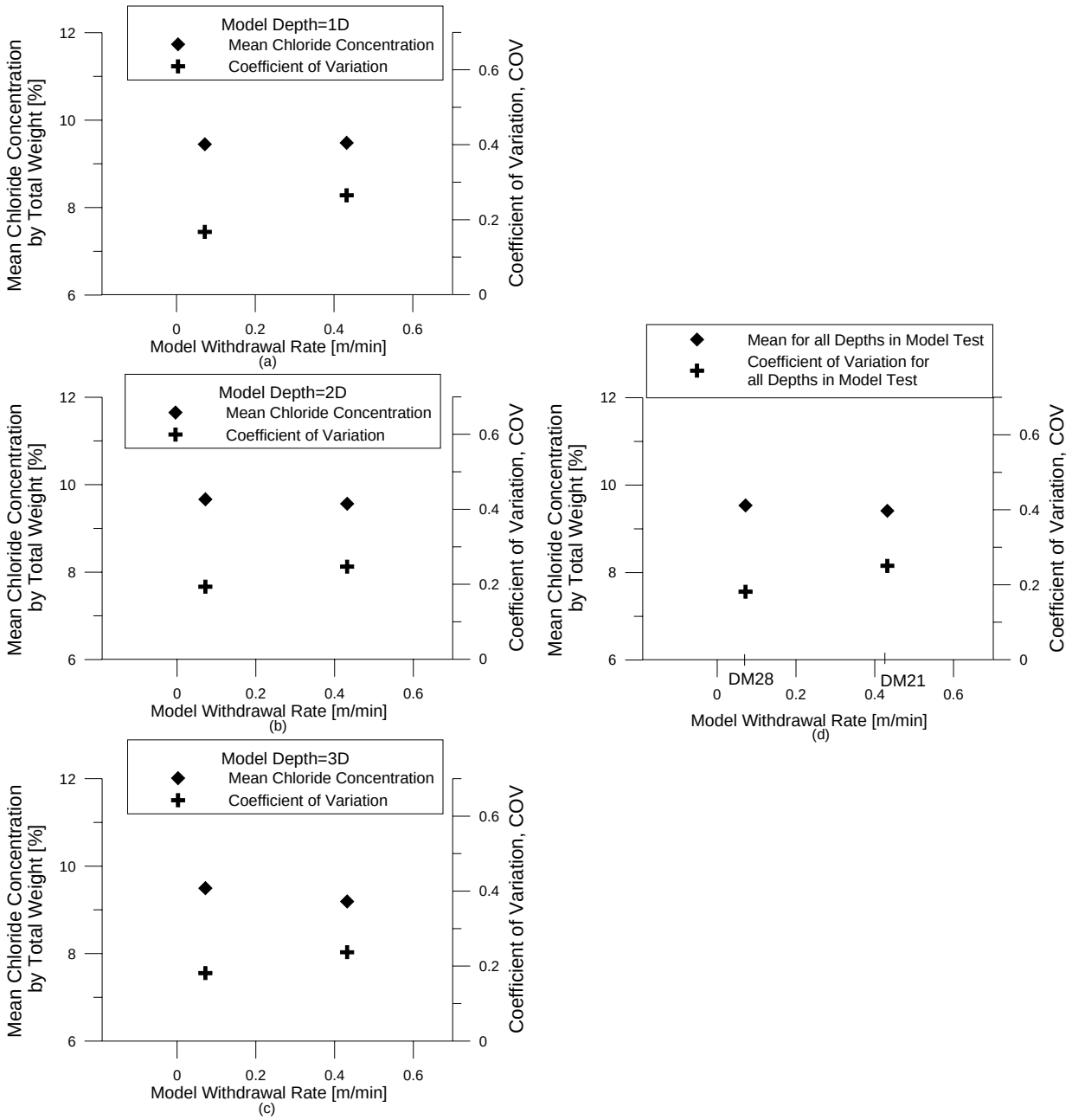

Fig. 5.20 Mean chloride concentration and coefficient of variation within the DM column for model tests DM21 and DM28.

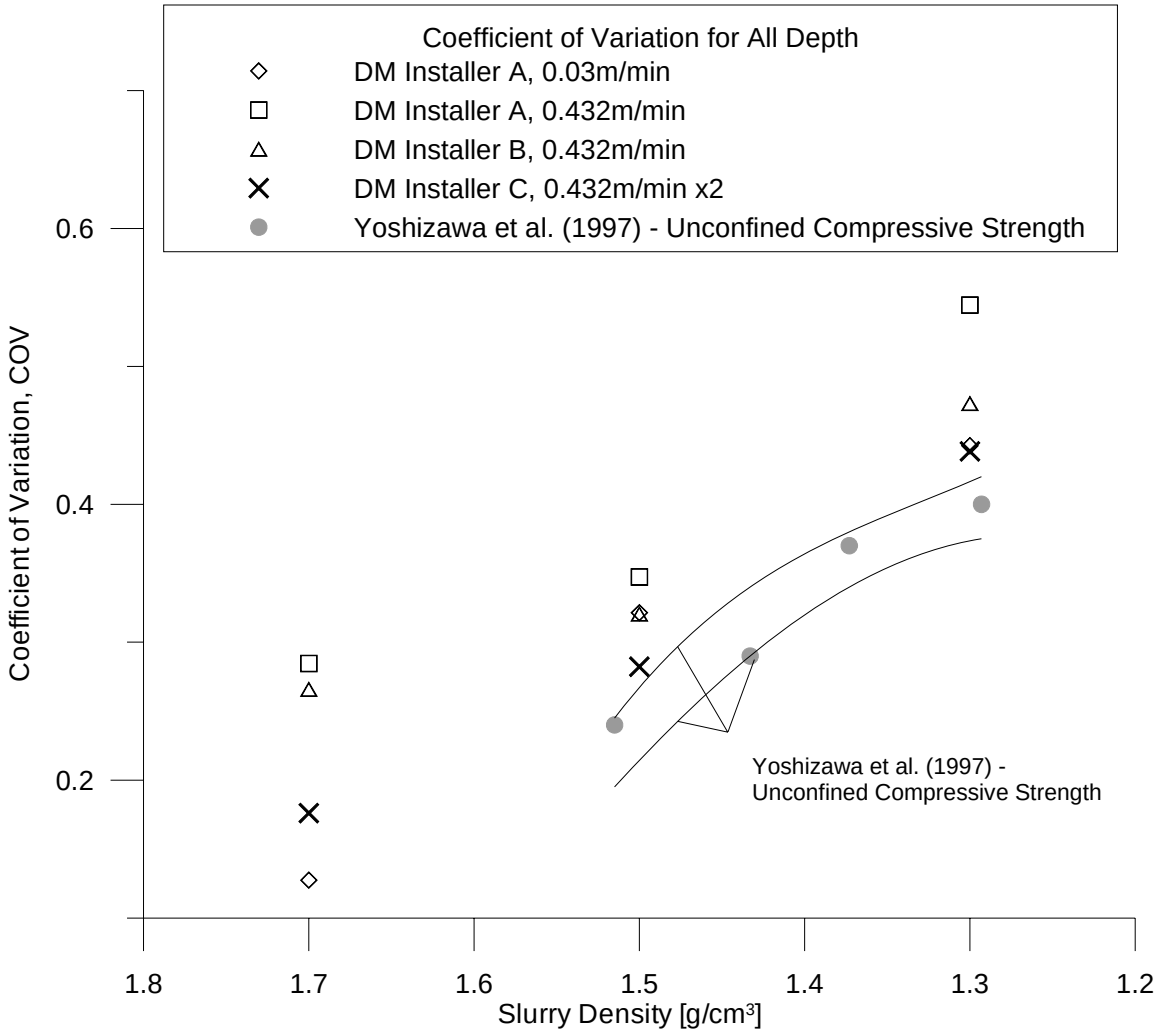

Fig. 5.21 Coefficient of variation within the DM column for high-g and 1-g model tests at difference slurry density of 1.3g/cm^3, 1.5g/cm^3 and 1.7g/cm^3.

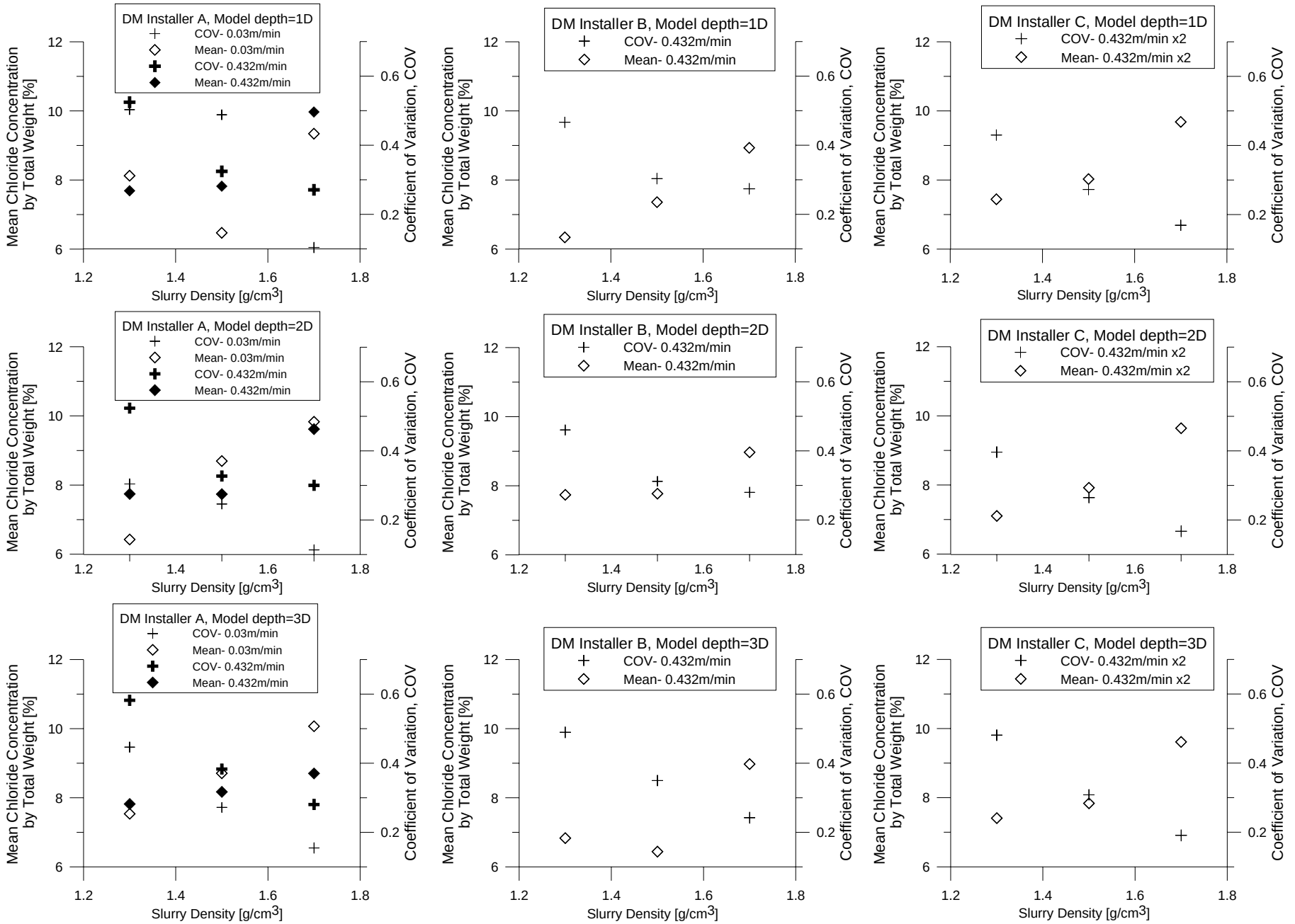

Fig. 5.22 Coefficient of variation for different model depth within the DM column at different slurry density of 1.3g/cm^3, 1.5g/cm^3 and 1.7g/cm^3.

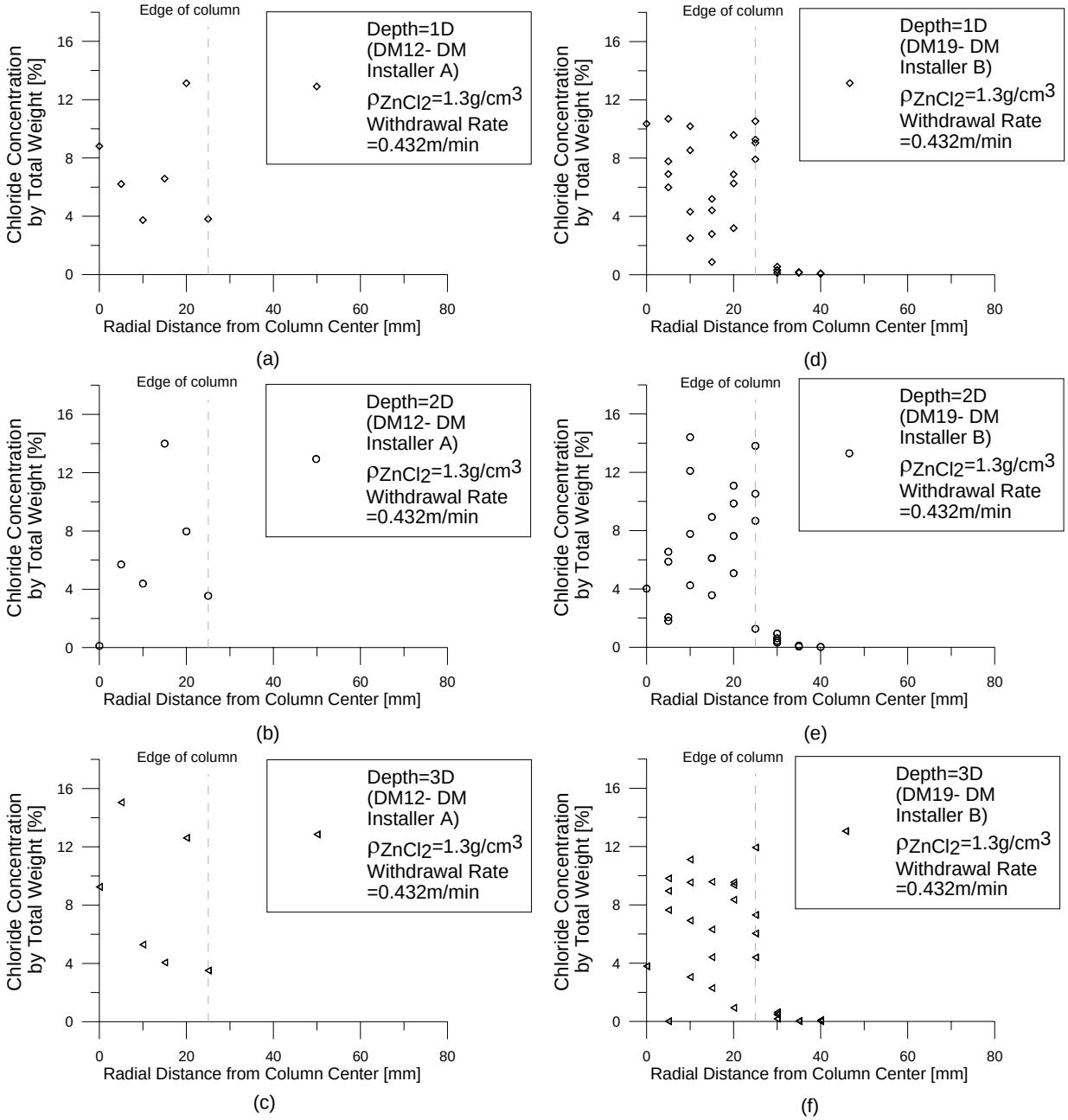

Fig. 5.23 Spot chloride concentration for model tests DM12 and DM19.

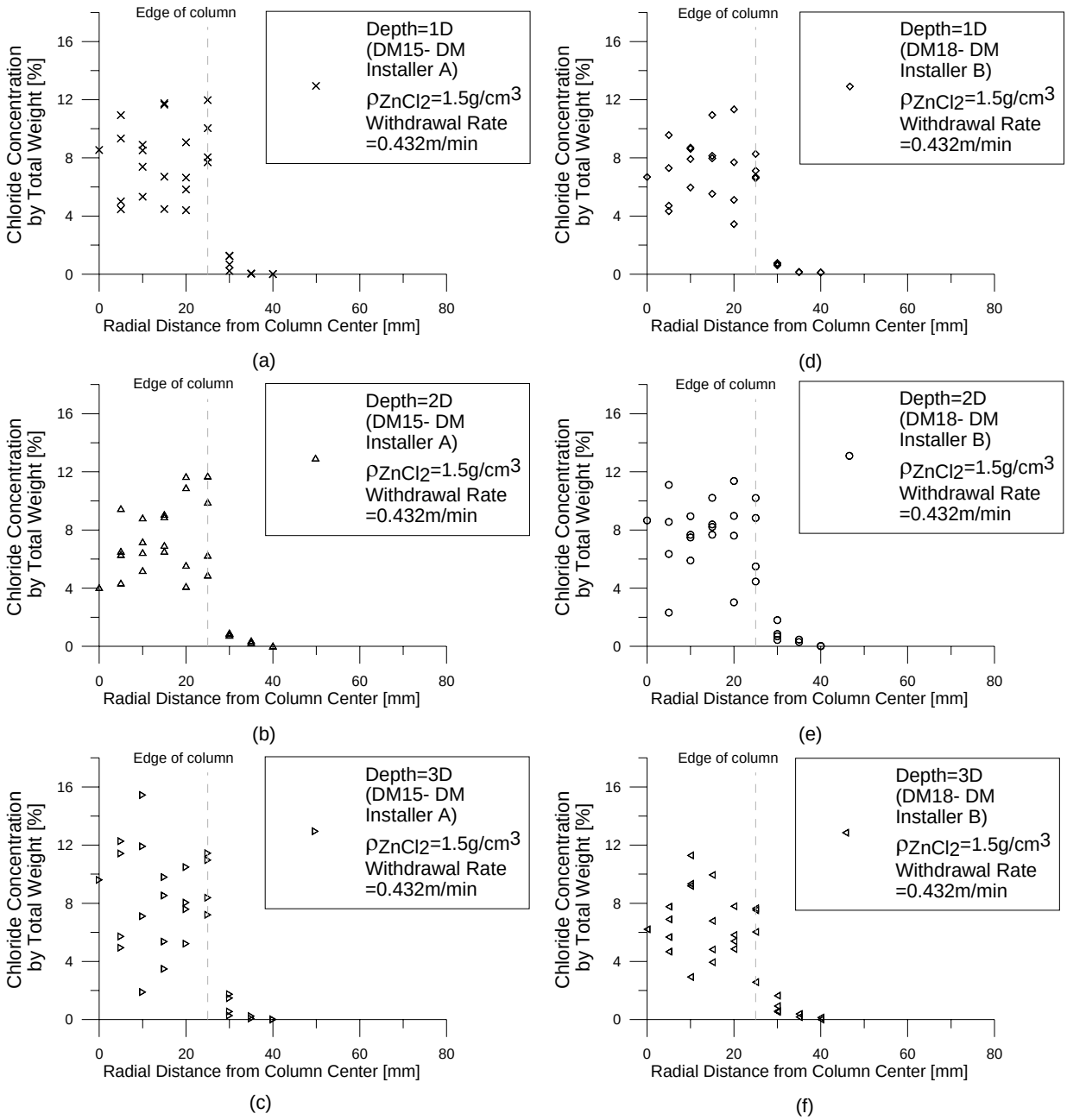

Fig. 5.24 Spot chloride concentration for model tests DM15 and DM18.

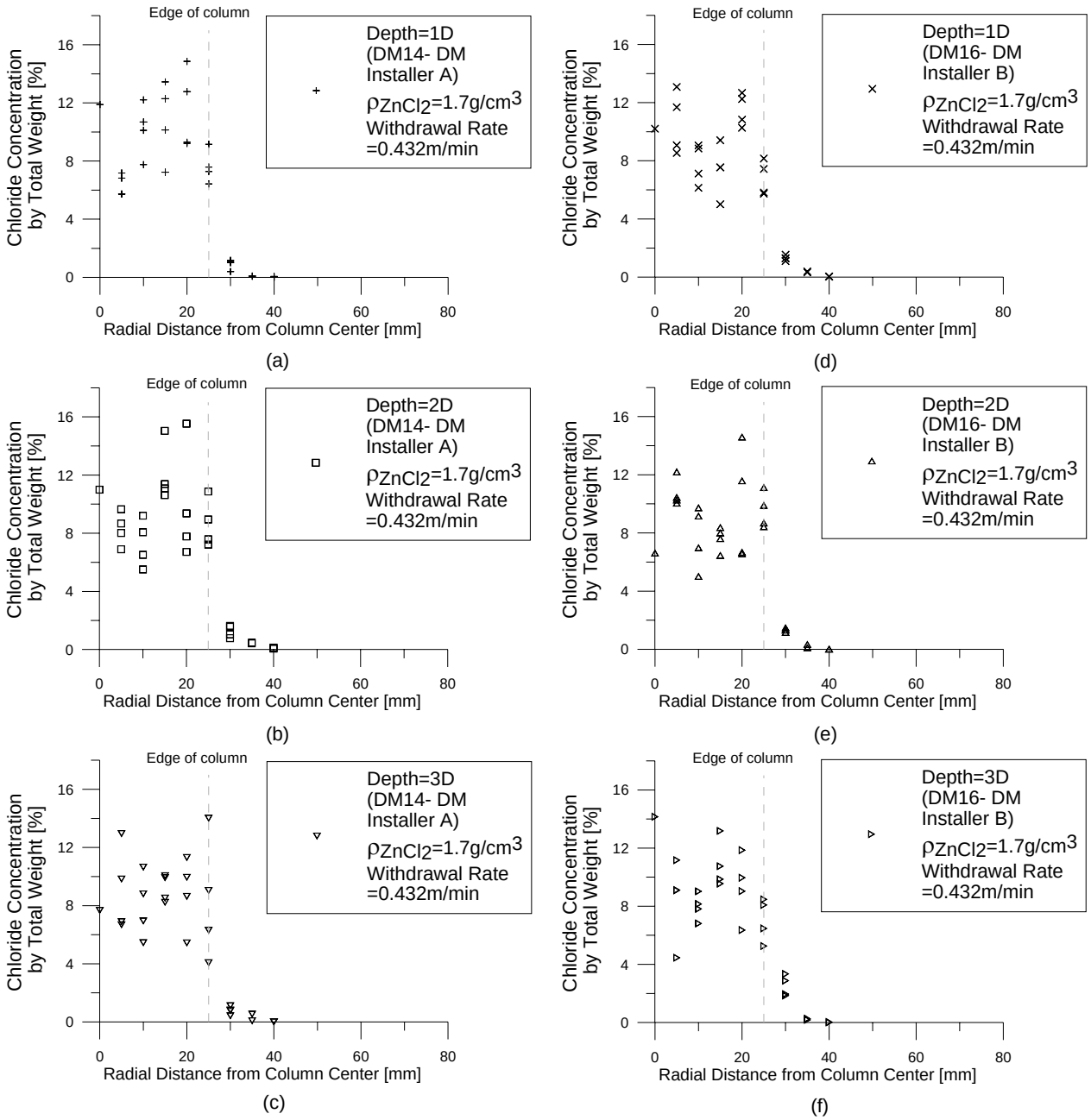

Fig. 5.25 Spot chloride concentration for model tests DM14 and DM16.

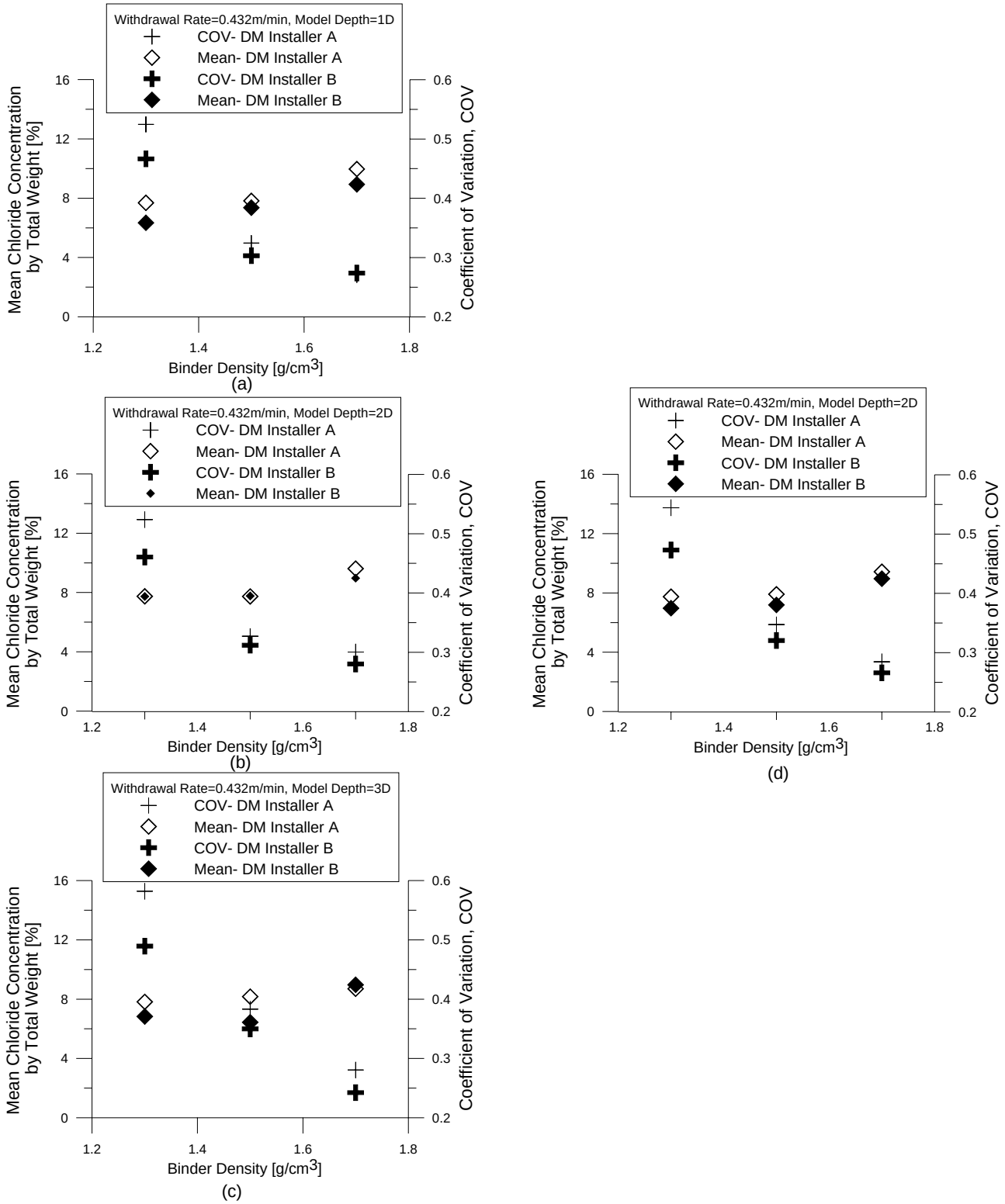

Fig. 5.26 Mean chloride concentration and coefficient of variation within the DM column for model tests conducted using DM installer A and DM installer B at different binder density.

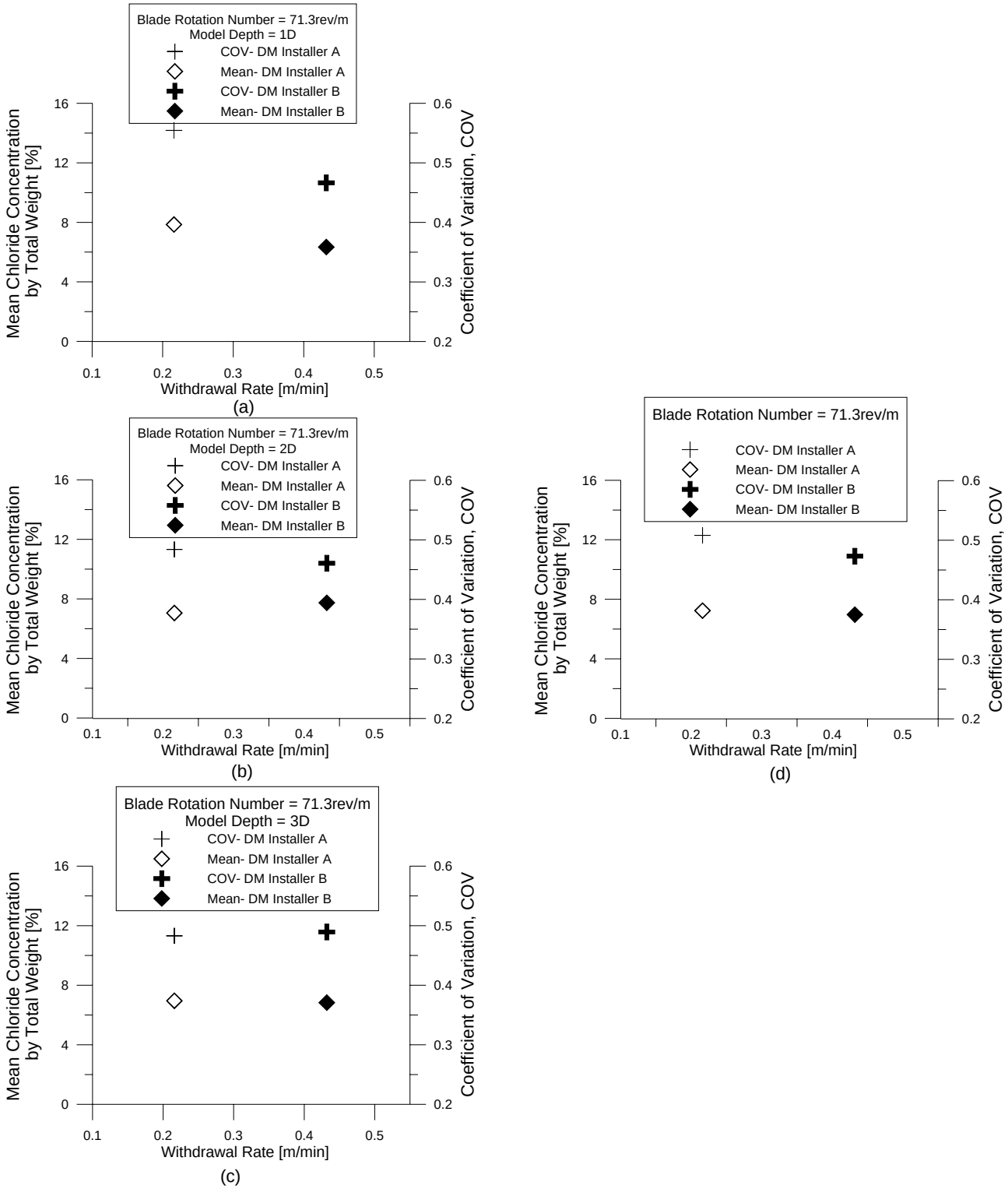

Fig. 5.27 Mean chloride concentration and coefficient of variation within the DM column for model tests conducted using DM installer A and DM installer B at same blade rotation number.

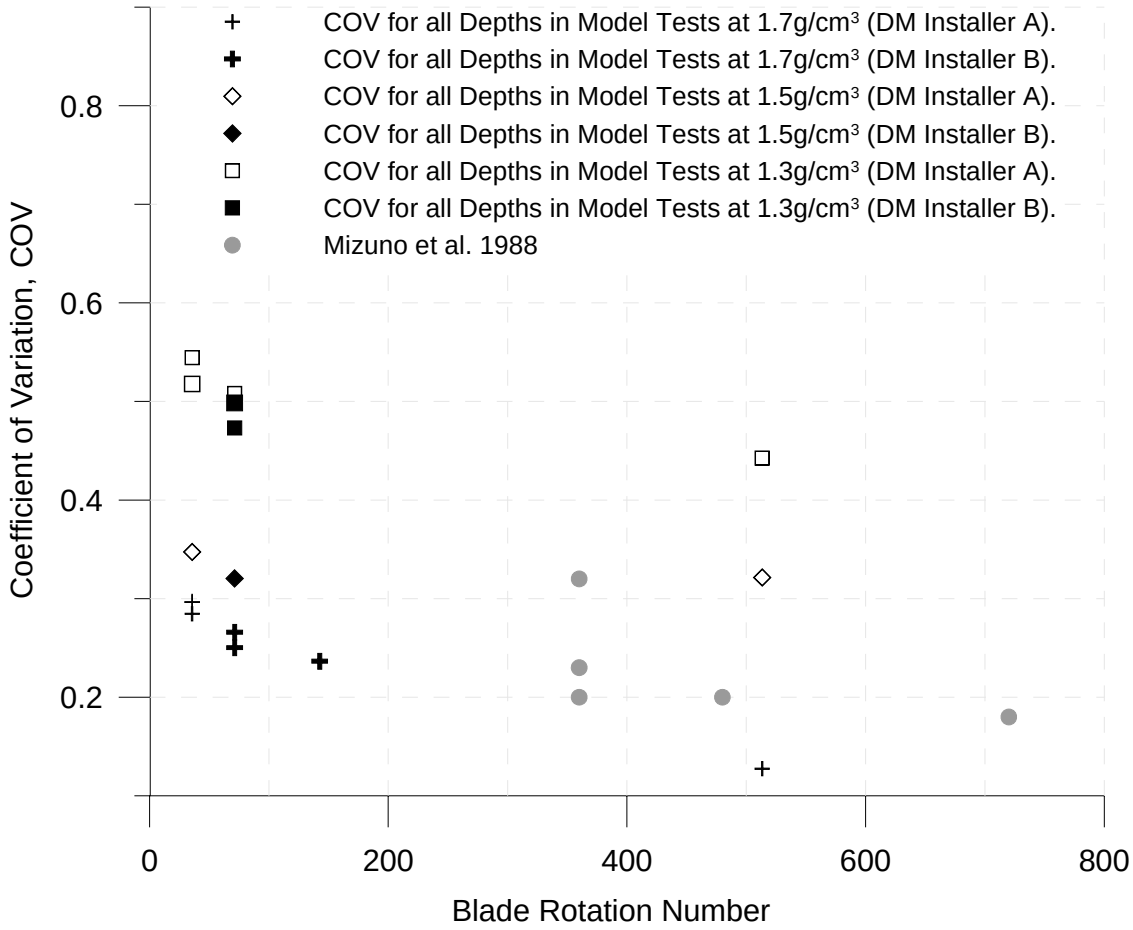

Fig. 5.28 Variation of COV at difference model withdrawal rate (DM installer A is equipped with single twisted-blades inclined at 45°, DM installer B is equipped with 2 twisted-blades inclined at 45° arranged in double layers).

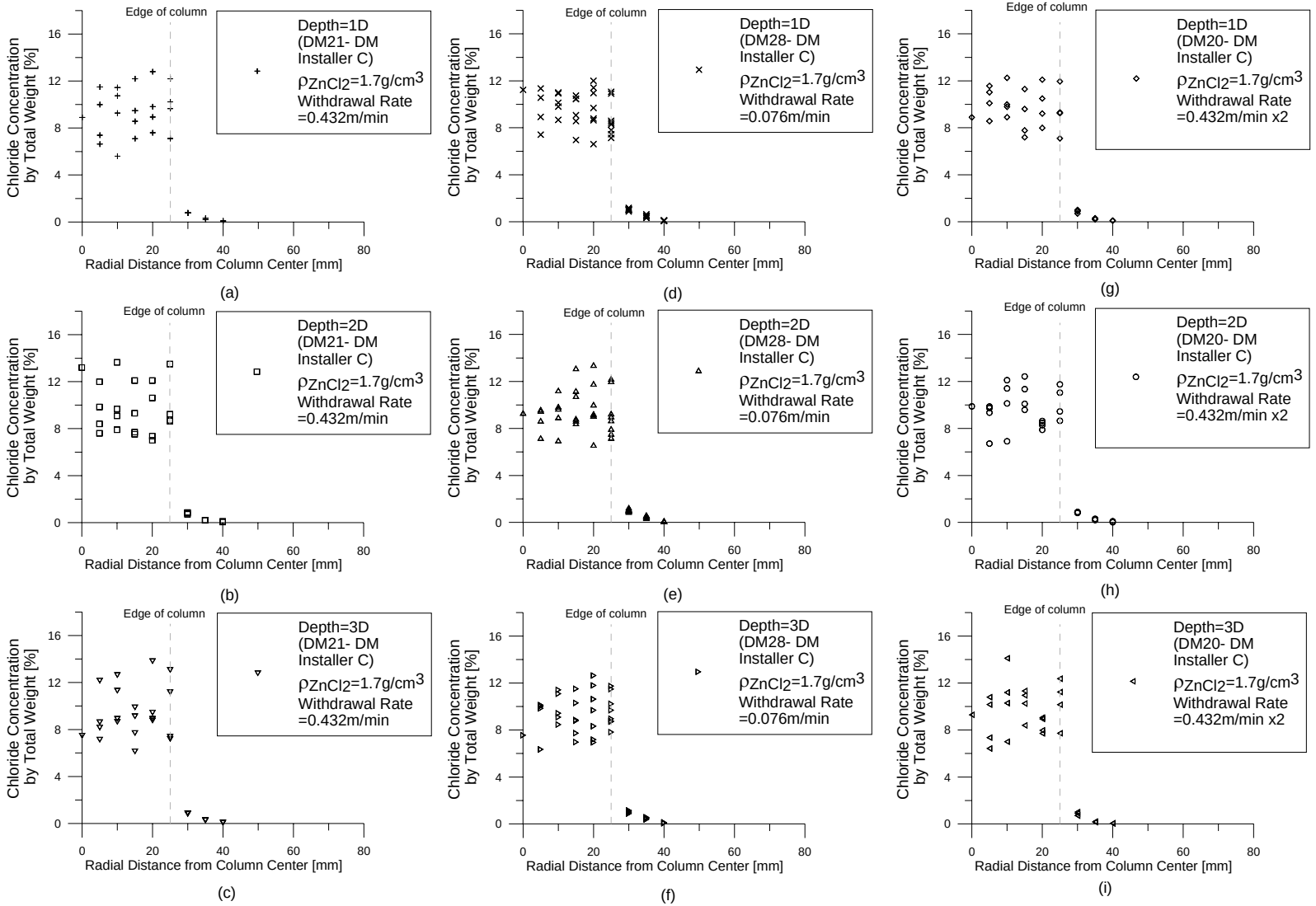

Fig. 5.29 Spot chloride concentration for model tests DM21, DM28 and DM20.

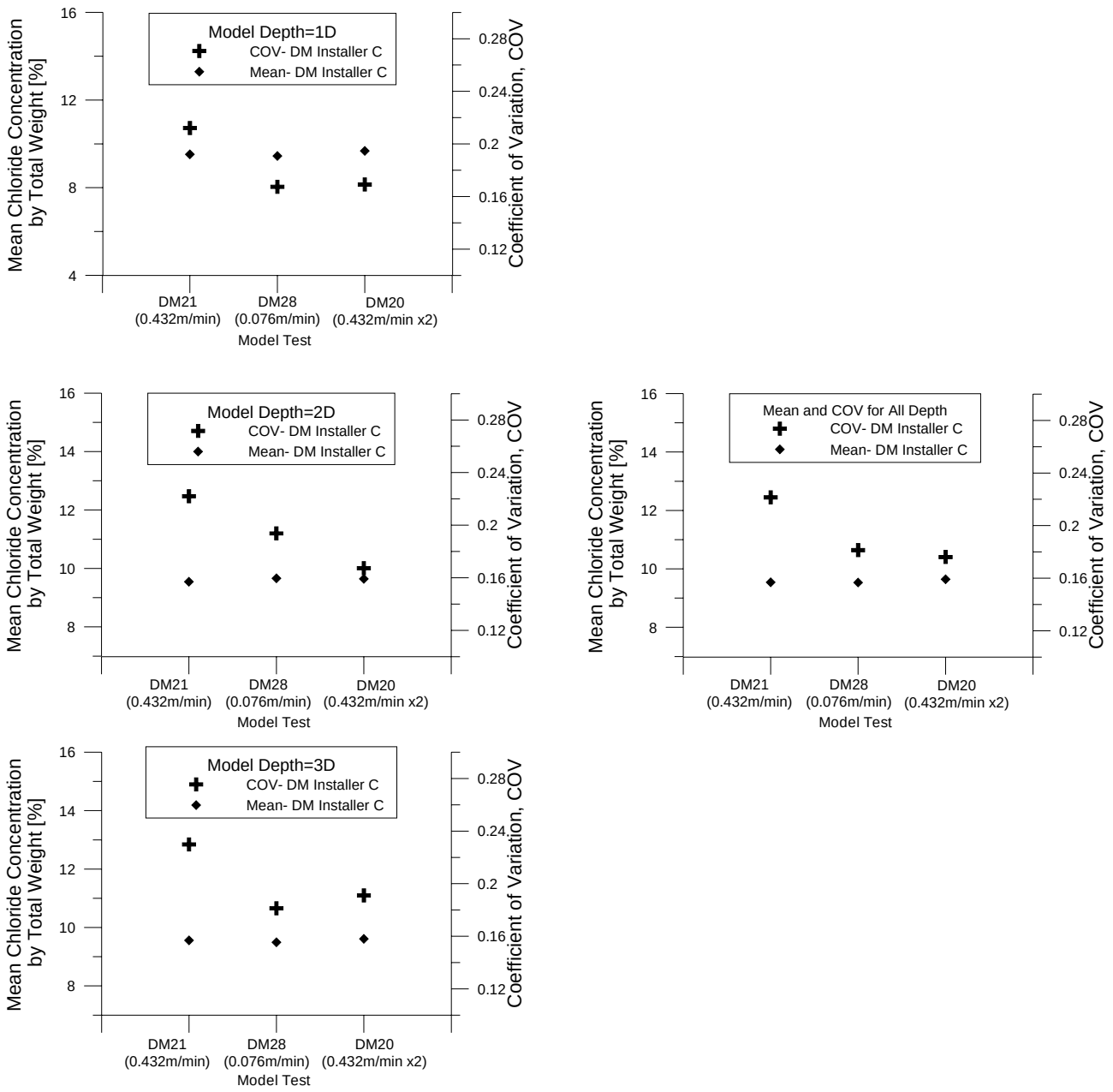

Fig. 5.30 Mean chloride concentration and coefficient of variation within the DM column for model tests conducted using DM installer C for model tests DM21, DM28 and DM20.

Chapter 6: Stress and Pore Pressure Changes in Surrounding Soil

Field results have shown that the stresses and pore pressures in surrounding soil changes during installation of the DM column (Shen 1998, Shen et al. 2003). Shen (1998) observed soil fracturing in laboratory vane shear study, 1-g model column installation and field DM installation. According to Shen (1998), the interaction mechanism between the installation of DM column and the surrounding clay gives rise to two kinds of forces acting on the wall of a DM column, i.e. (1) a shearing force from the rotating blades cutting the soil, (2) an expansion force from the injection of binder. These two forces contribute to the high excess pore pressure in clay. Shen (1998) postulated that this interaction mechanism is different from the displacement type of columnar inclusions such as pile driving and sand compaction pile installation, since both of latter processes do not consider the pore pressure generated due to pure shear. In DM installation, Shen (1998) showed the existence of additional shearing force during mixing may contribute towards soil fracturing around DM column. Shen's (1998) 1-g laboratory study suggested that the occurrence of soil fracturing would accelerate the infiltration of the binder into the surrounding soil in the vicinity of DM column. In order to further elucidate the interaction of in-flight installation of DM column and the surrounding clay, five centrifuge model tests were conducted to study the changes in pore pressure and the total stress during DM installation. All tests were conducted at withdrawal rate of 0.03m/min using DM installer A. This effect on binder distribution will be examined in this chapter.

6.1 Interaction between In-flight Installation of DM Column and the Surrounding Clay

Fig. 3.28 shows the location of the pore pressure transducers. Figs. 6.1 to 6.12 show the pore-pressure-time histories during installation of single DM column for test DM05, DM06, DM07, DM08 and DM09 within the latent periods between the penetration of the DM installer, feeding of zinc chloride and successive DM installation after the withdrawal phase. The depth and radial distance from the column centre of the PPTs are normalized against model blade diameter, *D* and model radius, *Rc* respectively. The zinc chloride was introduced when the DM installer reached its full installation depth of 3.6D. In these figures, the zero time point refers to the moment when the DM installer started to penetrate into the clay bed. In addition, the points in time at which the tip of the mixer reached the depth of PPTs i.e. 1D, 2D and 3D, during the penetration and withdrawal phases were also indicated by a straight line. As shown in these figures, PPTs which were closer to the DM column recorded a higher increase in the pore pressure and total lateral stress during the installation of DM installer. Increases in the pore pressure and lateral stress were observed when the blades of the DM installer approached the depth of the transducers.

As Figs. 6.1 to 6.12 show, all the pore pressure transducers showed increases in pore pressure during penetration and withdrawal. The pore pressure transducers nearest to the DM column showed the largest increase in pore pressure, which attenuates rapidly with distance away from the column. In at least some of the cases, at a given depth, there appears to be a time lag in pore pressure rise between the nearest and furthest pore pressure transducer. For example, PPT2 and PPT5 are both located at depth of 2D

but at distances of $1.6R_c$ and $3R_c$ away from the DM cavity as shown in Fig. 3.28. In Figs. 6.2 and 6.5, PPT2 shows pore pressure rises before PPT5. In Figs. 6.8, the time lag is not evident. The quantum of the time lag is about 40seconds in model time. The relatively short time lag indicates that the pore pressure increase is likely to have taken place under largely undrained condition. If so, then it is likely to be largely due to stress induction rather than pore fluid diffusion. This is also what Shen (1998) observed in the field and indeed, is also the assumption of Shen's (1998) shear-expansion analysis. It should be noted that, since stresses are preserved at homologous points in a centrifuge model, it is likely that stress-induced pore pressure changes will also be reasonably captured. On the other hand, since consolidation phenomenon is accelerated N^2 times in a centrifuge model whereas the mixing event is only accelerated N times, there may be some scale distortion in capturing pore pressure diffusion in the surrounding soil. Due to this discrepancy of time similitude, the pore pressure diffusion process is N time faster than the DM event. Since both events cannot be correctly scaled at the same time, there will be scale distortion in the pore pressure diffusion process. However, this is not the main object of this study. In any case, the presence of cracks in the surrounding soil suggests that hydro-fracturing may well be a more significant means of pore pressure leakage into the surrounding soil than diffusion.

Shen's (1998) shearing-expansion of cylindrical cavity will be used in our back analysis of the excess expanding pressure ratio on the cavity wall, for a given excess pore pressure ratio inferred in our experimental results. Shen (1998) showed that the pore pressure ratio inferred from the field measurement agrees well with the predicted value based on the shearing-expansion of cylindrical cavity. The predicted slurry

injection pressure falls within the work pressure of the DM machine. In his analytical model, the stress change due to shearing-expansion of cylindrical cavity is assumed to take place in an ideal elasto-plastic homogeneous material with initially isotropic stress conditions. The soil in the plastic zone is assumed to behave as a plastic material defined by the Mohr-Coulomb criterion. Beyond the plastic zone, the soil is assumed to behave as an elastic isotropic material defined by the deformation modulus, E and μ. The body force is also neglected and all of the plastic strain occurs under undrained and unconsolidated (UU) condition. The excess pore pressure Δu within the plastic zone can be expressed in term of the mean normal stress change $\Delta\sigma_{oct}$ and the mean shear stress change $\Delta\tau_{oct}$. The excess pore pressure in the plastic zone is given by

$$\Delta u = \beta \times \Delta\sigma_{oct} + \alpha \times \Delta\tau_{oct} \qquad (6.1)$$

For saturated soil, β is equal to 1. According to Shen's (1998) shearing-expansion of cylindrical cavity, the $\Delta\sigma_{oct}$ and $\Delta\tau_{oct}$ are given by

$$\Delta\sigma_{oct} = \Delta p_c^{'} - 2 \times c_{u0} \times In\left(\frac{r}{R_c}\right) - c_{uo} \times In\left(\frac{1+B_{r1}}{1+B_{rt}}\right) - c_{uo} \times B_{rt} \qquad (6.2)$$

$$\Delta\tau_{oct} = 0.816 \times c_{u0} \qquad (6.3)$$

in which Δp_c' is the excess expanding pressure on the cavity wall, c_{uo} is the in-situ undrained shear strength of soil and

$$B_{r1} = \sqrt{1 - t_c^2 \times \left(\frac{R_c}{r}\right)^4} \qquad (6.4)$$

$$B_{rt} = \sqrt{1 - t_c^2} \qquad (6.5)$$

$$t_c = \frac{T_Q}{c_{uo}} \qquad (6.6)$$

in which T_Q is the shearing force on the cavity wall, R_c is the radius of column and r is radial distance from column centre.

Substituting Eqs. 6.2 and 6.3 into Eq. 6.1 lead to excess pore pressure ratio $\frac{\Delta u}{c_{uo}}$, such that

$$\frac{\Delta u}{c_{uo}} = \frac{\Delta p_c^{'}}{c_{u0}} - 2 \times In\left(\frac{r}{R_c}\right) - In\left[\frac{1+B_{r1}}{1+B_{rt}}\right] - B_{rt} + 0.816 \times \alpha_f \qquad (6.7)$$

in which α_f is the Henkel's pore pressure parameter at failure state and can be calculated from Skempton's pressure parameter A_f (e.g. Shen 1998)

$$\alpha_f = 0.707 \times \left(3 \times A_f - 1\right) \qquad (6.8)$$

According to Shen (1998), the excess pore pressure ratio in the elastic zone can be calculated from Lame's solution (Vesic, 1972)

$$\frac{\Delta u}{c_{uo}} = 0.816 \times \alpha \times \left(\frac{R_p}{r}\right)^2 \qquad (6.9)$$

in which R_p is the plastics zone and α represents Henkel's pore pressure parameter, $0 < \alpha < \alpha_f$.

At the boundary of plastic zone, there is no mean normal stress increment, thus the radius of plastic zone can be calculated from (Shen 1998)

$$\frac{\Delta \sigma_{oct}}{c_{uo}} = \frac{\Delta p_c^{'}}{c_{u0}} - 2 \times In\left(\frac{R_p}{R_c}\right) - In\left[\frac{1+B_{r1}}{1+B_{rt}}\right] - B_{rt} = 0 \qquad (6.10)$$

As discussed earlier, the existence of shearing force during mixing might caused the hydraulic fracturing of the soil to be much easier induced around DM column as compared to pure expansion of cavity. For soft clay, the lower limit of ΔP_f can be expressed by the relationship (Yanagisawa and Panah 1994, Shen 1998)

$$\Delta P_f = P_f - \sigma_h = c_{uo} \qquad (6.11)$$

in which P_f is total hydraulic fracture pressure, ΔP_f is hydraulic pressure increment and σ_h is minor principal in-situ stress. Shen (1998) observed that with a cement mix of 2% to 4%, the excess expanding pressure on the cavity wall Δp_c' will generally be greater than the minimum hydraulic fracturing increment, ΔP_f which indicates that the surrounding clay is readily fractured during DM installation.

Fig. 6.13 shows the excess pore pressure ratio, $\frac{\Delta u}{c_{uo}}$ inferred from the test results to the normalised distance $\frac{r}{R_c}$. The excess pore pressures ratios $\frac{\Delta u}{c_{uo}}$ were also calculated based on the assumption that $G_s = 2.65$, $w = 61\%$ and $\frac{c_{uo}}{q'} = 0.22$ in which q' is the vertical effective stress using Shen's (1998) shearing-expansion of cylindrical cavity. Shen et al. (2003) shows that for undisturbed samples extracted using a block sampler, A_f value for Ariake clay range from 1.1 to 1.4; for samples taken using a think wall sampler, A_f range from 0.8 to 1.2. For this analysis, A_f = 1.0 was used. The shearing force T_Q was set to the same value as c_{uo}. As Fig. 6.13 shows, the measured and predicted excess pore pressures ratios $\frac{\Delta u}{c_{uo}}$ fall within the same range when the excess

expanding pressure ratio on the cavity wall $\frac{\Delta P_c^{'}}{c_{uo}}$ is set to a range of 2 to 5 in Shen's shear-expansion model. This prediction gives an insight into the ratio of excess expanding pressure to in situ undrained shear strength $\frac{\Delta P_c^{'}}{c_{uo}}$ in our model tests. As shown in Fig. 6.13, the measured values of $\frac{\Delta u}{c_{uo}}$ are consistent with those predicted by Shen's shear expansion theory, if the ratio $\frac{\Delta P_c^{'}}{c_{uo}}$ falls within the range of 2 and 5. Shen further noted that, for Ariake clay, $\frac{\Delta P_c^{'}}{c_{uo}}$ falls between 5 and 6. Thus, the back-deduced values of $\frac{\Delta P_c^{'}}{c_{uo}}$ from the centrifuge pore pressure measurements are lower than those for Ariake clay. This discrepancy may be due to the occurrence of diffusion in the surrounding soil as a result of the accelerated pore pressure dissipation process in the centrifuge model, arising from the mis-scaling of the diffusion process discussed above.

As discussed earlier, the minimum incremental hydraulic fracturing pressure is $\Delta P_f = c_{uo}$ (Yanagisawa and Panah 1994, Shen 1998). Fig. 6.13 also shows that the excess pore pressure ratio increased with the decrease of radial distance ratio, being largest in the immediate vicinity of the DM column. From Fig. 6.13, the pore pressure ratio in the immediate soil around DM column was much greater than 1. As discussed above, the minimum hydraulic pressure increment to cause soil fracturing is 1. This suggests that soil fracturing might have occurred in the immediate surrounding of the DM column. In such an eventuality, the zinc chloride would have infiltrated into the soil via the fractures around the DM column. This explains the reason, in which a

small portion of zinc chloride was able to infiltrate to the outside of the DM column within the short duration of the DM installation, as observed earlier.

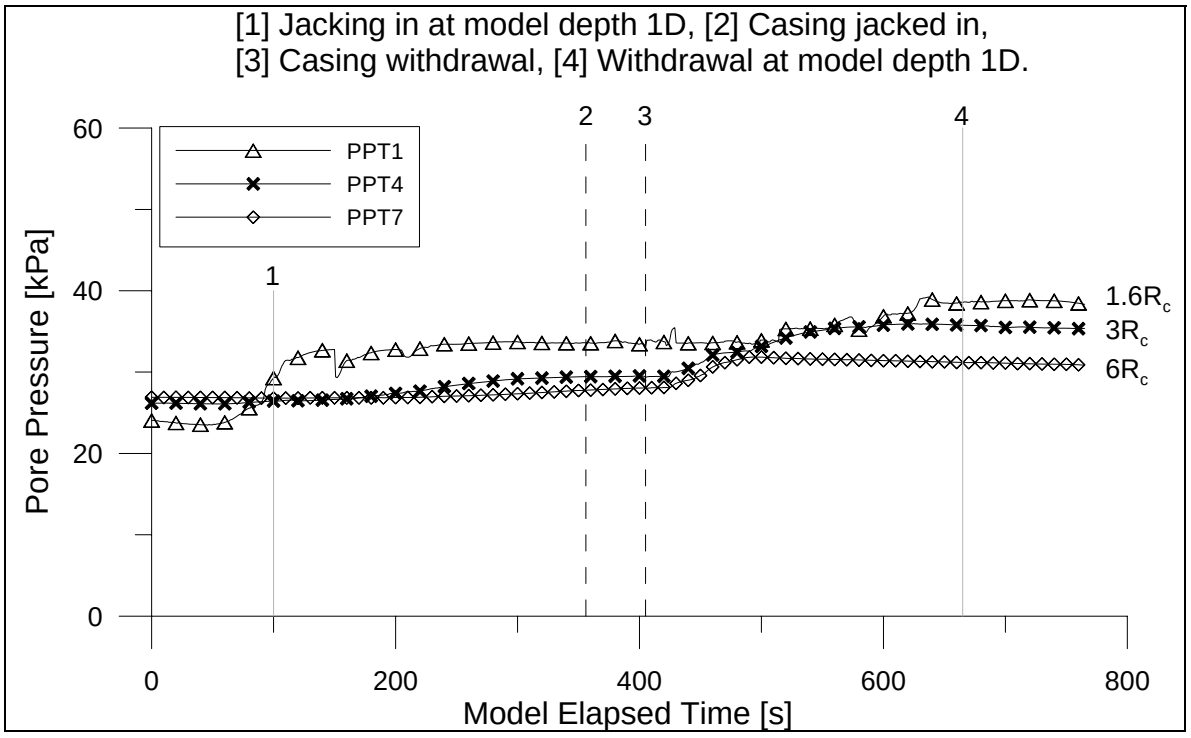

Fig. 6.1 Pore pressure recorded by PPTs at model depth 1D during installation of single DM column for test DM05.

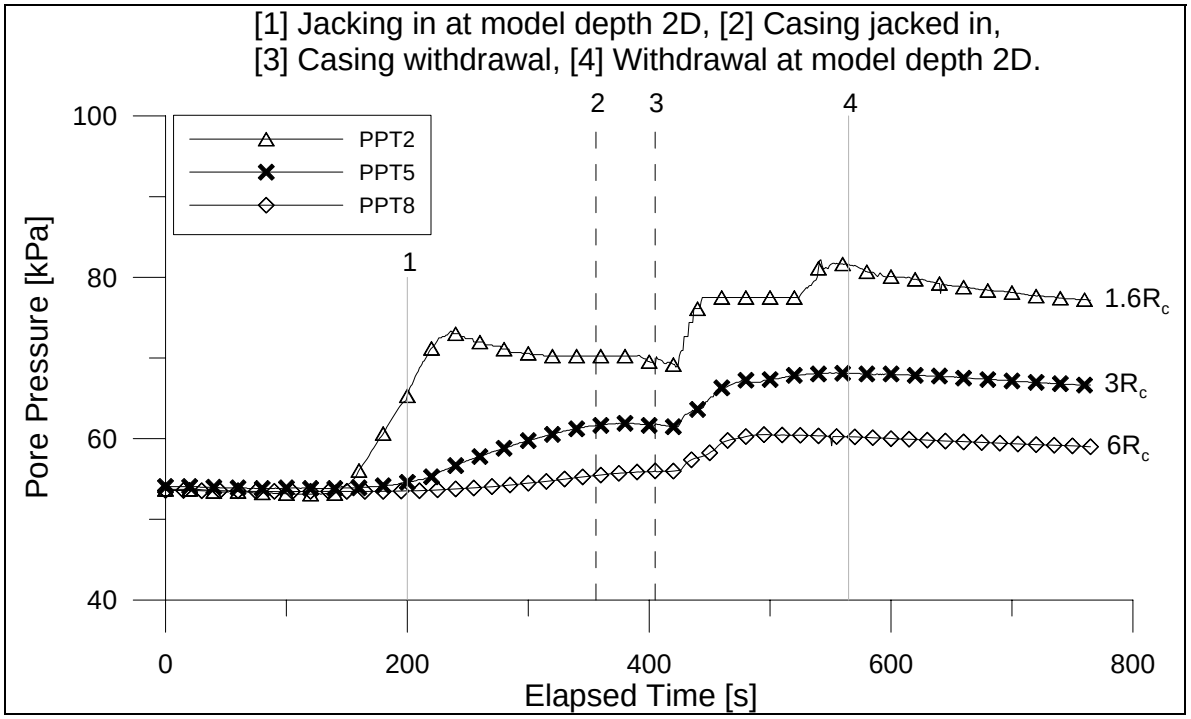

Fig. 6.2 Pore pressure recorded by PPTs at model depth 2D during installation of single DM column for test DM05.

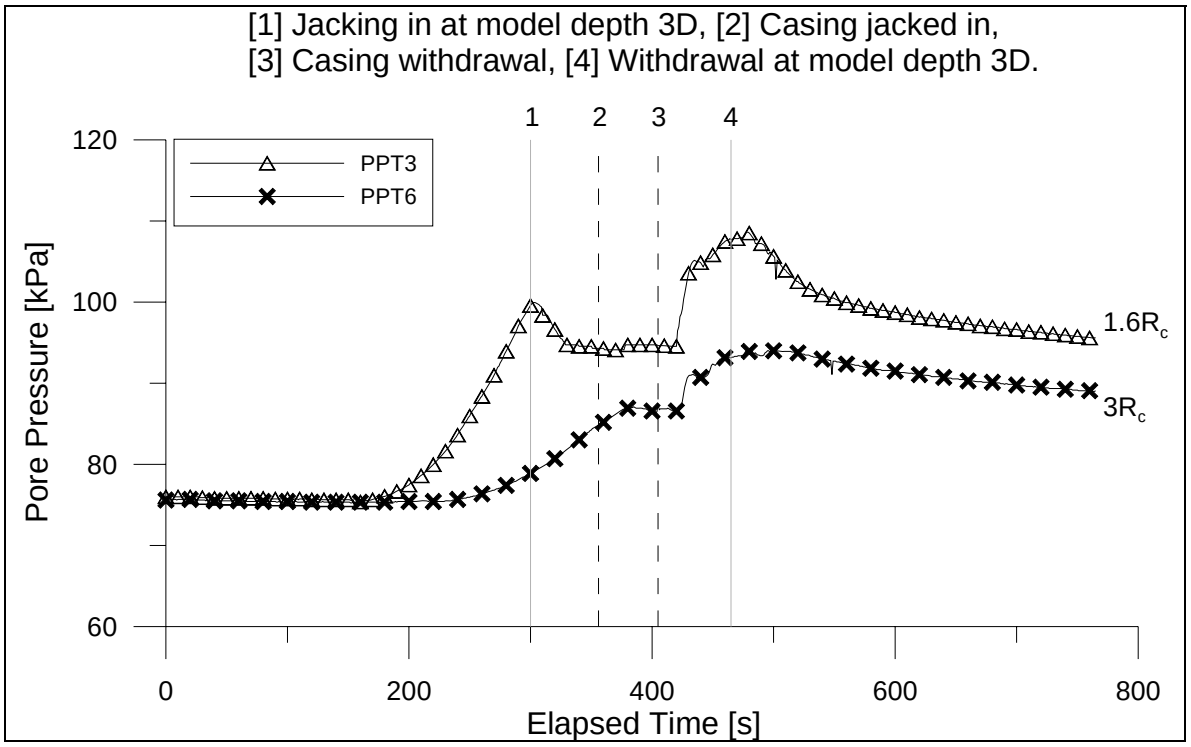

Fig. 6.3 Pore pressure recorded by PPTs at model depth 3D during installation of single DM column for test DM05.

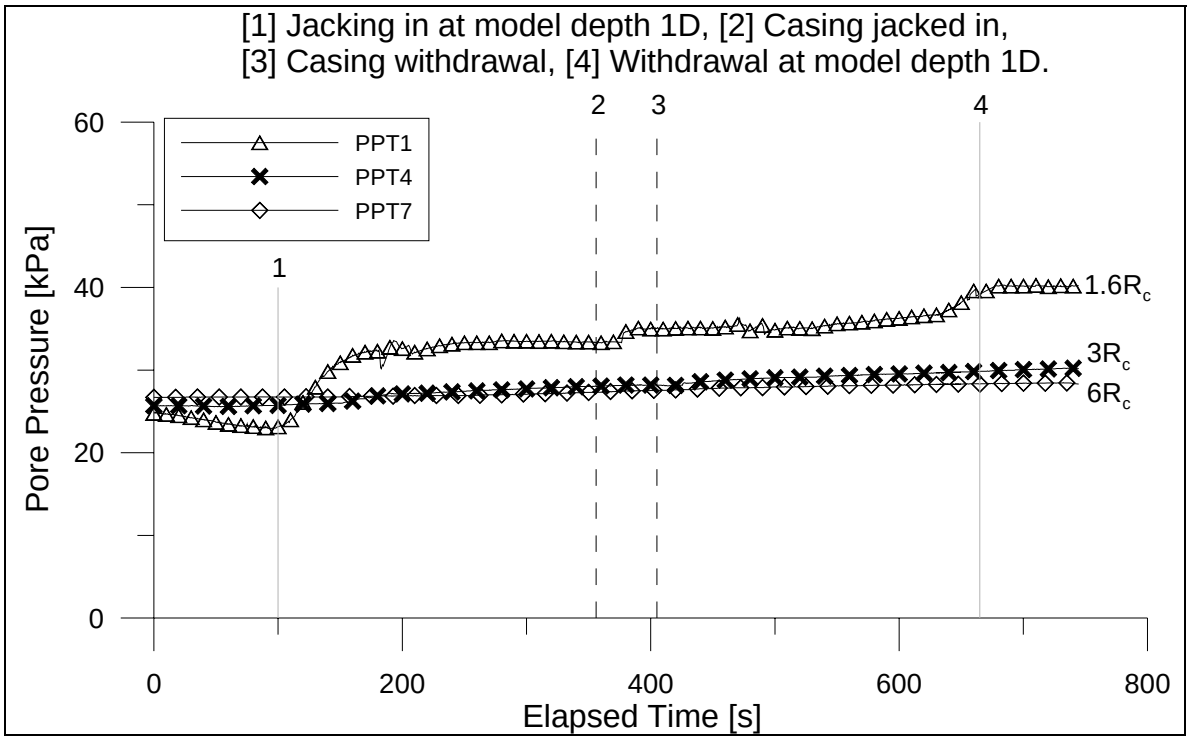

Fig. 6.4 Pore pressure recorded by PPTs at model depth 1D during installation of single DM column for test DM06.

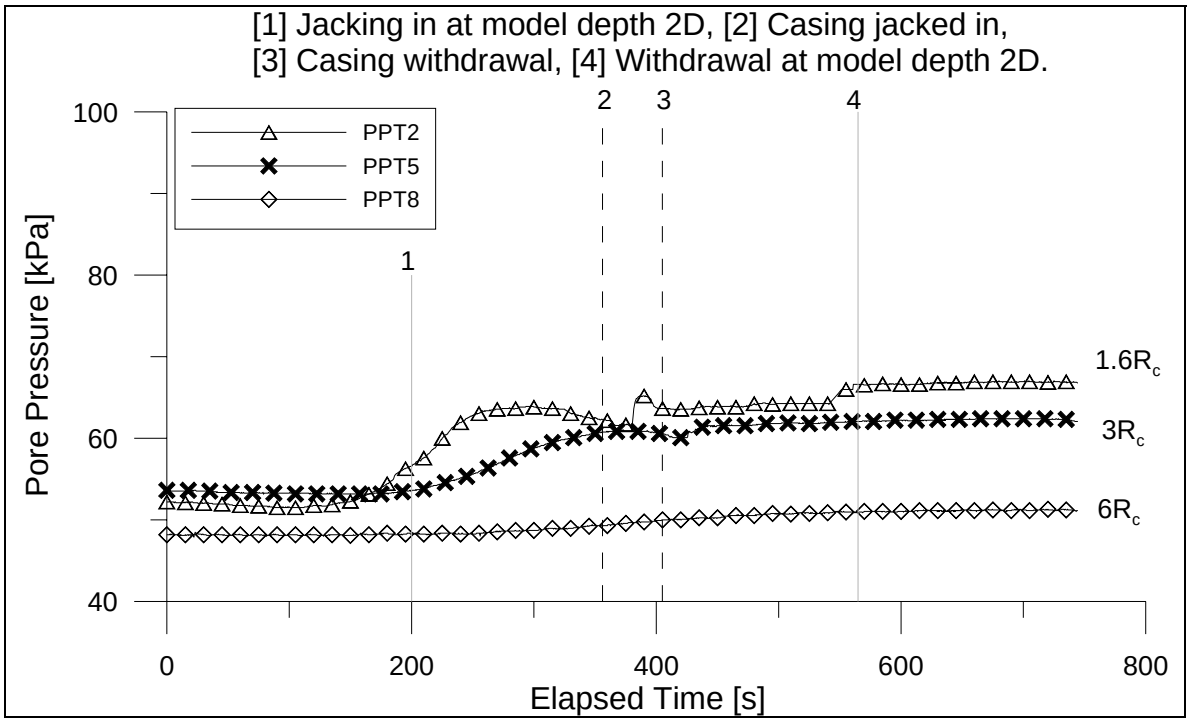

Fig. 6.5 Pore pressure recorded by PPTs at model depth 2D during installation of single DM column for test DM06.

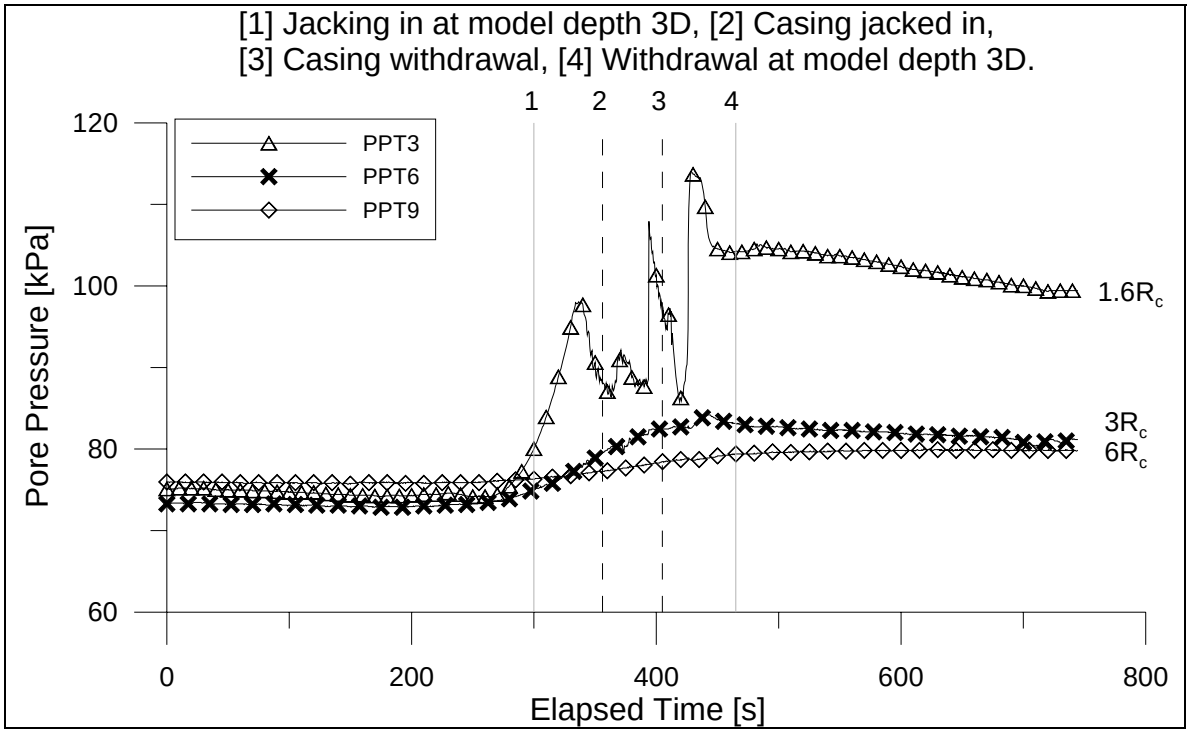

Fig. 6.6 Pore pressure recorded by PPTs at model depth 3D during installation of single DM column for test DM06.

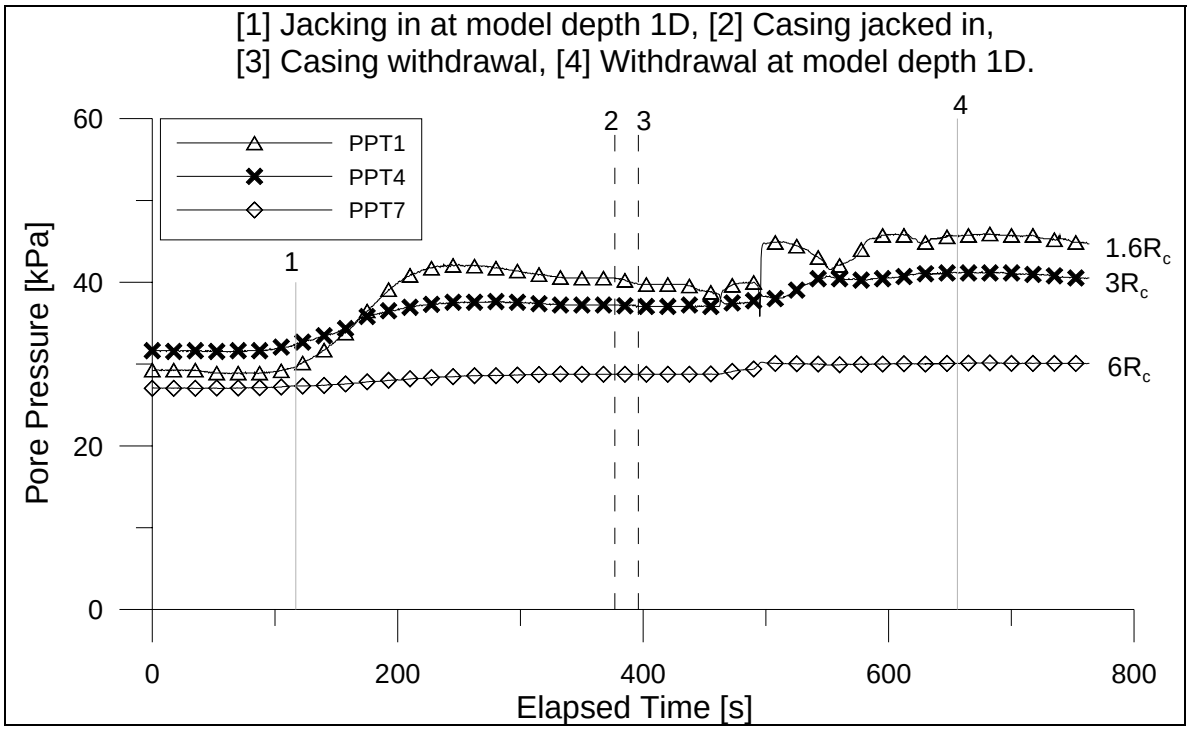

Fig. 6.7 Pore pressure recorded by PPTs at model depth 1D during installation of single DM column for test DM07.

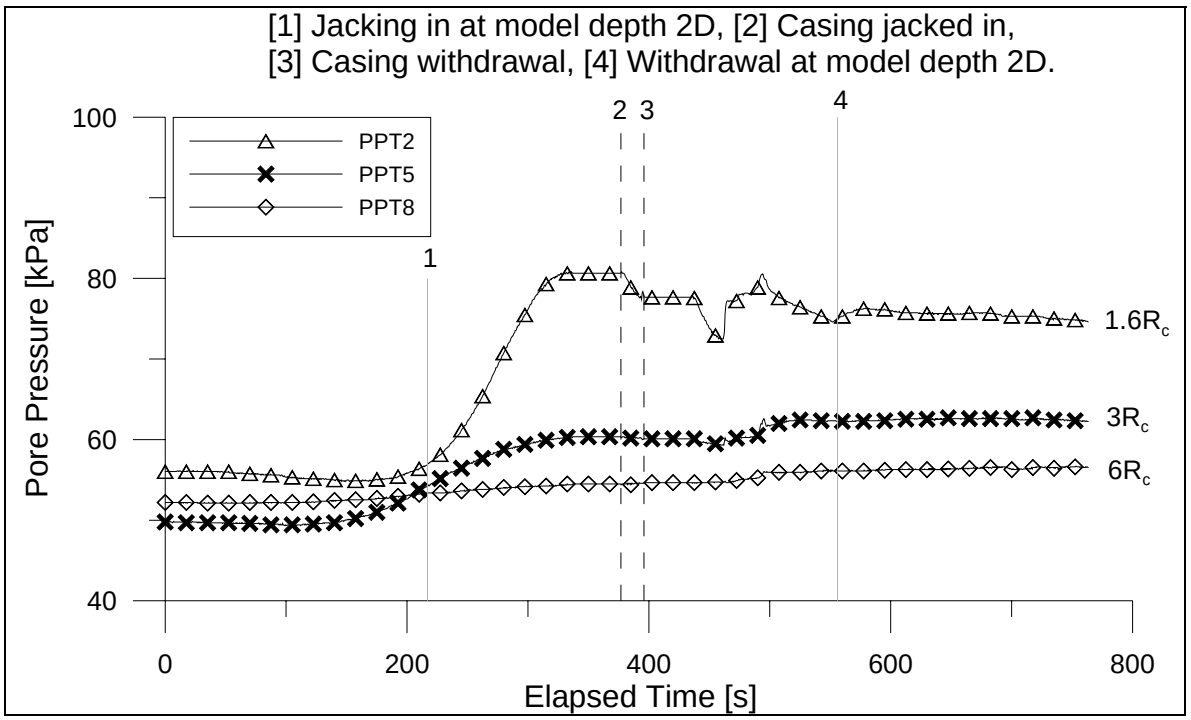

Fig. 6.8 Pore pressure recorded by PPTs at model depth 2D during installation of single DM column for test DM07.

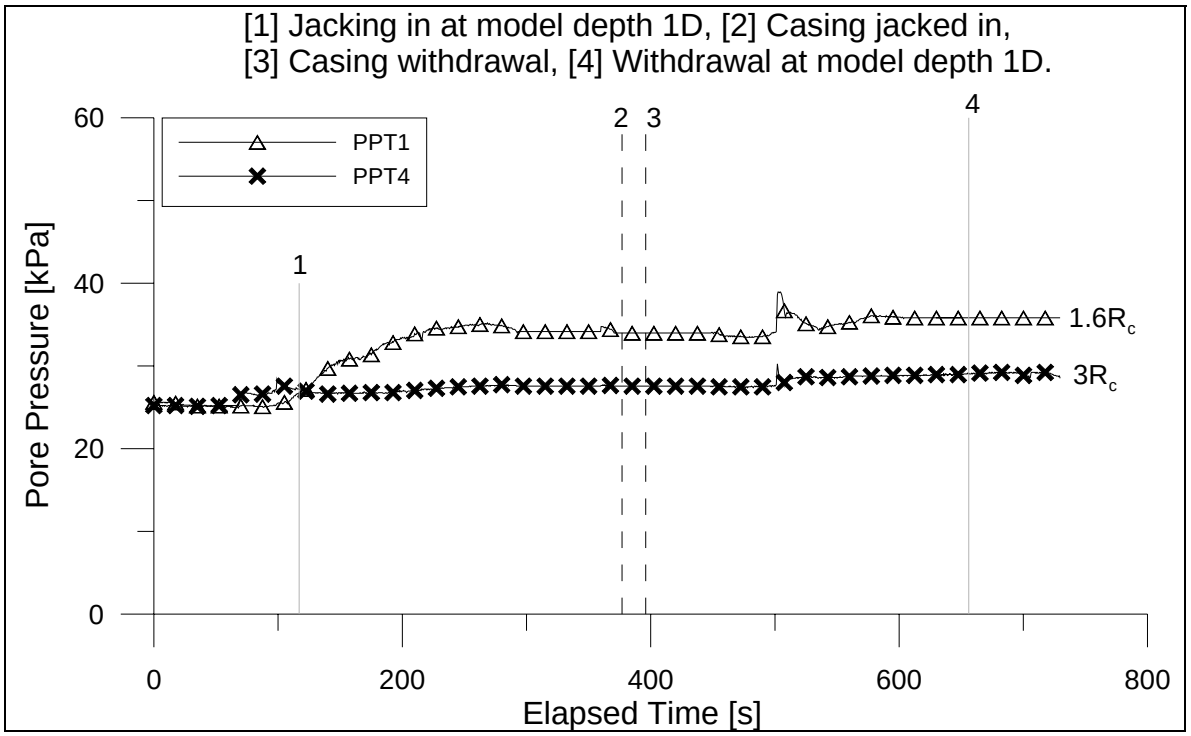

Fig. 6.9 Pore pressure recorded by PPTs at model depth 1D during installation of single DM column for test DM08.

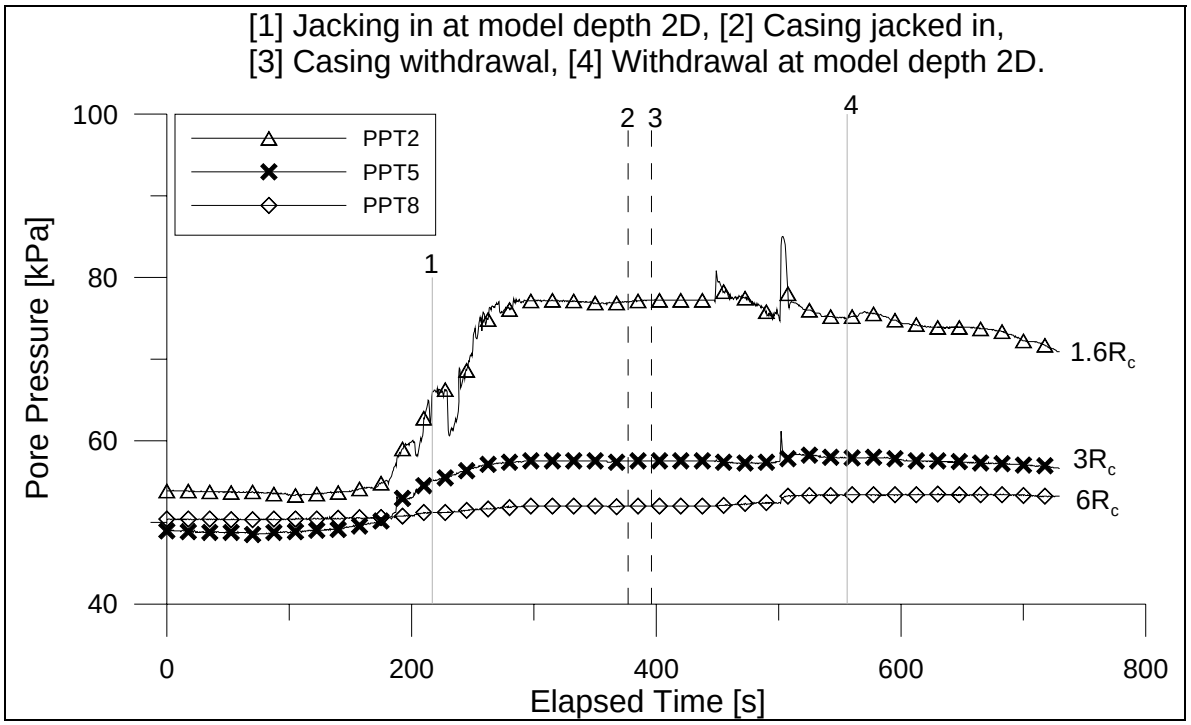

Fig. 6.10 Pore pressure recorded by PPTs at model depth 2D during installation of single DM column for test DM08.

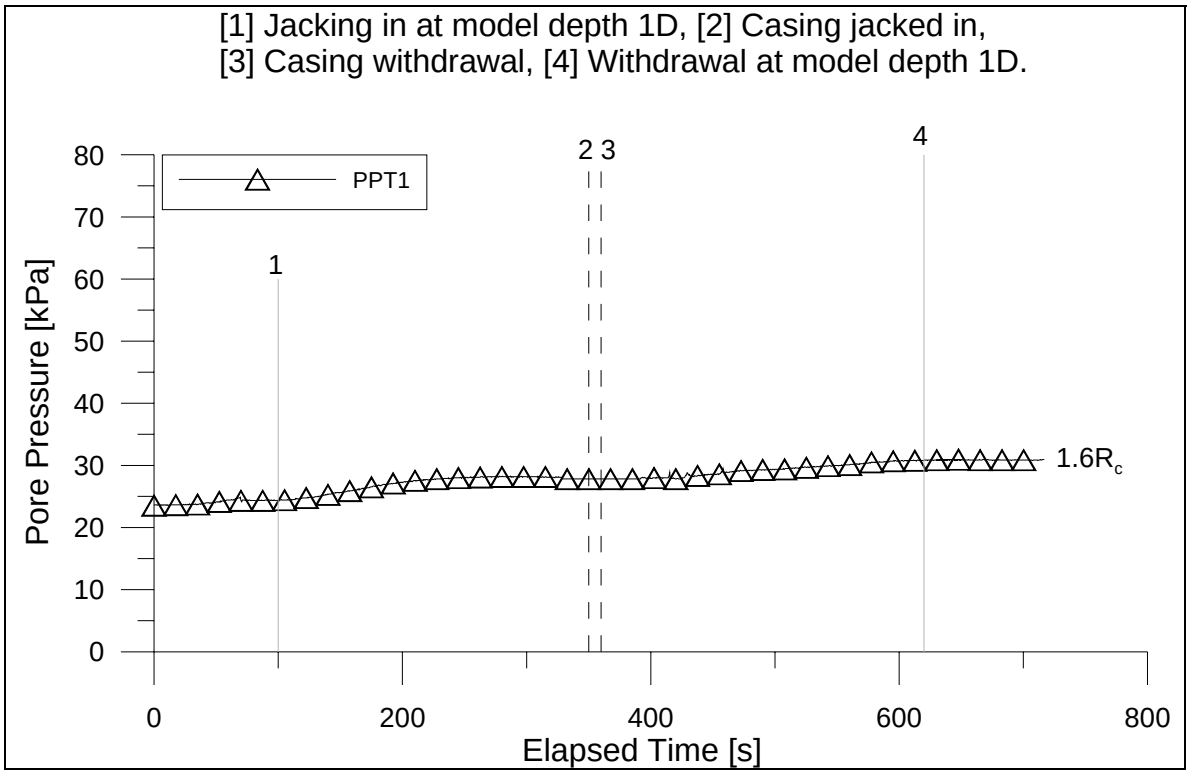

Fig. 6.11 Pore pressure recorded by PPT at model depth 1D during installation of single DM column for test DM09.

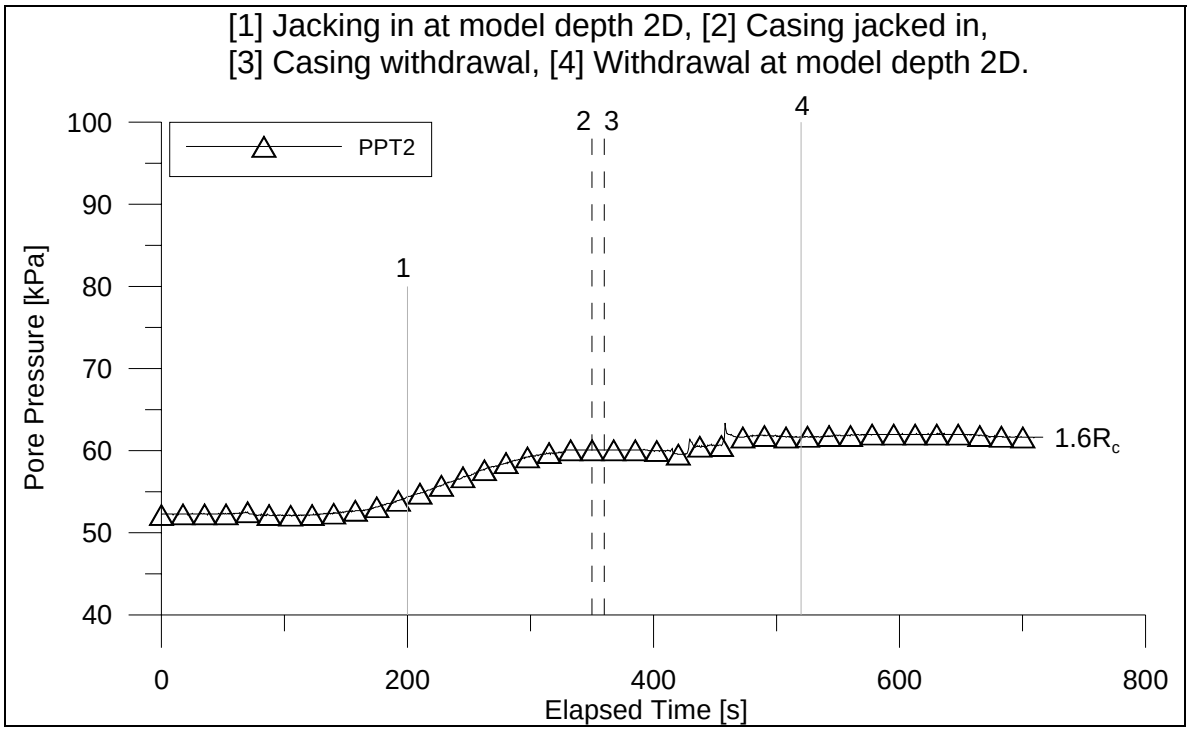

Fig. 6.12 Pore pressure recorded by PPT at model depth 2D during installation of single DM column for test DM09.

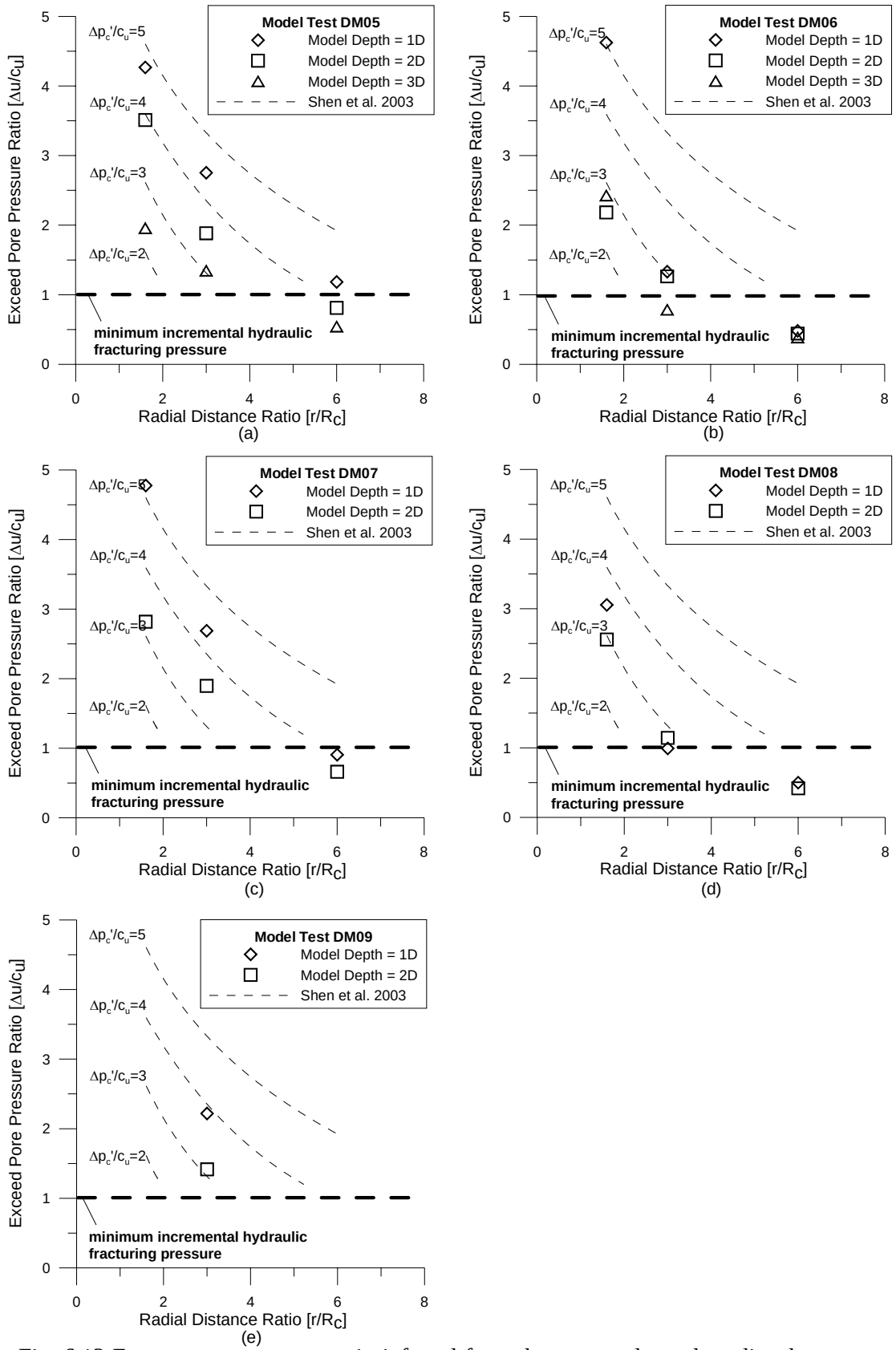

Fig. 6.13 Excess pore pressures ratio inferred from the test results and predicted excess expanding pressure ratio on the cavity wall calculated based on the shearing-expansion of cylindrical cavity model.

Chapter 7: Conclusion

7.1 Summary of Findings

The main findings arising from the foregoing discussion can be summarized as follows:

1. Examination of the scaling relationships showed that significant parameters governing the mixing process in wet DM method are Froude number, Reynolds number, Mobility number, Richardson number, centrifugal effect arising from mixing and work done in mixing. The scaling of gravity used in centrifuge modelling allows the Froude, Mobility and Richardson numbers to be preserved between prototype and model, thereby ensuring similitude between inertial, gravity and buoyancy forces. Centrifugal effect arising from mixing is automatically preserved between prototype and model in a geometrically similar model. The work done in mixing can be preserved between prototype and model via correct scaling of withdrawal rate. The withdrawal rate was calculated by considering both work done in mixing and Froude number. Among all the significant parameters that govern the mixing process, Reynolds number is most difficult to preserve since both the cement and soil slurries are non-Newtonian fluids. In particular, proper scaling of the viscosity of the cement slurry typically used in the prototype DM would require that the viscosity of the binder used in model to be less than that of water, while maintaining the same density, which is difficult to achieve. One way of mitigating this problem is to use a liquid tracer with the same density but a

lower viscosity, so that overscaling of the viscous shear stresses can be mitigated. An example of such a liquid tracer is zinc chloride solution, the density of which can be adjusted to be approximately equal to that of cement slurry. Further examination of viscous scaling of binder-soil mixture showed that prototype viscous shear stress level is much better preserved with zinc chloride as a model binder instead of cement slurry. Clearly, these scaling relationships discussed may serve as a basis for modelling of DM in a reduced-scale model. It should be noted that using zinc chloride solution in place of cement slurry does not model the hardening process. In any case, the hardening process involves chemical reactions that do not scale correctly in centrifuge environment.

2. The comparison between 1-g laboratory model mixing and centrifuge model mixing not only shows that there are significant differences between these two approaches, but it also highlights the important influence of viscous forces on the mixing quality and the significance of viscosity scaling to achieve a proper modelling. The viscous force could be modelled in 1-g models by increasing the rate of rotation, R_m to $N^2 \cdot R_p$. However, by increasing the rate of rotation, R_m beyond $\sqrt{N} \cdot R_p$ will lead to overscaling of inertial and centrifugal forces in relation to gravity forces. Because of this, the DM cannot be modelled correctly in 1-g reduced-scale model. In contrast, centrifuge modelling with appropriate viscosity scaling offers a better approach to study DM processes in the ground.

3. Both centrifuge and 1-g model test showed that raising the viscosity of the binder leads to an increase in the coefficient of variation, which is an indication

of a poorer mixing quality. Those results were consistent with the fact that a higher viscosity suppresses turbulence which promotes efficient mixing (e.g. Harnby et al. 1992). The centrifuge results emphasized the need to take viscosity into consideration when scaling the DM processes in a reduced-scale centrifuge model. In addition, it also implied that the quality of field mixing can be improved if the viscosity of cement slurry can be lowered, by using chemical additives.

4. The current study confirmed Yoshizawa et al.'s (1997) field study which showed that reducing the density difference between soil and slurry can enhance the quality of mixing. One possible explanation is that buoyancy force due to density difference between soil and slurry would affect the mixing process. Matsuo et al. (1996) also noted that similar variation in the coefficient of variation of the unconfined compressive strength with water-cement ratio and suggested that the degradation in mixing quality can be attributed to buoyancy effects arising out of density differences between slurry and soil. The significance of density differences in the mixing of fluids has been noted by Rielly & Pandit (1988) who characterised the mixing behaviour using the Richardson number. The similarity in the two trends i.e. model tests and reported field study, implies that under correctly scaled centrifuge conditions the model tests are able to demonstrate the effect of buoyancy force that arises from the density difference between soil and slurry.

5. The current study confirms that the withdrawal rate of the DM installer has significant influence on the quality of the mixing irrespective of their blade

configurations, under a constant blade revolution rate. This is also consistent with the field observation that the final quality of the DM treated ground is improved at a slower withdrawal rate. In addition, under same withdrawal rate, the quality of the mixing is affected by the blade rotation number which takes the withdrawal rate and the number of mixing blades into account. A more uniform mixing is achieved at a higher blade rotation number. From test results, it is obvious that, under the same blade rotation number, a comparable if not similar mixing quality can be achieved by using DM installer A, DM installer B and DM installer C regardless of their different blade number and blade configuration. This may be due to the fact that all types of mixing blades used in our study are simple twisted-blades inclined at blade angle of 45°. This simplicity and similarity in blade design might contribute to the similar mixing efficiency of these DM installers. However, a slightly more sophisticated design and a larger number of blades introduced in DM installer B and DM installer C surpass the simple-designed DM installer A by reducing the total DM installation time. The total DM installation time proportionally decreases with the number of blades installed along the installer shaft. For DM installer C, re-penetration is introduced due to the under-utilization of its additional blades. The advantage of introducing re-penetration in our study is two-fold. First, all blades on DM installer C can be better utilized after re-penetration and remixing are conducted. Second, re-penetration also increases the blade rotation number and thus increases the mixing quality as well as the mixing efficiency.

6. Experimental results of the high-g model tests have shown that pore pressure and lateral stress increase substantially upon installation of single DM column. Soil fracturing happens around the DM column. This conclusion is derived from the observation of measured excess pore pressure around the vicinity of DM column exceeded the minimum incremental hydraulic fracturing pressure proposed by Yanagisawa and Panah (1994) and Shen (1998). In such an eventuality, the zinc chloride would have infiltrated into the soil via the fractures around the DM column. This explains the reason, in which a portion of zinc chloride was able to infiltrate to the outside of the DM column within the short duration of the DM installation, as observed earlier.

7. The consistency between the coefficient of variation of concentration obtained in centrifuge and that for strength obtained from field measurements indicate that the centrifuge modelling approach is promising and merits further study. So far, much of the studies into the DM have been largely empirical in nature. The discussion shows that, notwithstanding the apparent complexity of the DM process, significant fundamental insight can still be glimpsed through appropriate theoretical considerations and physical modelling.

7.2 Implications of Centrifuge Modelling in Deep Mixing

This study demonstrated that, given the current technology, centrifuge modelling with appropriate scaling offers a theoretically consistent and experimentally viable approach to study DM processes in the ground. Comparison of 1-g reduced-scale data and centrifuge model data shows that 1-g reduced-scale models result in much higher

coefficient of variation in the mixing and that this observation can be readily explained through the proposed scaling relations, by the mis-scaling of the viscous stresses. Comparison of model results on coefficient of variation on binder concentration with field data on coefficient of variation of unconfined compressive strength shows remarkable similarity in magnitude and trend. Notwithstanding this, it should be emphasized that whereas the reduced-scale model data relate to concentration whereas the field data relate to unconfined compressive strength. More field data which relates directly to concentration would have been useful. However, the dearth of field data is an indication of the difficulty of studying mixing processes in the field. The objective of this study is precisely to find an approach which is theoretically viable, shows experimental promise and avoids the difficulties associated with field study.

7.3 Recommendations for Further Research

We acknowledge that the model equipment developed for the model test is different from the actual field DM machine. Furthermore, a variety of DM machines are used in the actual field. Therefore, the model test results cannot be directly applied to predict the performance of other DM machines used in actual field. However, in future work, the modelling technique outlined in this study can be replicated with a specific DM machine used in actual field. Furthermore, marine clay can be used in place of kaolin clay used in our tests. Hence a more direct comparison between model and field results can be conducted.

Difficulty in finding a liquid tracer with viscosity lower than water while maintaining a same density as cement slurry impedes a more accurate scaling of viscosity in

centrifuge model. A good alternative which is zinc chloride was chosen in our centrifuge model and put into tests. A wide range of parametric study in our tests showed a good agreement between model and prototype. In future work, efforts to search for a better liquid tracer should be continued in order to refine the model.

References

Al-Tabbaa, A. and Evans, C.W. (1999). Laboratory-scale soil mixing of a contaminated site. *Ground Improvement*, **3**, No. 3, 119-134.

Al-Tabbaa, A., Evans, C.W. and Wallace, C.J. (1998). Pilot in situ auger mixing treatment of a contaminated site. Part 2: Site trial. *Proceedings of the Institution of Civil Engineers, Geotechnical Engineering*, April, 131, 89-95.

Babasaki, R., and Suzuki, K. (1998). Design procedure for self-supporting earth retaining wall using deep mixing method. *Proceedings of International Conference Centrifuge 98, IS-Tokyo 98, Kimura, Kusakabe and Takemura (eds.)*, 673-678.

Babasaki, R., Terashi, M., Suzuki, T., Maekawa, A., Kawamura, M. and Fukazawa, E. (1996). JGS TC Report: Factor influencing the strength of the improved soil. *Grouting and Deep Mixing, Proceedings of IS-Tokyo 96', the Second International Conference on Ground Improvement Geosystems, Tokyo, 14-17 May, Yonekura, Terashi & Shibazaki (eds.)*, Vol. 1, 913-924.

Bourne, J.R. (1964). The mixing of powders, pastes and non-Newtonian fluids. *Industrial Research Fellow Report, The Institute of Chemical Engineers, September 1964*, 202-216.

Bruce, D.A. (2001). Practitioner's guide to the deep mixing method. *Ground Improvement* **5**, No. 3, 95-100.

Bruce, D.A., Bruce, M.E.C. and Dimillio, A.F. (1998). Deep mixing method: A global perspective. *Soil Improvement for Big Digs: Proceedings of Sessions of Geo-Congress 98*, 1-26.

Coastal Development Institute of Technology (CDIT), Japan. (2002). *The deep mixing method: principle design and construction.* A.A. Balkema Publishers, Lisse, Abingdon, Exton (PA), Tokyo.

Day C. and Ryan C.R., (1995). Containment, stabilisation and treatment if contaminated soils using in situ soil mixing. *ASCE Geotechnical Special Publication,* **46**, *Characterisation, Containment, Remediation and Performance in Environmental Geotechnics (Geoenvironment 2000),* 1349-1365.

Dinsdale, A. and Moore, F. (1962). *Viscosity and its measurement.* The Institute of Physics and the Physical Society, Chapman and Hall Limited, London, Reinhold Publishing Corporation, New York.

Dong, J., Hiroi, K. and Nakamura, K. (1996). Experimental study on behaviour of composite ground improved by deep mixing method under lateral earth pressure. *Grouting and Deep Mixing, Proceedings of IS-Tokyo 96', the Second International Conference on Ground Improvement Geosystems, Tokyo, 14-17 May, Yonekura, Terashi & Shibazaki (eds.),* Vol. 1, 585-590.

European Committee for Standardization (draft April 2003). *Execution of special geotechnical works- deep mixing.* European Standard.

Fang, Y.S., Chung, Y.T., Yu, F.J. and Chen, T.J. (2001). Properties of soil-cement stabilised with deep mixing method. *Ground Improvement* **5**, No. 2, 69-74.

Ferguson, J. and Kemblowski, Z. (1991). *Applied fluid Rheology.* Elsevier Science Publishers Ltd.

Gallagher, P.M. (2000). *Passive site remediation for mitigation of liquefaction risk.* PhD thesis, The Virginia Polytechnic Institute and State University, USA.

Gelfgat, A.Y., Yarin, A.L. and Yoseph, P.Z.B. (2001). Stability of a two-layer dean flow with a capillary liquid-liquid interface. *12th International Couette-Taylor Workshop, 6-8 Sep, Evanston, IL, USA.*

Govier, G.W. and Aziz, K. (1972). *The flow of complex mixtures in pipes*. Van Nostrand Reinhold Company.

Hanes, D.M., Alymov, V., Chang, Y.S. and Jette, C. (2001). Wave-formed sand ripples at Duck, North Carolina. *Journal of Geophysical Research*, Vol. 106, No. c10, 22, 575-22, 592.

Harnby, N., Edwards, M.F. and Nienow, A.W. (1992). *Mixing in the process industries*. Butterworth-Heinemann Ltd.

Harris, J. (1977). *Rheology and non-Newtonian flow*. Longman Group Limited.

Hashizume, H., Okochi, Y., Dong, J., Horii, N., Toyosawa, Y. and Tamate, S. (1998). Study on the behaviour of soft ground improved using Deep Mixing Method by low improvement ratio. *Proceedings of International Conference Centrifuge 98, IS-Tokyo 98, Kimura, Kusakabe and Takemura (eds.),* 851-856.

Hosomi, H. Nishioka, S. and Takei, S. (1996). Method of deep mixing at Tianjin Port, China. *Grouting and Deep Mixing, Proceedings of IS-Tokyo 96', the Second International Conference on Ground Improvement Geosystems, Tokyo, 14-17 May, Yonekura, Terashi & Shibazaki (eds.),* 491-494.

Inagaki, M., Abe, T., Yamamoto, M., Nozu, M., Yanagawa, Y. and Li, L. (2002). Behaviour of cement deep mixing columns under road embankment. *Physical Modelling in Geotechnics: ICPMG 02, Phillips, Guo and Popescu (eds.),* 967-972.

Isobe, K., Samura, Y., Aoki, C., Sogo, K. and Murakami, T. (1996). Large scales deep soil mixing and quality control. *Grouting and Deep Mixing, Proceedings of IS-Tokyo 96', the Second International Conference on Ground Improvement*

Geosystems, Tokyo, 14-17 May, Yonekura, Terashi & Shibazaki (eds.), Vol. 1, 619-624.

Kawasaki, T., Saitoh, S., Suzuki, Y. and Babasaki, R. (1984). Deep mixing method using cement slurry as hardening agent. *Proceedings of Seminar on Soil Improvement and Construction Techniques in Soft Ground, 10 – 11 January*, 17-38.

Khatib, Z. and Richardson, J.F. (1984). Vertical co-current flow of air and shear thinning suspensions of kaolin. *Chemical Engineering Research and Design*, Vol. 62, 139-154.

Kimura, M., and Matsuura, Y. (2002). Centrifuge model tests on laterally loaded steel pile and soil-cement composite pile. *Physical Modelling in Geotechnics: ICPMG 02, Phillips, Guo and Popescu (eds.)*, 619-624.

Kitazume, M., Ikeda, T. and Miyajima, S. (1996). Bearing capacity of improved ground with column type DMM. *Grouting and Deep Mixing, Proceedings of IS-Tokyo 96', the Second International Conference on Ground Improvement Geosystems, Tokyo, 14-17 May, Yonekura, Terashi & Shibazaki (eds.)*, Vol. 1, 503-508.

Kitazume, M., Okano, K. and Miyajima, S. (2000). Centrifuge model tests on failure envelope of column type deep mixing method improved ground. *Soils and Foundations*, Vol. 40, No. 4, 43-55.

Kitazume, M., Okano, K. and Miyajima, S. (2001). Centrifuge model tests on failure envelope of column type DMM improved ground (Discussions). *Soils and Foundations*, Vol. 41, No. 4, 108.

König, D., Jessberger, H.L., Bolton, M., Phillips, R., Bagge, G., Renzi, R. and Garnier, J. (1994). Pore pressure measurement during centrifuge model tests:

Experience of five laboratories. *Proceedings of the International Conference Centrifuge 94, Leung, Lee and Tan (eds.)*, 101-108.

Larsson, S. (2001). Binder distribution in lime-cement columns. *Ground Improvement* **5**, 111-122.

Larsson, S., Dahlstrom, M. and Nilsson, B. (2005b). A complementary field study on the uniformity of lime-cement columns for deep mixing. *Ground Improvement* **9**, No. 2, 67-77.

Larsson, S., Dahlstrom, M. and Nilsson, B. (2005a). Uniformity of lime-cement columns for deep mixing: a field study. *Ground Improvement* **9**, No. 1, 1-15.

Lee, C.H., Lee, F.H. & Dasari, G.R. (2004). Modelling of Deep Mixing Processes in Centrifuge. *5th Asian Young Geotechnical Engineers Conference, Taipei, Taiwan, 14-16 June*. 143-147.

Lee, F.H., Lee, C.H. and Dasari, G.R. (2006). Centrifuge modelling of deep mixing processes in soft clays. *Geotechnique* (in press).

Lee, F.H., Juneja, A., Tan, T.S. and Yong, K.Y. (2002). Excess pore pressure due to sand compaction installation in soft clay. *Physical Modelling in Geotechnical: ICPMG 02, Phillips, Guo and Popescu (eds.)*, 955-960.

Lee, F.H., Ng, Y.W. and Yong, K.Y. (2001). Effect of installation method on sand compaction piles in clay in the centrifuge. *Geotechnical Testing Journal*, **24**, No. 3, 314-323.

Lee. F.H., Tan, T.S., Leung, C.F., Yong, K.Y., Karunaratne, G.P. and Lee, S.L. (1991). Development of geotechnical centrifuge facility at the National University of Singapore. *Proceeding of the International Conference Centrifuge 91, Ko (ed.)*. Balkema, Rotterdam, 11-17.

Lee, F.H. (1992). *The National University of Singapore geotechnical centrifuge users' manual*. Research Report CE001, NUS, 48.

Matsuo, T., Nisibayashi, K. and Hosoya, Y. (1996). Studies on soil improvement adjusted at low compressive strength in deep mixing method. *Grouting and Deep Mixing, Proceedings of IS-Tokyo 96', the Second International Conference on Ground Improvement Geosystems, Tokyo, 14-17 May, Yonekura, Terashi & Shibazaki (eds.),* Vol. 1, 421-424.

McDonough, R.J. (1992). *Mixing for the process industries*. Van Nostrand Reinhold.

Miyake, M., Wada, M. and Satoh, T. (1991). Deformation and strength of ground improved by cement treated soil columns. *Proceedings of the International Conference on Geotechnical Engineering for Coastal Development: Theory and Practice on Soft Ground,* 369-372.

Mizuno, T., Namura, Y. and Matsumoto, J. (1998). An experimental on the improvement of sandy soil using the deep mixing method. *Proceeding of the 23rd Japan National Conference on Soil Mechanics and Foundation Engineering*, 2301-2304.

Mizutani, T., Kanai, S. and Fujii, M. (1996). Assessment of quality of soil-cement columns of square and rectangular shapes formed by deep mixing method. *Grouting and Deep Mixing, Proceedings of IS-Tokyo 96', the Second International Conference on Ground Improvement Geosystems, Tokyo, 14-17 May, Yonekura, Terashi & Shibazaki (eds.),* Vol. 1, 637-642.

Montgomery, D.C. and Runger, G.C. (1999). *Applied statistics and probability for engineers.* John Wiley & Sons, Inc.

Mori, F., Furukawa, S., Kikuchi, Y. and Matsumoto, K. (1997). Analysis and field loading tests of building foundations treated by new soil improvement methods. *Ground Improvement Geosystems, Proceedings of the 3rd International Conference on Ground Improvement Geosystems, London, 3-5 June 1997*, 246-252.

Ng, Y.W., Lee, F.H. and Yong, K.Y. (1998). Development of an in-flight Sand Compaction Piles (SCPs) installer. *Proceedings of the International Conference Centrifuge 98. Kimura, Kusakabe and Takemura (eds.)*, 837-843.

Niranjan, K., Smith, D.L.O., Rielly, C.D., Lindley, J.A. and Phillips, V.R. (1994). Mixing processes for agricultural and food materials: Part 5, review of mixer types. *Journal of Agricultural Research,* **59**, 145-161.

Nishibayashi, K. (1998). Research on low strength improvement using deep mixing method for the purpose of post improvement excavation: Part 2. *23rd Annual meeting, JSSMFE*, 2297-2300.

Nishida, K., Koga, Y. and Miura, N. (1996). Energy consideration of the dry jet mixing methods. *Grouting and Deep Mixing, Proceedings of IS-Tokyo 96', the Second International Conference on Ground Improvement Geosystems, Tokyo, 14-17 May, Yonekura, Terashi & Shibazaki (eds.)*, Vol. 1, 643-648.

Olson, R.M. (1966). *Essential of engineering fluid mechanics*. International Textbook Company, Scranton, Pennsylvania.

Ong, E.L. (2004). *Pile behaviour subject to excavation-induced soil movement in clay*. PhD thesis, Center for Soft Ground Engineering. National University of Singapore.

O'Neill, M.P. and Randolph, M.F. (2001). Modelling drag anchors in a drum centrifuge. *International Journal of Physical Modelling in Geotechnics*, Vol. 1, No. 2, 29-42.

O'Neill, M.P., Bransby, M.F. and Randolph, M.F. (2003). Drag anchor fluke-soil interaction in clays. *Canadian Geotechnical Journal*, Vol. 40(1), 78-94.

Porbaha, A., Raybaut, J.L., Nicholson, P. (2001). State of the art in construction aspects of deep mixing technology. *Ground Improvement,* **5**, No. 3, 123-140.

Porbaha, A., Shibuya, S., and Kishida, T. (2000). State of the art in deep mixing technology. Part III: geomaterial characterization. *Ground Improvement,* **3**, 91-110.

Porbaha, A. (1998a). State of the art in deep mixing technology: Part I: Basic concepts and overview. *Ground Improvement* **2**, 81-92.

Porbaha, A. (1998b). State of the art in deep mixing technology: Part II: Applications. *Ground Improvement* **2**, 125-139.

Porbaha, A. (2002). State of the art in quality assessment of deep mixing technology. *Ground Improvement,* **6**, No. 3, 91-110.

Rielly, C.D. and Pandit, A.B. (1988). The mixing of Newtonian liquids with large density and viscosity differences in mechanically agitated contactors. *Mixing, Proceedings of the 6th European Conference, Pavia, Italy, 24-26 May 1998*, 69-77.

Rielly, C.D., Smith, D.L.O., Lindley, J.A., Niranjan, K. and Phillips, V.R. (1994). Mixing processes for agricultural and food materials: Part 4, assessment and monitoring of mixing systems. *Journal of agricultural Engineering Res.* **59**, 1-18.

Shen, S.L. (1998). *Behaviour of the deep mixing columns in composite clay ground*. PhD thesis. Division of Engineering Systems and Technology, Graduate School of Science and Engineering, Saga University.

Shen, S.L., Miura, N. and Koga, H. (2003). Interaction mechanism between deep mixing column and surrounding clay during installation. *Canadian Geotechnical Journal*, 40(2), 293-307.

Silvester, T., (1999). Deep soil mixing. *Report on Joint BGS/ICE Meeting, Environmental and Engineering Applications of Deep Soil Mixing, 13 Jan 1999. Ground Engineering*, 29-32.

Springer, A.M. (2003). *Aerospace design: aircraft, spacecraft, and the art of modern flight*. New York, Merrell.

Sterbacek, Z. and Tausk, P. (1965). *Mixing in the chemical industry*. Pergamon Press Ltd., Headington Hill Hall, Oxford 4 & 5 Fitzroy Square, London W.1.

Taylor, R.N. (1995). Geotechnical centrifuge technology. *Blackie Academic and Professional.*

Topolnicki, M. (2004). In situ soil mixing. *Ground Improvement 2nd edition, edited by Moseley, M.P. and Kirsch, K.*, 331-428.

Ulbrecht, J.J. and Patterson, G.K. (1985). *Mixing of liquids by mechanical agitation*. Gordon and Breach Science Publishers.

Unami, K. and Shima, M. (1996). Deep mixing methods at Ukishima site of the Trans-Tokyo Bay highway project. *Grouting and Deep Mixing, Proceedings of IS-Tokyo 96', the Second International Conference on Ground Improvement Geosystems, Tokyo, 14-17 May, Yonekura, Terashi & Shibazaki (eds.),* Vol. 1, 777-782.

Usui, H. (2002). Quality control of cement deep mixing method (wet method). *Proceedings of Deep Mixing Workshop 2002 in Tokyo, The International Workshop on Deep Mixing, Tokyo, 15-18 October, Kitazume and Terashi (eds.),* 116-123.

Vesic, A.S. (1972). Expansion of cavities in infinite soil mass. *Journal of Soil Mechanics and Foundation Engineering Division, Proceeding of American Society of Civil Engineers (ASCE)*, Vol. 98, No. SM3, 265-290.

Yanagisawa, E and Panah, A.K. (1994). Two-dimensional study of hydraulic fracturing criteria in cohesive soil. *Soil and Foundations, Japanese Geotechnical Society (JGS)*, Vol. 34, No.1, 1-9.

Yoshida, S. (1996). Shear Strength of improved soils at lap-joint-face. *Grouting and Deep Mixing, Proceedings of IS-Tokyo 96', the Second International Conference on Ground Improvement Geosystems, Tokyo, 14-17 May, Yonekura, Terashi & Shibazaki (eds.)*, Vol. 1, 461-466.

Yoshizawa, H., Okumura, R., Hosoya, Y., Sumi, M. and Yamada, T. (1997). JGS TC report: Factor affecting the quality of treated soil during execution of DMM. *Grouting and Deep Mixing, Proceedings of IS-Tokyo 96', the Second International Conference on Ground Improvement Geosystems, Tokyo, 14-17 May, Yonekura, Terashi & Shibazaki (eds.)*, Vol. 2, 931-937.

Zorev, N.N. (1966). *Metal cutting mechanics; translated [from the Russian] by Massey. H.S.H., edited by Shaw, M.C.* Oxford, London: Pergamon.